1
Interfacial Catalysis at Oil/Water Interfaces

ALEXANDER G. VOLKOV Oakwood College, Huntsville, Alabama, U.S.A.

I. INTRODUCTION

From thermodynamic and kinetic principles the interface between two immiscible liquids can have catalytic properties for interfacial charge-transfer reactions [1–10]. It is also possible to shift the redox potential scale in a desired direction by selecting appropriate solvents, thereby permitting reactions to occur that are highly unfavorable in a homogeneous phase [1,11–15]. The kinetic mechanism underlying the catalytic properties of the liquid/liquid interface was discussed first by Kharkats and Volkov [4–7] as they introduced a new term "interfacial catalysis."

Redox reactions at the interface between immiscible liquids fall into two classes. The first class includes spontaneous processes that occur in the absence of external electromagnetic fields [16–77]. This type of redox transformation has been investigated in bioenergetics, model membrane systems and at oil/water interfaces [78–99]. Redox reactions in the second class occur at the interface between immiscible electrolytes when external electrical fields are applied to the interface, and under these conditions interfacial charge-transfer reactions take place at controlled interfacial potentials [100–139].

Michael Faraday first studied nanochemistry and electron-transfer reactions at oil/water interfaces to prepare colloidal metals by reducing metal salts at the ether/water or carbon disulfide/water interfaces [140]. Vectorial charge transfer at the interface between two dielectric media is an important stage in many bioelectrochemical processes such as those mediated by energy-transducing membranes. Boundary membranes play a key role in the cells of all contemporary organisms, and simple models of membrane function are therefore of considerable interest [11,141–143]. The interface of two immiscible liquids has been widely used for this purpose. For example, the fundamental processes of photosynthesis, biocatalysis, membrane fusion, ion pumping, and electron transport have all been investigated in such interfacial systems [11–15,18–33,53,83,144–153]. Bell [154] conducted the first experiments on multielectron redox reactions at the interface between two immiscible liquids. Bell studied the oxidation of benzoyl-*o*-toluidide in benzene solution to benzoyl-anthranilic acid by a neutral aqueous solution of potassium permanganate. Since then many studies have been made on redox and hydrolysis reactions catalyzed by enzymes, photosynthetic pigments, porphyrins, bacteria, and submitochondrial particles, as well as in systems with an extended surface—in microemulsions, vesicles, and reversed micelles. Naturally immobilized enzymes and pigments embedded in a hydrophilic–hydrophobic interface have properties similar to their functional state in a membrane.

For instance, certain enzymes can be highly active at the interface, but virtually inactive in a homogeneous medium.

The interface between two immiscible liquids with immobilized photosynthetic pigments can also serve as a simple model for investigating photoprocesses accompanied by spatial separation of charges across a membrane. Such light-dependent redox reactions at the oil/water interface have been discussed in recent reviews and books [1–3,11,14,15,94–96,155]. Here, we will present some theoretical aspects of interfacial catalysis.

Liquid interfaces can work not only as catalysts or inhibitors of redox reactions, but they can also shift the Gibbs free energy or redox potentials from the values found in a homogeneous medium. For example, at the oil/water interface the following redox reaction can occur:

$$\mathrm{Red} \leftrightarrow \mathrm{Ox} + n\mathrm{e}^- + m\mathrm{H}^+ \tag{1}$$

The electrons that are the products of Eq. (1) can be accepted at the interface by another substance (acceptor or catalyst) if it is dissolved in one of the two phases. The standard Gibbs free energies of Eq. (1) for each phase, α and β, are

$$\Delta G^\circ_\alpha = {}_\alpha\mu^\circ_{\mathrm{Red}} - {}_\alpha\mu^\circ_{\mathrm{Ox}} - n\mu^\circ_{\mathrm{e}^-} - m_\alpha\mu^\circ_{\mathrm{H}^+} \tag{2}$$

$$\Delta G^\circ_\beta = {}_\beta\mu^\circ_{\mathrm{Red}} - {}_\beta\mu^\circ_{\mathrm{Ox}} - n\mu^\circ_{\mathrm{e}^-} - m_\beta\mu^\circ_{\mathrm{H}^+} \tag{3}$$

Subtraction of Eq. (2) from Eq. (3) gives the change in the standard Gibbs energy at the interface if the electron acceptor is located in one phase only, or localized at the phase boundary:

$$\Delta G^\circ_\beta - \Delta G^\circ_\alpha = ({}_\beta\mu^\circ_{\mathrm{Red}} - {}_\alpha\mu^\circ_{\mathrm{Red}}) - ({}_\beta\mu^\circ_{\mathrm{Ox}} - {}_\alpha\mu^\circ_{\mathrm{Ox}}) - m({}_\beta\mu^\circ_{\mathrm{H}^+} - {}_\alpha\mu^\circ_{\mathrm{H}^+}) \tag{4}$$

or

$$\Delta G^\circ = RT \ln \frac{P_{\mathrm{Red}}}{P_{\mathrm{Ox}}(P_{\mathrm{H}^+})^m} \tag{5}$$

where P_i is the partition coefficient of the ith ion:

$$RT \ln P_i = {}_\beta\mu^\circ_i - {}_\alpha\mu^\circ_i \tag{6}$$

In the case of an n-electron reaction, the standard redox potential ΔE° at the interface is determined by

$$\Delta E^\circ = -\frac{RT}{nF} \ln \frac{P_{\mathrm{Red}}}{P_{\mathrm{Ox}}(P_{\mathrm{H}^+})^m} \tag{7}$$

A thermodynamic analysis of redox and mixed potentials at the liquid/liquid interface was published by Markin and Volkov [153,157–161].

A system of two immiscible liquids can form six types of structures, as shown in Fig. 1:

1. Two individual immiscible liquids
2. Water-in-oil emulsion/aqueous phase
3. Oil/oil-in-water emulsion
4. Two immiscible liquids and emulsion on the interface
5. Oil-in-water emulsion or water-in-oil emulsion
6. Water-in-oil emulsion/oil-in-water emulsion

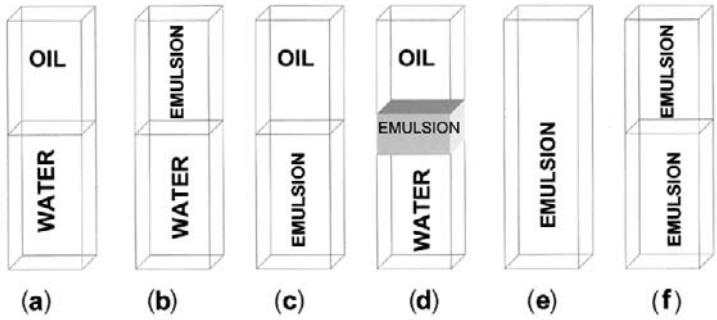

FIG. 1 Various types of structure arising in the oil/water system.

While reactions are being studied at the oil/water interface, one of the six possible structures should be specified. It should also be noted that transitions from one structure to another can occur if concentrations of surface-active compounds or electrolyte are varied, or if components of the system are altered by chemical reactions. In the present chapter we will consider flat and sharp oil/water interfaces as shown in Fig. 1(a).

Two types of heterogeneous catalysis are most frequently encountered in nature, namely, processes in which the catalyst is in the liquid or solid phase and the reactant is in another immiscible liquid, solid, or gaseous phase, and interfacial processes in which catalysts and substrate are soluble in one phase, but catalytic reactions take place at the interface with another immiscible phase.

Heterogeneous catalytic process can be divided into five steps:

- Diffusion of reactant to the interface
- Adsorption of reactants onto the interface
- Chemical reaction at the interface
- Desorption of products from the interface
- Diffusion of products from the interface

Depending on the conditions in which a process is conducted and its features, any of the five steps may be the slowest one. Hence, the rate of the catalytic process may be limited by one of them. An interfacial chemical reaction may proceed only with continuous molecular or convective diffusion of the reactants to the surface on which the given reaction is proceeding, and also with continuous reverse diffusion of the products. The rate of a process as a whole will be determined by the rate of its slowest step. If the rate of a reaction on the surface of a catalyst is greater than that of diffusion, the rate of the process as a whole will be determined by the rate of diffusion. The observed macroscopic kinetics of the reaction will obey equations that can be obtained by considering only processes of diffusion and will not reflect the true rate of the chemical reaction at the interface. Such a process is a diffusion-controlled one. It is most frequently described by a first-order reaction equation, since the rate of diffusion is directly proportional to the concentration.

If the rate of chemical reaction is considerably slower than that of diffusion, the rate of the process as a whole will be determined by that of the chemical reaction. Such process is a kinetically controlled one. If the rate of diffusion and that of the chemical reaction, when considered independently of each other, are commensurable, we have a process that is intermediate between a kinetically and diffusion controlled one. The same process, depending on the conditions under which it is conducted, may be kinetically or diffusion controlled.

Of special importance for heterogeneous processes is the transfer of a substrate from the bulk of a liquid or gas to the interface between two immiscible phases. Fick's law for diffusion in a given direction is

$$\mathrm{d}n = -DA\frac{\mathrm{d}x}{\mathrm{d}l}\mathrm{d}t \tag{8}$$

where $\mathrm{d}n$ is the amount of a substance passing during time $\mathrm{d}t$ through a surface with area A, D is the diffusion coefficient, and $\mathrm{d}x/\mathrm{d}l$ is the gradient of concentration. Assume that at the interface the concentration of a reactant is equal to c_s, and at a certain distance δ from it to c_x. Hence,

$$-\frac{\mathrm{d}x}{\mathrm{d}l} = \frac{c_s - c_x}{\delta} \tag{9}$$

and

$$\mathrm{d}n = DA\frac{c_s - c_x}{\delta}\mathrm{d}t \tag{10}$$

Dividing the right- and left-hand sides of Eq. (10) by the volume and passing over to concentrations, we obtain

$$\frac{dn}{V} = \mathrm{d}c = \frac{DA}{V}\frac{c_s - c_x}{\delta}\mathrm{d}l \tag{11}$$

We finally obtain for the rate of the diffusion process:

$$\frac{\mathrm{d}c}{\mathrm{d}t} = \frac{DA}{V\delta}(c_s - c_x) \tag{12}$$

Thus, the rate of diffusion kinetically obeys a first-order equation relative to the concentration c_x in the bulk of the solution, which was confirmed by experimental data. The rate of diffusion grows with the temperature according to a law similar to the Arrhenius equation:

$$D = k\mathrm{e}^{-E/RT} \tag{13}$$

It should be noted, however, that the value of E rarely exceeds 5 kJ/mol, i.e., it is only a small fraction of the activation energies of most chemical reactions. Consequently, with increasing temperature, the rate of diffusion will increase considerably slower than the rate of the chemical process.

II. ELECTRON TRANSFER REACTIONS AT LIQUID/LIQUID INTERFACES

Synchronous multielectron reactions in membranes have recently drawn the attention of both chemists and biologists. These reactions function to use its energy very economically. Furthermore, the biotechnological application of multielectron reactions makes it possible to drive redox reactions in relatively mild conditions under the action of weak oxidants or reductants. Synchronous multielectron reactions may proceed without forming highly reactive intermediate radicals, which have the potential to damage the catalytic complex. Since multielectron reactions do not produce significant toxic intermediates, they are used by living organisms for biochemical energy conversion in respiration and photosynthesis. In multielectron reactions that occur as consecutive one-electron stages, the Gibbs energy necessary per single electron transfer obviously cannot be uniformly distributed over the

stages. The energy needs for various stages will be different and the excess energy in the lower energy stages will be converted into heat.

The term *synchronous multielectron* reaction does not mean that all n electrons started synchronously, since this is impossible according to quantum mechanics. Instead, each electron is transferred from donor to acceptors individually. However, the time required for "intermediate" formation is much less than the time of the reorganization of the medium, so that "intermediates" as individual chemical compounds do not exist.

The quantum theory of chemical reactions in polar media can be used as the basis for the theory of charge transfer at the interface between two dielectric media—oil/water and biomembrane/water; by this theory one can express the electron transfer rate in terms of the dielectric properties of the medium and the characteristics describing the electronic properties of reactants.

The problem of theoretically describing the elementary charge-transfer act across interfaces between two condensed media has a long history. The earliest studies of interfacial electrochemical phenomena focused on metal/electrolyte or semiconductor/electrolyte interfaces. Considerable progress has been made recently in extending the theory to liquid/liquid interfaces [6,7,127,162–173].

Kharkats first calculated the energy of activation and solvent reorganization of charge transfer across the interface between two immiscible liquids [6,7,162]. The expression for the probability of electron transfer can be written as

$$W = A \exp\left\{ -\frac{U_i}{kT} - \frac{\left[E_s + \Delta G_c + U_f - U_i\right]^2}{4E_s kT} \right\} \tag{14}$$

where U_i is the work that must be performed on the system to place the reactants at distances h_1 and h_2 from the interface (Fig. 2), U_f is the corresponding work for the reaction products, ΔG_c is the configurational Gibbs free energy, E_s is the solvent reorganization energy, and A is the pre-exponential factor, which is proportional to the transmission coefficient. The transmission coefficient, κ, of the reaction for a nonadiabatic process is proportional to the square of the electronic matrix element. Theoretical analysis shows that the most effective electron transfer takes place at the closest disposition of reaction centers. If κ is smaller than unity, the process may be considered to be nonadiabatic. The transmission coefficient for multielectron transfer also corresponds to a

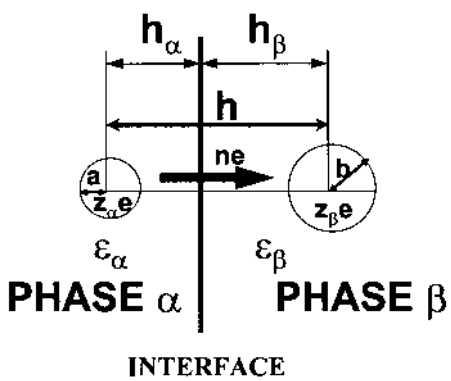

FIG. 2 Geometric factors for an interfacial electron-transfer reaction.

nonadiabatic process and may be substantially lower with respect to κ for a one-electron reaction. At the same time the activation factors for one- and multi-electron processes may differ considerably.

The difference between Gibbs free energies for substrates and products can be found by using the Born equation corrected for the solvophobic effect:

$$\Delta G_c = \Delta G_c(svp) + \frac{e_0^2}{4\pi\varepsilon_0}\left(\frac{n^2 + 2z_\alpha n}{2\varepsilon_\alpha a} + \frac{n^2 - 2z_\beta n}{2\varepsilon_\beta b}\right) \tag{15}$$

where the solvophobic component of Gibbs free energy ΔG_c (svp) does not depend on the dielectric properties of media α and β. The calculated Born electrostatic contribution to the solvation Gibbs free energy is not very precise, and a more accurate calculation can be performed using nonlocal electrostatics. The configurational Gibbs free energy ΔG_c in Eq. (15) is the part of the free energy not depending on the transpositional contribution to entropy. The configurational Gibbs free energy is different from the standard Gibbs free energy ΔG°:

$$\Delta G_c = \Delta G^\circ + RT \ln \frac{\prod\limits_n \mathrm{X}_i^\circ}{\prod\limits_m \mathrm{X}_f^\circ} \tag{16}$$

Here, X_i° and X_f° are the mole fractions of n initial (i) and m final (f) reagents in their standard states. If the reaction is not accompanied by changes in the number of particles, there is no difference between the standard free energy and the configurational free energy. However, if the number of particles changes, for instance, by decomposition of a molecule, the expression for the basic reaction involves only the configurational free energy, which does not include the entropy related to commutation of the particles. ΔG_c is the free energy of the reaction and it differs from the work of the reaction by the work of mixing reagents, depending on the concentration. In the case of interfacial reactions, the quantity that corresponds to ΔG_c will be a configurational interfacial potential:

$$\Delta_\beta^\alpha \phi_c = -\frac{\Delta G_c}{nF} \tag{17}$$

When the interfacial potential equals $\Delta_\beta^\alpha \phi_c$, the free energy of the interfacial reaction:

$$\mathrm{Ox} + e^- \leftrightarrow \mathrm{Red} \tag{18}$$

is zero. At interfacial potentials $\Delta_\beta^\alpha \phi$ different from $\Delta_\beta^\alpha \phi_c$ the free energy of the reaction will be $nF(\Delta_\beta^\alpha \phi - \Delta_\beta^\alpha \phi_c)$. Calculations of the configurational Gibbs energy, configurational redox, and electrode potentials, and the comparison of their values with standard Gibbs energies and standard redox potentials can be found in the literature [94,174,175].

Marcus [166–169] estimated the rate constant k_r for an electron-transfer reaction between two redox components dissolved in two different liquid phases (Fig. 3):

$$-\frac{\mathrm{d}n_1}{\mathrm{d}t} = -k_r c_1 c_2 S \tag{19}$$

where n_1 is the number of molecules of type 1 in the phase α, c_1 is the mean concentration of reactant 1 in phase α, c_2 is the mean concentration of reactant 2 in phase β, and S is the interfacial area. The rate constant k_r can be approximately determined as

$$k_r = \kappa \nu v \exp\left(-\frac{E_\mathrm{a}}{RT}\right) \tag{20}$$

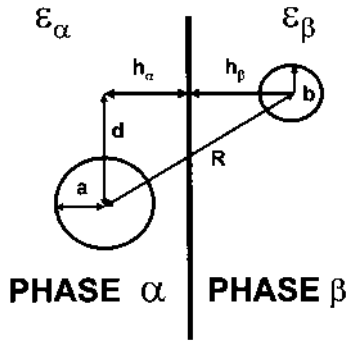

FIG. 3 Locations of charge donors and acceptors at the interface between two immiscible electrolyte solutions.

where v is some relevant frequency for the molecular motion, and E_a is the activation energy. If the liquid/liquid interface is a sharp boundary and if $h_\alpha \geq a$ and $h_\beta \geq b$, Marcus' expression for v is

$$v = 2\pi(a+b)(\Delta R)^3 \tag{21}$$

where ΔR is the center-to-center distance between reagents (Fig. 2). In the system shown in Fig. 1, $\Delta R = h_\alpha + h_\beta$. If the ions penetrate to a second contacting phase, but the reactants do not overlap, another equation, derived by Marcus, is used:

$$v \approx \pi(a_1 + a_2)^3 \Delta R \tag{22}$$

III. SOLVENT REORGANIZATION FREE ENERGY

The solvent reorganization energy is an important parameter in the quantum theory describing charge transfer in polar media. In the case of homogeneous reactions that take place in one phase it can be estimated by the relation:

$$E_s = \frac{1}{2\varepsilon_0}\left(\frac{1}{\varepsilon_{\text{op}}} - \frac{1}{\varepsilon_{\text{s}}}\right) \int\limits_{\infty - V_a - V_b} \left(\vec{D}_i - \vec{D}_f\right)^2 \mathrm{d}V \tag{23}$$

where ε_{op} and ε_{s} are the optical and the static dielectric permittivities of the medium, and $\vec{D}_i$ and $\vec{D}_f$ are the inductions of the electric fields, which are created in the solvent during the initial and final state of charge transfer. Integration in Eq. (23) is carried out over the entire volume of the medium except the reactant volumes.

An approximate calculation of the solvent reorganization energy during homogeneous charge transfer was first performed by Marcus [176]. Assuming that the distance h_{12} between the reactant centers is much larger than their radii a and b, and that the reactants can be described as nonpolarizable spheres with charges rigidly and uniformly distributed over the surfaces, the expression for the reorganization energy is

$$E_s = \frac{e_0^2 n^2}{4\pi\varepsilon_0}\left(\frac{1}{\varepsilon_{\text{op}}} - \frac{1}{\varepsilon_{\text{s}}}\right)\left(\frac{1}{2a} + \frac{1}{2b} - \frac{1}{h_{12}}\right) \tag{24}$$

The reorganization free energy at the liquid/liquid interface was first calculated by Kharkats [162] for the one-dimensional case where the two reactants are located at various positions along the line normal to the interface. The interface is modeled as a mathematically ideal plane separating the two bulk phases. If the charge transfer occurs between reactants in two different dielectric media, Eq. (23) can be written as

$$E_s = \frac{1}{2\varepsilon_0}\left[\int_{\infty-V_a-V_b} \frac{1}{\varepsilon_s}\left(\vec{D}_f - \vec{D}_i\right)^2 dV\right]_{\text{static}} - \frac{1}{2\varepsilon_0}\left[\int_{\infty-V_a-V_b} \frac{1}{\varepsilon_{op}}\left(\vec{D}_f - \vec{D}_i\right)^2 \mathrm{d}V\right]_{\text{optical}} \tag{25}$$

Girault [177] stressed the need for heterogeneous electron-transfer reactions to differentiate static from optical integrals.

For a sharp interface between two immiscible liquids the solvent reorganization energy according to Kharkats' theory [162] can be written as

$$\begin{aligned} E_s = &\frac{(ne_0)^2}{8\pi\varepsilon_0 a}\left(\frac{1}{\varepsilon_{op\alpha}} - \frac{1}{\varepsilon_\alpha}\right) + \frac{(ne_0)^2}{8\pi\varepsilon_0 b}\left(\frac{1}{\varepsilon_{op\beta}} - \frac{1}{\varepsilon_\beta}\right) \\ &+ \frac{(ne_0)^2}{16\pi\varepsilon_0 h_\alpha}\left(\frac{\varepsilon_{op\alpha} - \varepsilon_{op\beta}}{\varepsilon_{op\alpha}\left(\varepsilon_{op\alpha} + \varepsilon_{op\beta}\right)} - \frac{\varepsilon_\alpha - \varepsilon_\beta}{\varepsilon_\alpha\left(\varepsilon_\alpha + \varepsilon_\beta\right)}\right) \\ &- \frac{(ne_0)^2}{16\pi\varepsilon_0 h_\beta}\left(\frac{\varepsilon_{op\alpha} - \varepsilon_{op\beta}}{\varepsilon_{op\beta}\left(\varepsilon_{op\alpha} + \varepsilon_{op\beta}\right)} - \frac{\varepsilon_\alpha - \varepsilon_\beta}{\varepsilon_\beta\left(\varepsilon_\alpha + \varepsilon_\beta\right)}\right) \\ &- \frac{(ne_0)^2}{2\pi\varepsilon_0 (h_\alpha + h_\beta)}\left(\frac{1}{\varepsilon_{op\alpha} + \varepsilon_{op\beta}} - \frac{1}{\varepsilon_\alpha + \varepsilon_\beta}\right) \end{aligned} \tag{26}$$

where ne_0 is the charge transferred in the reaction, subscripts α and β denote the dielectric permittivities in media α and β, and the reactants are spheres of radii a and b, which are located at distances h_1 and h_2 from the interface with charges z_1e_0 and z_2e_0, respectively (Fig. 1).

Figure 3 shows a more complicated boundary when the direction of electron transfer between reactants is not perpendicular to the interface. Marcus derived an expression for the reorganization energy in which the reactants can have any orientation with respect to the interface, but each reactant is restricted to one medium and cannot cross the interface. The expression for solvent reorganization energy in this case is

$$\begin{aligned} E_s = &\frac{(ne_0)^2}{8\pi\varepsilon_0 a}\left(\frac{1}{\varepsilon_{op\alpha}} - \frac{1}{\varepsilon_\alpha}\right) + \frac{(ne_0)^2}{8\pi\varepsilon_0 b}\left(\frac{1}{\varepsilon_{op\beta}} - \frac{1}{\varepsilon_\beta}\right) \\ &+ \frac{(ne_0)^2}{16\pi\varepsilon_0 h_\alpha}\left(\frac{\varepsilon_{op\alpha} - \varepsilon_{op\beta}}{\varepsilon_{op\alpha}\left(\varepsilon_{op\alpha} + \varepsilon_{op\beta}\right)} - \frac{\varepsilon_\alpha - \varepsilon_\beta}{\varepsilon_\alpha\left(\varepsilon_\alpha + \varepsilon_\beta\right)}\right) \\ &- \frac{(ne_0)^2}{16\pi\varepsilon_0 h_\beta}\left(\frac{\varepsilon_{op\alpha} - \varepsilon_{op\beta}}{\varepsilon_{op\beta}\left(\varepsilon_{op\alpha} + \varepsilon_{op\beta}\right)} - \frac{\varepsilon_\alpha - \varepsilon_\beta}{\varepsilon_\beta\left(\varepsilon_\alpha + \varepsilon_\beta\right)}\right) \\ &- \frac{(ne_0)^2}{2\pi\varepsilon_0 (l)}\left(\frac{1}{\varepsilon_{op\alpha} + \varepsilon_{op\beta}} - \frac{1}{\varepsilon_\alpha + \varepsilon_\beta}\right) \end{aligned} \tag{27}$$

Similarly, U_i and U_f can be expressed according to Kharkats [6,7,162] in terms of integrals of inductions $\vec{D}_i$ and $\vec{D}_f$:

$$U_i = \frac{1}{32\pi^2\varepsilon_0\varepsilon_1}\int_{\mathrm{I}} D_i^2 \mathrm{d}V + \frac{1}{32\pi^2\varepsilon_0\varepsilon_2}\int_{\mathrm{II}} D_i^2 \mathrm{d}V - \frac{z_1^2 e_0^2}{8\pi\varepsilon_0 a\varepsilon_1} - \frac{z_2^2 e_0^2}{8\pi\varepsilon_0 b\varepsilon_2} \tag{28}$$

$$U_f = \frac{1}{32\pi^2\varepsilon_0\varepsilon_1}\int_{\mathrm{I}} D_f^2 dV + \frac{1}{8\pi\varepsilon_2}\int_{\mathrm{II}} D_f^2 \mathrm{d}V - \frac{(z_1+n)^2 e_0^2}{8\pi\varepsilon_0 a\varepsilon_1} - \frac{(z_2-n)^2 e_0^2}{8\pi\varepsilon_0 b\varepsilon_2} \tag{29}$$

where the integration ranges I and II represent the two half-spaces of media α and β excluding the volume of reactants.

Calculation of the integrals in Eqs. (28) and (29) is conveniently carried out by changing to surface integrals. For instance, Kharkats calculated for $\int_{\mathrm{I}} D_i^2 \mathrm{d}V$ with an accuracy of $(a/h)^3$, $(b/h)^3$:

$$\int_{\mathrm{I}} D_i^2 \mathrm{d}V = \frac{4\pi e_0^2 z_1^2}{a} - \frac{2\pi e_0^2 z_1^2}{h_1} + \pi e_0^2\left(\frac{2\varepsilon_1}{\varepsilon_1+\varepsilon_2}\right)^2\left(\frac{z_1^2}{h_1}+\frac{z_2^2}{h_2}+\frac{4z_1^2 z_2^2}{h_1+h_2}\right) \tag{30}$$

The expression for $\int_{II} D_i^2 \mathrm{d}V$ is obtained from Eq. (28) by making the substitutions $a \to b$, $\varepsilon_1 \to \varepsilon_2$, $h_1 \to h_2$, and $z_1 \to z_2$. The corresponding expression for $\int_{\mathrm{I,2}} D_f^2 \mathrm{d}V$ can be obtained by making substitutions $z_1 \to (z_1+n)$ and $z_2 \to (z_2-n)$.

The simplest expressions for E_s, U_i, and U_f are obtained [6] when the reactions take place at equal distances from the interface, $h_1 = h_2 = h$:

$$E_s = \frac{(ne_0)^2}{8\pi\varepsilon_0 a}\left(\frac{1}{\varepsilon_{\mathrm{op}\alpha}}-\frac{1}{\varepsilon_\alpha}\right) + \frac{(ne_0)^2}{8\pi\varepsilon_0 b}\left(\frac{1}{\varepsilon_{\mathrm{op}\beta}}-\frac{1}{\varepsilon_\beta}\right) - \frac{(ne_0)^2}{4\pi\varepsilon_0 h}\left(\frac{1}{\varepsilon_{\mathrm{op}\alpha}+\varepsilon_{\mathrm{op}\beta}}-\frac{1}{\varepsilon_\alpha+\varepsilon_\beta}\right) \tag{31}$$

$$U_i = \frac{z_\alpha z_\beta e_0^2}{4\pi\varepsilon_0(\varepsilon_\alpha+\varepsilon_\beta)h} + \frac{z_\alpha^2 e_0^2(\varepsilon_\alpha-\varepsilon_\beta)}{16\pi\varepsilon_0\varepsilon_\alpha(\varepsilon_\alpha+\varepsilon_\beta)h} - \frac{z_\beta^2 e_0^2(\varepsilon_\alpha-\varepsilon_\beta)}{16\pi\varepsilon_0\varepsilon_\beta(\varepsilon_\alpha+\varepsilon_\beta)h} \tag{32}$$

$$U_f = \frac{(z_\alpha+n)(z_\beta-n)e_0^2}{4\pi\varepsilon_0(\varepsilon_\alpha+\varepsilon_\beta)h} + \frac{(z_\alpha+n)^2 e_0^2(\varepsilon_\alpha-\varepsilon_\beta)}{16\pi\varepsilon_0\varepsilon_\alpha(\varepsilon_\alpha+\varepsilon_\beta)h} - \frac{(z_\beta-n)e_0^2(\varepsilon_\alpha-\varepsilon_\beta)}{16\pi\varepsilon_0\varepsilon_\beta(\varepsilon_\alpha+\varepsilon_\beta)h} \tag{33}$$

$$E_a = U_i + \frac{\left(E_s+\Delta G_c+U_f-U_i\right)^2}{4E_s} \tag{34}$$

In the case of homogeneous electron transfer in a dielectric medium, the work required to bring the reactants or reaction products together approaches zero when one of the reactants or products is electrically neutral, whereas in the process discussed here, U_i values are never zero because of the interactions with image charges.

IV. SELECTIVE CATALYTIC PROPERTIES OF LIQUID INTERFACES

The activation energy of electron transfer depends on the charges of the reactants and dielectric permittivity of the nonaqueous phase. This dependence can be useful when choosing a pair of immiscible solvents to decrease the activation energy of the reaction in question or to inhibit an undesired process. For example, suppose that an electron is

transferred from a donor in the aqueous phase α to an acceptor in organic phase β (Fig. 2). Assuming that ΔG_c is negligible compared to E_s, the activation energy E_a depends on the dielectric permittivity of nonaqueous phase ε_2:

$$E_a \cong U_i + \frac{(E_s + U_f - U_i)^2}{4E_s} \tag{35}$$

The reorganization energy increases with ε_α to a maximum asymptotic value at $\varepsilon_\beta >> \varepsilon_{op\beta}$:

$$E_s = \frac{(ne_0)^2}{8\pi\varepsilon_0 a}\left(\frac{1}{\varepsilon_{op\alpha}} - \frac{1}{\varepsilon_\alpha}\right) + \frac{(ne_0)^2}{8\pi\varepsilon_0 b}\left(\frac{1}{\varepsilon_{op\beta}}\right) - \frac{(ne_0)^2}{4\pi\varepsilon_0 h}\left(\frac{1}{\varepsilon_{op\alpha} + \varepsilon_{op\beta}} - \frac{1}{\varepsilon_\alpha + \varepsilon_\beta}\right) \tag{36}$$

and at $\varepsilon_\beta = \varepsilon_{op\,\beta}$ reorganization energy is minimal and equal to

$$E_s = \frac{(ne_0)^2}{8\pi\varepsilon_0 a}\left(\frac{1}{\varepsilon_{op\alpha}} - \frac{1}{\varepsilon_\alpha}\right) - \frac{(ne_0)^2}{4\pi\varepsilon_0 h}\left(\frac{1}{\varepsilon_{op\alpha} + \varepsilon_{op\beta}} - \frac{1}{\varepsilon_\alpha + \varepsilon_\beta}\right) \tag{37}$$

Examples of the dependencies of E_s, E_a, and U_i for different sets of parameters z_1, z_2, and h/a are plotted in Figs 4–6.

Figure 4 shows how the dielectric constant of the organic phase ε_2 and the distance from the interface or between reagents affect the medium reorganization energy. A decrease in h or ε dramatically decreases E_s (Fig. 4), which reaches a minimum value as ε approaches 2.

Equation (35) is plotted in Figs 5 and 6, which show that the activation energy of the process decreases (or increases) greatly at low ε_β. Accordingly, the rate constant of charge transfer across the interface increases (or decreases) sharply at relatively low ε_β. Figure 6 shows that the liquid–liquid interface has selective properties and can catalyze or inhibit interfacial charge-transfer reactions due to electrostatic effects.

To summarize, the kinetic parameters of interfacial charge transfer depend on the charge being transferred, the charges of reactants, their location in relation to the interface, and the dielectric properties of the media forming the liquid–liquid interface. Charge-transfer processes in simple models are described by equations that can in turn be extended to more complicated processes, including phase transfer, micellar catalysis, and bioenergetic processes taking place in biomembranes.

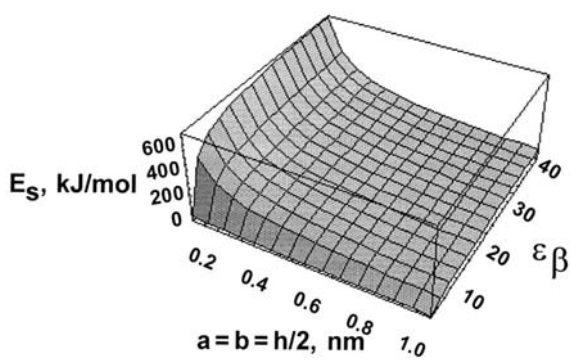

FIG. 4 Dependence of solvent reorganization free energy on dielectric permittivity of nonaqueous phase ε_2 and radii of reagents $a = b = h/2 = h_\alpha = h_\beta$ from the interface at parameters: $\varepsilon_{op\alpha} = \varepsilon_{op\beta} = 1.8$, $\varepsilon_\alpha = 78$, $n = 1$.

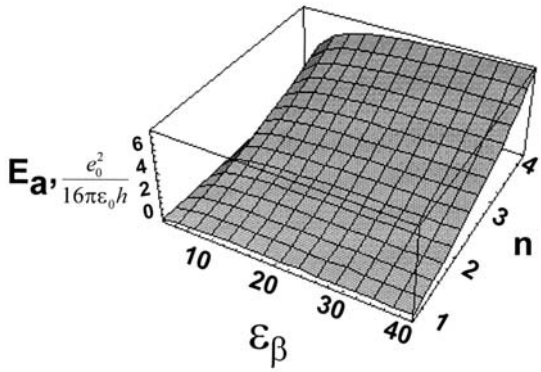

FIG. 5 Dependence of activation energy, E_a, on dielectric permittivity of nonaqueous phase ε_β and number of transferred electrons with parameters: $\varepsilon_{op\alpha} = \varepsilon_{op\beta} = 1.8$, $\varepsilon_\alpha = 78$, $a = b = h/2$, $z_\alpha = 0$, $z_\beta = 0$, $\Delta G_c = -0.05e^2/16\pi\varepsilon_0 h$.

Kuznetsov and Kharkats [165] have investigated electron-transfer rates near an interface between two immiscible liquids as functions of the positions of the electron donor and acceptor relative to this interface as it is shown in Fig. 7. They found that under certain conditions the electron-transfer rates should rise to values several times higher than those found in the interior of each of the phases. Three basic cases for the reactant positions relative to the interface were considered:

I. The two reactants are located in the solvent with dielectric permittivity ε_1.
II. One of the reactants A is located in the solvent with dielectric permittivity ε_1, the another reactant B in that with dielectric permittivity ε_2.
III. The two reactants are located in the solvent with dielectric permittivity ε_2.

The electron-transfer reaction rate for all these three cases can be presented as follows:

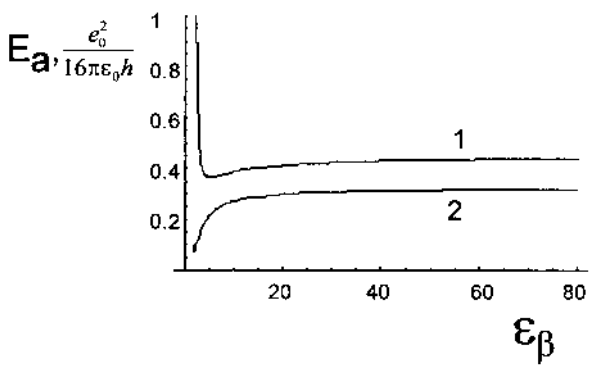

FIG. 6 Dependence of the activation energy, E_a, on dielectric permittivity of a nonaqueous phase ε_β with parameters: $a = b = h/2$, $n = 1$ and (1) $z_\alpha = 0, z_\beta = -1$, $\Delta G_c = -0.35e^2/16\pi\varepsilon_0 h$; (2) $z_\alpha = 0, z_\beta = 0, \Delta G_c = -0.05e^2/16\pi\varepsilon_0 h$.

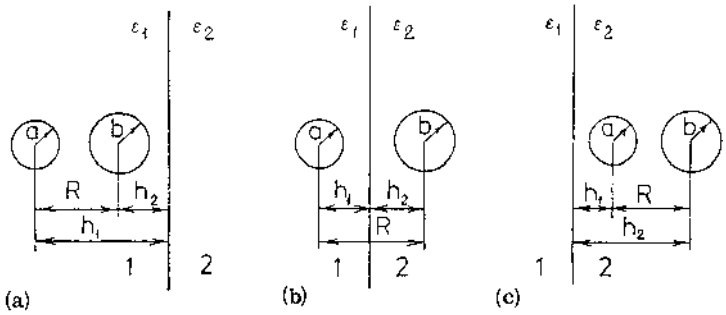

FIG. 7 Schematic drawing of the reactant positions relative to an interface between two immiscible liquids with dielectric permittivities ε_1 and ε_2: (a) case I, both reactants with radii a and b, located in phase 1; (b) case II, one reactant located in phase 1, the other located in phase 2; (c) case III, both reactants located in phase 2. (From Ref. 163.)

$$k_{\mathrm{I}} = k_0 c_{\mathrm{A}}^{\mathrm{I}} c_{\mathrm{B}}^{\mathrm{I}} \exp\left\{ -\frac{U_i^{\mathrm{I}}}{RT} - \frac{\left(E_s^{\mathrm{I}} + \Delta G^o + U_f^{\mathrm{I}} - U_i^{\mathrm{I}}\right)^2}{4E_s^{\mathrm{I}} RT} \right\} \tag{38}$$

$$k_{\mathrm{II}} = k_0 c_{\mathrm{A}}^{\mathrm{I}} c_{\mathrm{B}}^{\mathrm{I}} \exp\left\{ -\frac{J^{\mathrm{II}} - J^{\mathrm{I}}}{RT} - \frac{U_i^{\mathrm{II}}}{RT} - \frac{\left(E_s^{\mathrm{II}} + \Delta G^o + U_f^{\mathrm{II}} - U_i^{\mathrm{II}}\right)^2}{4E_s^{\mathrm{I}} RT} \right\} \tag{39}$$

$$k_{\mathrm{II}} = k_0 c_{\mathrm{A}}^{\mathrm{I}} c_{\mathrm{B}}^{\mathrm{I}} \exp\left\{ -\frac{J^{\mathrm{II}} - J^{\mathrm{I}}}{RT} - \frac{U_i^{\mathrm{II}}}{RT} - \frac{\left(E_s^{\mathrm{II}} + \Delta G^o + U_f^{\mathrm{II}} - U_i^{\mathrm{II}}\right)^2}{4E_s^{\mathrm{I}} RT} \right\} \tag{40}$$

Here,

$$J^{\mathrm{I}} = \frac{z_A^2 e^2}{8\pi\varepsilon_o\varepsilon_1 a} + \frac{z_{\mathrm{B}}^2 e^2}{8\pi\varepsilon_o\varepsilon_1 b} \tag{41}$$

$$J^{\mathrm{II}} = \frac{z_A^2 e^2}{8\pi\varepsilon_o\varepsilon_1 a} + \frac{z_B^2 e^2}{8\pi\varepsilon_o\varepsilon_2 b} \tag{42}$$

$$J^{\mathrm{III}} = \frac{z_A^2 e^2}{8\pi\varepsilon_o\varepsilon_2 a} + \frac{z_B^2 e^2}{8\pi\varepsilon_o\varepsilon_2 b} \tag{43}$$

Figures 8–10 show the dependencies of energy of reorganization, activation energy, and rate constants of the electron-transfer reaction for three basic systems.

Benjamin and Kharkats [173] considered a model with all possible locations of the ions including the cases where one or both ions are located across the interface (Fig. 11). They have found that for a fixed distance of the center of the ion pair from the interface and at a fixed distance between ions the reorganization free energy is only mildly affected by the orientation of the ion pair (Fig. 12). For a fixed distance from the interface the reorganization free energy is maximum for the perpendicular orientation if the ion pair is on the high dielectric side, and it is maximum for the parallel orientation of the ion pair in the low dielectric constant medium (Figs 13 and 14). Theoretical estimations by Kharkats and coworkers [6,7,162,165,173] are extremely important for understanding reaction mechanisms in phase transfer catalysis (PTC).

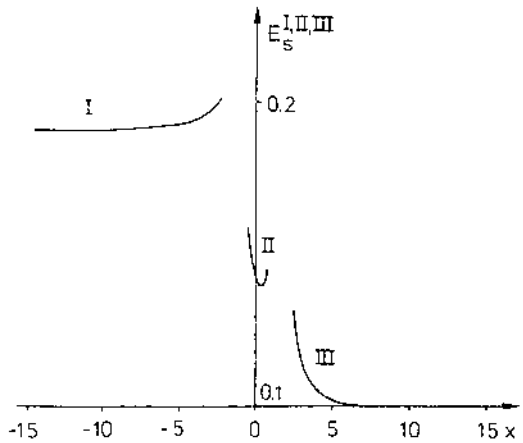

FIG. 8 Dimensionless medium reorganization energies $E_s^{I,II,III}/(e^2/0.4\pi\varepsilon_0 nm)$ as function of distance x for three cases (see Fig. 7) of reactant locations relative to the interface: $a = b = 0.2$ nm, $R = 0.6$ nm, $z_1 = -1$, $z_2 = 0, n = 1$, $\Delta G = 0$, $\varepsilon_{01} = 1.76$, $\varepsilon_1 = 78$, $\varepsilon_{02} = 2.5$, and $\varepsilon_2 = 10$. (From Ref. 163.)

PTC has been widely used by chemists for preparative purposes. The essence of the method is to create a two-phase system (usually with an organic and an aqueous phase), in which nonpolar and ionic reactants are present in the different phases, and to use the catalysts as a source of lipophilic cations. The role of the catalysts is to form lipophilic ion pairs between the cation of the catalyst and the reacting anion, which then are capable of migrating within the organic phase. PTC is one of the simplest and most economical methods of intensifying the production of a wide range of organic materials. The main advantage of the PTC method is that it is general, mild, and catalytic. PTC is limited by

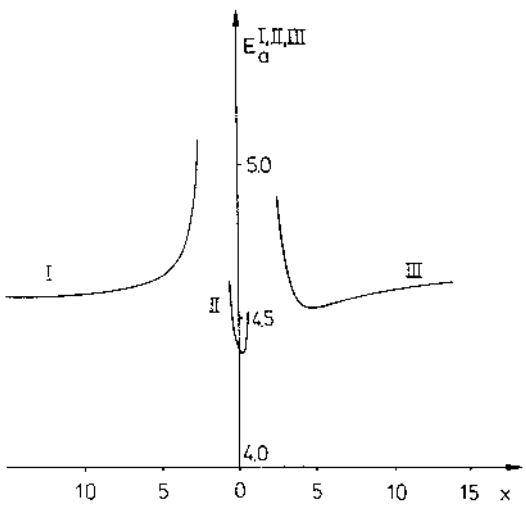

FIG. 9 Dimensionless activation factors $E_a^{I,II,III}/(e^2/0.4\pi\varepsilon_0 nm)$ as functions of reactant locations relative to the interface. The values of parameters are the same as in Fig. 8. (From Ref. 163.)

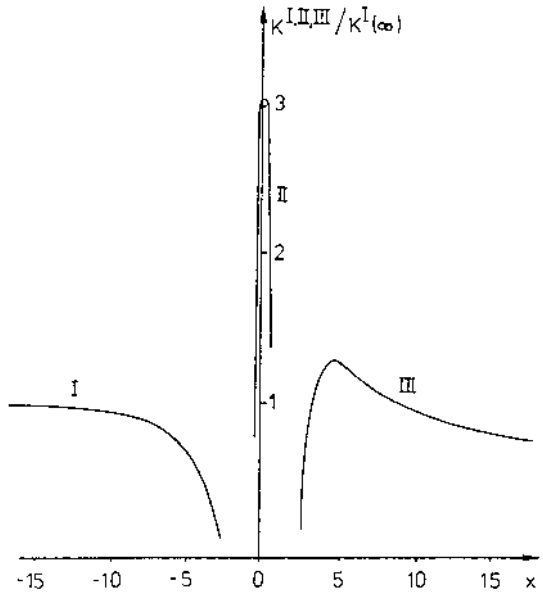

FIG. 10 Dependence of the relative charge-transfer rates $k^{\mathrm{I,II,III}}/k^{\mathrm{I}}(8)$ on the position of reactants relative to the interface, $T = 300$ K; the other parameters are the same as in Figs. 8 and 9. (From Ref. 163.)

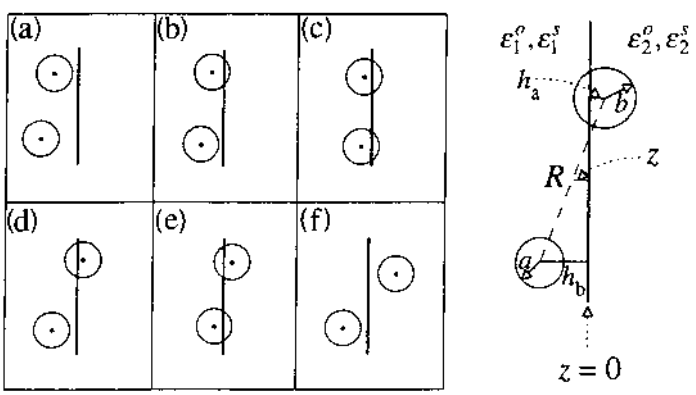

FIG. 11 Schematic representation of the geometry of a system with two ions at the liquid/liquid interface. The top panel defines the different parameters in the system. The bottom panel shows the different situations that need to be considered. In (a), (b), and (c) the centers of two ions are in the same liquid, and in (d), (e), and (f) they are in different liquids. Other cases can be obtained from these six cases by simple reflection through the interface plane. (From Ref. 173.)

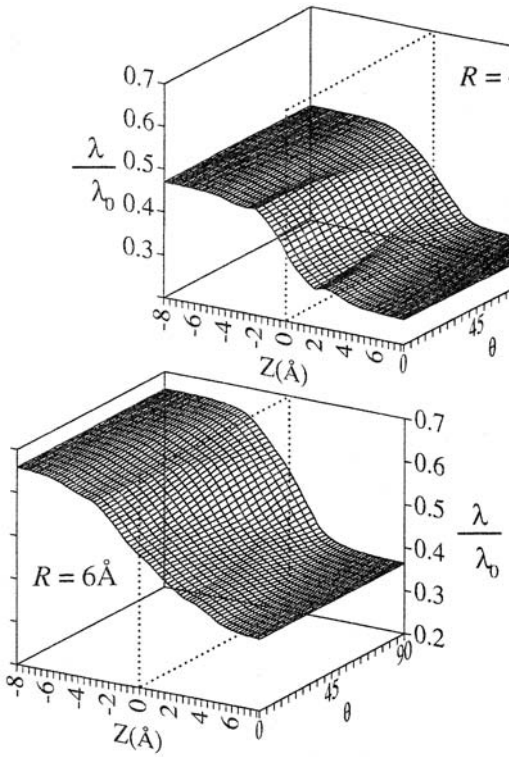

FIG. 12 Reorganization free energy as a function of the distance of the center of the ion pairs from the interface (z) and the angle (Θ) between the line joining the two ions and the interface normal. The two panels are for two different values of the interionic distance R. (From Ref. 173.)

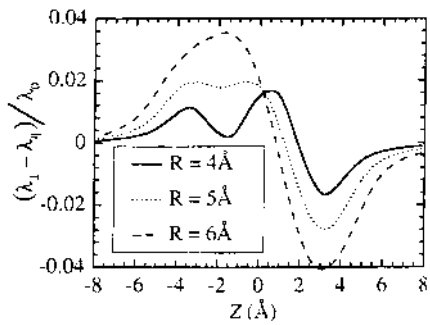

FIG. 13 Difference between the reorganization free energy for the parallel and perpendicular orientations of the ion pair as a function of the distance from the interface for three different values of the interionic distance R. (From Ref. 173.)

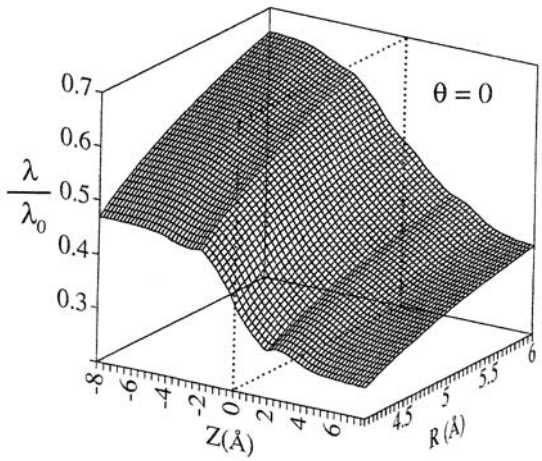

FIG. 14 Reorganization free energy as a function of the distance of the center of the ion pairs from the interface (z) and the interionic distance R for the perpendicular orientation of the ions ($\Theta = 0$). (From Ref. 173.)

separation of the catalyst from the reaction medium, the tendency to form stable emulsions, and the impossibility of performing repeated or continuous processes. These disadvantages can be eliminated by three-phase catalysis in which a catalyst is immobilized on a polymeric support. The insoluble catalysts are easily separated from the reaction medium by simple filtration and can be used repeatedly.

PTC requires a phase transfer agent in catalytic amounts, which transfers substrates from one phase to a second phase where they can react with other reagents. A typical scheme of phase transfer catalysis is shown in Fig. 15. Details of PTC catalysis can be found in numerous books [178,179].

If a catalytic reaction of electron or ion transfer takes place at the oil/water interface between reagents located in two different contacting phases, we have deal with an example of *interfacial catalysis* discovered by Volkov and Kharkats [4–7]. The interface itself can serve as a catalyst for heterogeneous charge-transfer reactions. If the interfacial catalysis requires an electrical field, the reaction can take place at the interface between two immiscible electrolyte solutions having a fixed interfacial potential, a process called interfacial electrocatalysis.

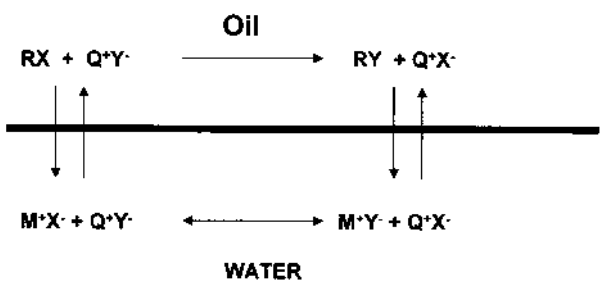

FIG. 15 Schematic representation of phase transfer catalysis.

REFERENCES

1. AG Volkov. J. Electroanal Chem 173: 5–24, 1984.
2. AG Volkov. Sov Electrochem 21:91–98, 1985.
3. AG Volkov. J Electroanal Chem 205:245–257, 1986.
4. AG Volkov, YuI Kharkats. Kinet Katal 26:1322–1326, 1985.
5. AG Volkov, YuI Kharkats. Chem Phys 5:964–971, 1986.
6. YuI Kharkats, AG Volkov. J Electroanal Chem 184:435–439, 1985.
7. YuI Kharkats, AG Volkov. Biochim Biophys Acta 891:56–67, 1987.
8. YuI Kharkats, AG Volkov, LI Boguslavsky. Dokl Akad Nauk SSSR 220:1441–1444, 1975.
9. YuI Kharkats, AG Volkov, LI Boguslavsky. Biophysics 21:634–638, 1976.
10. YuI Kharkats, AG Volkov, LI Boguslavsky. J Theor Biol 65:379–391, 1977.
11. AG Volkov, D Deamer, D Tanelian, VS Markin. Liquid Interfaces in Chemistry and Biology. New York: John Wiley, 1998.
12. AG Volkov, DW Deamer, eds. Liquid–Liquid Interfaces: Theory and Methods. Boca Raton, FL: CRC Press, 1996.
13. AG Volkov, DW Deamer. Progr Colloid Polym Sci 103:21–27, 1997.
14. OS Ksenzhek, AG Volkov. Plant Energetics. New York: Academic Press, 1998.
15. AG Volkov, ed. Liquid Interfaces in Chemical, Biological, and Pharmaceutical Applications, New York: Marcel Dekker, 2001.
16. AG Volkov. Electrochim Acta 44:139–153, 1998.
17. AG Volkov. Uspekhi Sovr Biol (Progr Modern Biol) 105:467–487, 1988.
18. LI Boguslavsky, AA Kondrashin, IA Kozlov, ST Metelsky, VP Skulachev, AG Volkov. FEBS Lett 50:223–226, 1975.
19. LI Boguslavsky, AG Volkov. Dokl Akad Nauk SSSR 224:1201–1204, 1975.
20. LI Boguslavsky, AG Volkov. In: VE Kazarinov, ed. The Interface Structure and Electrochemical Processes at the Boundary Between Two Immiscible Liquids. Berlin: Springer Verlag, 1987, pp 143–178.
21. LI Boguslavsky, AG Volkov, VG Boytsov, IA Kozlov, ST Metelsky. Bioorg Khim 2:1125–1131, 1976.
22. LI Boguslavsky, AG Volkov, MD Kandelaki. Biophysics 21:808–811, 1976.
23. LI Boguslavsky, AG Volkov, MD Kandelaki. FEBS Lett 65:155–158, 1976.
24. LI Boguslavsky, AG Volkov, MD Kandelaki. Bioelectrochem Bioenerg 4:68–72, 1977.
25. LI Boguslavsky, AG Volkov, MD Kandelaki, EA Nizhnikovsky. Dokl Akad Nauk SSSR 227:727–730, 1976.
26. LI Boguslavsky, AG Volkov, MD Kandelaki, EA Nizhnikovsky, MA Bibikova. Biofizika 22:223–227, 1977.
27. LI Boguslavsky, AG Volkov, AA Kondrashin, ST Metelsky, AA Yasaitis. Biokhimiya 41:1047–1051, 1976.
28. LI Boguslavsky, AG Volkov, AA Kondrashin, VP Skulachev, AA Yasaitis. Bioorg Khim 1:1783–1791, 1975.
29. LI Boguslavsky, AG Volkov, IA Kozlov, AV Kargopolov, EI Mileykovskaya. Bioorg Khim 2:846–854, 1976.
30. LI Boguslavsky, AG Volkov, IA Kozlov, AN Mal'yan. Biophysics 21:286–289, 1976.
31. LI Boguslavsky, AG Volkov, IA Kozlov, ST Metelsky, VP Skulachev. Dokl Akad Nauk SSSR 218:963–966, 1974.
32. LI Boguslavsky, AG Volkov, IA Kozlov, ST Metelsky, VP Skulachev. Bioorg Khim 1:1369–1378, 1975.
33. LI Boguslavsky, AG Volkov, IA Kozlov, EI Mileykovskaya. Dokl Akad Nauk SSSR 222:726–729, 1975.
34. DW Deamer, AG Volkov. In: AG Volkov, DW Deamer, eds. Liquid–Liquid Interfaces. Theory and Methods. Boca Raton, FL: CRC Press, 1996, pp. 375–400.
35. MC Goodall, G Sachs. Biophys J 17:182a-182a, 1977.

36. MI Gugeshashvili, VI Portnov, AG Volkov, LN Chekulaeva, VS Markin. Bioelectrochem Bioenerg 26:139–158, 1991.
37. MI Gugeshashvili, AG Volkov, A Tessier, PF Blanchet, D Cote, G Munger, RM Leblanc. Biol Membr 9:862–873, 1992.
38. MI Gugeshashvili, AG Volkov, B Zelent, J Galant, G Munger, RM Leblanc. Membr Cell Biol 9:1–12, 1995.
39. MI Gugeshashvili, AG Volkov, LS Yaguzhinsky, AF Mironov, LI Boguslavsky. Sov Electrochem 19:1629–1632, 1983.
40. MI Gugeshashvili, AG Volkov, LS Yaguzhinsky, AF Mironov, LI Boguslavsky. Bioelectrochem Bioenerg 10:493–498, 1983.
41. P Hajkova, D Homolka, V Marecek, AG Volkov, Z Samec. Sov Electrochem 21:209–215, 1985.
42. MD Kandelaki, AG Volkov. Can J Chem 69:151–156, 1991.
43. MD Kandelaki, AG Volkov. Russ J Electrochem 29:1158–1164, 1993.
44. MD Kandelaki, AG Volkov, AL Levin, LI Boguslavsky. Dokl Akad Nauk SSSR 271:462–465, 1983.
45. MD Kandelaki, AG Volkov, AL Levin, LI Boguslavsky. Bioelectrochem Bioenerg 11:167–172, 1983.
46. MD Kandelaki, AG Volkov, VV Shubin, LI Boguslavsky. Biochim Biophys Acta 893:170–176, 1987.
47. MD Kandelaki, AG Volkov, VV Shubin, AL Levin, LI Boguslavsky. Sov Electrochem 24:288–294, 1988.
48. VS Markin, MI Gugeshashvili, AG Volkov, G Munger, RM Leblanc. J Colloid Interface Sci 154:264–275, 1992.
49. VS Markin, MI Gugeshashvili, AG Volkov, G Munger, RM Leblanc. J Electrochem Soc 139:455–455, 1992.
50. VS Markin, MI Gugeshashvili, AG Volkov, G Munger, RM Leblanc. Extended abstracts. Proceddings of Fall Meeting, Toronto: The Electrochemical Society, vol. 92–2, 1992, pp 978–978.
51. FM Menger. Chem Soc Rev 1:229–253, 1972.
52. NM Mirsalikhova, LI Boguslavsky, AG Volkov, BA Tashmuchamedov, FA Umarova. Dokl Akad Nauk SSSR 229:1473–1476, 1976.
53. A Post, SE Young, RN Robertson. Photobiochem Photobiophys 8:153–162, 1984.
54. AG Volkov, MA Bibikova, AF Mironov, LI Boguslavsky. Sov Elektrochem 19:1398–1401, 1983.
55. AG Volkov, MA Bibikova, AF Mironov, LI Boguslavsky. Bioelectrochem Bioenerg 10:477–483, 1983.
56. AG Volkov, MI Gugeshashvili, MD Kandelaki, VS Markin, B Zelent, G Munger, RM Leblanc. Proc Soc Photo-Opt Instrum Eng 1436:68–79, 1991.
57. AG Volkov, MI Gugeshashvili, AF Mironov, LI Boguslavsky. Bioelectrochem Bioenerg 9:551–558, 1982.
58. AG Volkov, MI Gugeshashvili, AF Mironov, AN Nizhnik, LI Boguslavsky. Sov Electrochem 18:1628–1634, 1982.
59. AG Volkov, MI Gugeshashvili, AF Mironov, LI Boguslavsky. Sov Electrochem 19:1194–1198, 1983.
60. AG Volkov, MI Gugeshashvili, AF Mironov, LI Boguslavsky. Bioelectrochem Bioenerg 10:485–491, 1983.
61. AG Volkov, MI Gugeshashvili, VI Portnov, VS Markin, LN Chekulaeva. In: MJ Allen, SF Cleary, AE Sowers, DD Shillady, eds. Charge and Field Effects in Biosystems—3. Boston, MA: Birkhauser, 1992, pp 365–372.
62. AG Volkov, MI Gugeshashvili, G Munger, RM Leblanc, B Zelent, J Galant, HA Tajmir-Riahi, J Aghion. Biol Membr 9:874–880, 1992.
63. AG Volkov, MI Gugeshashvili, G Munger, RM Leblanc. Biol Membr 9:576–580, 1992.

64. AG Volkov, MI Gugeshashvili, G Munger, RM Leblanc. Bioelectrochem Bioenerg 29:305–314, 1993.
65. AG Volkov, MI Gugeshashvili, DW Deamer. Electrochim Acta 40:2849–2868, 1995.
66. AG Volkov, MI Gugeshashvili, B Zelent, D Cote, G Munger, A Tessier, PF Blanchet, RM Leblanc. Bioelectrochem Bioenerg 38:333–342, 1995.
67. AG Volkov, VD Kolev, AL Levin, LI Boguslavsky. Photobiochem Photobiophys 10:105–111, 1985.
68. AG Volkov, VD Kolev, AL Levin, LI Boguslavsky. Sov Electrochem 22:1303–1307, 1986.
69. AG Volkov, BT Lozhkin, LI Boguslavsky. Dokl Akad Nauk SSSR 220:1207–1210, 1975.
70. AG Volkov, VS Markin, RM Leblanc, MI Gugeshashvili, B Zelent, G Munger. J Solut Chem 23:223–248, 1994.
71. AG Volkov, AF Mironov, LI Boguslavsky. Sov Electrochem 12:1326–1329, 1976.
72. I Wilner, WE Ford, JW Otvos, M Calvin. Nature 280:823–824, 1979.
73. LS Yaguzhinsky, AG Volkov, LI Boguslavsky. Biochemistry 41:1203–1207, 1976.
74. LS Yaguzhinsky, AG Volkov, LI Boguslavsky. Bioelectrochem Bioenerg 4:225–230, 1977.
75. LS Yaguzhinsky, LI Boguslavsky, AG Volkov, AB Rakhmaninova. Dokl Akad Nauk SSSR 221:1465–1468, 1975.
76. LS Yaguzhinsky, LI Boguslavsky, AG Volkov, AB Rakhmaninova. Nature 259:494–496, 1975.
77. B Zelent, J Gallant, AG Volkov, MI Gugeshashvili, G Munger, HA Tajmir-Riahi, RM Leblanc. J Mol Struct 297:1–11, 1993.
78. MK Aliev, LI Boguslavsky, AG Volkov, IA Kozlov, DO Levicky, ST Metelsky. Bioorg Khim 2:1132–1137, 1976.
79. JF Danielli. Nature 156:468–470, 1945.
80. JF Danielli, JT Davies. Adv Enzymol Relat Subj Biochem 11:35–89, 1951.
81. GJ Hanna, RD Noble. Chem Rev 85:583–598, 1985.
82. SB Hwang, JI Korenbrot, W Stoeckenius. J Membr Biol 36:137–158, 1977.
83. IA Kozlov, VP Skulachev. Biochim Biophys Acta 463:29–89, 1977.
84. VS Markin, AG Volkov. In: AG Volkov, DW Deamer, eds. Liquid–Liquid Interfaces. Theory and Methods. Boca Raton, FL: CRC Press, 1996, pp 63–75.
85. G Munger, RM Leblanc, B Zelent, J Gallant, HA Tajmirriahi, J Aghion, MI Gugeshashvili, AG Volkov. Biol Membr 9:874–880, 1992.
86. G Munger, RM Leblanc, B Zelent, AG Volkov, MI Gugeshashvili, J Gallant, HA Tajmirriahi, J Aghion. Thin Solid Films 210:739–742, 1992.
87. HT Tien, SP Verma. Nature 227:1232–1234, 1970.
88. HT Tien. Progr Surf Sci 30:1–199, 1989.
89. HT Tien. Bioelectrochem Bioenerg 15:19–38, 1986.
90. HT Tien, A Ottova-Leitmannova. Membrane Biophysics as Viewed from Experimental Bilayer Lipid Membranes (Planar Lipid Bilayers and Spherical Liposomes). Amsterdam: Elsevier, 2000.
91. HT Tien. Bilayer Lipid Membranes (BLM). Theory and Practice. New York: Marcel Dekker, 1974.
92. AG Volkov. Mol Biol 20:728–736, 1986.
93. AG Volkov. Photobiochem Photobiophys 11:1–7, 1986.
94. AG Volkov. Biol Membr 4:984–993, 1987.
95. AG Volkov. Biophysics 30:491–491, 1985.
96. AG Volkov. Bioelectrochem Bioenerg 21:3–24, 1989.
97. AG Volkov, YuI Kharkats. Biol Membr 5:920–931, 1988.
98. YuI Kharkats, AG Volkov. Anal Sci 14:29–32, 1998.
99. AG Volkov. Anal Sci 14:21–27, 1998.
100. AR Brown, LJ Yellowlees, HH Girault. J Chem Soc, Faraday Trans 89:207–212, 1993.
101. M Brust, M Walker, D Bethell, DJ Schiffrin, R Whyman. J Chem Soc, Chem Commun 801–802, 1994.

102. QZ Chen, K. Iwamoto, M Seno. Electrochim Acta 36:291–296, 1991.
103. Y Cheng, DJ Schiffrin. J Electroanal Chem 314:153–163, 1991.
104. Y Cheng, DJ Schiffrin. J Chem Soc, Faraday Trans 89:199–205, 1993.
105. Y Cheng, DJ Schiffrin. J Chem Soc, Faraday Trans 90:2517–2523, 1994.
106. V Cunnane, L Murtomaki. In: AG Volkov, DW Deamer, eds. Liquid–Liquid Interfaces. Theory and Methods. Boca Raton, FL: CRC Press, 1996, pp 401–416.
107. VJ Cunnane, DJ Schiffrin, C Beltran, G Geblewicz, T Solomon. J Electroanal Chem 247:203–214, 1988.
108. MK De Armond, AH De Armond. In: AG Volkov, DW Deamer, eds. Liquid–Liquid Interfaces. Theory and Methods. Boca Raton, FL: CRC Press, 1996, pp 255–276.
109. M Guainazzi, G Silvestri, G Serravalle. J Chem Soc, Chem Commun 200–201, 1975.
110. T Kakiuchi. J Electroanal Chem 322:55–61, 1992.
111. T Kakiuchi. In: AG Volkov, DW Deamer, eds. Liquid–Liquid Interfaces. Theory and Methods. Boca Raton, FL: CRC Press, 1996, pp 1–18.
112. T. Kakiuchi. In: AG Volkov, DW Deamer, eds. Liquid–Liquid Interfaces. Theory and Methods. Boca Raton, FL: CRC Press, 1996, pp 317–331.
113. T Kakiuchi, T Usui, M Senda. Bull Chem Soc Jpn 63:2044–2050, 1990.
114. H Katano, K Maeda, M. Senda. J Electroanal Chem 396:391–396, 1995.
115. S Kihara, M Suzuki, K Maeda, K Ogura, M Matsui, Z Yoshida. J Electroanal Chem 271:107–125, 1989.
116. T Kondo, T Kakiuchi. Bioelectrochem Bioenerg 36:53–56, 1995.
117. AK. Kontturi, K Konturri, L Murtomaki, DJ Schiffrin. J Chem Soc, Faraday Trans 91:3433–3439, 1995.
118. NA Kotov, MG Kuzmin. Sov Electrochem 26:1484–1488, 1990.
119. NA Kotov, MG Kuzmin. J Electroanal Chem 285:223–240, 1990.
120. NA Kotov, MG Kuzmin. Sov Electrochem 27:76–81, 1991.
121. NA Kotov, MG Kuzmin. J Electroanal Chem 338:99–124, 1992.
122. NA Kotov, MG Kuzmin. In: AG Volkov, DW Deamer, eds. Liquid–Liquid Interfaces. Theory and Methods. Boca Raton, FL: CRC Press, 1996, pp 213–253.
123. KL Kott, DA Higgins, RJ McMahon, RM Corn. J Am Chem Soc 115:5342–5345, 1993.
124. K Maeda, S Kihara, M Suzuki, M Matsui. J Electroanal Chem 303:171–184, 1991.
125. K Nakatani, T Uchida, H Misawa, N Kitamura, H Masuhara. J Electroanal Chem 367:109–114, 1994.
126. VS Markin, AG Volkov. Electrochim Acta 35:715–724, 1990.
127. Z Samec. J Electroanal Chem 99:197–205, 1979.
128. Z Samec. In: AG Volkov, DW Deamer, eds. Liquid-Liquid Interfaces. Theory and Methods. Boca Raton, FL: CRC Press, 1996, pp 155–178.
129. Z Samec, T Kakiuchi. In: H Gerischer, CW Tobias, eds. Advances in Electrochemical Science and Electrochemical Engineering. Weinheim: VCH, vol. 4, 1995, pp 297–361.
130. M Senda, Y Yamamoto. In: AG Volkov, DW Deamer, eds. Liquid-Liquid Interfaces. Theory and Methods. Boca Raton, FL: CRC Press, 1996, pp 375–400.
131. YuA Shchipunov. In: AG Volkov, DW Deamer, eds. Liquid–Liquid Interfaces. Theory and Methods. Boca Raton, FL: CRC Press, 1996, pp 295–315.
132. NK Zaitsev, NF Gorelik, NA Kotov, MG Kuzmin. Sov Electrochem 24:1243–1247, 1988.
133. NK Zaitsev, II Kulakov, MG Kuzmin. Sov Electrochem 21:1293–1297, 1985.
134. B Quinn, K Kontturi. J Electroanal Chem 483:124–134, 2000.
135. M Senda, Electrochim Acta 40:2993–2997, 1995.
136. T Kakiuchi. In: AG Volkov, ed. Liquid Interfaces in Chemical, Biological, and Pharmaceutical Applications. New York: Marcel Dekker, 2001, pp 105–121.
137. DJ Fermin, R Lahtinen. In: AG Volkov, ed. Liquid Interfaces in Chemical, Biological, and Pharmaceutical Applications. New York: Marcel Dekker, 2001, pp 179–227.

138. S Kihara, H Ohade, K Maeda, Y Yoshida, O Shirai. In: AG Volkov, ed. Liquid Interfaces in Chemical, Biological, and Pharmaceutical Applications. New York: Marcel Dekker, 2001, pp 487–514.
139. L Murtomaki, J Manzanares, S Mafe, K Kontturi. In: AG Volkov, ed. Liquid Interfaces in Chemical, Biological, and Pharmaceutical Applications. New York: Marcel Dekker, 2001, pp 533–551.
140. M Faraday. Phil Trans R Soc London 147:145–181, 1857.
141. K Maeda, S Kihara. In: AG Volkov, ed. Liquid Interfaces in Chemical, Biological, and Pharmaceutical Applications, New York: Marcel Dekker, 2001, pp. 609–628.
142. M Senda, Y Kubota, H Katano. In: AG Volkov, ed. Liquid Interfaces in Chemical, Biological, and Pharmaceutical Applications. New York: Marcel Dekker, 2001, pp 683–697.
143. H Watarai. In: AG Volkov, ed. Liquid Interfaces in Chemical, Biological, and Pharmaceutical Applications. New York: Marcel Dekker, 2001, pp 355–372.
144. F Millich, CE Carraher. Interfacial Synthesis. vols 1 and 2. New York: Marcel Dekker, 1977.
145. M Rosenberg. Crit Rev Microbiol 18:159–173, 1991.
146. S Paula, AG Volkov, AN Van Hoek, TH Haines, DW Deamer. Biophys J 70:339–348, 1996.
147. VS Markin, AG Volkov. Sov Electrochem 23:1105–1112, 1987.
148. AG Volkov, AA Kornyshev. Sov Electrochem 21:814–817, 1985.
149. AG Volkov. Langmuir 12:3315–3319, 1996.
150. S Sjolin. Acta Physiol Scand 4:365–372, 1942.
151. YuI Kharkats, AG Volkov. Bioelectrochem Bioenerg 22:91–103, 1989.
152. YuI Kharkats, AG Volkov. In: MJ Allen, SF Cleary, AE Sowers, eds. Charge and Field Effects in Biosystems—4. Singapore, New Jersey, London: World Scientific, 1994, pp 70–77.
153. VS Markin, AG Volkov. Adv Colloid Interface Sci 31:111–152, 1990.
154. RP Bell. J Phys Chem 32:882–1137, 1928.
155. AA Kornyshev, AG Volkov. J Electroanal Chem 180:363–381, 1984.
156. VS Markin, AG Volkov. Sov Electrochem 23:1405–1413, 1987.
157. VS Markin, AG Volkov. J Colloid Interface Sci 131:382–392, 1989.
158. VS Markin, AG Volkov. Russ Chem Rev 57:1963–1989, 1988.
159. VS Markin, AG Volkov. Electrochim Acta 34:93–107, 1989.
160. VS Markin, AG Volkov. Russ Chem Rev 56:1953–1972, 1987.
161. VS Markin, AG Volkov. J Electroanal Chem 235:23–40, 1987.
162. YuI Kharkats. Sov Electrochem 12:1370–1377, 1976.
163. YuI Kharkats. Sov Electrochem 26:1032–1039, 1990.
164. YuI Kharkats, AM Kuznetsov. In: AG Volkov, DW Deamer, eds. Liquid–Liquid Interfaces. Theory and Methods. Boca Raton, FL: CRC Press, 1996, pp 139–154.
165. AM Kuznetsov, YuI Kharkats. In: VE Kazarinov, ed. The Interface Structure and Electrochemical Processes at the Boundary Between Two Immiscible Liquids. Berlin: Springer-Verlag, 1987, pp 11–46.
166. RA Marcus. J Phys Chem 94:1050–1055, 1990.
167. RA Marcus. J Phys Chem 94:4152–4155, 1990.
168. RA Marcus. J Phys Chem 95:2010–2013, 1991.
169. RA Marcus. J Phys Chem 99:5742–5742, 1995.
170. RA Marcus. J Chem Phys 113:1618–1629, 2000.
171. I Benjamin. J Phys Chem 95:6675–6683, 1991.
172. I Benjamin. In: AG Volkov, DW Deamer, eds. Liquid–Liquid Interfaces. Theory and Methods. Boca Raton, FL: CRC Press, 1996, pp 179–211.
173. I Benjamin, YuI Kharkats. Electrochim Acta 44:133–138, 1998.
174. LI Krishtalik. Biochim Biophys Acta 849:162–171, 1986.
175. LI Krishtalik, AM Kuznetsov. Sov Electrochem 22:218–221, 1986.
176. RA Marcus. J Chem Phys 24:966–978, 1956.

177. HHJ Girault. J Electroanal Chem 388:93–100, 1995.
178. EV Dehmlow, SS Dehmlow. Phase Transfer Catalysis. New York: VCH, 1993.
179. CM Starks, CL Liotta, NM Halper. Phase Transfer Catalysis. New York: Chapman & Hall, 1994.

2

Electrochemistry of Chemical Reactions at Polarized Liquid–Liquid Interfaces

TAKASHI KAKIUCHI Kyoto University, Kyoto, Japan

I. INTRODUCTION

Chemical reactions at the interface between two immiscible liquid phases take place in a variety of systems, ranging from biological cells to the earth environment with regard to the circulation of chemicals. Life on earth probably would not have been possible without the cradle of a mixed "soup" composed of hydrophilic and lipophilic substances. In contemporary chemistry, solvent extraction and phase-transfer catalysis (PTC), making use of two-phase reactions, are indispensable at both industrial and laboratory scales. One notable feature of the chemical reactions in liquid/liquid systems is that the two-phase systems permit the reaction between lipophilic substances with hydrophilic substances in the vicinity of the interface. Another inherent property is that both reactants and products can be transported from or to the adjacent bulk phases, depending on their hydrophilicity–lipophilicity balances, which constitute the basis of directional transport and facilitation of chemical reactions. On the other hand, however, these virtues, which provide a multitude of possibilities in designing chemical reactions, complicate the quantitative understanding of the mechanism. For example, while PTC has been widely utilized for organic synthesis, fully making use of the advantages of two-phase reactions, little is known for sure about the detailed mechanism of PTC, because of the involved interplay of homogeneous and heterogeneous processes, such as mass transports in homogeneous and heterogeneous media, heterogeneous and homogeneous chemical reactions, and adsorption.

To decipher this complexity, electrochemistry at the polarized liquid–liquid interface developed over the past two decades has been proven to be a powerful tool, as shown in elucidation of the mechanism of ion-pair extraction [1–4] and the response of ion-selective electrodes of liquid-membrane type to different types of ions [5–7]. Along this line, several attempts have been made to use polarized liquid|liquid interfaces for studying two-phase S_N2 reactions [8–10], two-phase azo-coupling [11], and interfacial polymerizations [12]. Recently, kinetic aspects of complexation reactions in facilitated ion transfer with ionophores and the rate of protonation of amines have been treated quantitatively [13–16]. Their theoretical framework, which was adapted from the theories of kinetic currents in polarography, can be directly applicable to analyze quantitatively the chemical reactions in the two-phase systems. In what follows is the introduction to recent advances in electrochemical studies of the chemical reactions at polarized liquid–liquid interfaces, mainly focusing on

those accompanying the formation or breaking of covalent bonds. Electron-transfer reactions at the liquid|liquid interface almost always accompany following chemical reactions, which complicates the interpretation of the interfacial electron-transfer processes. This subject will not be covered in this chapter, partly because little is known about the quantitative aspects of the following chemical reactions and partly because the diversity of the following reactions after the interfacial electron transfer would necessitate a new chapter.

II. ION TRANSFER WITH PRECEDING CHEMICAL REACTIONS

The transfer of amines [17–19] and weak acids [20,21] between the aqueous phase (W) and the organic phase (O) across the O|W interface is a typical example of the ion transfer with preceding chemical reactions. In the case of the transfer of ammonium ions across the interface, the interfacial ion transfer:

$$BH^+(W) \rightleftarrows BH^+(O) \tag{1}$$

is accompanied by the protonation reaction in W:

$$B(W) + H^+(W) \underset{k_b}{\overset{k_f}{\rightleftharpoons}} BH^+(W) \tag{2}$$

or in a well-buffered medium:

$$B(W) \underset{k_b}{\overset{k_f'}{\rightleftharpoons}} BH^+(W) \tag{3}$$

If B is soluble in both O and W, the partition of B also occurs:

$$B(W) \rightleftarrows B(O) \tag{4}$$

The partition coefficient of B may be defined as

$$K_D = {}^b c_B^O / {}^b c_B^W \tag{5}$$

where ${}^b c_B^O$ and ${}^b c_B^W$ are the bulk concentrations of B in O and W, respectively. Using the concept of reaction-layer thickness, μ, developed in the theory of kinetic currents in polarography [22] and the assumption that the distribution of B and also the ion transfer of BH^+ across the interface are reversible, Senda and coworkers [13,14] derived expressions for the limiting current in ion-transfer polarograms for two initial conditions: B and BH^+ being only in W (Case 1) and B being only in O while no B and BH^+ in W (Case 2). In Case 1:

$$i_\ell^1 = i_d^1(1 + K'/(1 + \lambda))/(1 + K') \tag{6}$$

where i_ℓ^1 is the limiting current for Case 1. The diffusion-limited current for Case 1, i_d^1, is defined by

$$i_d^1 = zFA(D^W/\delta^W)({}^b c_{BH^+}^W + {}^b c_B^W) \tag{7}$$

where z is the charge number of ion BH^+, F is the Faraday constant, A is the area of the planar interface between O and W, D^W is the diffusion coefficient of the relevant species, assuming that D^W values for all species have the same magnitude, and δ^W is the thickness of the diffusion layer in W. In Eq. (6), $K' = k_b/k_f'$, and

$$\lambda = (D^W/\delta^W)(1 + (D^O/D^W)^{1/2}K_D)/\mu k_f' \tag{8}$$

where μ is related to the rate constants in the protonation reaction through

$$\mu = \sqrt{D^{W}/(k_f' + k_b)} \tag{9}$$

The limiting current for Case 2, i_ℓ^2, is given by

$$i_\ell^2 = i_d^2/(1 + \lambda) \tag{10}$$

where i_d^2 is the diffusion current for Case 2 defined by

$$i_d^2 = zFA(D^{O}/\delta^{O})\,{}^{b}c_B^{O} \tag{11}$$

where ${}^{b}c_B^{W}$ is the bulk concentration of B in O. On the other hand, the half-wave potential, $E_{1/2}$, is given by

$$E_{1/2} = E^{\circ}_{BH^+} - \frac{RT}{2zF}\ln\frac{D^{O}}{D^{W}} + \frac{RT}{2zF}\ln[1 + K'(1 + \sqrt{D^{O}/D^{W}}K_D)/(1 + \lambda)] \tag{12}$$

From the analysis of polarograms for the transfer of procaine in Case 2, Senda et al. concluded that the transfer of procaine is described by the CE mechanism, that is, the transfer of the protonated form of procaine with the preceding protonation reaction in W. The major contribution to k_f' was found to be proton donation from the acid form of a buffer component, AH, employed. The values of $k_{AH} = k_f'/[AH]$ at pH 8.0 are given in Table 1 for three different buffers. In this example, the reaction-layer thickness is much thinner, of the order of 10^{-6} cm^{-1}, than the diffusion-layer thickness, which ensures the applicability of the concept of the reaction layer [22].

A. Two-Phase Nucleophilic Substitution Reaction

Nucleophilic substitution reactions of a lipophilic substance, such as 2,4-dinitrofluorobenzene (DNFB), with OH^- ions are facilitated when lipophilic substrates are incorporated into cationic micelles [23] and microemulsions [24]:

TABLE 1 Rate Constant of Proton Transfer, k_{AH}, from AH to Procaine at pH 8.0 in 0.1 mol dm^{-3} LiCl and pK_a values at 25°C

Buffer	k_{AH}/(dm^3 mol^{-1} s^{-1})	pK_a
TAPSO[a]	5.4×10^6	7.7
EPPS[b]	2.1×10^6	8.0
TAPS[c]	8.5×10^5	8.4

[a] *N*-Tris(hydroxymethyl)methyl-2-hydroxy-3-aminopropanesulfonic acid.
[b] *N*-2-Hydroxyethylpiperazine-*N*′-3-propanesulfonic acid.
[c] *N*-Tris(hydroxymethyl)methyl-3-aminopropanesulfonic acid.
Source: Ref. 14.

$$\mathrm{DNFB(M) + OH^-(W) \underset{k_b}{\overset{k_f}{\rightleftharpoons}} DNP^-(M) + F^-(W) + H^+} \tag{13}$$

where M designates the micellar or microemulsion phase and DNP^- stands for 2,4-dinitrophenolate anions. DNP^- ions are moderately hydrophilic and can distribute between the organic phase and the aqueous phase, depending on the phase-boundary potential, $\Delta_O^W\phi = \phi^W - \phi^O$, whereas OH^-, F^-, and H^+ are hydrophilic. By varying $\Delta_O^W\phi = \phi^W - \phi^O$ at the polarized liquid|liquid interface, it is thus possible to detect the formation of DNP^- ions through monitoring the current accompanied by its transfer across the interface. Kong et al. studied, using the dropping-electrolyte-solution interface (DESI) between nitrobenzene (NB) and W, the nucleophilic substitution reactions of DNFB and 1-*p*-toluenesulfonyl-2,4-dinitronaphthalene (TSDNN) with OH^- ions. The reaction of TSDNN with OH^- is

$$\mathrm{TSDNN(NB) + OH^-(W) \underset{k_b}{\overset{k_f}{\rightleftharpoons}} DNN^-(W/O) + tosylate^-(W) + H^+} \tag{14}$$

where DNN^- stands for 2,4-dinitronaphthalate and tosylate (p-toluenesulfonate) is hydrophilic enough to be present only in W with the potential window of the system employed. The use of DESI was necessary to define experimentally the initial conditions regarding the partitioning of DNFB and TSDNN, as the partition coefficients of DNFB and TSDNN between NB and W are 1.2×10^{-3} and 3.4×10^{-4}, respectively; the partition of DNFB and TSDNN in W may not be negligible, as are the cases of the transfer of amines described above. Figure 1 shows a polarogram recorded with DESI for the reaction (14) in which the limiting current appeared corresponding to the transfer of DNN^- ions from W to O. The values of k_f for reactions (13) and (14) evaluated from the limiting currents, using the theory for Case 2 above, are 1.0×10^{-1} and 1.03 $dm^3\ mol^{-1}\ s^{-1}$ at 25°C.

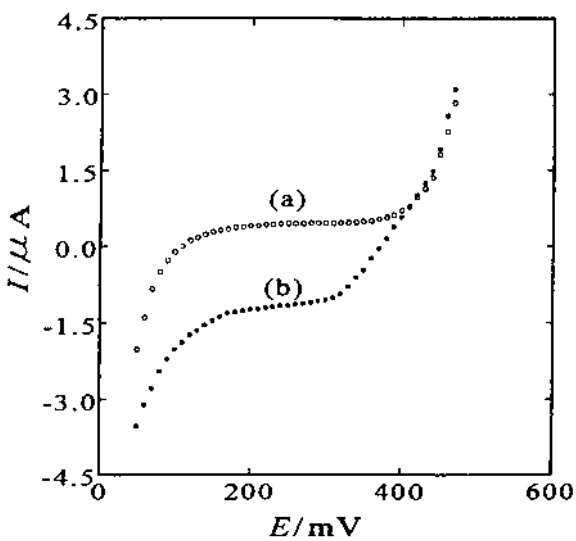

FIG. 1 Polarograms recorded using the dropping electrolyte solution interface between 0.5 mol dm^{-3} LiOH + 0.1 mol dm^{-3} LiCl and 0.05 mol dm^{-3} tetrapentylammonium tetraphenylborate in nitrobenzene in the absence (a) and the presence (b) of 40 mmol dm^{-3} TSDNN in W. (From Ref. 9.)

In both reactions (13) and (14), no appreciable dependence of k_f values on the supporting electrolyte concentration was observed. From values of the pseudo-first order rate constant in the present examples, the reaction-layer thickness is evaluated to be of the order of 1.5×10^{-3} cm, which is far greater than the thickness of the electrical double layer at the interface, explaining the absence of the appreciable change in the rate constant for the substitution reactions for both DNFB and TSDNN. A difference between the dropping electrolyte interface and micelles is the thickness of the diffusion layer: in the latter the steady-state spherical diffusion should prevail and the diffusion-layer thickness is simply the radius of the micelles. A rigorous treatment of the coupling of chemical reactions and diffusion has to be considered, instead of the reaction-layer concept, under the influence of the electrical double layer, as the thickness of the double layer is comparable to that of the diffusion layer.

B. Facilitated Ion Transfer with Preceding Dissociation of Metal Ion Complexes

According to Katano and Senda [15,16], the transfer of Pb^{2+} ions in the presence of citrate in W facilitated by 1,4,7,10,13,16-hexathiacyclo-octadecane is limited by the dissociation reaction of Pb^{2+} ions from their complexes with citrate in W, while the transfer of Pb^{2+} ions across the interface and the complex formation of Pb^{2+} ions with the ionophore in O are fast. The quantitative analyses of linear-sweep voltammograms and normal-pulse polarograms consistently show that the entire process is described by a CE mechanism and that the dissociation and association rate constants of the Pb^{2+}-citrate^{3-} complex are 1.2×10^4 s^{-1} and 1.2×10^{10} dm^3 mol^{-1} s^{-1}, respectively [15,16]. In this case, a planar interface can be used as no partition of neutral components relevant to the facilitated ion transport exists.

III. ION TRANSFER WITH FOLLOWING CHEMICAL REACTIONS

Ions transferred from one phase to the other can be subject to succeeding chemical reactions [25]. A classical example of this type of two-phase reaction is PTC, in which reactant anions are brought from the aqueous phase to the organic phase in the presence of cationic phase-transfer catalysts, such as tetra-alkylammonium ions [26,27], which presumably function to establish the phase-boundary potential favorable for the transfer of relatively hydrophilic ions into the organic phase [28]. A polarized liquid|liquid interface allows us to drive moderately lipophilic ions into the organic phase by externally changing the phase-boundary potential, instead of using phase-transfer catalysts. This idea of phase-boundary potential-driven PTC was first demonstrated for the two-phase azo-coupling reactions [11].

A. Phase-Boundary Potential-Driven Interfacial Chemical Reactions

1. Two-Phase Azo-Coupling

The azo coupling between diazonium ions and coupling components is an important reaction for synthesizing dye compounds [29,30]. Usually, this reaction proceeds in a homogeneous solution phase. However, in certain cases, the reaction in a two-phase system is advantageous, as many coupling components are lipophilic, while diazonium

ions are relatively hydrophilic [31]. The two-phase azo coupling of this type is facilitated by the reverse-PTC in which hydrophilic cations are transferred from W to O by ion-pairing with large hydrophobic anions [32–40], e.g., tetrakis[3,5-bis(trifluoromethyl)phenyl]borate anion [36,37]. Kong et al. recently used the phase-boundary potential-driven ion transfer of arenediazonium ions from W to 1,2-dichloroethane (DCE), instead of using phase-transfer catalysts, to effect the two-phase azo-coupling reactions [11].

The mechanism of the phase-boundary potential-driven azo-coupling reaction at the DCE|W interface may be composed of the following steps:

$$\mathrm{Ar-N_2^+(W)} \underset{k_{\mathrm{DCE}}}{\overset{k_{\mathrm{W}}}{\rightleftharpoons}} \mathrm{Ar-N_2^+(DCE)} \tag{15}$$

$$\mathrm{Ar-N_2^+(DCE) + Y(DCE)} \underset{k_{-1}}{\overset{k_1}{\rightleftharpoons}} \mathrm{Ar-N{=}N-Y^+-H(DCE)} \tag{16}$$

$$\mathrm{Ar-N=N-Y^+-H(DCE) + B} \xrightarrow{k_2} \mathrm{Ar-N=N-Y(DCE) + HB^+(DCE)} \tag{17}$$

where Ar-N_2^+ are arenediazonium ions and constitute a coupling component, k_{W} and k_{DCE} are the rate constants of ion transfer in the forward and backward directions, and k_1 and k_{-1} are the forward and backward rate constants of the formation of the σ complex, Ar-N=N-Y^+-H; B is a base, and k_2 is the rate constant for the release of the proton [41]. When $k_{-1} << k_2$[B], which probably holds in the present case, the reaction in DCE is expressed by

$$\mathrm{Ar-N_2^+ + Y} \xrightarrow{k_1} \mathrm{Ar-N=N-Y + H^+} \tag{18}$$

Such a heterogeneous charge transfer across the interface followed by a chemical reaction of the reactants formed by the preceding electrochemical process is known as the E_rC_i mechanism in electrode reactions, that is, the electrochemically reversible charge transfer followed by an irreversible chemical reaction [42].

Figure 2 shows cyclic voltammograms for the transfer of Fast Red TR (4-chloro-2-methylbenzenediazonium) cations ($FRTR^+$) across the DCE|W interface in the presence of 20 mM *N*, *N*′-dimethyl-1-naphthylamine (DMNA) in DCE. With decreasing scan rate, the negative currents on the reverse scan, corresponding to the transfer of $FRTR^+$ cations from DCE to W diminished, indicating that the transfer of $FRTR^+$ is represented by the E_rC_i mechanism. In reaction (18), H^+ ions are formed in DCE together with the azo dye, Ar − N = N − Y. If H^+ is in free form, the back transfer of H^+ ions from DCE to W, giving a negative current, would cancel out the positive current due to the transfer of $FRTR^+$ even in the forward scan. The fact that the presence of positive current on voltammograms in Fig. 2 suggests that, after reaction (17), H^+ ions are kept in O by forming protonated species in O.

Potential-step chronoamperometry is a more convenient and accurate way of determining the rate of chemical reactions than cyclic voltammetry. The current responses for the transfer of $FRTR^+$ shown in Figure 3 were analyzed quantitatively. The analysis of current-time curve for the E_rC_i mechanism is simplified when we examine the ratio of the current at t_r in the reverse step to that at $t_r - \tau$ in the forward step, where τ is the time of the potential reversal, as a function of $(t_r - \tau)/\tau$ [43]. The ratio for the E_rC_i mechanism is given by [43]

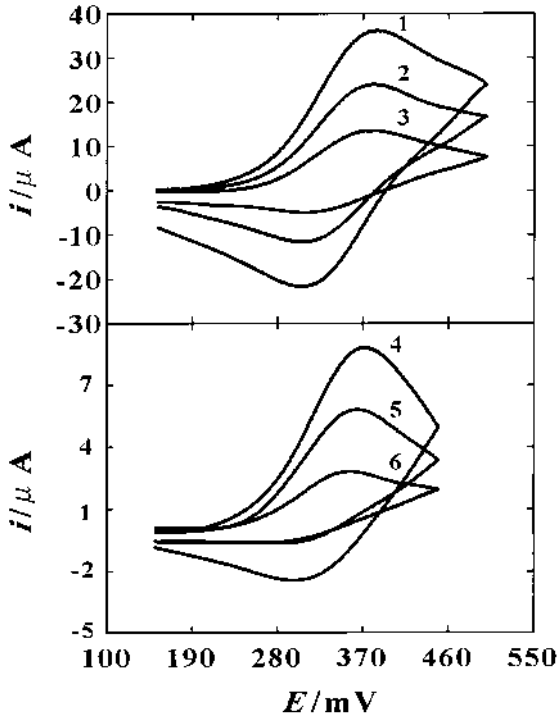

FIG. 2 Cyclic voltammograms for the transfer of Fast Red TR across the DCE|W interface in the presence of 20 mM *N,N*-dimethyl-1-naphthylamine in DCE. Concentration of Fast Red TR in W: 1 mM; voltage scan rate: 1000 (curve 1), 500 (curve 2), 200 (curve 3), 100 (curve 4), 50 (curve 5), and 20 (curve 6) mV s^{-1}. (From Ref. 11.)

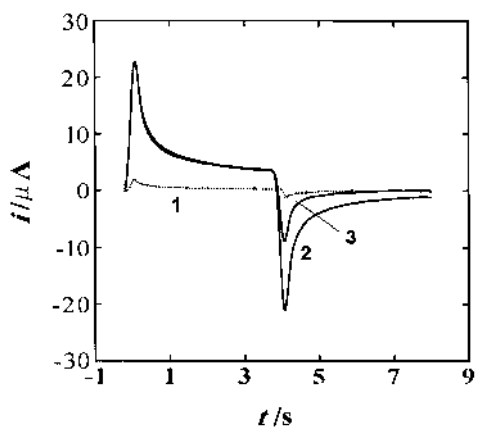

FIG. 3 Chronoamperometry curves for a base supporting electrolytes in the absence of Fast Red TR and *N,N*-dimethyl-1-naphthylamine (curve 1), in the presence of 1 mM Fast Red TR in W (curve 2), and in the presence of 1 mM Fast Red TR in W and 20 mM *N,N*-dimethyl-1-naphthylamine (curve 3) in DCE. Initial potential: 0.15 V; second potential: 0.50 V; and switching time: 4 s. (From Ref. 11.)

$$-\frac{i_a}{i_c} = \phi[k_f\tau, (t_r - \tau)/\tau] - \left[\frac{(t_r - \tau)}{1 + (t_r - \tau)/\tau}\right]^{1/2} \tag{19}$$

where t_r is the time of the potential reversal and ϕ represents a function involving a confluent hypergeometric series. The ratio of the current in the forward step over that in the reverse step, i_a/i_c, is plotted against $(t_r - \tau)/\tau$ in Fig. 4. Solid lines are working curves calculated using Eq. (19) and the points represent experimental values for Fast Red ITR (curve 1), Fast Red TR (curve 2), and Fast Red B (curve 3) in the presence of DMNA. It is shown that experimental points are well fitted to working curves over the range of $(t_r - \tau)/\tau$ examined. Table 2 summarizes the values of k_1 for four different diazonium ions and four couplers.

Recent further studies of the electrochemical two-phase azo-coupling reactions revealed that in certain cases the transfer of H^+ ions formed in DCE from DCE to W is not always negligible [44]. In this case, the current transients in potential-step chronoamperometry have to be analyzed using the $E_rC_iE_r$ or $E_rC_rE_r$ model, taking account of the H^+ transfer to W after reaction (18).

2. Phase-Boundary Potential-Driven Two-Phase S_N2 Reactions

There are several conceivable variations in the phase-boundary potential-driven two-phase reactions. Recently, Forssten et al. [10] reported cyclic voltammograms shown in Fig. 5 for the transfer of I^- in the presence of 2-bromo-3-methylbutyric acid (RBr) in DCE. The overall mechanism is

$$RBr(DCE) + OH^-(W) \rightleftarrows ROH(DCE) + Br^-(W) \tag{20}$$

The actual mechanism of this reaction is not clear as to the location of the chemical reaction, as RBr, if it has a finite solubility in W, can react with OH^- in W and then partition back to DCE. When I^- is added in W, I^- apparently catalyzes reaction (20) (Fig. 5). The mechanism proposed for the catalytic effect of I^- is [10]

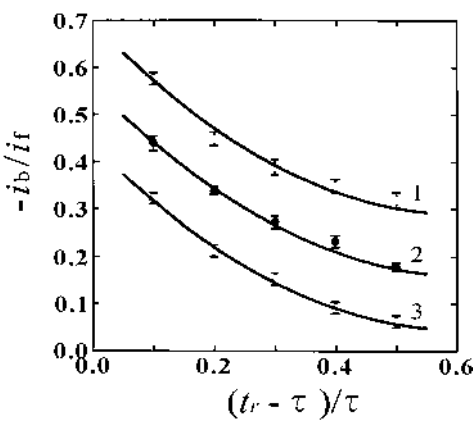

FIG. 4 Plots of the ratio of negative current to positive current versus $(t_r - \tau)/\tau$ for the transfer of Fast Red ITR (◆), Fast Red TR (●), and Fast Red B (■) in the presence of 20 mM *N,N*-dimethyl-1-naphthylamine in DCE at 20±0.5°C: $\tau = 5$ s. The dashed line and solid lines are theoretical curves calculated using Eq. (19) for $k\tau = 0$ (curve 1), 0.3 (curve 2), 0.7 (curve 3), and 1.4 (curve 4). (From Ref. 11.)

TABLE 2 Values of Pseudo-First Order Rate Constants of Azo-Coupling Reaction in DCE Evaluated from Potential-Step Measurements at the DCE|W Interface at 20±0.5°C

	k_f ($dm^3\ mol^{-1}s^{-1}$)			
	1-NA	DMNA	1-Naphthol	2-Naphthol
Fast Red B	95.5±7.5	20.5±1.3	9.9±1.5	3.3±0.1
Fast Red TR	15.7±1.3	12.5±1.2	9.3±0.9	1.5±0.1
Fast Red ITR	8.5±2.5	5.6±1.2	4.8±0.4	4.0±0.7
Fast Red PDC	2.7±0.4	12.2±1.4	2.0±0.5	2.8±0.4

Fast Red B: 2-methoxy-4-nitrobenzenediazonium 1,5-naphthalenedisulfonate; Fast Red ITR: 5-diethylaminosulfonyl-2-methoxybenezenediazonium chloride; Fast Red PDC: 5-butylaminosulfonyl-2-methoxybenezenediazonium chloride; 1-NA: 1-naphthylamine; DMNA: *N*,*N*′-dimethyl-1-naphthylamine.

$$RBr(DCE) + I^-(W) \rightleftarrows RI(DCE) + Br^-(W) \tag{21}$$

$$RI(DCE) + OH^-(W) \rightleftarrows ROH(DCE) + I^-(W) \tag{22}$$

The locations of both reactions are again not self-evident. These two steps may be further decomposed into several steps, even when we exclude the possibility of finite dissolution of RBr into W and also the possibility of direct interfacial reaction of RBr on the DCE side with OH^- or I^- ions on the W side of the interface:

$$I^-(W) \rightleftarrows I^-(DCE) \tag{23}$$

$$RBr(DCE) + I^-(DCE) \rightleftarrows RI(DCE) + Br^-(DCE) \tag{24}$$

$$Br^-(DCE) \rightleftarrows Br^-(W) \tag{25}$$

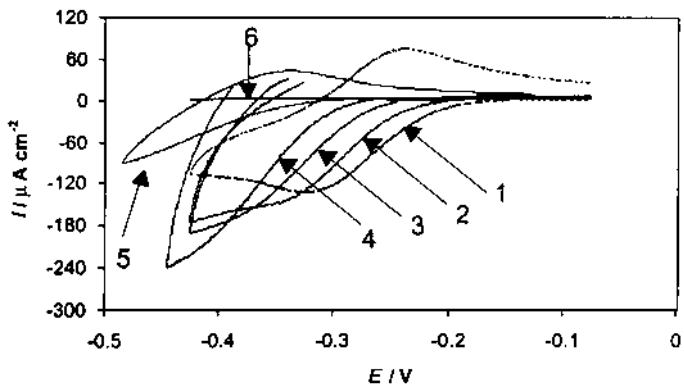

FIG. 5 Effect of substrate (RBr) concentration on the apparent iodide transfer curve: $[I^{-1}] = 1$ mmol dm^{-3}, no RBr (curve 1); $[I^{-1}] = 1$ mmol dm^{-3}, $[RB] = 1$ mmol dm^{-3} (curve 2); $[I^{-1}] = 1$ mmol dm^{-3}, $[RB] = 2$ mmol dm^{-3} (curve 3); $[I^{-1}] = 1$ mmol dm^{-3}, $[RB] = 3$ mmol dm^{-3} (curve 4); $[Br^{-1}] = 1$ mmol dm^{-3}, no $[I^-]$ (curve 5); baseline (curve 6). Scan rate 10 mV s^{-1}. (From Ref. 10.)

$$OH^-(W) \rightleftarrows OH^-(DCE) \tag{26}$$

$$RI(DCE) + OH^-(DCE) \rightleftarrows ROH(DCE) + I^-(DCE) \tag{27}$$

$$I^-(DCE) \rightleftarrows I^-(W) \tag{28}$$

In this mechanism, it is necessary that OH^- ions are transferred into DCE and then react with RI in DCE, which is the basis of the proposed mechanism, that is, the two-phase S_N2 reaction involving the electrochemically driven transfer of I^- and OH^- from the aqueous to organic phase coupled with transfer of Br^- in the other direction and an S_N2 reaction in the organic phase [10]. Their results indeed show that the increase in pH in W from 3 to 9 leads to an increase in the negative current, corresponding to the net transfer of negative ion from W to DCE. This clearly points to the possible role of OH^- ions in the overall process, though it seems difficult for OH^- ions to exist in a significant amount in DCE even at pH 9.

B. Ion Transfer Followed by Homogeneous Electron-Transfer Reaction

Voltammetry usually does not provide unequivocal evidence as to the location of the chemical reaction, as has been pointed out in facilitated ion transfer [45]. The difficulty in determining the mechanism is inherent to all electrochemical processes involving chemical reactions in liquid|liquid two-phase systems, including several examples described above. The source of the difficulty is that liquid|liquid two-phase systems allow any component in the systems to partition between the two phases. The reaction mechanism in these systems can only have a relativistic meaning; the mechanism that dominates the flux of an overall charge-transfer reaction may be considered to be the primary mechanism. The following is a clear-cut example of the E_rC_i mechanism in liquid|liquid two-phase systems in this sense.

Arenediazonium ions are dediazonized upon reduction:

$$Ar - N_2^+ \overset{e^-}{\rightleftharpoons} Ar^{\cdot} + N_2 \tag{29}$$

Figure 6 shows voltammograms for the transfer of $FRTR^+$ cations across the DCE|W interface in the absence and presence of 20 mM decamethylferrocene in DCE [12]. The negative current on the backward scans completely disappeared on addition of decamethylferrocene in DCE. In view of the lipophilicity of decamethylferrocene, this is a good example of the ion-transfer process described by the E_rC_i mechanism. From the shift of the peak potential, E_p, with the scan rate, v, the pseudo-first order rate constant, k_f, can be estimated using the Nicholson and Shain's equation for the peak shift in the case of E_rC_i mechanism [42]:

$$E_m - E_p = -\frac{RT}{zF}\left(0.780 - \ln\sqrt{k_f/(zFv/RT)}\right) \tag{30}$$

where E_m is the midpoint potential for the transfer of $FRTR^+$. The results in Fig. 6 give a value of 230 s^{-1} for k_f for the reaction (29) or 1.2×10^4 mol^{-1} dm^3 s^{-1}.

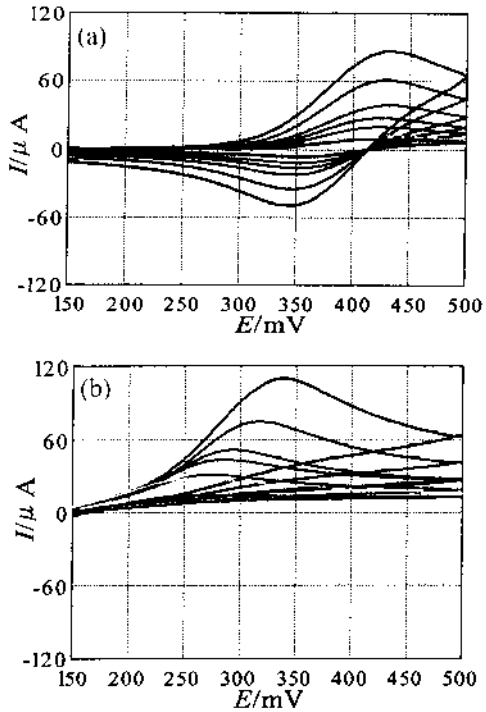

FIG. 6 Cyclic voltammograms for the transfer of Fast Red TR across the DCE|W interface in the absence (a) and the presence (b) of 20 mmol dm^{-3} decamethylferrocene in DCE; the concentration of Fast Red TR in W is 4 mmol dm^{-3}. Voltammograms in (a) and (b) with increasingly greater peak currents correspond to those recorded at the scan rate of 10, 20, 50, 100, 200, 500, and 100 mV s^{-1}, respectively. (From Ref. 12.)

IV. ELECTROCHEMICAL POLYMERIZATION REACTIONS AT THE LIQUID|LIQUID INTERFACE

Polymerization reactions at the liquid|liquid interface are of fundamental importance in emulsion polymerization, which has been used on the industrial scale [46]. Electrochemical polymerization at the liquid|liquid interface was first reported by Cunnane and Evans [47] for the oxidation of 1-methylpyrrole and 1-phenylpyrrole dissolved in DCE with Fe^{3+} in W. A similar surface polymerization of surface-active derivatives of pyrrole by the oxidation with $Ce(SO_4)_2$ has been recently reported [48]. Surface films gradually formed at the interface impede the transfer of tetramethylammonium (TMA^+) ions across the DCE|W interface and, to a lesser extent, the transfer of PF_6^- ions. These two examples are the interfacial radical polymerization initiated by the direct oxidation of monomers.

Another approach of the interfacial radical polymerization is the use of aryl radicals formed by the reduction of arenediazonium ions described above as the initiator of radial polymerization. Styrene monomers dissolved in DCE can be polymerized by this scheme. Oligomers formed in the vicinity of the interface appreciably reduce the rate of transfer of tetraethylammonium ions across the interface [12].

V. CONCLUSIONS

Recent electrochemical studies of chemical reactions at the polarized liquid|liquid interface have been briefly summarized. All chemical reactions seem to occur in either one of the two adjacent bulk phases before or after the interfacial charge transfer. No effect of the double layers at the interface on the chemical reactions has been confirmed. No evidence has been obtained for the specific role of adsorption in the interfacial chemical reactions.

Electrochemical methods have been shown to be useful for quantitatively studying the heterogeneous ion-transfer reactions coupled with chemical reactions. Theoretical developments of the kinetic current in polarography mainly made in the 1950s and 1960s and also of other voltammetric studies are important resources for studying the charge transfer at liquid|liquid interfaces and thus provide us with not only powerful means for precise data analysis but also a conceptual framework and guideline in studying fairly involved two-phase chemical reactions.

Given the significance of chemical reactions associated with the ion and electron transfers across the liquid|liquid interfaces of various types, further elaborations of both experimental and theoretical studies are to be seen in the future along the lines illustrated above.

REFERENCES

1. T Kakutani, Y Nishiwaki, M Senda. Bunseki Kagaku 33:E175–E182, 1984.
2. J Koryta. J Electroanal Chem 213:323–325, 1987.
3. J Koryta, M Skalický. J Electroanal Chem 229:265–271, 1987.
4. Y Yoshida, M Matsui, O Shirai, K Maeda, S. Kihara. Anal Chim Acta 373:213–225, 1998.
5. T Kakiuchi, M Senda. Bull Chem Soc Jpn 57:1801–1808, 1984.
6. S Kihara, Z Yoshida. Talanta 31:789–797, 1984.
7. Y Yoshida, M Matsui, K Maeda, S. Kihara. Anal Chim Acta 374:269–281, 1998.
8. YT Kong, T Kakiuchi. J Electroanal Chem 446:19–23, 1998.
9. YT Kong, S Imabayashi, T Kakiuchi. Anal Sci 14:121–125, 1998.
10. C Forssten, K Kontturi, L Murtomäaki, HC Hailes, DE Williams. Electrochem Commun 3:379–383, 2001.
11. YT Kong, S Imabayashi, T Kakiuchi. J Am Chem Soc 122:8215–8219, 2000.
12. T Kakiuchi, H Sasao. to be published.
13. M Senda, Y Kubota, H Katano. Anal Sci 1997; 72 (suppl):285–288.
14. Y Kubota, H Katano, K Maeda, M Senda. Electrochim Acta 44:109–116, 1998.
15. H Katano, M Senda. Bull Chem Soc Jpn 71:2359–2363, 1998.
16. H Katano, M Senda. Bull Chem Soc Jpn 72:2085–2090, 1999.
17. D Homolka, V Mareček, Z Samec, K Baše, H Wendt. J Electroanal Chem 163:159–170, 1984.
18. K Arai, F Kusu, K Takamura. In: AG Volkov, DW Deamer, ed. Liquid–Liquid Interfaces: Theory and Methods. Boca Raton, FL: CRC Press, 1996, pp 375–400.
19. M Senda, Y Kubota, H Katano. In: AG Volkov, ed. Liquid Interfaces in Chemical, Biological, and Pharmaceutical Applications. New York: Marcel Dekker, 2001, pp 683–697.
20. T Ohkouchi, T Kakutani, M Senda. Bioelectrochem Bioenerg 25:71–80, 1991.
21. T Ohkouchi, T Kakutani, M Senda. Bioelecrochem Bioenerg 25:81–89, 1991.
22. J Heýrovsky, J Kuta. Principles of Polarography. New York: Academic Press, 1966, ch. 17.
23. CA Bunton L Robinson. J Am Chem Soc 92:356–361, 1970.
24. EN Durantini, CD Borsarelli. J Chem Soc, Perkin Trans 2: 719–723, 1996.
25. AK Kontturi, K Kontturi, L Murtomaki, DJ Schiffrin. J Chem Soc, Faraday Trans 91:3433–3439, 1995.

26. ME Halpern. Phase-Transfer Catalysis, Mechanism and Syntheses. Washington, DC: American Chemical Society, 1997.
27. EV Dehmlow, SS Dehmlow. Phase Transfer Cataysis. Weinheim: VCH, 1983.
28. SN Tan, RA Dryfe, HH Girault. Helv Chim Acta 77:231–242, 1994.
29. H Gilman. Organic Chemistry. vol. III. An Advanced Treatise. London: John Wiley, 1953.
30. H Zollinger. Diazo Chemistry I. Weinheim: VCH, 1994.
31. YT Kong, T Kakiuchi. J Electroanal Chem 483:22–28, 2000.
32. SH Korzeniowski, GW Gokel. Tetrahedron Lett 1637–1640, 1977.
33. K Bredereck, S Karaca. Tetrahedron Lett 39:3711–3712, 1979.
34. M Ellwood, J Griffiths. J Chem Soc, Chem Commun 181–183, 1980.
35. Y Hashida, K Kubota, S Sekiguchi. Bull Chem Soc Jpn 61:905–909, 1988.
36. H Kobayashi, T Sonoda, H Iwamoto, M Yoshimura. Chem Lett 579–580, 1981.
37. H Kobayashi, T Sonoda, H Iwamoto. Chem Lett 1185–1186, 1982.
38. M Iwamoto, T Sonoda, H Kobayashi. Tetrahedron Lett 24:4703–4706, 1983.
39. H Iwamoto, M Yoshimura, T Sonoda, H Kobayashi. Bull Chem Soc Jpn 56:796–801, 1983.
40. H Iwamoto, H Kobayashi, P Murer, T Sonoda, H Zollinger. Bull Chem Soc Jpn 66:2590–2602, 1993.
41. H Zollinger. Diazo Chemistry I. Weinheim: VCH, 1994, ch. 12.
42. RS Nicholson, I Shain. Anal Chem 36:706–723, 1964.
43. WM Schwarz, I Shain. J Phys Chem 69:30–40, 1965.
44. M Chiba. "Voltammetry of Interphase Chemical Reactions at the Potential–Controlled Liquid/Liquid Interface." Master's thesis, Graduate School of Engineering, Kyoto University, Kyoto, Japan, 2001.
45. T Kakutani, Y Nishiwaki, T Osakai, M Senda. Bull Chem Soc Jpn 59:781–788, 1986.
46. RG Gilbert. Emulsion Polymerization. London: Academic Press, 1995.
47. VJ Cunnane, U Evans. Chem Commun 2163–2164, 1998.
48. K Maeda, H Jänchenová, A Lhotský, I Stibor, J Budka, V Mareček. J Electroanal Chem 516:103–109, 2001.

3
Interfacial Catalysis in Metal Complexation

HITOSHI WATARAI Osaka University, Osaka, Japan

I. INTRODUCTION

The liquid–liquid interface is an extremely thin liquid region with a few nanometers thickness, where it is predicted that properties such as cohesive energy density, electrical potential, dielectric constant, and viscosity are drastically changed along with the coordinate from an organic phase to an aqueous phase. Therefore, various specific chemical phenomena, which are not observed in bulk liquid phases, occur at liquid–liquid interfaces. However, the nature of the liquid–liquid interface and its chemical function are still not fully understood. This situation is mainly due to the lack of suitable experimental methods, for the determination of the chemical species adsorbed at the interface and for the measurement of chemical reaction rates at the interface [1,2]. Recently, some new methods were developed in our laboratory [3], which attained a breakthrough in the study of interfacial reactions.

The solvent-extraction process for metal ions depends intrinsically on the mass transfer to or across the interface and the chemical reaction in the interfacial region. Therefore, the study of the role of the interface is very important for analyzing the real extraction mechanism and for controlling the extraction kinetics. In the early 1980s, the high-speed stirring (HSS) method was developed by Watarai and Freiser [4,5]. Thereafter, some new methods were proposed in our laboratory, which included the two-phase stopped-flow method [6], the capillary plate method [7], reflection spectrometry [8], the centrifugal liquid membrane (CLM) method [9], and the two-phase sheath flow method [10].

The most specific role of liquid–liquid interfaces that we found is a catalytic effect in the solvent extraction of metal ions and interfacial complexation kinetics. Shaking or stirring of a solvent-extraction system generates a wide interfacial area or a high specific interfacial area defined as the interfacial area divided by the bulk phase volume. Almost all extractants, and an auxiliary ligand in some cases, are more or less interfacially active, since they have both hydrophilic and hydrophobic groups. Interfacial adsorption of the extractant or an intermediate complex at the liquid–liquid interface can very effectively facilitate the extraction rate. In this chapter, the catalytic role of the interface in metal complexation will be discussed.

II. EXPERIMENTAL METHODS

There are many classical methods for investigating extraction kinetics, which include a Lewis cell, a single-drop method, and a rotating-disk method [11]. None of these methods, however, could be used to measure the extraction rate and interfacial concentration of extractant simultaneously. A modern experimental method for interfacial reactions has to be able to determine the interfacial concentration of an extractant or complex as a function of time through the extraction.

A. High-Speed Stirring Method

The high-speed stirring (HSS) method [4,5] made it possible to measure both an interfacial concentration and an extraction rate for the first time by a simple principle. When a two-phase system is vigorously stirred or agitated in a vessel and the interfacial area is extremely extended, the interfacial amount of an adsorbed compound is increased and thus the concentration in the organic phase is decreased. The interfacial area can easily be increased 500 times that under standing conditions. The specific interfacial area in HSS conditions can reach as high as 400 cm^{-1}. The maximum interfacial concentration of an ordinary compound is of the order of 10^{-10} mol/cm^2. This means that the maximum amount of the adsorbable solute at the interface corresponds to a 50 mL solution of 10^{-4} M concentration. This solute is removed from the organic phase to the interface; it is then ready to be measured by a conventional spectroscopic method such as spectrophotometry or fluorometry. In the original HSS method, the concentration depression in the organic phase was measured spectrophotometrically using a PTFE phase separator and a photodiode array spectrometer. Furthermore, the extraction rate could also be simultaneously measured by this method [4]. A schematic drawing of the apparatus used is shown in Fig. 1. The measurements were carried out by employing 50 mL for each phase at a stirring speed of 5000 rpm. From the spectral change effected by stirring, the decrease or increase in absorbance of a ligand or a complex was observed as a function of time.

B. Centrifugal Liquid Membrane Method

Both the requirements of a high specific interfacial area and a direct spectroscopic observation of the interface were attained by the centrifugal liquid membrane (CLM) method [12] shown in Fig. 2. A two-phase system of about 100 μL for each phase is introduced into a cylindrical glass cell with a diameter of 19 mm. The cell is rotated at a speed of 10,000 rpm. By this procedure, a two-phase liquid membrane with a thickness of 50–100 μm is produced inside the cell wall, which attains a specific interfacial area > 100 cm^{-1}. Ultraviolet/visible spectrometry was used in the original work for measurements of the interfacial species as well as of those in thin bulk phases. This method can be readily applied to the measurement of interfacial reaction rates of the order of seconds.

The CLM method can be combined with any kind of spectroscopic method. The fluorescence lifetime of an interfacially adsorbed zinc–tetraphenylporphyrin complex was observed by a nanosecond time-resolved laser-induced fluorescence method [13]. Microscopic resonance Raman spectrometry was also combined with the CLM method. This combination was highly advantageous for measuring the concentration profile at the interface and in a bulk phase [14].

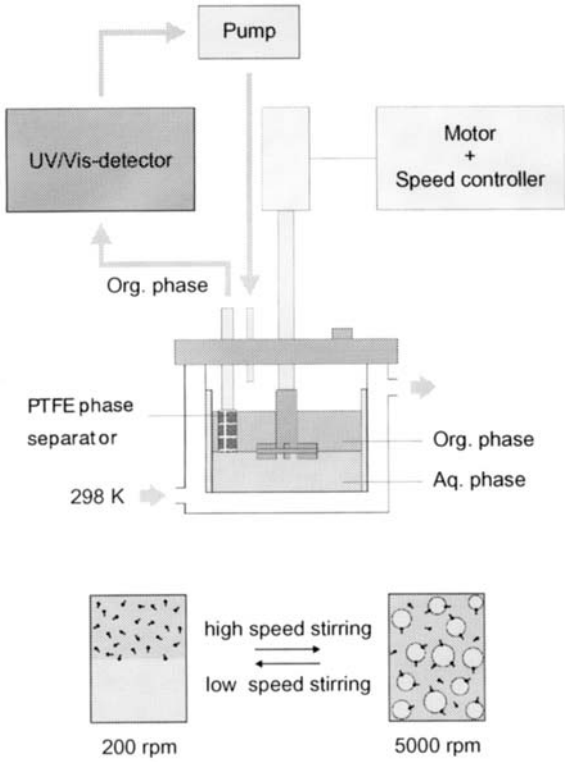

FIG. 1 Schematic drawing of the high-speed stirring (HSS) apparatus. The organic phase was continuously separated by a PTFE phase separator and circulated through the flow cell in the UV/VIS photodiode array spectrometer.

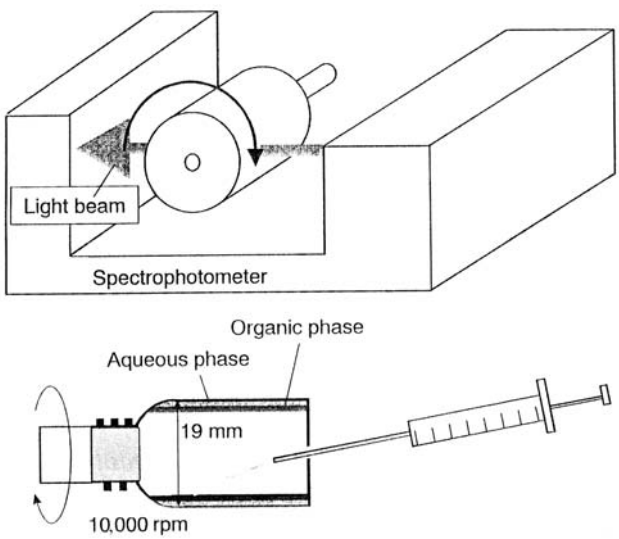

FIG. 2 Schematic drawing of the centrifugal liquid membrane (CLM) spectrometer with a modified cell having a sample injection hole in the base.

C. Two-Phase Stopped-Flow Method

Stopped-flow mixing of organic and aqueous phases is an excellent way to produce dispersions within a few milliseconds [9]. The specific interfacial area of the dispersion becomes as high as 700 cm^{-1} and the interfacial reaction in the dispersed system can be measured by a photodiode-array spectrophotometer. A drawback of this method is the limitation of a measurable time, since the dispersion system starts to separate after $\simeq$. 200 ms, even in a rather viscous solvent such as dodecane. However, it is unique as a method applicable to relatively fast interfacial reactions such as diffusion-rate limiting reactions as observed in the protonation reaction of tetraphenylporphyrin at a dodecane/acid interface [9].

D. Total Internal Reflection Spectrometry

Under total internal reflection (TIR) conditions at a liquid–liquid interface, one can observe interfacial reactions in the evanescent layer, which is a very thin layer of $\simeq$100 nm thickness. Fluorometry is the most sensitive method for detection of interfacial species and their dynamics [15]. Time-resolved laser spectrofluorometry is a powerful tool for the elucidation of rapid dynamic phenomena at the interface [16]. Time-resolved total-reflection fluorometry can be used for evaluation of the rotational relaxation time of octadecylrhodamine B and thus the viscosity of the interface [17]. Laser excitation can produce excited states of the adsorbed compound at the interface. As an example, the decay of the triplet state of porphyrin was observed at the interface [18].

E. External Reflection Spectrometry

In the case of an organic phase containing light-absorbing compounds, external reflection (ER) absorption spectrometry [19] is more useful than TIR spectrometry. Another advantage of the ER method is that its sensitivity is higher than that of the TIR method, especially when using s-polarized light, polarized parallel to the interface. Therefore, it can be used as a universal absorption spectrometry method for adsorbed species.

F. Micro Two-Phase Sheath Flow Method

The measurement of fast interfacial reactions is very difficult, since the reaction has started just after contact of the two phases. The HSS method could measure a reaction several seconds after the contact, and the two-phase stopped-flow method could measure the reaction in the range from a few tenths of a millisecond to several hundred milliseconds. The micro two-phase sheath flow method can measure reactions as fast as <1 ms [10]. A schematic drawing of the laser-induced fluorescence measurement in the sheath flow system is shown in Fig. 3. An inner organic phase and an outer aqueous phase flow with the same line velocity. The fluorescence at the interface is observed as a function of the distance from the end of the fused-silica capillary. The distance is converted into time.

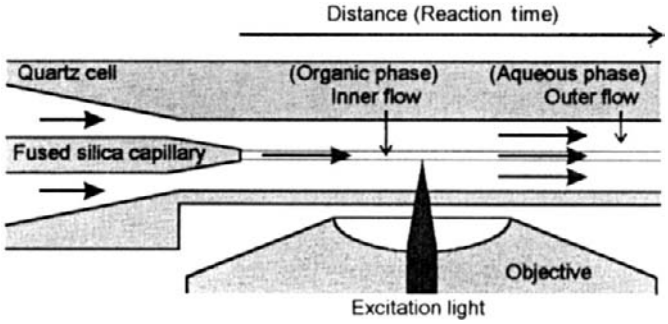

FIG. 3 Schematic drawing of laser-induced fluorescence measurement in the two-phase sheath flow system.

III. INTERFACIAL CATALYSIS IN METAL EXTRACTION SYSTEMS

A. Chelate Extraction

The HSS method was applied for the first time to the measurement of the extraction kinetics of Ni(II) and Zn(II) with *n*-alkyl-substituted dithizone (HL) [20]. The observed extraction rate constants linearly depended on both the metal ion concentration $[M^{2+}]$ and the hydrogen ion concentration in the aqueous phase. However, the observed extraction rate constant k' was not decreased with increase in the distribution constant K_D of the ligands as expected from the aqueous phase mechanism. Furthermore, the HSS method revealed that the dissociated form of the *n*-alkyl-dithizone did adsorb at the interface, generated by the vigorous agitation [5]. From these experimental results, the following scheme was concluded by considering both the aqueous phase reaction and the interfacial reaction between M^{2+} and the dissociated form of the ligand L^-:

$$M^{2+} + L^- \rightarrow ML^+ \quad k : \text{formation rate constant in bulk aqueous phase}$$

$$M^{2+} + L_i^- \rightarrow ML_i^+ \quad k_i : \text{interfacial formation rate constant}$$

The rate law for the extraction was obtained as

$$-\frac{d[M^{2+}]}{dt} = k' \frac{[M^{2+}][HL]_0}{[H^+]} \tag{1}$$

and the observed extraction rate constant k' was represented by

$$k' = (k + k_i K_L' A_i/V) K_a/K_D \tag{2}$$

where A_i/V refers to the specific interfacial area, K_a is the dissociation constant, and K_L' is the adsorption constant of L^- from the aqueous phase to the interface. Under the conditions of $k << k_i K_L' A_i/V$, Eq. (2) is reduced to

$$\log k' K_D/K_a = \log k_i + \log K_L' A_i/V \tag{3}$$

The value of $K_L' A$i was determined by the HSS method. Linear relationships for Eq. (3) were proved experimentally and gave $\log (k_i/M^{-1}s^{-1}) = 8.08$ for the Zn^{2+} system and $\log (k_i/M^{-1}s^{-1}) = 5.13$ for the Ni^{2+} system [4].

From these results, one could understand that the liquid–liquid interface catalyzed the extraction rate through the adsorption of extractants such as a solid catalyst. Kinetic

parameters in the extraction of Zn^{2+} and Ni^{2+} with dialkyl-substituted dithizones in chloroform are listed in Table 1.

A primary criterion of the interfacial catalysis is whether the ligand concentration dependence of the extractant rate shows a Nernstian isotherm or an adsorption isotherm. This was determined in the extraction of Ni(II) with a 2-hydroxy oxime such as 5-nonylsalicylaldoxime (P50) [21], 2-hydroxy-5-nonylacetophenone oxime (SME529) [22], and 2-hydroxy-5-nonylbenzophenone oxime (LIX65N) [23]. These extractants adsorbed at the interface in their neutral forms, obeying the Langmuir isotherm:

$$[HL]_i = aK'[HL]_o/(a + K'[HL]_o) \tag{4}$$

where $[HL]_i$ and $[HL]_o$ refer to the concentrations at the interface and organic phase, respectively, a is the saturated interfacial concentration, and K' is the interfacial adsorption constant defined by $K' = [HL]_i/[HL]_o$ under the condition of $[HL]_o \to 0$. The interfacial adsorptivity was confirmed also by the interfacial tension measurement as shown in Fig. 4. The initial rate constant for the extraction, r°, was represented by

$$r^\circ = k_i K_a' n_i [Ni^{2+}]/[H^+] \tag{5}$$

where K_a' is the dissociation constant at the interface and n_i is the interfacial amount of the ligand in the present experimental conditions. As shown in Fig. 5, the linear relationship between r° and n_i was experimentally confirmed. It was then concluded that the reaction between the dissociated form, L^-, and metal ions at the interface governed the extraction rate. The complex formed at the interface was not adsorbed at the interface, but extracted into the organic phase. We determined the adsorption constants of the three 2-hydroxy oximes and the complexation rate constants with Ni(II) and Cu(II) ions at the interface by means of the HSS method as listed in Table 2. The adsorption constants (K') of the neutral forms were all of the order of 10^{-3} cm and the complexation rate constants of the dissociated form with Ni(II) ion at the interface were of the order of $10^5 M^{-1}s^{-1}$ for the three extractants, though the distribution constants ($\log K_D$) were significantly different. The complexation rate constants were not seriously affected by the heptane/water interface in comparison with those in bulk aqueous solution. However, in the chloroform system, the magnitude of k_i was decreased by about two orders. This can be thought of as a specific solvent effect at the interface. The ligand might be solvated by chloroform molecules even when it was adsorbed.

The adsorptivity and the orientation of the 2-hydroxy oxime were well simulated by molecular dynamics (MD) simulations [25]. In Fig. 6, the polar groups of − OH and = N-OH of the adsorbed P50 molecule are accommodated in the aqueous phase so as to react with the Ni(II) ion in the aqueous phase [26]. The diffusive behavior of LIX65N around

TABLE 1 Kinetic Parameters in the Extraction of Zn^{2+} and Ni^{2+} with Dialkyl-Substituted Dithizones in Chloroform at 25°C

Ligand	$\log K_D/K_a$	$\log K_L' A_i/V$	$\log k'(Zn^{2+})$	$\log k'(Ni^{2+})$
Dithizone	10.17	—	−3.33	−6.42
Dimethyldithizone	11.89	−0.35	−3.05	−7.51
Diethyldithizone	12.80	0.57	−4.00	−6.93
Dibutyldithizone	15.50	3.00	−4.51	−7.45
Dihexyldithizone	17.80	5.02	−4.50	−7.51

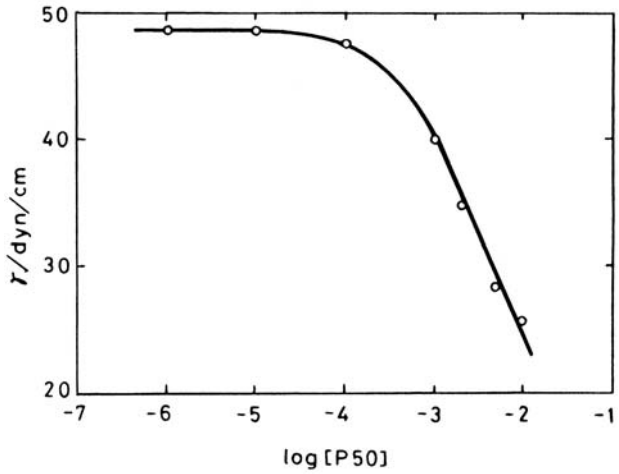

FIG. 4 Interfacial tension lowering in the heptane/aqueous phase (pH 5.53) system by the addition of 5-nonylsalicylaldoxime (P50).

the interface was also simulated for 1 ns. Figure 7 clearly shows that LIX65N is more stable at the interface than in the heptane phase. This is thought to be the reason why the reaction rate constants of Ni(II) at the heptane/water interface have almost the same magnitude as those in the aqueous phase.

Pyridylazo-ligands have been widely used in the extraction photometry of various metal ions. For example, 1-(2-pyridylazo)-2-naphthol (Hpan) is one of the most well known reagents, but it shows a slow extraction rate for some metal ions such as Ni(II) and Pd(II). 2-(5-Bromo-2-pyridylazo)-5-diethylaminophenol (5-Br-PADAP) is a relatively new reagent, which is more sensitive than Hpan for Cu(II), Ni(II), Co(II), and Zn(II), giving the metal complexes molar absorptivities of the order of 10^5 $M^{-1}cm^{-1}$.

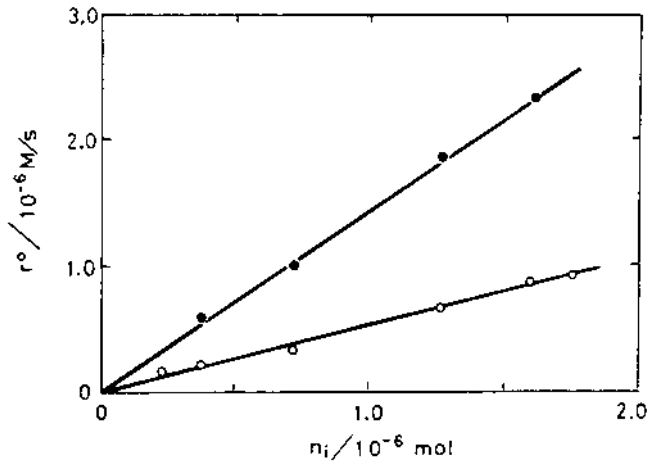

FIG. 5 Linear correlation between the initial extraction rate and the interfacial amount of P50: (●) $[Ni^{2+}] = 8.0 \times 10^{-3}$M; (○)$[Ni^{2+}] = 1.0 \times 10^{-3}$M.

TABLE 2 Parameters in the Adsorption and Extraction of Ni(II) and Cu(II) with 2-Hydroxy Oxime in 0.1M (H, Na)ClO_4 at 25°C

2-Hydroxy oxime	pK_a	$\log K_D$ (org. solvent)	$\log a$ (mol/cm^2)	$\log A_i$ (cm^2)	$\log K'$ (cm)	$\log k_i$ ($M^{-1}s^{-1}$)
Ni(II)/5-Nonylsalicyl aldoxime(P50)	9.00	3.36 (heptane)	−9.60	4.11	−3.34	4.57
Ni(II)/2-Hydroxy-5-nonylacetophenone oxime(SME529)	9.79	3.99 (heptane)	−9.70	4.29	−3.29	5.11
Ni(II)/2-Hydroxy-5-nonylbenzophenone oxime (LIX65N)	8.70	5.69 (heptane)	−9.76	4.28	−2.97	5.14
		4.6[a] (chloroform)	$\log aA_I = -6.50$	$\log K_i(cm^3) = -0.16$		3.33
Cu(II) /LIX65N	8.70	5.69 (heptane)	−9.76	4.28	−2.97	9.87

[a] *Source*: Ref. 24.

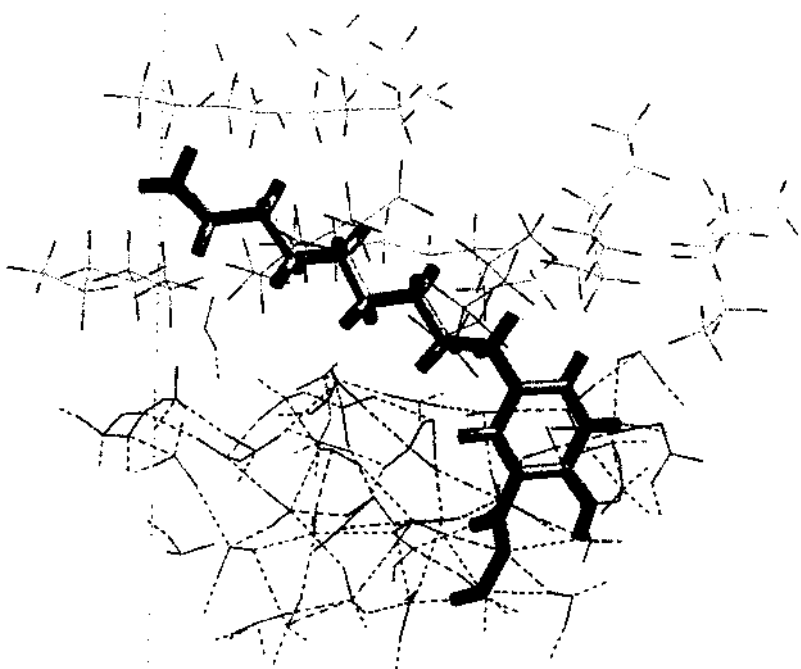

FIG. 6 Preferential hydration around the =N−OH and −OH groups of 5-nonylsalicylaldoxime (P50) in the spherical region with a radius of 8.5 Å at the heptane/water interface. Hydrogen-bonding interactions are shown with dotted lines.

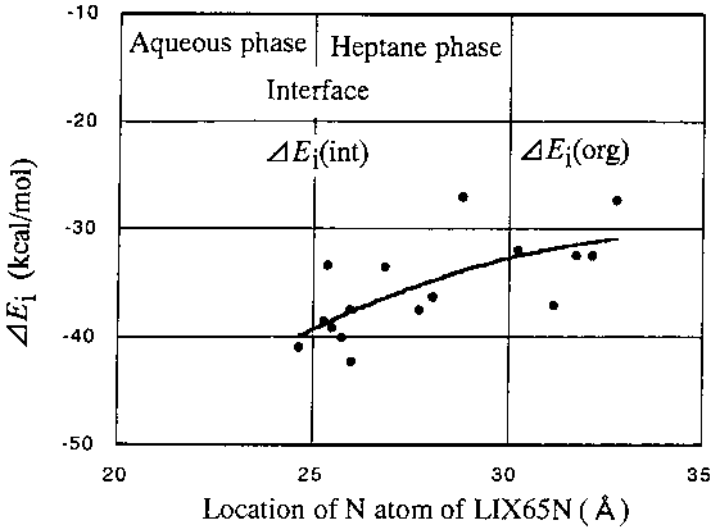

FIG. 7 Change in the solvation energy with position of the N atom of a LIX65N molecule estimated by the molecular dynamics simulation for 1 ns. It is indicated that the LIX65N molecule is stabilized at the interface during its diffusion between the interface and the bulk heptane phase.

5-Br-PADAP showed a significant adsorption at the interface of heptane/water under HSS conditions (5000 rpm). On the other hand, the adsorptivity at the toluene/water interface was very low. Hpan did not adsorb at the toluene/water interface at all. The adsorption constants of 5-Br-PADAP (HL) at the heptane/water and toluene/water interfaces were obtained as $\log K'A_i\,(\mathrm{cm}^3) = 1.64$ and $\log K'A_i\,(\mathrm{cm}^3) = -0.367$, respectively [6]. The solvent effect on the adsorptivity of the ligand directly affected the interfacial reaction rate. In the heptane system, the Ni(II) complex was not extracted into the heptane phase. On the other hand, in the toluene system the complex was extracted very slowly. Recently, the extraction rates of Ni(II) and Zn(II) with 5-Br-PADAP were studied by means of the CLM method [27]. Based on Reaction Scheme 1, the initial formation rate was represented by

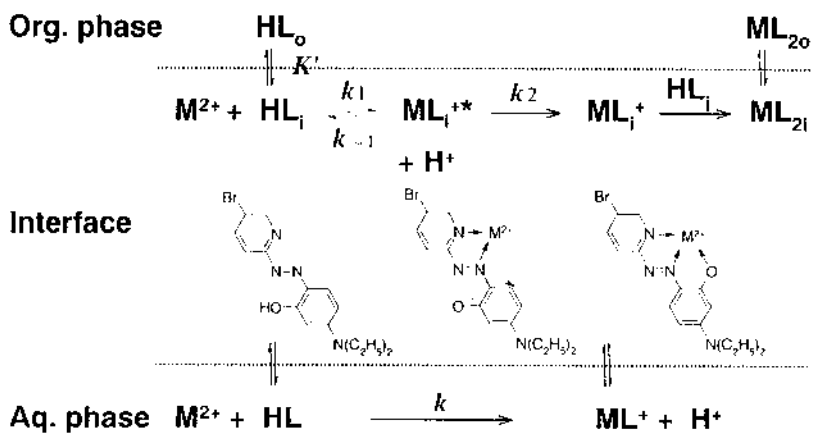

SCHEME 1

$$r_0 = \left\{ k[\mathrm{HL}]\frac{V_a}{V_o} + \left(\frac{k_1 k_2 [\mathrm{HL}]_i}{k_2 + k_{-1}[\mathrm{H}^+]}\right)\frac{A_i}{V_o} \right\} [\mathrm{M}^{2+}] \tag{6}$$

where V_a and V_o refer to the aqueous and organic phase volumes, and the definitions of k, k_1, k_2 and k_{-1} are shown in Scheme 1. The complexation proceeds almost completely at the interface. The values of the interfacial complexation rate constants are listed in Table 3. The rate constant of $k = 5.3 \times 10^2 \mathrm{M}^{-1}\mathrm{s}^{-1}$ was determined by stopped-flow spectrometry in the region where the formation rate was independent of pH. The conditional interfacial rate constants represented by $k_i = k_1 k_2 [\mathrm{HL}]_i/(k_2 + k_{-1}[\mathrm{H}^+])$ were larger at the heptane/water interface than at the toluene/water interface, regardless of metal ions. The MD simulation of the adsorptivities of 5-Br-PADAP at heptane/water and toluene/water interfaces suggested that 5-Br-PADAP could be adsorbed in the interfacial region more closely than in the aqueous phase, but that 5-Br-PADAP at the toluene/water interface was still surrounded by toluene, which might lower the probability of reaction with aqueous Ni(II) ions.

Recently, the fast reaction rate between Zn(II) ions with 5-octyloxymethyl-8-quinolinol (Hocqn) at the 1-butanol/water interface was measured by the two-phase sheath flow method [10]. The formation of a fluorescence complex at the interface was measured in a period of < 5 ms after the two-phase contact, as shown in Fig. 8. This approach is promising for the measurement of rapid interfacial reactions.

B. Ion-Association Extraction

In ion-association extraction systems, hydrophobic and interfacially adsorbable ions are included. Complexes of Fe(II), Cu(II), and Zn(II) with 1,10-phenanthroline (phen) and its hydrophobic derivatives exhibited remarkable interfacial adsorptivity, although the ligands themselves can hardly adsorb at the interface, unless protonated [28–30]. Solvent-extraction photometry of Fe(II) with phen is widely used for the determination of trace amounts of Fe(II). The extraction-rate profiles of Fe(II) with phen and its dimethyl (DMP) and diphenyl (DPP) derivatives into chloroform were investigated by the HSS method. In the presence of 0.1 M $NaClO_4$, both the formation rate of the phen complex and its interfacial adsorption were remarkably dependent on the anions of Cl^- and ClO_4^-. The initial extraction rate was described by the equation:

$$(\mathrm{d}[\mathrm{FeL_3X_2}]/\mathrm{d}t)_{t=0} = k_1[\mathrm{Fe}^{2+}][\mathrm{L}] + k_1'[\mathrm{Fe}^{2+}][\mathrm{L}]_i A_i/V_o \tag{7}$$

where k_1 and k_1' stand for the 1:1 formation rate constants of FeL^{2+} in the aqueous phase and at the interface, respectively. The apparent extraction rate constant, k_{obs}, was written as

$$k_{obs} = \frac{1}{1 + K_c' A_i/V_o}\left(\frac{k_1}{K_D} + k_i K_L' \frac{A_i}{V_o}\right) \tag{8}$$

where K_L' and K_C' refer to the adsorption constants of L and $\mathrm{FeL_3X_2}$ from the organic phase to the interface, respectively. The values of the parameters are listed in Table 3. The results showed that the rate-determining step was the 1:1 complex formation in the aqueous phase and at the interface; the adsorption of ligand accelerated the extraction (a positive catalytic effect), but the adsorption of the complex apparently suppressed the extraction rate (a negative catalytic effect). The effects of anion and solvent on the extraction rate can be explained through the change in the adsorption constant K_C' of the tris-complex ion [31].

TABLE 3 Interfacial Complexation Rate Constants of Ni(II) and Zn(II) with 5-Br-PADAP in Heptane/Water and Toluene/Water Interfaces

Metal ion	$k_1(M^{-1}s^{-1})$	$k_{-1}(M^{-1}s^{-1})$	$k_2(s^{-1})$
Heptane/water interface			
Ni(II)	1.1×10^3	4.3×10^5	4.4×10^{-2}
Zn(II)	4.4×10^4	6.9×10^5	1.1×10^{-1}
Toluene/water interface			
Ni(II)	3.2×10	2.9×10^4	3.5×10^{-1}
Zn(II)	5.1×10^4	2.0×10^6	4.8×10^{-2}

C. Synergistic Extraction

A typical kinetic synergism has been reported for the Ni(II)–dithizone (HDz)–phen chloroform system [32]. The extraction equilibrium constant ($\log K_{ex}$) was enhanced from -0.7 to 5.3 by the addition of phen:

$$Ni^{2+} + 2HDz_o + phen \rightarrow NiDz_2phen_o + 2H^+ \tag{9}$$

At the same time, the extraction rate was accelerated by the reactions in the aqueous phase [33]. The catalytic effect of phen was explained by the formation of the interfacial adsorptive complex of $NiDzphen^+$:

$$Ni^{2+} + phen \rightarrow Niphen^{2+} \qquad k = 6.8 \times 10^3 M^{-1}s^{-1} \tag{10}$$

$$Niphen^{2+} + Dz^- \rightarrow NiDzphen^+ \qquad k = 9.2 \times 10^4 M^{-1}s^{-1} \tag{11}$$

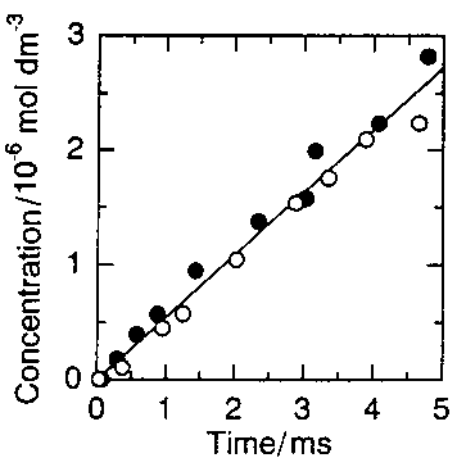

FIG. 8 Formation of a fluorescent Zn–ocqn complex at a 1-butanol/water interface measured by laser-induced fluorescence in the two-phase sheath flow system. The linear flow velocities are 0.26 $m\,s^{-1}$(●) and 0.20 $m\,s^{-1}$(○). The aqueous phase included 1.1×10^{-2}MZn^{2+} and 1.0×10^{-3} M MES buffer (pH 6.3).

The synergistic effect of DPP on the extraction of Ni(II) with dithizone was also studied and confirmed the formation of an interfacial complex [34].

It was suggested that the kinetic synergism included an interfacial intermediate complex, which was neutralized by the bonding of another ligand or by the ligand substitution to form a more extractable complex. The catalytic effect of *N,N*−dimethyl-4-(2-pyridylazo)aniline (PADA) on the extraction of $Ni(pan)_2$ is a typical example of the latter case [35]. The extraction rate of $Ni(pan)_2$ into toluene is very slow even under HSS conditions, whereas the addition of PADA at the diluted concentration of 10^{-5}M can accelerate the extraction rate by about 10 times, as shown in Fig. 9. There was observed only extraction of $Ni(pan)_2$ and no consumption in PADA after the extraction, while a significant decrease in the organic phase concentration of PADA was observed during the extraction under HSS conditions. These results were analyzed by the mechanism of the interfacial ligand-substitution reaction:

$$Ni(pada)_i^{2+} + Hpan_o \rightarrow Ni(pan)(pada)_i^{+} + H^{+} \qquad k': \text{ formation rate constant}$$

$$Ni(pan)(pada)_i^{+} + Hpan_o \rightarrow Ni(pan)_{2,o} + pada_o + H^{+}$$

The value of k' was obtained as 90 $M^{-1}s^{-1}$ [35]. The key process of the catalytic extraction of Ni(II)–Hpan–PADA system was the fast aqueous phase formation of $Ni(pada)^{2+}$, which adsorbed at the interface and increased the reaction probability with Hpan in the organic phase.

Usually, acidic conditions decrease the extraction rate of metal ions with acidic ligands, because of the suppression of the dissociation of extractant. However, in the extraction of Pd(II) with 5-Br-PADAP, the lowering of pH accelerated the extraction rate [36]. The protonation of 5-Br-PADAP increased its adsorptivity, but did not decrease the reactivity with Pd(II) as the nitrogen atom of diethylamine or azo-group was protonated. Interfacial reactions in this system are represented by Scheme 2. The rate constants obtained in heptane/water and toluene/water interfaces by the CLM method are listed in Table 4 [12]. The rate constant is greater for the reaction with protonated 5-Br-PADAP, because Pd(II) is coordinated by chloride ions charged negatively as $PdCl_3^-$ and $PdCl_4^{2-}$. This finding should provide an inspiration for the design of a new type of catalytic extractant being interfacially adsorbable and strongly reactive for a specific metal ion.

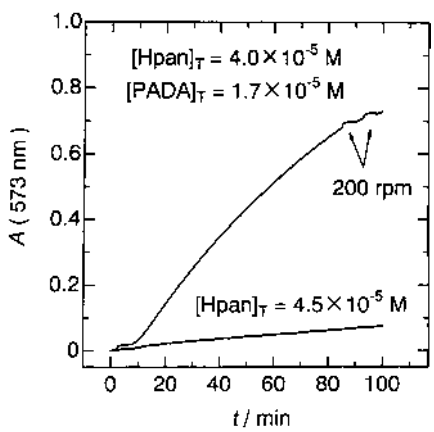

FIG. 9 Catalytic effect of PADA on the extraction rate of Ni^{2+} with Hpan; $[Ni^{2+}]_T = 1.0 \times 10^{-3}$ M and pH 5.4–5.5. The subscript T refers to the total concentration.

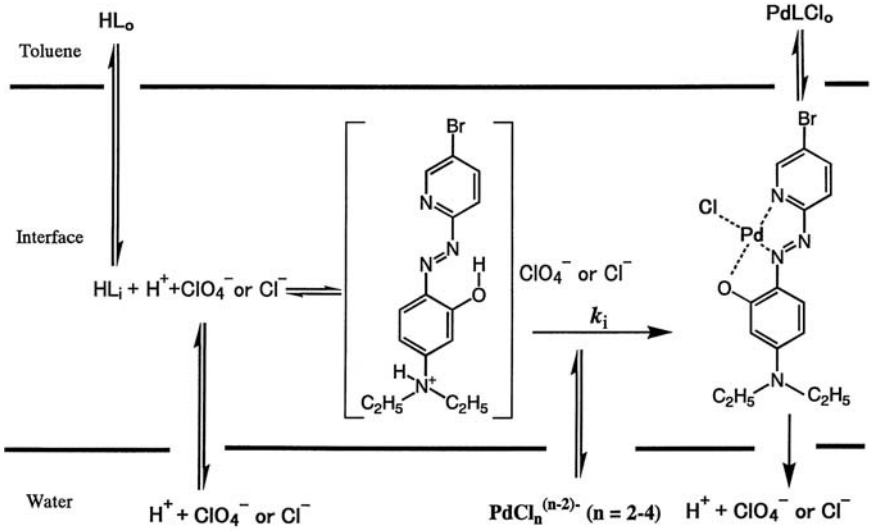

SCHEME 2

IV. INTERFACIAL AGGREGATION OF METAL COMPLEXES

A unique feature of the interfacial catalysis for metal complexes is the formation of the aggregate of the complex. As pointed out in many studies [3], the liquid–liquid interface can be saturated by an adsorbate with a saturated interfacial concentration of 10^{-10} mol/cm^2, which can be attained even under a diluted bulk concentration. This means that the interface is ready to become a two-dimensionally condensed state for the adsorbate. This is realized in, e.g., the formation of aggregates of the metal complex at a liquid–liquid interface. In a procedure for the solvent extraction of metal ions, the formation of some precipitate at the interface is encountered. This kind of phenomenon should be studied more carefully from the viewpoint of the interfacial aggregation of metal complexes.

A typical example of interfacial aggregation is that of the interfacial protonation of tetraphenylporphyrin (TPP). The aggregation rate of H_2TPP^{2+} in a dodecane/sulfuric acid solution was measured by a two-phase stopped-flow method [9] and a CLM method [37]. In the former method, it was found that the stagnant layer of 1.4 μm still existed in the dodecane phase side of the droplet interface even under the highly dispersed system. In

TABLE 4 Rate Constants ($M^{-1}s^{-1}$) for the Reaction of Pd(II) with Neutral and Protonated 5-Br-PADAP in the Aqueous Phase and at the Heptane/Water and Toluene/Water Interfaces

Reaction site	Neutral 5-Br-PADAP (HL)	Protonated 5-Br-PADAP (H_2L^+)
Aqueous phase	5.7×10^2	5.7×10^2
Heptane/water interface	5.3×10	5.1×10^2
Toluene/water interface	6.6×10	3.3×10^2

the CLM method, the liquid membrane phase of 50–100 μm thickness behaved as a stagnant layer where the TPP molecule migrated according to its self-diffusion rate, followed by a rapid protonation and aggregation of the diprotonated species.

Recently, the formation of a dinuclear Eu(II) complex at a toluene/water interface was measured by time-resolved total-reflection fluorometry. When bathophenanthroline sulfate (bps) was added to the extraction system of Eu(III) with 2-thenoyltrifuluoroacetone (Htta), a double-component luminescence decay profile was observed and it showed the presence of a binuclear complex at the interface [16]. The observed lifetimes $\tau = 22\,\mu$s and 203 μs were attributed to the binuclear complex $Eu_2(tta)_2(bps)_2$ and the mononuclear complex $Eu(tta)_2bps^-$. A lifetime of the binuclear complex shorter than $\tau = 98\,\mu$s for an aqua-Eu(III) ion suggested charge-transfer deactivation in the complex.

An aggregate of the Pd(II)–tetrapyridylporphyrin (tpyp) complex was formed at a toluene/water interface, when a tpyp toluene solution was contacted with a $PdCl_2$ aqueous solution under acidic conditions. Palladium(II) was bound to the nitrogen atoms of the pyridyl group, not to the central pyrrole nitrogens. Depending on the concentration ratio of Pd(II)/tpyp, it formed two kinds of aggregates: an aggregate (AS1) observed at a lower tpyp concentration had a 3:1 Pd/tpyp ratio with a shorter lifetime of 0.15 ns, and another one (AS2) observed at higher tpyp concentration had a 1:1 ratio with a longer lifetime of 1.1 ns. The 1:1 aggregate ($\lambda_{max} = 668$ nm) showed a red-shift of 12 nm from the 3:1 aggregate ($\lambda_{max} = 656$ nm), and suggested a π stacking interaction in the 1:1 aggregate (Fig. 10) [38]. By considering the result obtained by rotational relaxation measurements, the structures of AS1 and AS2 were postulated as shown in Fig. 11.

V. CONCLUDING REMARKS

Interfacial catalysis in the solvent-extraction system for metal ions, and, in particular, in an oil/water system, is described in this chapter and some important features of the interfacial catalysis are remarked:

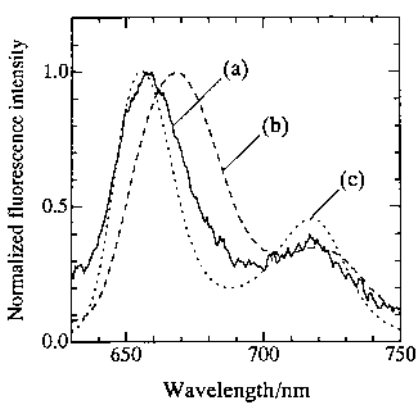

FIG. 10 Fluorescence spectra of a Pd(II)–tpyp complex at a toluene/water interface (a and b). The spectra of (a) and (b) correspond to a 3:1 and a 1:1 composition aggregate, respectively. The spectrum (c) is the fluorescence spectrum of tpyp in toluene.

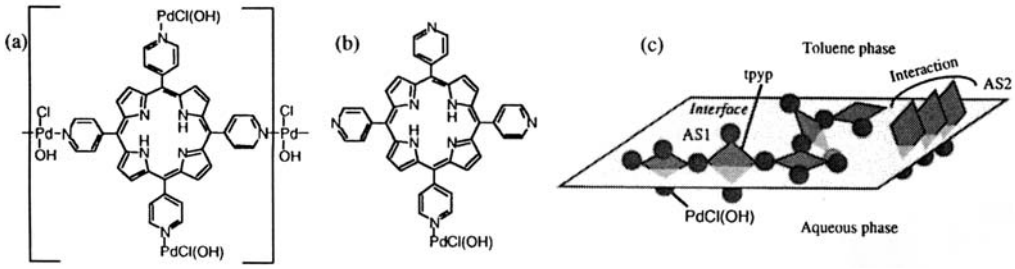

FIG. 11 Probable structures of (a) AS1 and (b) AS2 units and (c) a schematic illustration of AS1 and AS2 at the interface.

1. The most important step in the interfacial catalysis in complex formation is the adsorption of extractant, which increases the interfacial concentration; thus, the interfacial complexation and extraction rate are accelerated. The kinetic solvent effect of the liquid–liquid interface is very sensitive to the location where the ligand molecule is adsorbing. The interfacial solvent effect in the nanometer region has to be studied more extensively.
2. Formation and adsorption of a labile and charged complex at the interface can greatly facilitate a subsequent ligand-exchange reaction to produce a more extractable or neutral complex.
3. Interfacial catalysis in metal complexation facilitates the formation of aggregates of a complex by its accumulation at the interface. This is why the interfacial concentration can be greatly increased over the saturated one expected from a monomolecular layer model.
4. Interfacial catalysis should be designed by using the knowledge of the interfacial adsorptivity of ligands and complexes, and their reactivity, which all depend on their molecular structure.
5. MD simulations have proved to be very useful in a prediction of interfacial adsorptivity and reactivity of ligands.
6. The design of new experimental methods to measure the interfacial reaction is very important for the development of the chemistry of interfacial catalysis.

REFERENCES

1. PR Danesi. In:J Rydberg, C Musikas, GR Choppin, ed. Principles and Practices of Solvent Extraction. New York: Marcel Dekker, 1992, pp 157–207.
2. H Watarai. Trends Anal Chem 12:313–318, 1993.
3. H Watarai. In: AG Volkov, ed. Liquid Interfaces in Chemical, Biological, and Pharmaceutical Applications. New York: Marcel Dekker, 2000, pp 355–372.
4. H Watarai, H. Freiser. J Am Chem Soc l05:l89–190, l983.
5. H Watarai, H Freiser. J Am Chem Soc l05:l91–194, l983.
6. H Watarai, M Gotoh, N Gotoh. Bull Chem Soc Jpn 70:957–964, 1997.
7. H Watarai, Y Chida. Anal Sci 10:105-107, 1994.
8. H Watarai, Y Saitoh. Chem Lett 283–284, 1995.
9. H Nagatani, H Watarai. Anal Chem 68:1250–1253, 1996.
10. T Tokimoto, S Tsukahara, H Watarai. Chem Lett 204–205, 2001.
11. GJ Hanna, RD Noble. Chem Rev 85:583–598, 1985.

12. A Ohashi, H Watarai. Anal Sci 17:1313–1319, 2001.
13. H Nagatani, H Watarai. Chem Lett 701–702, 1999.
14. A Ohashi, H Watarai. Chem Lett 1238–1239, 2001.
15. H Watarai, F Funaki. Langmuir 12:6717–6720, 1996.
16. M Fujiwara, S Tsukahara, H Watarai. Phys Chem Chem Phys 1:2949–2951, 1999.
17. S Tsukahara, Y Yamada, T Hinoue, H Watarai. Bunseki Kagaku 47:945–952,1998.
18. S Tsukahara, H. Watarai. Chem Lett 89–90, 1999.
19. K Fujiwara, H Watarai. Bull Chem Soc. Jpn 74:1885–1890, 2001.
20. H Watarai, L Cunningham, H Freiser. Anal Chem 54:2390–2392, 1982.
21. H Watarai, K Satoh. Langmuir 10:3913–3915, 1994.
22. H Watarai, M Takahashi, K Shibata. Bull Chem Soc Jpn 59:3469–3473, 1986.
23. H Watarai, M Endo. Anal Sci 7:137–140, 1991.
24. K Akiba, H Freiser. Anal Chim Acta 136:329–337, 1982.
25. Y Onoe, H Watarai. Anal Sci 14:237–239, 1998.
26. H Watarai, Y Onoe. Solv Extr Ion Exch 19:155–166, 2001.
27. Y Yulizar, A Ohashi, H Watarai. Anal Chim Acta 447:247–254, 2001.
28. H Watarai. J Phys Chem 89:384–387, 1985.
29. H Watarai. Talanta 32:817–820, 1985.
30. H Watarai, Y Shibuya. Bull Chem Soc Jpn 62:3446–3450, 1989.
31. H Watarai, K Sasaki, N Sasaki. Bull Chem Soc Jpn 63:2797–2802, 1990.
32. B Freiser, H Freiser. Talanta 17:540-543, 1970.
33. H Watarai, K Sasaki, K Takahashi, J Murakami. Talanta 42:1691–1700, 1995.
34. H Watarai, K Takahashi, J Murakami. Solv Extr Res Dev Jpn 3:109–116, 1996.
35. Y Onoe, S Tsukahara, H Watarai. Bull Chem Soc Jpn 71:603–608, 1998.
36. A Ohashi, S Tsukahara, H Watarai. Anal Chim Acta 364:53–62, 1998.
37. H Nagatani, H Watarai. Anal Chem 70:2860–2865, 1998.
38. N Fujiwara, S Tsukahara, H Watarai. Langmuir 17:5337–5342, 2001.

4

The Role of Water Molecules in Ion Transfer at the Oil/Water Interface

TOSHIYUKI OSAKAI Kobe University, Kobe, Japan

I. INTRODUCTION

It is well known that water molecules are coextracted into water-immiscible organic solvents with hydrophilic ions such as Li^+, Na^+, K^+, Ca^{2+}, Ba^{2+}, Cl^-, and Br^- [1–17]. Even water-immiscible organic solvents such as nitrobenzene (NB) usually dissolve a considerable amount of water (e.g., 0.168 M H_2O in NB [15]). Accordingly, such phenomena can be elucidated in terms of selective hydration of ions in mixed solvents [18]. This is a key concept intimately related to important ion-transfer processes in artificial systems such as solvent extraction, membrane transport, phase-transfer catalysis, and ion-selective electrodes. Also, it has a fundamental significance for understanding the role of water in biological systems including lipid membranes, ion channels, etc. For instance, a significant role of water molecules in hydrophobic cores in proteins has been recognized (e.g., a light-driven proton pump, bacteriorhodopsin [19]). Furthermore, in recent years, the cotransport of water by ions has been dealt with in molecular dynamics simulations [20–22].

Nevertheless, in previous Born-type theories [23–28] of the standard Gibbs energy ($\Delta G_{tr}^{\circ,o\to w}$) of ion transfer at the oil (O)/water (W) interface, it is postulated or tacitly understood that when an ion is transferred across the O/W interface, it strips off solvated molecules completely, and hence the crystal ionic radius is usually employed for the calculation of $\Delta G_{tr}^{\circ,o\to w}$. Although Abraham and Liszi [26], in considering the transfer between mutually saturated solvents, were aware of the effects of hydration of ions in organic solvents in which water is quite soluble (e.g., 1-octanol, 1-pentanol, and methyl isobutyl ketone), they concluded that in solvents such as NB and 1,2-dichloroethane, the solubility of water is rather low and most ions in the water-saturated solvent exist as unhydrated entities. As described above, however, even a *water-immiscible* organic solvent such as NB dissolves a considerable amount of water. In such a medium, hydrophilic ions such as Li^+, Na^+, Ca^{2+}, Ba^{2+}, Cl^-, and Br^- are selectively solvated by water. This phenomenon has become apparent since at least 1968 by solvent-extraction studies with the Karl Fischer method [1–15]. Rais et al. [1] and Iwachido and coworkers [2–5] determined hydration numbers, i.e., the number of coextracted water molecules, for alkali and alkaline earth metal ions in NB. Some inorganic anions (Cl^-, Br^-, I^-, SCN^-, ClO_4^-, and NO_3^-) have also been found to coextract water into NB [6–9]. Similar phenomena have further been observed in solvents other than NB (e.g., 1,1- and 1,2-dichloroethane, 4-methyl-2-pentanone, chloroform, NB–benzene mixtures, and hexane) [8–14]. If these observations are valid, we should reconsider the previous theories of $\Delta G_{tr}^{\circ,o\to w}$ in which the hydration of

ions in O is not properly taken into account. From this point of view, Osakai et al. [15] reaffirmed the coextraction of water into NB for a variety of common ions and determined their accurate hydration numbers in NB. Based on the experimental data, a new, nonBornian theory has been proposed, in which a hydrophilic ion, being preferentially hydrated in the O phase, is assumed to transfer across the interface as the hydrated ion [29].

The purpose of this chapter is to discuss mainly the hydration behavior of ions in NB and its significance in the theory of $\Delta G_{\mathrm{tr}}^{\circ,\mathrm{o}\to\mathrm{w}}$.

II. HYDRATION NUMBER OF IONS IN NITROBENZENE

A. Distribution Behavior of Ions at the NB/W Interface

Since NB has a relatively high permittivity ($\varepsilon^{\circ} = 34.8$), the ion-pair formation in NB is usually of less significance. Thus, in the "ion-pair" extraction systems using NB, the formation of ion pairs is not necessarily required to be considered for low overall concentrations of the salts. According to the proposed theory [30–33], the distribution equilibrium in such a system can be described in terms of the standard ion-transfer potential [$\Delta_{\mathrm{o}}^{\mathrm{w}}\phi^{\circ} = -(\Delta G_{\mathrm{tr}}^{\circ,\mathrm{o}\to\mathrm{w}}/zF)$; z, the charge number of the ion; F, the Faraday constant] as a measure of extractability (or hydrophobicity) of an individual ion. When m kinds of ions are distributed at equilibrium between the O/W interface, the Galvani potential difference $\Delta_{\mathrm{o}}^{\mathrm{w}}\phi \equiv \phi^{\mathrm{w}} - \phi^{\mathrm{o}}$ across the O/W interface is given by [30–32]

$$\sum_{i=1}^{m} \frac{z_i c_i^{0,\mathrm{w}}}{1 + \exp\left[\dfrac{z_i F}{RT}(\Delta_{\mathrm{o}}^{\mathrm{w}}\phi - \Delta_{\mathrm{o}}^{\mathrm{w}}\phi_i^{\circ})\right]} + \sum_{i=1}^{m} \frac{z_i c_i^{0,\mathrm{o}}}{1 + \exp\left[\dfrac{z_i F}{RT}(\Delta_{\mathrm{o}}^{\mathrm{w}}\phi - \Delta_{\mathrm{o}}^{\mathrm{w}}\phi_i^{\circ})\right]} = 0 \tag{1}$$

where z_i and $\Delta_{\mathrm{o}}^{\mathrm{w}}\phi_i^{\circ}$ are, respectively, the charge number (including the sign) and the standard ion-transfer potential of ion i ($= 1, 2, 3, \ldots m$), $c_i^{0,\mathrm{w}}$ and $c_i^{0,\mathrm{o}}$ are the initial concentrations of the ion in W and O, and R and T have their usual meanings. In Eq. (1), it is assumed that the volume ratio of the two phases is 1. If the values of $\Delta_{\mathrm{o}}^{\mathrm{w}}\phi_i^{\circ}$ are known for all ions in the system of interest, the value of $\Delta_{\mathrm{o}}^{\mathrm{w}}\phi$ can be determined from Eq. (1). The distribution ratio of each ion can then be calculated from the Nernst equation:

$$D_i \equiv \frac{c_i^{\mathrm{o}}}{c_i^{\mathrm{w}}} = \exp\left[\frac{z_i F}{RT}(\Delta_{\mathrm{o}}^{\mathrm{w}}\phi - \Delta_{\mathrm{o}}^{\mathrm{w}}\phi_i^{\circ})\right] \tag{2}$$

where c_i^{o} and c_i^{w} are the equilibrium concentrations of ion i in O and W, respectively. Here, it is assumed for simplicity that the concentration of an ion is equal to the activity.

In our previous study [15], various kinds of cations [alkali and alkaline earth metal ions, Me_4N^+, Et_4N^+, n-Bu_4N^+, and tetraphenylarsonium ($TPAs^+$) ion] and anions [halide ions, SCN^-, ClO_4^-, NO_3^-, and tetraphenylborate (TPB^-) ion] were distributed in the NB–W system, in order to determine their accurate hydration numbers in NB. The distribution experiments for the cations were performed by using TPB^- or dipicrylaminate (DPA^-) as an extractant. For the distribution experiments on the anions, some hydrophobic cations including n-Bu_4N^+, n-Pen_4N^+, n-Hep_4N^+, and tris(1,10-phenanthroline)iron(II) [$Fe(phen)_3^{2+}$] were used as extractants.

As an example, the results of distribution experiments for alkali and alkaline earth metal ions with DPA^- are shown in Fig. 1. In these experiments, DPA^- salts of Li^+, Na^+, Ca^{2+}, or Ba^{2+} were added to the aqueous phase, whereas the DPA^- salts of K^+ or Rb^+

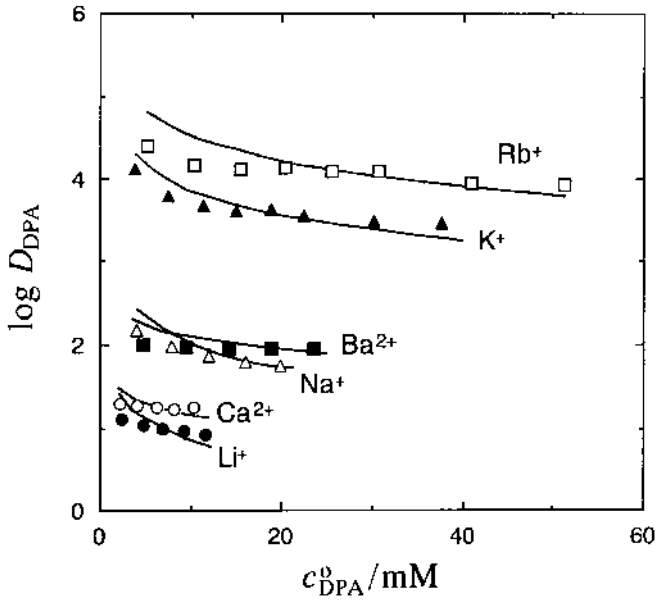

FIG. 1 Dependences of distribution ratios of alkali and alkaline earth metal ions on the "equilibrium" concentration of DPA^- in NB (the legend for Fig. 2 in Ref. 15 should be revised). Each solid line shows a regression curve obtained with Eqs. (1) and (2). (From Ref. 15.)

were added to the NB phase. In order to prevent formation of emulsions, the nitrate or chloride salt of each ion was added to the aqueous solution (the ionic strength, $I = 0.1$). The pH of the aqueous phase was adjusted to 10 by using a hydroxide of the respective metal ion. The equilibrium concentration of DPA^- in the aqueous phase was then determined spectrophotometrically. In Fig. 1, the logarithm of the distribution ratio of DPA^- is plotted against the equilibrium concentration of DPA^- in NB. Each solid line shows the regression curve, which was calculated using Eqs (1) and (2). In the fitting analysis, the $\Delta^{w}_{o}\phi^{\circ}_{i}$ value of each metal ion was an adjusting parameter, whereas the $\Delta^{w}_{o}\phi^{\circ}_{i}$ value of DPA^- was fixed to the literature value (i.e., 0.407 V [34]). The $\Delta^{w}_{o}\phi^{\circ}_{i}$ values for Li^+, Na^+, K^+, Rb^+, Ca^{2+}, and Ba^{2+} obtained in the regression analysis are 0.420, 0.347, 0.237, 0.190, 0.364, and 0.307 V, respectively, which are consistent with the literature values [34,35]: 0.395, 0.354, 0.242, 0.201, 0.349, and 0.320 V, respectively. Thus, Eqs (1) and (2), which were obtained by assuming no ion-pair formation, were available for this system, suggesting that the metal ions were mostly unassociated in NB. Similar results were obtained for other distribution experiments for cations with TPB^- and for anions with n-Bu_4N^+ and $Fe(phen)^{2+}_3$ (for further details, see Ref. 15).

B. Number of Coextracted Water Molecules

In the above-mentioned distribution experiments [15], the equilibrium concentration of water in the NB phase was determined by means of a Karl Fischer coulometer. The increase in water concentration in NB ($\Delta[H_2O]$) with extraction of an ion was then evaluated as a function of equilibrium concentration of the ion in NB. A typical example, obtained in the DPA^- system, is shown in Fig. 2. As seen in the figure, hydrophobic

organic cations (Me_4N^+, Et_4N^+, and $TPAs^+$) showed no increase in water concentration, indicating that these cations as well as DPA^- had no ability to transport water to NB. In contrast, hydrophilic metal ions showed a distinguishing increase. The slope of each linear plot should correspond to the number (n_{ex}) of water molecules coextracted to NB with a metal ion, which are listed in Table 1 together with those determined in other systems. In Table 1, some literature values of n_{ex} [1,2,7–9] are shown in parentheses, being in fair agreement with those determined here. As is also seen in the table, for both cations and anions, the n_{ex} values determined were only slightly dependent on the nature of the extractant (i.e., co-ion). This implies that ion-pair formation in NB is of less significance or that the ions are almost dissociated. Accordingly, the n_{ex} value determined for each ion can be considered as the true hydration number (n_h) of the ion in NB, i.e., the number of water molecules being certainly associated with an individual ion in NB. Thus, it has been reaffirmed that alkali and alkaline earth metal ions and some hydrophilic inorganic anions have the ability to transport 0.2–14 water molecules to NB.

III. RELEVANCE TO THE GIBBS ENERGY OF ION TRANSFER

A. Proposed Model of Interfacial Transfer of a Hydrophilic Ion

On the basis of the above experimental findings, we proposed a new model, as depicted in Fig. 3 [15]. In this model, the hydrophilic ion transfers from W to O with some water molecules associated with the ion. A typical example in the figure shows that a sodium ion transfers across the NB/W interface with four water molecules. In the theoretical treatment of transfer energy of such a hydrophilic ion the transferring species should, therefore,

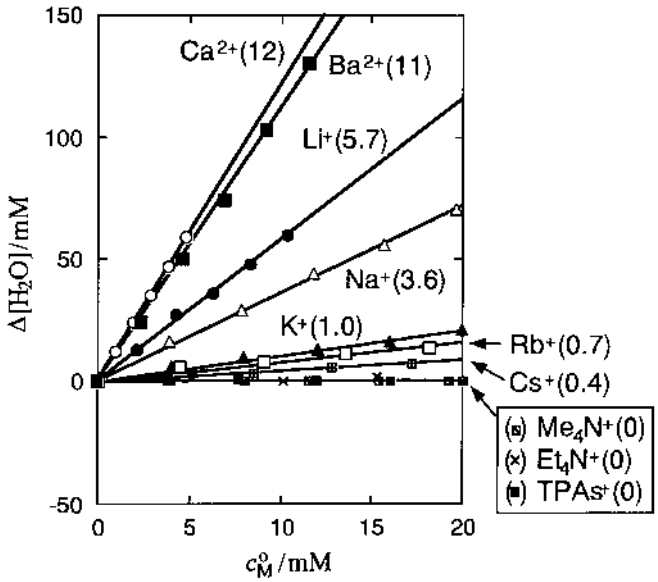

FIG. 2 Plots of the increase in water concentration in NB ($\Delta[H_2O]$) with extraction of cations with DPA^- against the equilibrium cation concentration in NB. Each value in parentheses shows the number (n_{ex}) of coextracted water molecules per ion. (From Ref. 15.)

TABLE 1 Numbers (n_{ex}) of Coextracted Water Molecules in NB and Radii (r_h) of Hydrated Ions at 25°C

Cation	n_{ex}			r_h (nm)	r_c^a (nm)
	TPB^- system	DPA^- system	av		
Li^+	6.3	5.7 (4.2 [1]; 5.5 [2])	6.0±0.4	0.351	0.073
Na^+	4.0	3.6 (3.6 [1]; 3.5 [2])	3.8±0.3	0.307	0.116
K^+		1.0 (1.0 [1]; 1.3 [2])	1.0	0.220	0.152
Rb^+		0.7 (0 [1]; 0.7 [2])	0.7	0.212	0.166
Cs^+		0.4 (0 [1]; 0.7 [2])	0.4	0.206	0.181
Ca^{2+}	15	12 (13 [2])	14±2	0.467	0.114
Ba^{2+}	10	11 (9.4 [2])	11±1	0.435	0.149
Me_4N^+		0	0		0.279
Et_4N^+	0	0	0±0		0.337
n-Bu_4N^+	0 (∼0 [8])		0		0.413
Ph_4As^+		0	0		0.426

Anion	n_{ex}					r_h (nm)	r_c^a (nm)
	n-Bu_4N^+ system	n-Pen_4N^+ system	n-Hep_4N^+ system	$Fe(phen)_3^{2+}$ system	av		
Cl^-		4.0 (3.3 [9])			4.0	0.322	0.167
Br^-	2.1 (1.8 [9])	2.1	2.0	—[b] (5.5 [7])	2.1±0.1	0.276	0.182
I^-	0.9	0.8	1.0	1.0[c] (2.1 [7])	0.9±0.1	0.248	0.206
SCN^-	1.1	1.1	1.0	1.1[c] (1.9 [7])	1.1±0.1	0.260	0.213
ClO_4^-	0.3	0.2	0.2	0.1[c] (0.64 [7])	0.2±0.1	0.244	0.236
NO_3^-	(∼1.4 [8])			1.7[c]	1.7	0.267	0.189
TPB^-	0 (∼0 [8])	0	0	0[c]	0		0.421

[a] Crystal (or bare) ionic radii.
[b] No reliable value could be obtained due to extremely low extractability (the distribution ratio $D < 0.03$).
[c] Corrected for the contribution ($n_{ex} = 0.3$) from $Fe(phen)_3^{2+}$.
Source: Ref. 15.

be regarded as the "hydrated" ion. Consequently, the radii (r_h) of hydrated ions in NB were estimated from the hydration numbers ($n_h = n_{ex}$) and crystal ionic radii (r_c) by

$$r_h = \sqrt[3]{\frac{3n_h}{4\pi d} + r_c^3} \tag{3}$$

where d is the density of water in the hydration shell (here, the value of d is assumed to be the same as that of bulk water, i.e., 3.33×10^{28} molecule m^{-3}). The estimated values of r_h are also shown in Table 1.

As shown in Fig. 4, an excellent correlation of r_h with the Stokes radius (r_s) [36] was observed for hydrated cations (alkali and alkaline earth metal ions):

$$(r_h/\text{nm}) = 1.310(r_s/\text{nm}) + 0.055 \quad (R = 0.997) \tag{4}$$

although there was no clear correlation for anions. In this equation and the following remarks, R represents the correlation coefficient. This correlation suggests the similarity of

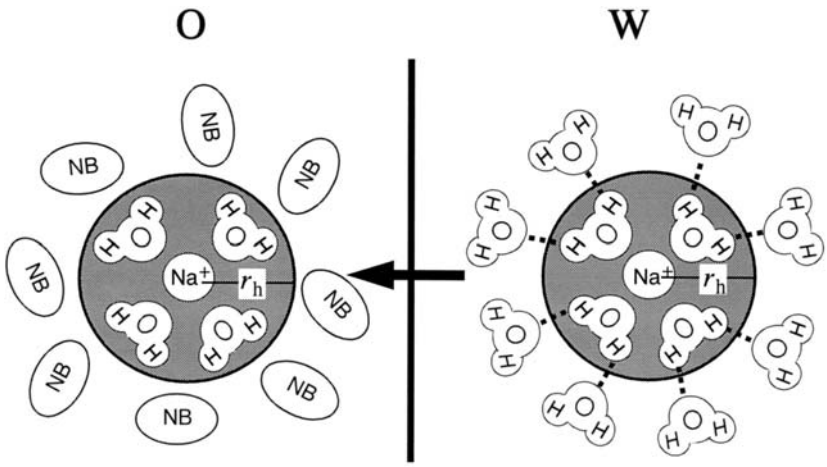

FIG. 3 Proposed model of the transfer of a hydrophilic ion across the O/W interface. The illustration shows the transfer of Na^+ from W to NB as a typical example. (From Ref. 15.)

transfer processes of these metal ions at the O/W interface to their transport properties in bulk water. The water molecules, which are strongly bound to the metal ions in W, appear to be undissociated even in their transfers across the O/W interface. In this connection, Zavitsas [37] has recently reported that the hydration numbers of Li^+ (6.6 ± 0.6), Na^+ (3.9 ± 0.5), K^+ (1.7 ± 0.5), Cs^+ (0.0 ± 1), Ca^{2+} (12 ± 2), and Ba^{2+} (10.5 ± 1.5) obtained from measurements of a classical colligative property (i.e., freezing-point depression) are in remarkable agreement with those obtained from our extraction experiments (cf. Table 1).

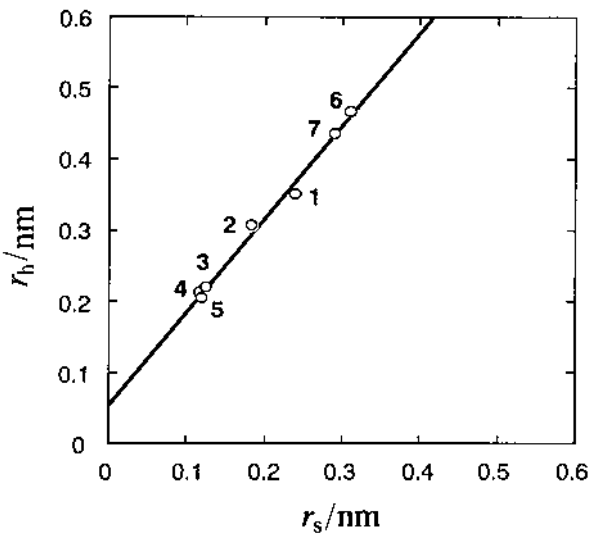

FIG. 4 Correlation of the hydrated radius (r_h) with the Stokes radius (r_s) for alkali and alkaline earth metal ions: (1) Li^+, (2) Na^+, (3) K^+, (4) Rb^+, (5) Cs^+, (6) Ca^{2+}, and (7) Ba^{2+}. The solid line represents the regression line, which is given by Eq. (4). (From Ref. 15.)

For prediction of $\Delta G_{tr}^{\circ,o\to w}$ of the hydrophilic ion whose n_h value is unknown, it is desirable that the n_h value can be obtained from the ionic radius (r_c) and charge (z) only. It has been found that the plots of n_h (i.e., n_{ex}) against the quantity z/r_c lie on a quadratic curve [29]:

For cations:

$$n_h = -0.566 + 0.0091(z/r_c) + 0.04745(z/r_c)^2 \quad (R = 0.966) \tag{5}$$

For anions:

$$n_h = 5.844 + 3.775(z/r_c) + 0.5661(z/r_c)^2 \quad (R = 0.930) \tag{6}$$

where r_c is in nanometers. Equations (5) and (6) are applicable in the range of $z/r_c > 5$ and $z/r_c < -4$, respectively. Using these equations, though somewhat roughly, we can predict the n_h value of a hydrophilic ion. Regarding the cations, however, their n_h values would be obtained more accurately from the Stokes radii by using the relations of Eqs (3) and (4).

B. Invalidity of Bornian Electrostatic Models

As seen in Table 1, the order of the magnitude of r_h for alkali metal ions is the reverse of that of the magnitude of r_c. This means that a more hydrophilic ion has a larger r_h. However, this fact does contradict the expectation from Bornian electrostatic theories. In the classical Born model [23], an ion is considered as a hard sphere of a given radius (r) immersed in a continuous medium, and its resolvation energy, i.e., $\Delta G_{tr}^{\circ,o\to w}$, is then expressed as a difference between electrostatic energies for charging the ion up to ze (e is the elementary charge) in O and W:

$$\Delta G_{tr}^{\circ,o\to w}(\text{Born}) = -\frac{N_A z^2 e^2}{8\pi\varepsilon_0 r}\left(\frac{1}{\varepsilon^o} - \frac{1}{\varepsilon^w}\right) \tag{7}$$

where N_A is the Avogadro constant, ε_0 is the permittivity of vacuum, and ε^o and ε^w are relative permittivities of O and W, respectively. As can be seen from this equation, it is expected that the larger radius an ion has, the less negative $\Delta G_{tr}^{\circ,o\to w}$ value the ion has, i.e., the more hydrophobic it becomes. This would show that, e.g., Li^+ with $r_h = 0.351$ nm is more hydrophobic than Cs^+ with $r_h = 0.206$ nm, but this is of course not the case. An invalidity of the Born model will be shown by the following more quantitative analysis.

So far it has been customary to divide $\Delta G_{tr}^{\circ,o\to w}$ into two (or three) parts corresponding to electrostatic and nonelectrostatic (and specific) ion–solvent interactions [24,27,28,38,39]. Such a division is to a certain degree arbitrary since different effects may overlap. However, it is useful to evaluate the individual effects. In an analogous manner we divided $\Delta G_{tr}^{\circ,o\to w}$ into two terms:

$$\Delta G_{tr}^{\circ,o\to w} = \Delta G_{tr}^{\circ,o\to w}(z\text{-dep}) + \Delta G_{tr}^{\circ,o\to w}(z\text{-indep}) \tag{8}$$

where $\Delta G_{tr}^{\circ,o\to w}(z\text{-dep})$ is the charge-dependent term, which has so far been considered mainly as describing the electrostatic (long-range) ion–solvent interaction, and $\Delta G_{tr}^{\circ,o\to w}(z\text{-indep})$ is the charge-independent term corresponding to the solvophobic interaction or the energy of the formation of a cavity in solvents.

The evaluation of the nonelectrostatic term is usually empirical and multifarious. Based on a skillful argument, however, Volkov and coworkers [27,28] proposed that the nonelectrostatic term of the ion-transfer energy, i.e., $\Delta G_{tr}^{\circ,o\to w}(z\text{-indep})$, should be expressed by a semiempirical equation called the Uhlig equation [40], which is given by

$$\Delta G_{tr}^{\circ,o\to w}(z\text{-indep}) = 4\pi N_A r^2 \sigma_{o,w} \quad (9)$$

when the surface tension at the boundary of the organic solvent (O) with air is less than that of water (W) with air. In this formula, the difference in the energies for forming a surface around an ion in O and in W is to be evaluated simply by using the interfacial tension ($\sigma_{o,w}$) between the two phases. The Uhlig formula is shown to be valid for $\sigma_{o,w} > 10$ mN m^{-1} and $r > 0.2$ nm [28]. Accordingly, the formula may be applied to the hydrated ions ($r_h > 0.21$ nm) in the present NB–W system ($\sigma_{o,w} = 25.2$ mN m^{-1} [41]); then, we have tentatively employed the Uhlig formula to evaluate $\Delta G_{tr}^{\circ,o\to w}(z\text{-indep})$ for the hydrated ions with $r = r_h$. By subtracting $\Delta G_{tr}^{\circ,o\to w}(z\text{-indep})$ from the literature values of $\Delta G_{tr}^{\circ,o\to w}$ [34,35,42–45], $\Delta G_{tr}^{\circ,o\to w}(z\text{-dep})$ are evaluated (see Table 2). If the Born equation [Eq. (7)] is valid, $\Delta G_{tr}^{\circ,o\to w}(z\text{-dep})$ should be proportional to z^2/r_h. In practice, however, the plot of $\Delta G_{tr}^{\circ,o\to w}(z\text{-dep})$ against z^2/r_h has not exhibited a straight line, as shown in Fig. 5. Although several modifications [24–28] of the Born equation, in which the dielectric effect

TABLE 2 Gibbs Energies of Transfer of Ions at the NB/W Interface and Its Charge-Independent and -Dependent Components at 25°C

Ion	$\Delta G_{tr}^{\circ,o\to w}$ (kJ mol^{-1})	$\Delta G_{tr}^{\circ,o\to w}(z\text{-indep})$[a] (kJ mol^{-1})	$\Delta G_{tr}^{\circ,o\to w}(z\text{-dep})$ (kJ mol^{-1})
Cation			
Li^+	−38.2[b]	23.6	−61.8
Na^+	−34.2[b]	17.9	−52.1
K^+	−23.5[b]	9.2	−32.7
Rb^+	−19.4[b]	8.6	−28.0
Cs^+	−15.4[b]	8.1	−23.5
Ca^{2+}	−67.3[c]	41.6	−108.9
Ba^{2+}	−61.8[c]	36.0	−97.8
Me_4N^+	−3.4[b]	14.8	−18.2
Et_4N^+	5.3[d]	21.7	−16.4
n-Bu_4N^+	26.5[e]	32.5	−6.0
$TPAs^+$	35.9[b]	34.6	1.3
Anion			
Cl^-	−38.2[f]	19.8	−58.0
Br^-	−27.8[g]	14.6	−42.4
I^-	−18.4[g]	11.7	−30.1
SCN^-	−15.8[g]	12.9	−28.7
NO_3^-	−25.2[g]	13.5	−38.7
ClO_4^-	−7.9[g]	10.6	−18.5
TPB^-	35.9[b]	33.8	2.1

[a] Evaluated by the Uhlig equation [Eq. (9)] with $r = r_h$ (for the inorganic ions) or $r = r_c$ (for the organic ions).
[b] Ref. 34.
[c] Ref. 35.
[d] Ref. 42. The value is revised by employing Me_4N^+ as a reference ion in place of n-Bu_4N^+.
[e] Ref. 43.
[f] Ref. 44.
[g] Ref. 45.
Source: Ref. 29.

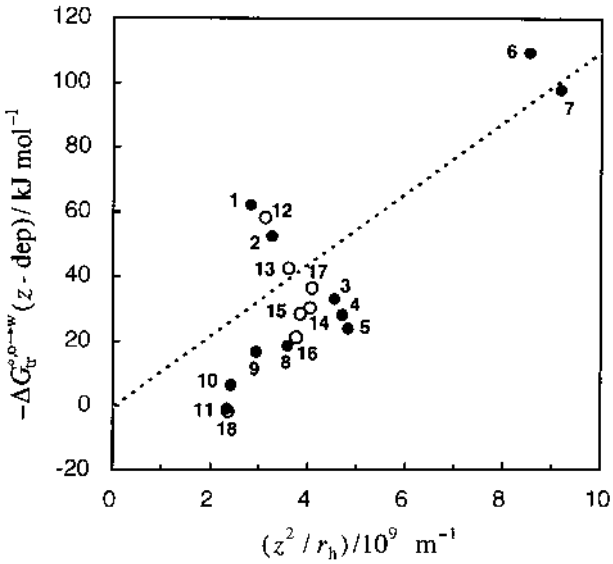

FIG. 5 Plots of $\Delta G_{tr}^{\circ,o\to w}(z\text{-dep})$ against (z^2/r_h) based on the simple Born model, for cations (●): (1) Li^+, (2) Na^+, (3) K^+, (4) Rb^+, (5) Cs^+, (6) Ca^{2+}, (7) Ba^{2+}, (8) Me_4N^+, (9) Et_4N^+, (10) n-Bu_4N^+, (11) $TPAs^+$, and for anions (○): (12) Cl^-, (13) Br^-, (14) I^-, (15) SCN^-, (16) ClO_4^-, (17) NO_3^-, (18) TPB^-. For the organic ions, (8), (9), (10), (11), (18), $\Delta G_{tr}^{\circ,o\to w}(z\text{-dep})$ is plotted against (z^2/r_c). The dotted line represents the dependence expected from the Born equation [Eq. (7)] with $\varepsilon^o = 34.8$ and $\varepsilon^w = 78.5$.

is taken into consideration, have been proposed, there is no essential difference between the simple Born equation and its modifications in the r-dependence of $\Delta G_{tr}^{\circ,o\to w}$. Accordingly, any modification could not serve as a rational explanation of the dispersed plots in Fig. 5. We conclude that, if the hydrated ion is regarded as the transferring species at the O/W interface, Bornian electrostatic models are invalid.

C. A New Approach Based on Quantum Chemical Considerations

The invalidity of Bornian electrostatic models seems to be due to the neglect of the important contribution of short-range interactions between an ion and solvents. For a better account of $\Delta G_{tr}^{\circ,o\to w}$ for the hydrated ions, we have made a new approach that recognizes short-range interactions of a hydrated ion with solvents. By this approach, $\Delta G_{tr}^{\circ,o\to w}$ for hydrophilic ions could be elucidated on the basis of the proposed model in Fig. 3 [15,29,46]. A similar model was also employed by Sánchez et al. [47] to elucidate $\Delta G_{tr}^{\circ,o\to w}$ for some hydrophilic ions, but using a Bornian electrostatic theory.

The charge-dependent term $\Delta G_{tr}^{\circ,o\to w}(z\text{-dep})$ in Eq. (8) is here assumed to be governed by short-range ion–solvent interactions. The long-range interactions of an ion with the solvents in the second and further solvation shells are ignored in the present theory. Because the short-range (i.e., chemical) interactions recognize some overlap of the electron orbitals of the ion and the solvent molecule in its immediate vicinity, they should be explained by quantum chemical considerations. In ab initio molecular orbital studies [48], the self-consistent-field (SCF) energy of the ion–molecule interaction, U_{SCF}, is parti-

tioned into several terms including Coulomb (COU), polarization (POL), charge-transfer (CT), and exchange (EX) terms:

$$U_{SCF} = U_{COU} + U_{POL} + U_{CT} + U_{EX} \tag{10}$$

The first two terms U_{COU} and U_{POL} correspond to the empirical energy of ion–dipole and ion–induced dipole interactions, being given by

$$U_{COU} = -\mu E\langle\cos\theta\rangle \tag{11}$$

and

$$U_{POL} = -\frac{1}{2}\alpha E^2 \tag{12}$$

where μ and α are the dipole moment and electronic polarizability of the solvent molecule, respectively, θ is the angle between the dipole axis and the line connecting the point dipole and point charge, $\langle\ \rangle$ indicates the ensemble average, and E is the "effective" electrical field strength, which can be approximated by the surface field strength of the ion given by

$$E = \frac{ze}{4\pi\varepsilon_0 r^2} \tag{13}$$

when r is much larger than the radius of the dipole (i.e., solvent molecule).

The third term, U_{CT}, on the right-hand side of Eq. (10) is due to the partial electron transfer between an ion and solvents in its immediate vicinity. The model Hamiltonian approach [39] has shown that U_{CT} ($= \Delta W$ in Ref. 39) per primary solvent molecule, for an ion such as the polyanion, can also be expressed as a function of E, approximately a quadratic equation:

$$U_{CT} = -\zeta_0 - \zeta_1 E - \zeta_2 E^2 \tag{14}$$

The coefficients ζ_0, ζ_1, and ζ_2 (denoted as α_0, α_1, and α_2 in Ref. 39) are influenced by various molecular properties of the solvent and an ion, including their electron-donating or -accepting abilities. Hence, these coefficients are specific to the ion. Nevertheless, they may be considered as common to a family of ions such as the polyanions whose surface atoms, directly interacting with solvents, are oxygens. This is the case for "hydrated" cations or anions whose surfaces are composed of some water molecules that interact with outer water molecules in the W phase or with organic solvents in the O phase.

The remaining term, U_{EX}, in Eq. (10) represents the nonclassical repulsion term, being inherently independent of E. By summarizing the above argument, we conclude that the short-range interaction energy, $U_{SR}(= U_{SCF})$, can be given by a quadratic function of E:

$$U_{SR} = -A - BE - CE^2 \tag{15}$$

with

$$A = \zeta_0 + U_{EX} \tag{16}$$

$$B = \mu\langle\cos\theta\rangle + \zeta_1 \tag{17}$$

$$C = \frac{\alpha}{2} + \zeta_2 \tag{18}$$

In Eq. (15) we should note that U_{SR} represents the interaction energy per primary solvent molecule. The number of solvent molecules that can interact directly with an ion in

phase S (= O or W) is then denoted as N^S. Accordingly, the contribution of the short-range interactions to the solvation energy ($\Delta G_{tr}^{\circ,vac\to S}$) of the ion in phase S (i.e., transfer energy from the vacuum) is given from Eq. (15) as

$$\Delta G_{tr}^{\circ,vac\to S}(SR) = N^S U_{SR} = -A^S N^S - B^S N^S E - C^S N^S E^2 \tag{19}$$

where the superscript s of A, B, and C represents the S phase. Because the transfer energy $\Delta G_{tr}^{\circ,o\to w}$ is the difference between the solvation energies in O and W, the contribution of short-range interactions to $\Delta G_{tr}^{o,O\to W}$ can be expressed as

$$\Delta G_{tr}^{\circ,o\to w}(SR) = -\Gamma_1 - \Gamma_2 E - \Gamma_3 E^2 \tag{20}$$

with

$$\Gamma_1 = A^w N^w - A^o N^o \tag{21}$$

$$\Gamma_2 = B^w N^w - B^o N^o \tag{22}$$

$$\Gamma_3 = C^w N^w - C^o N^o \tag{23}$$

In this manner, $\Delta G_{tr}^{\circ,o\to w}$ (SR) is given approximately by a quadratic equation of E. The coefficients Γ_1, Γ_2, and Γ_3 are related to various molecular properties of the ion and solvents [see Eqs (16)–(18) and Eqs (21)–(23)]. To estimate theoretically these coefficients using an appropriate model may not be impossible, but rather difficult at the present stage, because there is insufficient information on the above-mentioned molecular properties (in particular, the charge-transfer properties). Consequently, coefficients Γ_1, Γ_2, and Γ_3 in Eq. (20) have been determined *empirically* for hydrated cations and anions as well as nonhydrated ions [29]. The data analyses for the hydrated cations and anions are described below:

Unless noted otherwise, it has been assumed that the number of the solvent molecules N^S (S = O or W) that can be interact directly with a hydrated ion in phase S is equal to the hydration number:

$$N^o = N^w = n_h \tag{24}$$

For Ca^{2+} and Ba^{2+}, whose n_h values are larger than 10, however, it is thought that some hydrated water molecules not only in the first hydration shell but also in the second hydration shell are cotransferred into NB. Accordingly, it can be supposed that some water molecules in the first hydration shell (i.e., in the vicinity of the ion) are covered with the second hydration shell, so that they cannot be associated with outer solvent molecules (W or NB). Such an effect is here called shielding. In these cases, N^S cannot be equated simply to n_h and should be reduced to some extent. It has been found that, for the above two cations, the subtraction of 4 from the net n_h values may lead to the best result in the following regression analysis.

If we suppose that $\Delta G_{tr}^{\circ,o\to w}(z\text{-dep})$ for the hydrated ions is ruled only by short-range interactions, a combination of Eqs (20)–(23) and (24) yields

$$\Delta G_{tr}^{\circ,o\to w}(z\text{-dep})/n_h = -\Delta A - \Delta B E - \Delta C E^2 \tag{25}$$

with $\Delta A = A^w - A^o$, $\Delta B = B^w - B^o$, and $\Delta C = C^w - C^o$. In Fig. 6 the values of $\Delta G_{tr}^{o,o\to w}$ (z-dep)/n_h for the hydrated cations (○) and anions (●) are plotted against E, being calculated by Eq. (13) with $r = r_h$. Note that the plots of Ca^{2+} and Ba^{2+} have been compensated for the "shielding" effect: the marks (×) in Fig. 6 represent the plots with the net values of n_h (= 14 or 11 for Ca^{2+} or Ba^{2+}, respectively).

As seen in Fig. 6, in accordance with Eq. (25), $\Delta G_{tr}^{\circ,o\to w}(z\text{-dep})$ per hydrated water molecule becomes progressively greater as E is enhanced. Since the contribution from the interaction in W to $\Delta G_{tr}^{\circ,o\to w}(z\text{-dep})$ is probably more significant than that from the interaction in NB, the dependences shown in Fig. 6 seem to suggest that the hydrogen bonds, which are formed around a hydrated ion in W and which must be broken in its transfer to NB, are strengthened by the surface field of the hydrated ion.

The solid lines in Fig. 6 represent the quadratic curves obtained in regression analyses.

For hydrated cations:

$$\Delta G_{tr}^{\circ,o\to w}(z\text{-dep})/n_h = -8.90 + 4.506E - 4.853E^2 \quad (R = 0.931) \tag{26}$$

For hydrated anions:

$$\Delta G_{tr}^{\circ,o\to w}(z\text{-dep})/n_h = 50.17 - 52.51E - 19.33E^2 \quad (R = 0.999) \tag{27}$$

where $\Delta G_{tr}^{\circ,o\to w}(z\text{-dep})$ is in kJ mol^{-1} and E is 10^{10} V m^{-1}.

By using these regression equations for $\Delta G_{tr}^{\circ,o\to w}(z\text{-dep})$ and the Uhlig equation [Eq. (9)] for $\Delta G_{tr}^{\circ,o\to w}(z\text{-indep})$, the values of $\Delta G_{tr}^{\circ,o\to w}$ for hydrated ions can be predicted, though roughly, from Eq. (8), provided that their n_h values are known. In the calculation of $\Delta G_{tr}^{\circ,o\to w}(z\text{-dep})$ for highly hydrated cations such as Ca^{2+} and Ba^{2+} with $n_h > 10$ (e.g., Mg^{2+}, Sr^{2+}, Ni^{2+}, Fe^{2+}, Fe^{3+}), the n_h values should be corrected for the "shielding" effect, on the assumption that the corrected values of n_h are proportional to the surface area of the hydrated ion:

$$n_{corr} = f(4\pi r_h^2) \tag{28}$$

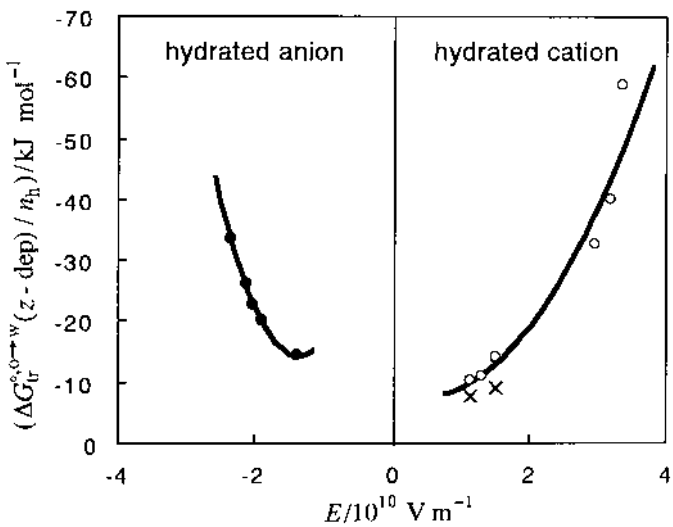

FIG. 6 Plots of $\Delta G_{tr}^{\circ,o\to w}(z\text{-dep})/n_h$ against E (with $r = r_h$) for hydrated cations (○) and anions (●). Note that the n_h values for the plots of Ca^{2+} and Ba^{2+} have been corrected for the "shielding" effect (see text) by subtracting 4 from their net values of n_h; (×) represents the plots with the net values. Solid lines show the regression curves [Eqs. (26) and (27)]. (From Ref. 29.)

The factor f has been tentatively determined to be 42.05 by a regression analysis so that the n_{corr} values of Ca^{2+} and Ba^{2+} may be approximated to be $n_h - 4$ (see above). For further details, see Ref. 29.

IV. PROTON NMR STUDY

In the above sections, coextraction of ions into water-immiscible solvents has been elucidated in terms of selective hydration of ions in mixed solvents. However, it has frequently been asked whether water molecules are actually bound with ions in organic solvent. Nevertheless, there seems to be no doubt about it, since the selective hydration of hydrophilic ions in water-miscible and -immiscible solvents has been confirmed by solubility [49,50], polarography [51], UV–visible [52,53], ^{1}H NMR [3,50,53–55], IR [55–57], and other methods [50,58] (see also Ref. 18). Among these methods, NMR is one of the most powerful techniques. In 1972, Kawasaki et al. [3] applied H NMR to calcium ions in water-immiscible NB, and observed changes in the chemical shift of water as a function of the water content. Ito et al. [53] measured the chemical shift of water protons for iodide ions in NB, and found that the low-field shift of water protons with water and ion concentrations can be explained in terms of the successive reaction mechanism, $I^- \rightleftharpoons I^-(H_2O) \rightleftharpoons I^-(H_2O)_2 \rightleftharpoons I^-(H_2O)_3$. While this mechanism is very likely, further verification of the mechanism has been needed.

In our recent study [59], we have utilized ^{1}H NMR spectroscopy at 400 MHz to study the selective hydration phenomena for typical univalent anions ($X^- = Cl^-$, Br^-, I^-, NO_3^-, ClO_4^-, and SCN^-) in deuterated nitrobenzene (NB-d_5). For the respective anions, dependences of the chemical shift of water on water and ion concentrations have been examined. We have found that the selective hydration of these anions can be explained in terms of the successive reaction mechanim [e.g., $Br^- \rightleftharpoons Br^-(H_2O) \rightleftharpoons Br^-(H_2O)_2$ $Br^-(H_2O)_3 \rightleftharpoons Br^-(H_2O)_4$]. In addition, measurements of spin–lattice relaxation times have shown that the rate of rotational diffusion of water molecules is considerably slowed by the hydration of the ions. The results are summarized below.

A. Chemical Shifts

Figure 7 shows a typical NMR spectrum, which was obtained for a 20 mM Br^- NB-d_5 solution containing 115 mM H_2O. As seen in the figure, the water protons always appear as a singlet, because the exchange of water molecules associated and unassociated with the anion is very fast. Under these conditions, the chemical shift of water protons should change with the distribution of water molecules between some different states.

In Fig. 8 the chemical shift of water protons, δ (ppm), is plotted against water concentration, $[H_2O]_{total}$, for six different anions. As seen in the figure, the chemical shift changed to lower magnetic fields in the order: $ClO_4^- < I^- < SCN^- < NO_3^- < Br^- < Cl^-$, showing that the ion–water interaction becomes stronger in this order. This order is in harmony with that of the crystal (or bare) ionic radii (nm) shown in Table 1: ClO_4^- (0.236) > SCN^- (0.213) > I^- (0.206) > NO_3^- (0.189) > Br^- (0.182) > Cl^- (0.167). Also, the sequence of the chemical shifts agrees with that of the hydration number in NB [15]: ClO_4^- (0.2) < I^- (0.9) < SCN^- (1.1) < NO_3^- (1.7) < Br^- (2.1) < Cl^- (4.0). Furthermore, the sequence correlates closely with the $\Delta G_{tr}^{\circ,o\rightarrow w}$ values for the anions that are listed in Table 2. Thus, the chemical shifts of water protons show a good correlation with the hydrophilicity of the anions.

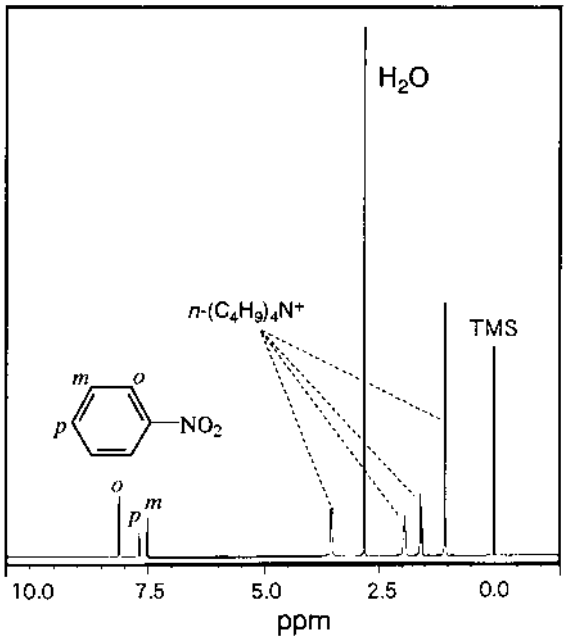

FIG. 7 ^{1}H NMR spectrum at 400 MHz for a 20 mM Br^- NB-d_5 solution containing 115 mM H_2O (25°C). (From Ref. 59.)

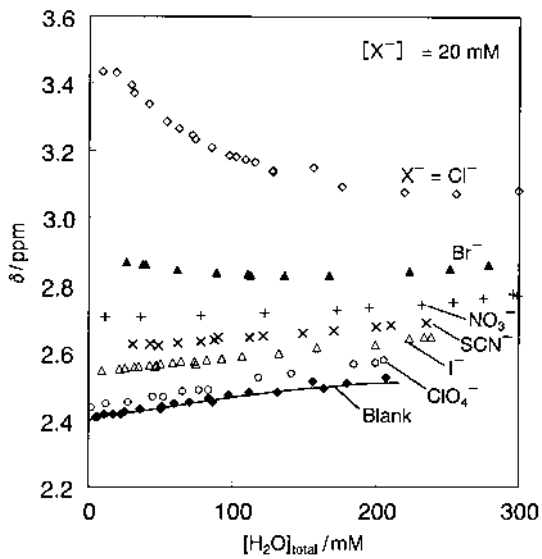

FIG. 8 Plots of the chemical shifts of water protons against water concentration for various anions: $X^- = ClO_4^-$, I^-, SCN^-, NO_3^-, Br^-, and Cl^- at 20 mM in NB-d_5. The "Blank" represents the chemical shifts of water protons in the absence of the anions. The solid line represents the regression curve based on the monomer–dimer equilibrium [Eq. (29)]. (From Ref. 59.)

The chemical shifts for the "blank" solvent, i.e., NB-d_5 containing no ions, depend on water concentration to some extent, as shown by the "Blank" in Fig. 8. The low-field shift with the water concentration can be analyzed on the basis of monomer–dimer equilibrium [60]:

$$2H_2O \rightleftharpoons (H_2O)_2 \tag{29}$$

By assuming this equilibrium, the chemical shift of water protons is given by

$$\begin{aligned}\delta_{\text{blank}} &= \frac{[H_2O]}{[H_2O]_{\text{total}}}\delta_{H_2O} + 2\frac{[(H_2O)_2]}{[H_2O]_{\text{total}}}\delta_{(H_2O)_2} \\ &= \frac{[H_2O]}{[H_2O]_{\text{total}}}\delta_{H_2O} + 2\frac{K_s[H_2O]^2}{[H_2O]_{\text{total}}}\delta_{(H_2O)_2}\end{aligned} \tag{30}$$

where δ_{H_2O} and $\delta_{(H_2O)_2}$ are intrinsic chemical shifts of the monomer and dimer, respectively, and K_s is the monomer–dimer equilibrium constant for water:

$$K_s = \frac{[(H_2O)_2]}{[H_2O^2]} \tag{31}$$

By using the reported value [53,60] of K_s(= 1.054 M^{-1}, at 25°C), curve fitting with Eq. (30) was performed to obtain the regression curve shown in Fig. 8. The intrinsic chemical shifts as fitting parameters were $\delta_{H_2O} = 2.40$ ppm and $\delta_{(H_2O)_2} = 2.87$ ppm. It should be noted that these values are very low compared with the chemical shift for bulk water ($\delta = 4.8$ ppm) or water clusters formed in certain organic solvents at low temperatures ($\delta \simeq 5$ ppm); however, they are comparable to the chemical shifts for water monomers in hydrophobic solvents (1 ppm $< \delta <$ 3 ppm) [61]. Thus, the observed higher-field signals for water protons allow us to suggest that water should hardly form any water clusters or hydrogen bond networks in such a hydrophobic solvent as NB.

As described above, the exchange processes of water molecules are too fast for the NMR to discriminate between their different states and only the averaged singlet lines for the protons of all different water molecules (free, autoassociated, and associated with the anions) are obtained. The interpretation of those spectra depends on the introduction of more or less speculative models whose validity can be verified indirectly. With a view to verifying the hydration models for the anions in NB, we then examined the dependence of δ on water and ion concentrations in detail. Figure 9 shows a typical example, in which the δ values for 10, 20, and 40 mM Br^- in NB-d_5 are plotted against the water concentration in the solvent. As seen in the figure, the chemical shift changed to lower fields with increasing ion concentration. A similar ion-concentration dependence of δ was also observed for all other anions, although the extent of the dependence differed from one anion to another.

The hydration number of Br^- is $n_h = 2.1$ in NB, as shown in Table 1. Under the assumption that the dihydrated ion is formed in one step:

$$Br^- + 2(H_2O) \rightleftharpoons Br^-(H_2O)_2 \tag{32}$$

the chemical shift of water protons is given by [cf. Eq. (30)]

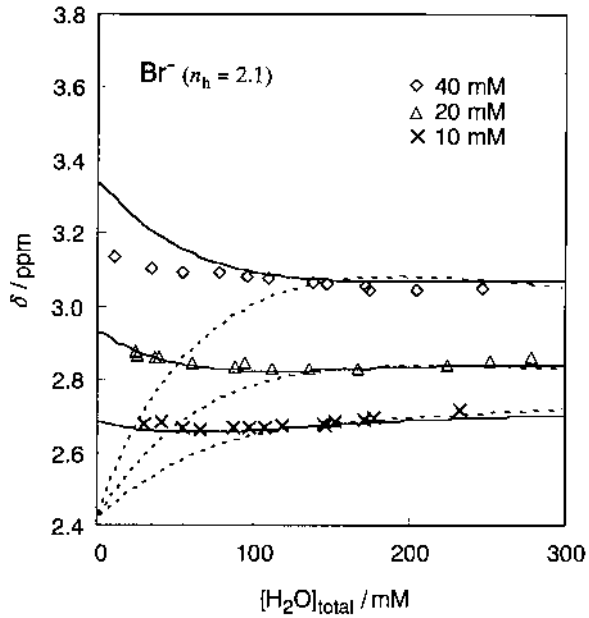

FIG. 9 Plots of the chemical shifts of water protons against water concentration for 10, 20, and 40 mM Br^- in NB-d_5. The solid lines show the best fit to the experimental data for the successive reaction mechanism [Eq. (36) with $m = 1$–4], while the dashed lines represent a set of theoretical curves based on the one-step reaction mechanism [Eq. (33)]. (From Ref. 59.)

$$\begin{aligned}\delta &= \delta_{\text{blank}} + 2\frac{[\text{Br}^-(\text{H}_2\text{O})_2]}{[\text{H}_2\text{O}]_{\text{total}}}\delta_{\text{Br}^-(\text{H}_2\text{O})_2} \\ &= \frac{[\text{H}_2\text{O}]}{[\text{H}_2\text{O}]_{\text{total}}}\delta_{\text{H}_2\text{O}} + 2\frac{K_s[\text{H}_2\text{O}]^2}{[\text{H}_2\text{O}]_{\text{total}}}\delta_{(\text{H}_2\text{O})_2} + 2\frac{K_{\text{one-step}}[\text{Br}^-][\text{H}_2\text{O}]^2}{[\text{H}_2\text{O}]_{\text{total}}}\delta_{\text{Br}^-(\text{H}_2\text{O})_2}\end{aligned} \tag{33}$$

where $\delta_{\text{Br}^-(\text{H}_2\text{O})_2}$ is the intrinsic chemical shift for the dihydrated ion, and $K_{\text{one-step}}$ is the equilibrium constant of the hydration reaction [Eq. (32)]. However, the curve fitting with Eq. (33) was unsuccessful. The dashed lines in Fig. 9 represent a set of theoretical curves based on the one-step reaction mechanism. As seen, the δ values at higher water concentrations can be simulated, but the dependence in the lower concentration range is entirely different from the observed one.

As an alternative approach, it can be assumed that Br^- is hydrated in a stepwise fashion:

$$\begin{aligned}&\text{Br}^- + \text{H}_2\text{O} \rightleftharpoons \text{Br}^-(\text{H}_2\text{O}) \\ &\text{Br}^-(\text{H}_2\text{O}) + \text{H}_2\text{O} \rightleftharpoons \text{Br}^-(\text{H}_2\text{O})_2 \\ &\text{Br}^-(\text{H}_2\text{O})_2 + \text{H}_2\text{O} \rightleftharpoons \text{Br}^-(\text{H}_2\text{O})_3\end{aligned} \tag{34}$$

In general, one can write for an X^- ion:

$$\text{X}^-(\text{H}_2\text{O})_{m-1} + \text{H}_2\text{O} \rightleftharpoons \text{X}^-(\text{H}_2\text{O})_m \quad (m = 1, 2, 3, \ldots) \tag{35}$$

Such a successive reaction mechanism was previously employed by Ito et al. [53] to explain the chemical shift of water for the hydration of I^- in NB. On the basis of this mechanism, the observed chemical shift of water protons should be given by

$$\begin{aligned}\delta &= \delta_{\text{blank}} + \frac{[X^-(H_2O)]}{[H_2O]_{\text{total}}}\delta_1 + 2\frac{[X^-(H_2O)_2]}{[H_2O]_{\text{total}}}\delta_2 \\ &+ 3\frac{[X^-(H_2O)_3]}{[H_2O]_{\text{total}}}\delta_3 + \cdots + m\frac{[X^-(H_2O)_m]}{[H_2O]_{\text{total}}}\delta_m + \cdots \\ &= \frac{[H_2O]}{[H_2O]_{\text{total}}}\delta_{H_2O} + 2\frac{K_s[H_2O]^2}{[H_2O]_{\text{total}}}\delta_{(H_2O)_2} \\ &+ \frac{K_1[X^-][H_2O]}{[H_2O]_{\text{total}}}\delta_1 + 2\frac{K_1K_2[X^-][H_2O]^2}{[H_2O]_{\text{total}}}\delta_2 \\ &+ 3\frac{K_1K_2K_3[X^-][H_2O]^3}{[H_2O]_{\text{total}}}\delta_3 + \cdots + m\frac{K_1K_2K_3\cdots K_m[X^-][H_2O]^m}{[H_2O]_{\text{total}}}\delta_m + \cdots\end{aligned} \tag{36}$$

where δ_m ($m = 1, 2, 3, \ldots$) is the intrinsic chemical shift for the m-hydrated ion, and K_m is the successive formation constant of the m-hydrated ion, which is defined by

$$K_m = \frac{[X^-(H_2O)_m]}{[X^-(H_2O)_{m-1}][H_2O]} \quad (m = 1, 2, 3, \ldots) \tag{37}$$

The terms in Eq. (36) are interdependent of each other, because each term involves the concentration of monomeric water $[H_2O]$. However, it should be noted that the crucial parameters involved in those terms (δ_m, K_m, K_s, etc.) are independent of each other, probably in the studied concentration range. By using the values of K_m, the concentration of the nonhydrated ion is given by

$$\begin{aligned}[X^-] = [X^-]_{\text{total}}/\{1 + K_1[H_2O] + K_1K_2[H_2O]^2 + K_1K_2K_3[H_2O]^3 + \cdots + \\ (K_1K_2K_3\cdots K_m)[H_2O]^m + \cdots\}\end{aligned} \tag{38}$$

where $[X^-]_{\text{total}}$ is the total concentration of X^-.

The experimental data were fitted with Eqs (36)–(38) by assuming that $m = 1, 2, 3$, and 4 for Br^-, which has an average hydration number of 2.1. First, Eq. (38) was used with the initial values of K_m to evaluate $[X^-]$ as a function of $[H_2O]$ and then an iterative calculation was carried out with Eq. (36) to minimize the standard deviation, $\sigma = [\Sigma(\delta_{\text{calcd}} - \delta_{\text{obsd}})^2/(N-1)]^{1/2}$, where δ_{calcd} and δ_{obsd} are calculated and observed chemical shifts, respectively, and N is the number of data points. In this curve-fitting procedure, the values K_m and δ_m were used as adjusting parameters. In Fig. 9, a set of the best regression curves for Br^- are shown by solid lines. In contrast to the one-step reaction mechanism, the successive reaction mechanism could reproduce the observed behaviors for δ reasonably well.

For other anions with $n_h > 1.5$, i.e., Cl^- ($n_h = 4.0$) and NO_3^- ($n_h = 1.7$), curve fitting was also successful only with the successive reaction mechanism. This is true of such a highly hydrophilic cation as Na^+ [62]. However, in the case of the anions with $n_h < 1.5$, i.e., SCN^- ($n_h = 1.1$), I^-($n_h = 0.9$), and ClO_4^- ($n_h = 0.2$), curve fitting was successful with both the successive and one-step reaction mechanisms. Nevertheless, since there would be

no essential difference in hydration mechanism between the two anion groups, the successive reaction mechanism was adopted for the latter group (with $n_h < 1.5$) as well.

In Table 3 the values of K_m and δ_m obtained from the curve fittings are listed. It must be noted that these values were obtained as adjusting parameters and that not less than six parameters were used for each anion. Accordingly, these parameters could not be uniquely determined; a set of parameters obtained for each anion should be regarded as one of the best parameter sets that could give us a satisfactory result of the curve fitting. Although this prevents us from examining these parameters closely, there seem to be notable dependences of the parameters, especially for the monohydrated anions. The values of K_1 and δ_1 increase with the hydration number in NB. Because the hydration number shows a good correlation with the ionic radius (r_c) as described above, the K_1 and δ_1 values also correlate with r_c. This suggests that the ion–water interaction should be strengthened by an increase in the surface electric field (E) which is inversely proportional to the ionic radius [see Eq. (13)].

The above-mentioned curve-fitting analyses clearly show that the selective hydration of anions (probably also cations) in NB can be explained in terms of the successive reaction mechanism. In Fig. 10, the distribution of the anions in several hydration states, calculated with the K_m values in Table 3, are shown as a function of $[H_2O]_{total}$ for (a) SCN^- and (b) Br^-. For SCN^- with $n_h = 1.1$, the nonhydrated and monohydrated ions are most dominant at $[H_2O]_{total} \approx 180$ mM where NB containing 10 mM SCN^- is saturated with water at 25°C. Such a relatively hydrophobic anion as SCN^- exists in the water-saturated NB mostly in the nonhydrated or monohydrated state, though there should be

TABLE 3 Values of K_m (M^{-1}) and δ_m (ppm) Obtained from the Curve Fittings Based on the Successive Reaction Mechanism (25°C)

	ClO_4^-	I^-	SCN^-	NO_3^-	Br^-	Cl^-
K_1	3.7	6.5	7.4	7.4	7.5	13
K_2	1.9	3.0	3.5	4.9	6.5	11
K_3	1.6	3.0	3.5	3.4	6.5	11
K_4	—	—	—	—	7.0	10
K_5	—	—	—	—	—	10
K_6	—	—	—	—	—	9
δ_1	2.9	3.5	4.2	4.7	6.5	7.8
δ_2	2.7	3.5	3.1	3.5	3.2	4.0
δ_3	6.1	4.5	5.7	6.0	3.4	4.0
δ_4	—	—	—	—	5.2	4.0
δ_5	—	—	—	—	—	4.0
δ_6	—	—	—	—	—	4.6
σ[a]	0.011	0.010	0.008	0.028	0.044	0.078
n_h[b]	0.2	0.9	1.1	1.7	2.1	4.0
$< n_h >$[c]	0.6	1.2	1.3	1.6	2.6	5.3

[a] Standard deviation, $\sigma = [\sum(\delta_{calcd} - \delta_{obsd})^2/(N-1)]^{1/2}$.
[b] Hydration number in NB (see Table 1).
[c] Average hydration number calculated using the K_m values.
Source: Ref. 59.

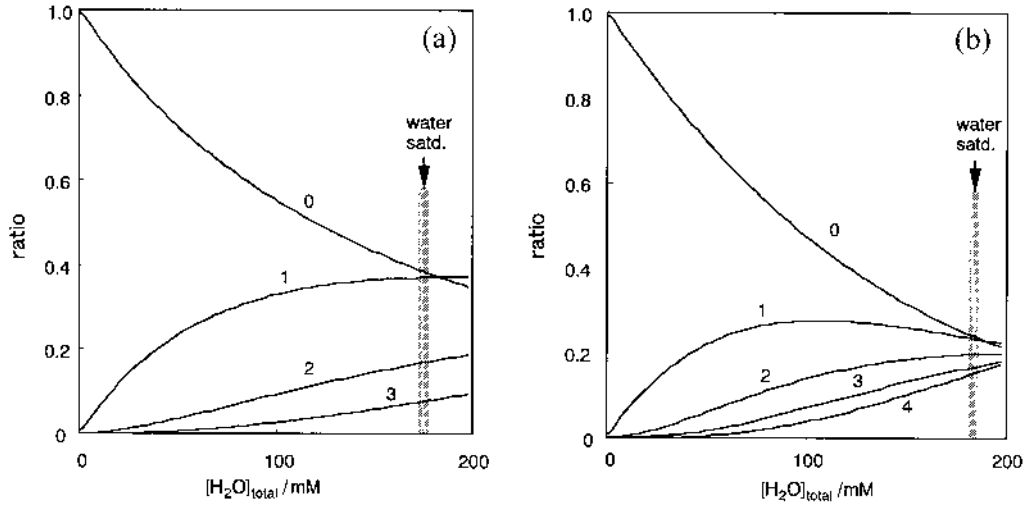

FIG. 10 Distribution of anions in several hydration states for (a) 10 mM SCN^- and (b) 10 mM Br^- as a function of water concentration: (0) nonhydrated; (1) monohydrated; (2) dihydrated; (3) trihydrated; (4) tetrahydrated. (From Ref. 59.)

some highly hydrated ions. For this reason, the chemical shifts for ClO_4^-, I^-, and SCN^- could also be explained by the one-step reaction mechanism. On the other hand, as shown in Fig. 10(b), the Br^- ion with a higher hydration number ($n_h = 2.1$) exists in the water-saturated solvent (with $[H_2O]_{total} \approx 190$ mM) as the nonhydrated and differently hydrated states. This is the reason the chemical shifts for NO_3^-, Br^-, and Cl^- could not be reproduced by the one-step reaction mechanism assuming only one hydration state.

As also pointed out by Kusakabe [13], our results clearly show that the hydration number has no need to be an integer because it is always given as an averaged value over several species with different hydration numbers. Table 3 also shows the "averaged" hydration numbers of the anions calculated by the following equation:

$$< n_h >= \frac{\sum_m m([X^-(H_2O)_m]_{sat})}{[X^-]_{total}} \tag{39}$$

where $[X^-(H_2O)_m]_{sat}$ stands for the concentration of the m-hydrated ion in the water-saturated solvent. As seen in Table 3, the values of $< n_h >$ are in accord with the values of n_h, which were previously obtained by the Karl Fischer method [15] (cf. Table 1).

B. Rotational Correlation Times

Spin–lattice relaxation times, T_1, for water in NB-d_5 solutions were measured by the inversion-recovery method with the pulse sequence of $(180°–t–90°)_n$. Under the extreme narrowing condition, which is realized here by the rapid molecular rotational motions, the spin–lattice relaxation rate $(1/T_1)$ for the ^1H nucleus with spin $I = 1/2$ is approximately expressed by [63]:

$$\frac{1}{T_1} = \frac{3\gamma^4\hbar^2}{2{r_{HH}}^6}\tau_c \tag{40}$$

where γ is the proton gyromagnetic ratio, $\hbar$ is Planck's constant (h) divided by 2π, r_{HH} is the intraproton distance of the water molecule, and τ_c is the rotational correlation time for the intramolecular ^1H–^1H axis. It is assumed here that $1/T_1$ consists of only the intramolecular ^1H–^1H interaction. Because γ is related to the nuclear magnetic moment (μ) as $\hbar\gamma = \mu/(\text{angular momentum}) = \mu/(1/2) = 2\mu$, Eq. (40) can be rewritten as

$$\frac{1}{T_1} = \frac{3(2\mu)^4}{2{r_{HH}}^6\hbar^2}\tau_c \tag{41}$$

The value of $r_{HH}(= 1.5143 \times 10^{-8}$ cm) is calculated from the O–H bond length (0.09575 nm) and ∠HOH angle (104.51°) for the gas-phase molecule of water; these values are available in Ref. 64. Using the r_{HH} value and the value of μ ($= 1.4106 \times 10^{-23}$ erg G^{-1}, one can obtain

$$\tau_c = \frac{1.41 \times 10^{-11}}{T_1}[\text{s}] \tag{42}$$

This relation enables us to obtain the value of τ_c from T_1 (in s).

Strictly speaking, the measured $1/T_1$ value consists of not only the intramolecular ^1H–^1H interaction [being given by Eq. (40)] but also the "intermolecular" dipole–dipole interaction between the water proton and a nucleus of the hydrated anion. Although the exact evaluation of its contribution is impossible because of the lack of structural information for the hydrated anions in NB, a rough estimation (for the detail, see Ref. 59) has shown that the contribution to $1/T_1$ is very small. Consequently, such outer-sphere relaxation has been neglected in determining the rotational correlation times of water molecules on the basis of Eq. (40).

In the same manner as the chemical shifts, the rotational correlation times should be considered as the averaged values over several hydration states of water molecules. Figure 11 shows the plots of the rotational correlation time (τ_c) against $[H_2O]_{total}$ for several concentrations of Br^- (0, 10, 20, and 40 mM). As seen in the figure, the observed correlation times exhibited a clear dependence on $[H_2O]_{total}$, reflecting the concentration changes of the anions in several hydration states.

The τ_c values for the blank solvent (i.e., for 0 mM Br^-) were only slightly dependent on $[H_2O]_{total}$ in the range 2.8–2.9 ps, but simulated in a similar manner as the chemical shifts:

$$\begin{aligned}\tau_{c,blank} &= \frac{[H_2O]}{[H_2O]_{total}}\tau_{H_2O} + 2\frac{[(H_2O)_2]}{[H_2O]_{total}}\tau_{(H_2O)_2} \\ &= \frac{[H_2O]}{[H_2O]_{total}}\tau_{H_2O} + 2\frac{K_s[H_2O]^2}{[H_2O]_{total}}\tau_{(H_2O)_2}\end{aligned} \tag{43}$$

where τ_{H_2O} and $\tau_{(H_2O)_2}$ are the intrinsic rotational correlation times for water monomer and dimer, respectively. The values of $\tau_{H_2O} = 2.8$ ps and $\tau_{(H_2O)_2} = 3.0$ ps were obtained as the fitting parameters. These values are somewhat larger than the τ value (1.96 ps) for pure water [65], in which hydrogen-bond networks are formed to retard the rotation of water molecules. However, on considering the high viscosity of NB ($\eta = 1.795 \times 10^{-3}$ Pa·s at 25°C; cf. $\eta = 0.890 \times 10^{-3}$ Pa·s for water) [66], the higher τ_c values in NB seem to be reasonable for water monomer or dimer in NB.

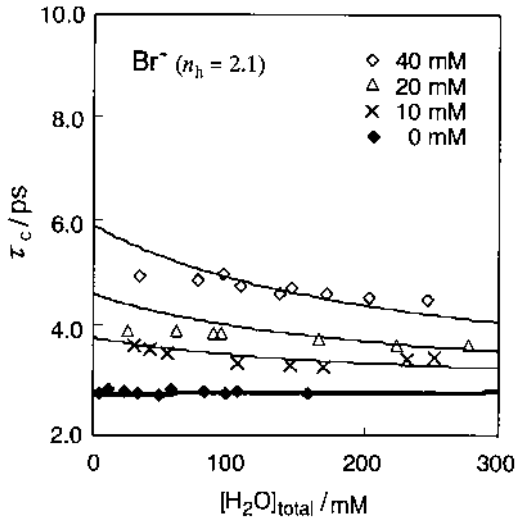

FIG. 11 Plots of the rotational correlation times (τ_c) of water molecules against water concentration for several concentrations of Br^- in NB-d_5. The solid lines show the regression curves obtained by using Eq. (43) (for 0 mM Br^-) or Eq. (44) (for 10, 20, and 40 mM Br^-) (From Ref. 59.)

As shown in Fig. 11, the τ_c values usually increased with the anion concentration. This dependence could also be expressed in terms of the successive reaction mechanism [Eq. (35)]. For this mechanism, the rotational correlation time of water molecules is generally given by

$$\begin{aligned}\tau_c &= \tau_{c,blank} + \frac{[X^-(H_2O)]}{[H_2O]_{total}}\tau_1 + 2\frac{[X^-(H_2O)_2]}{[H_2O]_{total}}\tau_2 \\ &\quad + 3\frac{[X^-(H_2O)_3]}{[H_2O]_{total}}\tau_3 + \cdots + m\frac{[X^-(H_2O)_m]}{[H_2O]_{total}}\tau_m + \cdots \\ &= \frac{[H_2O]}{[H_2O]_{total}}\tau_{H_2O} + 2\frac{K_s[H_2O]^2}{[H_2O]_{total}}\tau_{(H_2O)_2} \\ &\quad + \frac{K_1[X^-][H_2O]}{[H_2O]_{total}}\tau_1 + 2\frac{K_1K_2[X^-][H_2O]^2}{[H_2O]_{total}}\tau_2 \\ &\quad + 3\frac{K_1K_2K_3[X^-][H_2O]^3}{[H_2O]_{total}}\tau_3 + \cdots + m\frac{K_1K_2K_3\cdots K_m[X^-][H_2O]^m}{[H_2O]_{total}}\tau_m + \cdots\end{aligned} \tag{44}$$

where τ_m ($m = 1, 2, 3, \ldots$) is the intrinsic rotational correlation time of hydrated water molecules for the m-hydrated ion. Using the K_m values obtained for the chemical shifts (Table 3), similar fitting analyses have been performed to obtain the τ_m values as the fitting parameters. Thus, the present theoretical treatment enabled us to estimate the intrinsic contributions from hydrated water molecules in some different states.

As shown in Table 4, the τ_m values are greater than $\simeq 3$ ps for free water molecules, suggesting that the rotational motion of the hydrated water molecules should be restricted by the association with the anions. For the same reason as that given for the intrinsic

TABLE 4 Values of τ_m (ps) Obtained from the Curve Fittings Based on the Successive Reaction Mechanism (25°C)

	ClO_4^-	I^-	SCN^-	NO_3^-	Br^-	Cl^-
τ_1	4.9	7.8	6.9	8.0	13.8	27
τ_2	7.1	13.5	13.7	4.0	6.6	7.3
τ_3	11.8	15.5	18.7	10.7	8.0	7.3
τ_4	—	—	—	—	7.3	7.3
τ_5	—	—	—	—	—	7.3
τ_6	—	—	—	—	—	7.3
σ[a]	0.11	0.12	0.28	0.16	0.11	0.46

[a] Standard deviation, $\sigma = \left[\sum(\tau_{calcd} - \tau_{obsd})^2/(N-1)\right]^{1/2}$, where τ_{calcd} and τ_{obsd} stand for the calculated and observed rotational correlation times, respectively.
Source: Ref. 59.

chemical shifts mentioned above, the τ_m values obtained cannot be examined closely. Nevertheless, there is a notable tendency for τ_1 to increase with increasing hydration number in NB or the hydrophilicity of the anions. Regarding the relatively hydrophobic anions (ClO_4^-, I^-, and SCN^-), there is a marked tendency for τ_m to increase with m: $\tau_1 < \tau_2 < \tau_3$. However, this is not the case for other anions. It is probable that the τ_m values reflect the structures of the hydrated anions, which are still unknown at the present stage.

V. SELECTIVE HYDRATION OF ORGANIC IONS

Most previous studies on selective hydration in water-immiscible organic solvents have been confined mainly to inorganic ions. With regard to organic molecules, there had been only a negative report [67] that acetylacetonates and glyoximes as the neutral forms are not hydrated in NB. However, our recent studies have revealed that primary to tertiary ammonium ions [16] and carboxylate ions [17] have the ability to coextract some water molecules into NB, as described below.

A. Alkylammonium Ions

In the NB–W system, primary to tertiary ammonium ions with methyl (Me), ethyl (Et), and *n*-butyl (*n*-Bu) groups were distributed with DPA^- and TPB^-, and the number of water molecules being coextracted to NB by an alkylammonium ion ($R_mNH_{4-m}^+$) was measured by the Karl Fischer method [16].

In all the systems studied, the addition of an $R_mNH_{4-m}^+$ salt caused an increase of the water concentration in the NB phase. The increase in water concentration in NB ($\Delta[H_2O]$) was plotted against the "total" concentration ($[R_mNH_{4-m}^+]_o^t$) of the alkylammonium ion in the NB phase at equilibrium ("total" means including the ion pair as well as the free ion. See below). Some typical examples for the TPB^- and DPA^- systems are shown in Fig. 12(a) and (b), respectively. In all the cases, $\Delta[H_2O]$ was shown to be proportional to $[R_mNH_{4-m}^+]_o^t$. Because either TPB^- or DPA^- used as a counterion of $R_mNH_{4-m}^+$ is not

hydrated in NB as shown above, the slope of each linear plot should represent the number (n_{ex}) of coextracted water molecules per alkylammonium ion.

As shown in Table 5, the n_{ex} values of the primary to tertiary ammonium ions with Me, Et, or *n*-Bu groups have been found to range from 0.51 to 1.54. For the quaternary ammonium ions, their n_{ex} values have been found to be zero [15]. In general, the observed values of n_{ex} are dependent on the number of alkyl groups (i.e., the class) in an $R_mNH_{4-m}^+$ ion, but almost independent of the kind. The primary, secondary, tertiary, and quaternary ammonium ions have, respectively, their n_{ex} values of 1.5, 1.0, 0.7, and 0 in the DPA^- system, and those of 0.8, 0.8, 0.6, and 0 in the TPB^- system.

Thus, the n_{ex} values of tertiary and quaternary ammonium ions in the TPB^- system coincided well with the corresponding values in the DPA^- system. However, the n_{ex} values of the primary and secondary ammonium ions in the TPB^- system were somewhat less than those in the DPA^- system. So, we assumed that this discordance could be ascribed to the difference in tendencies of $R_mNH_{4-m}^+$ to associate with TPB^- and DPA^- in NB, and then performed conductivity measurements.

Based on the conductivity measurements, the association constants (K_As) of the TPB^- and DPA^- salts of $R_mNH_{4-m}^+$ in "water-saturated" NB (i.e., containing 0.168 M water) were determined in a conventional manner [68] (for further details, see Ref. 16). The results have shown that the K_As in the DPA^- system are close to zero, while those in the TPB^- system show comparatively large values (e.g., $K_A = 124.6$, 83.7, and 72.2 M^{-1} for $MeNH_3^+$, $EtNH_3^+$, and *n*-$BuNH_3^+$, respectively). Thus, ion association is significant in the TPB^- system.

Using the K_A value thus obtained, the concentration ($[R_mNH_{4-m}^+]_o$) of a free alkylammonium ion in NB was estimated, and the n_{ex} value was then corrected for the ion-pair effect to obtain the "true" hydration number (n_h) of the $R_mNH_{4-m}^+$ ion. Here, we assumed

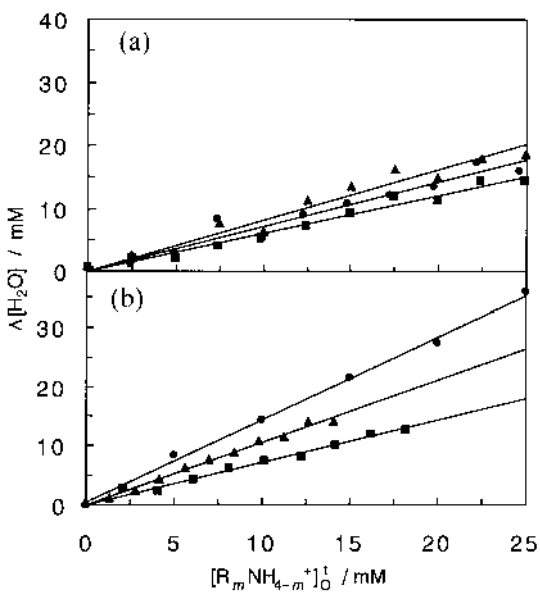

FIG. 12 Plots of the increase in water concentration in NB against the total concentration of $R_mNH_{4-m}^+$ distributed to the NB phase: (a) TPB^- system; (b) DPA^- system; ●, $MeNH_3^+$; ▲, *n*-$Bu_2NH_2^+$; ■, Et_3NH^+. (From Ref. 16.)

TABLE 5 n_{ex} Values of Water Molecules Coextracted with $R_mNH_{4-m}^+$ in NB

	n_{ex}	
$R_mNH_{4-m}^+$	TPB^- system	DPA^- system
$MeNH_3^+$	0.71±0.05	1.43±0.05
$EtNH_3^+$	0.88±0.08	1.53±0.06
n-$BuNH_3^+$	0.70±0.04	1.54±0.10
$Me_2NH_2^+$	—	1.02±0.04
$Et_2NH_2^+$	—	1.07±0.05
n-$Bu_2NH_2^+$	0.80±0.06	1.05±0.03
Me_3NH^+	0.65±0.06	0.62±0.05
Et_3NH^+	0.60±0.03	0.68±0.04
n-Bu_3NH^+	0.51±0.05	—
Me_4N^+	—[a]	0.00[a]
Et_4N^+	0.00[a]	0.00[a]
n-Bu_4N^+	0.00[a]	—[a]

[a] Ref. 15.
Source: Ref. 16.

that a hydrated $R_mNH_{4-m}^+$ ion in NB would release all water molecules by its ion-pair formation with TPB^- or DPA^-. In Fig. 13, the values of $\Delta[H_2O]$ are plotted against (a) the total concentration of $MeNH_3^+$ in NB and (b) the concentration of the free $MeNH_3^+$ ion. The plots (b) lie on a straight line with a slope of 1.83; the slope should correspond to the true n_h value of $MeNH_3^+$. This value has been found to be larger than the apparent value (i.e., $n_{ex} = 0.71$) obtained from the slope of the plots (a). For other $R_mNH_{4-m}^+$ ions in the TPB^- system, their n_h values were evaluated in a similar manner. Also, in the DPA^- system with much lower K_A values, the n_{ex} values were compensated for the ion-pair effects, unless the K_A values were zero. The n_h values thus determined in both systems are shown in Table 6.

As shown in Table 6, the n_h values in the TPB^- system became appreciably larger than the corresponding n_{ex} values in Table 5. The n_h values determined in both systems were found to be only slightly dependent on the nature of extractant (i.e., DPA^- or TPB^-). This suggested that correct values of n_h could be obtained for the $R_mNH_{4-m}^+$ ions in NB. This implies that the above assumption that ion pairs are not hydrated in NB is valid.

Table 6 clearly shows that the n_h values of $R_mNH_{4-m}^+$ ions are little affected by the alkyl chain length, but very dependent on the class of the ammonium ion: $n_h = 1.64$, 1.04, 0.66, and 0.00 for the primary, secondary, tertiary, and quaternary ammonium ions, respectively. For the primary to tertiary ammonium ions, it can be considered that water molecules interact with hydrogen atom(s) bound to the central nitrogen atom. In order to reinforce this argument, the optimized structure of a hydrated $MeNH_3^+$ ion was calculated by the PM3 method with a MOPAC program [68]. As shown in Fig. 14, the respective oxygen atoms of three water molecules form a hydrogen bond with hydrogen atoms of the $-NH_3^+$ group. Thus, the primary ammonium ion has a possibility of interacting directly with three water molecules without steric hindrance. However, a higher class of ammonium ion, e.g., a tertiary Me_3NH^+ ion, can be associated with only one water molecule; a similar MOPAC calculation, which included three water molecules

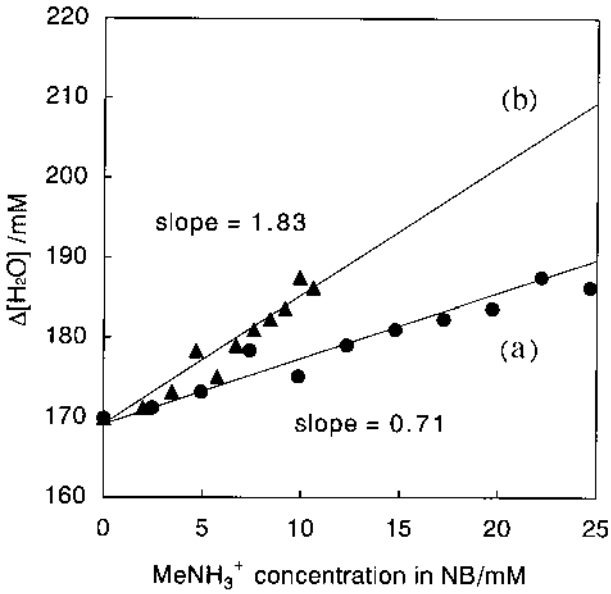

FIG. 13 Plots of the increase in water concentration in NB against the equilibrium concentration of $MeNH_3^+$ distributed to the NB phase. For the plots (a) and (b), the abscissa indicates, respectively, the total concentration of $MeNH_3^+$ (i.e., including the ion pair) and the concentration of the free $MeNH_3^+$ ion. (From Ref. 16.)

initially situated near the $\geqslant NH^+$ group, deflected away two water molecules. Thus, substitution of hydrogen atom(s) with alkyl group(s) indicates a reduction in binding sites. However, an increase in alkyl chain length (i.e., Me → Et → *n*-Bu) appears to provide no additional steric hindrance to the approach of water molecule(s), since the binding site is located at the apex of a pyramid composed of sp^3 hybrid orbitals [69].

TABLE 6 n_h Values of $R_mNH_{4-m}^+$ in NB Compensated for the Ion-Pair Effects

	n_h		
$R_mNH_{4-m}^+$	TPB^- system	DPA^- system	av
$MeNH_3^+$	1.83±0.16	1.67±0.07	1.75±0.09
$EtNH_3^+$	1.79±0.27	1.53±0.06	1.66±0.14
n-$BuNH_3^+$	1.50±0.12	1.54±0.10	1.52±0.08
$Me_2NH_2^+$	—	1.07±0.04	1.07±0.04
$Et_2NH_2^+$	—	1.07±0.05	1.07±0.05
n-$Bu_2NH_2^+$	0.97±0.06	1.05±0.03	1.01±0.03
Me_3NH^+	0.78±0.07	0.62±0.05	0.70±0.04
Et_3NH^+	0.70±0.04	0.69±0.03	0.70±0.03
n-Bu_3NH^+	0.51±0.05	—	0.51±0.05
Me_4N^+	—	0.00	0.00
Et_4N^+	0.00	0.00	0.00
n-Bu_4N^+	0.00	—	0.00

Source: Ref. 16.

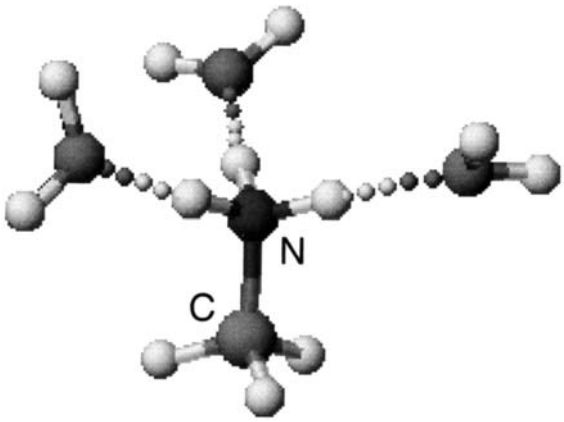

FIG. 14 Optimized structure of $MeNH_3^+$ associated with three water molecules. Dotted lines represent hydrogen bonds. (From Ref. 16.)

B. Carboxylate Ions

Eight different carboxylate ions (RCO_2^-; R = (**1**) Ph, (**2**) *o*-, (**3**) *m*-, (**4**) *p*-Tol, (**5**) Ph_2CH, (**6**) *cyc*-$(C_6H_{11})CH_2$, (**7**) *n*-C_5H_{11}, and (**8**) *n*-C_7H_{15}) were extracted from W to NB with a cationic dye, Crystal Violet [tris-(4-dimethylaminophenyl)methyl chloride] [17]. The sodium salts of the carboxylates and Crystal Violet chloride were initially added, respectively, to the W and NB phases (volume ratio 1:1) at the same concentration in the range 5–20 mM. Because Crystal Violet cation (CV^+) is very hydrophobic, it can draw RCO_2^- to NB by releasing Cl^- into W. In a similar manner as previously described [15,16], the equilibrium concentration of water in the NB phase was determined at 25°C by means of a Karl Fischer coulometer.

Spectrophotometric determination of CV^+ in the W phase showed that CV^+ almost completely remained in the NB phase. Potentiometric titration with a standard silver nitrate solution showed that a part (0.7–18%) of Cl^- initially added to the NB phase remained unexchanged with RCO_2^- in the W phase. The equilibrium concentration of RCO_2^- in NB was evaluated from its initial concentration and the concentration of Cl^- remaining in NB. Such distribution behavior of the ions in the NB–W system could be elucidated by using the above-mentioned theory [30–32], in which the standard ion-transfer potential $\Delta_o^w\phi_i^\circ$) is used as a measure of extractability of an individual ion. It could be thus concluded that, in this system, the ions are distributed individually without forming ion pairs.

The water extractability of CV^+ was examined in advance by performing a distribution experiment with no addition of carboxylate ions. The results showed that 3.8 mol of water molecules were extracted with 1 mol of CV^+Cl^-, but all the water molecules should be allocated to Cl^- that is known to convey four water molecules [15]. Therefore, it can be assumed that CV^+ transports no water molecules to NB.

In Fig. 15, the plot (a) shows a linear dependence of $\Delta[H_2O]$ on the equilibrium concentration of benzoate ion (**1**) in NB. However, since a part of Cl^- remained in NB as described above, its contribution to $\Delta[H_2O]$ should be evaluated to obtain the correct n_h value for the carboxylate ion. Using the value of $n_h = 4.0$ for Cl^- [15], the value of $\Delta[H_2O]$ was corrected to obtain the plot (b). From the slope of the linear

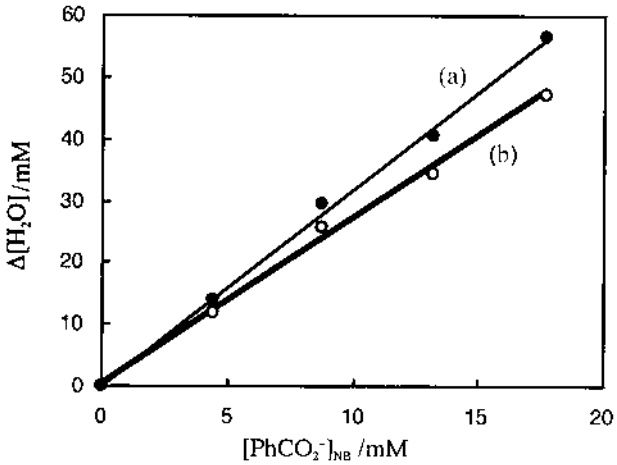

FIG. 15 (a) Plot of the increase in water concentration in NB ($\Delta[H_2O]$) with extraction of carboxylate ion **1** with CV^+ against the equilibrium concentration of the carboxylate ion in NB. (b) Plot corrected for the contribution of Cl^- to $\Delta[H_2O]$. When $[PhCO_2]_{NB} = 0$ mM, $[H_2O]$ was 185 mM in NB. (From Ref. 17.)

regression line, the n_h value for **1** was evaluated to be 2.7 ± 0.2. Similar linear plots were obtained for the other carboxylate ions (**2–8**), and their n_h values thus determined are shown in Table 7.

As seen in Table 7, the n_h values for the carboxylate ions examined are little dependent on their chemical structures. There is no noticeable difference in n_h between the aromatic and aliphatic groups. Thus, it has been found that a carboxylate ($-CO_2^-$) group is selectively hydrated by 2.4 ± 0.2 water molecules in NB. This hydration number determined for $-CO_2^-$ is larger than that observed for an amino group ($-NH_3^+$), i.e., $n_h = 1.64$ in NB [16]. As is generally well known, $-CO_2^-$ has a larger water-holding capacity, which has been confirmed here as well. It is expected that an amino acid having both $-CO_2^-$ and $-NH_3^+$ in its structure holds at least four water molecules in NB.

TABLE 7 Hydration Numbers of Carboxylate Ions (RCO_2^-) in NB at 25°C

Entry	R	n_h
1	Ph	2.7 ± 0.2
2	*o*-Tol	2.4 ± 0.2
3	*m*-Tol	2.4 ± 0.2
4	*p*-Tol	2.5 ± 0.2
5	Ph_2CH	2.1 ± 0.4
6	*cyc*-$(C_6H_{11})CH_2$	2.4 ± 0.2
7	*n*-C_5H_{11}	2.5 ± 0.4
8	*n*-C_7H_{15}	2.3 ± 0.3

Source: Ref. 17.

VI. CONCLUDING REMARKS

Solvent-extraction experiments combined with Karl Fischer coulometry have revealed that hydrophilic inorganic ions and some charged groups (e.g., $-CO_2^-$ and $-NH_3^+$) in organic ions have the ability to transport certain water molecules into water-immiscible NB. Such phenomena can be elucidated in terms of selective hydration of ions in organic solvent. It has been undoubtedly shown by the ^1H NMR study that the hydration of hydrophilic ions proceeds by a successive reaction mechanism. For this reason, the hydration number of ions in organic solvent is not necessarily an integer.

For understanding the transfer processes of hydrophilic ions at the O/W interface, it is essential to take into account the role of water molecules associated with the ions in the O phase. The assumption that a hydrophilic ion transfers across the interface as the hydrated ion has enabled us to elucidate the Gibbs energy of the ion transfer very well, on the basis of a nonBornian solvation model. The hydrogen bonds, which are formed around a hydrated ion in the W phase and which must be broken in its transfer to the O phase, seem to play a major role in the transfer energy.

Hydration phenomena of ions in organic solvents and their roles in interfacial ion-transfer processes have been extensively discussed for many years.. As discussed in this chapter, a marked development in this field may be recognized, at least from a thermodynamic viewpoint. However, no detailed molecular pictures of hydrated ions in organic solvent have been provided yet. Further experimental and theoretical approaches seem to be required. Vibrational spectroscopic and molecular dynamics simulation studies on solvation of ions in the gas phase [70,71] would shed light on the microscopic structure and dynamics of hydrated ions in organic solvents.

REFERENCES

1. J Rais, M Kyrš, M Pivoňková. J Inorg Nucl Chem 30:611–619, 1968.
2. S Motomizu, K Tôei, T Iwachido. Bull Chem Soc Jpn 42:1006–1010, 1969.
3. M Kawasaki, K Tôei, T Iwachido. Chem Lett 417–420, 1972.
4. T Iwachido, M Minami, A Sadakane, K Tôei. Chem Lett 1511–1514, 1977.
5. T Iwachido, M Minami, M Kimura, A Sadakane, M Kawasaki, K Tôei. Bull Chem Soc Jpn 53:703–708, 1980.
6. Y Yamamoto, T Tarumoto, T Tarui. Chem Lett 459–461, 1972.
7. Y Yamamoto, T Tarumoto, T Tarui. Bull Chem Soc Jpn 46:1466–1467, 1973.
8. T Kenjo, RM Diamond. J Phys Chem 76:2454–2459, 1972.
9. T Kenjo, RM Diamond. J Inorg Nucl Chem 36:183–188, 1974.
10. S Kusakabe, M Shinoda, K Kusafuka. Bull Chem Soc Jpn 62:333–335, 1989.
11. S Kusakabe, M Arai. Bull Chem Soc Jpn 69:581–588, 1996.
12. S Kusakabe. Solvent Extr Ion Exch 15:219–229, 1997.
13. S Kusakabe. Solvent Extr Res Dev Jpn 4:147–156, 1997.
14. S Kusakabe. Bull Chem Soc Jpn 73:1171–1177, 2000.
15. T Osakai, A Ogata, K Ebina. J Phys Chem B 101:8341–8348, 1997.
16. A Ogata, Y Tsujino, T Osakai. Phys Chem Chem Phys 2:247–251, 2000.
17. T Osakai, S Nakata, H Ogawa. Chem Lett 558–559, 2001.
18. Y Marcus, Ion Solvation. Chichester, UK: John Wiley, 1985, pp 184–217.
19. N Grigorieff, TA Ceska, KH Downing, JM Baldwin, R Henderson. J Mol Biol 259:393–421, 1996.
20. I Benjamin. Science 261:1558–1560, 1993.

21. I Benjamin. In AG Volkov, DW Deamer, eds. CRC Press, Liquid–Liquid Interfaces: Theory and Methods. Boca Raton, FL: 1996, pp 179–211.
22. M Lauterbach, G Wipff, A Mark, WF van Gunsteren. Gazz Chim Ital 127:699–708, 1997.
23. M Born. Z Phys 1:45–48, 1920.
24. MH Abraham, J Liszi. J Chem Soc, Faraday Trans 1 74:1604–1614; 2858–2867, 1978.
25. MH Abraham, J Liszi, L Mészáros. J Chem Phys 70:2491–2496, 1979.
26. MH Abraham, J Liszi. J Inorg Nucl Chem 43:143–151, 1981.
27. AA Kornyshev, AG Volkov. J Electroanal Chem 180:363–381, 1984.
28. VS Markin, AG Volkov. Electrochim Acta 34:93–107, 1989.
29. T Osakai, K Ebina. J Phys Chem B 102:5691–5698, 1998.
30. LQ Hung. J Electroanal Chem 115:159–174, 1980.
31. T Kakutani, Y Nishiwaki, M Senda. Bunseki Kagaku (Sect E). 33:E175–E182, 1984.
32. T Kakiuchi. In AG Volkov, DW Deamer, eds. Liquid-Liquid Interfaces: Theory and Methods. Boca Raton, FL: CRC Press, 1996, pp 1–18.
33. Y Yoshida, M Matsui, O Shirai, K Maeda, S Kihara. Anal. Chim. Acta. 373:213–225, 1998.
34. J Koryta, P Vanýsek, M Březina. J Electroanal. Chem 75:211–228, 1977.
35. V Mareček, Z Samec. Anal Chim Acta 151:265–269, 1983.
36. ER Nightingale Jr. J Phys Chem 63:1381–1387, 1959.
37. AA Zavitsas. J Phys Chem B 105:7805–7817, 2001.
38. S Kihara, M Suzuki, K Maeda, K Ogura, M Matsui. J Electroanal Chem 210:147–159, 1986.
39. T Osakai, K Ebina. J Electroanal Chem 412:1–9, 1996.
40. HH Uhlig. J Phys Chem 41:1215–1225, 1937.
41. T Kakiuchi, M Nakanishi, M Senda. Bull Chem Soc Jpn 61:1845–1851, 1988.
42. T Osakai, T Kakutani, Y Nishiwaki, M Senda. Bunseki Kagaku (Sect E) 32:E81–E84, 1983.
43. Z Samec, V Mareček, D Homolka. Faraday Discuss Chem Soc 77:197–208, 1984.
44. B Hundhammer, S Wilke. J Electroanal. Chem 266:133–141, 1989.
45. T Osakai, K Muto. Anal Sci 14:157–162, 1998.
46. T Osakai, K Ebina, In: AG Volkov, ed. Liquid Interfaces in Chemical, Biological, and Pharmaceutical Applications. New York: Marcel Dekker, 2000, pp 23–49.
47. C Sánchez, E Leiva, SA Dassie, AM Baruzzi Bull Chem Soc Jpn 71:549–554, 1998.
48. A Karpfen, P Schuster. In: RR Dogonadze, E Kálmán, AA Kornyshev, J Ulstrup, eds. The Chemical Physics of Solvation: Part A, Theory of Solvation. Amsterdam: Elsevier, 1985, pp 265–312.
49. MK. Chantooni Jr, IM Kolthoff. J Am Chem Soc 89:1582–1586, 1967.
50. RL Benoit, SY. Lam. J Am. Chem Soc 96:7385–7390, 1974.
51. K Izutsu, S Sakura, T Fujinaga. Bull Chem Soc Jpn 45:445–450, 1972.
52. MCR Symons, SE. Jackson. J Chem Soc, Faraday Trans 1 75:1919–1928, 1979.
53. K Ito, E Iwamoto, Y Yamamoto. Bull Chem Soc Jpn 56:2290–2292, 1983.
54. DR Cogley, JN. Butler, E Grunwald. J Phys Chem 75:1477–1486, 1971.
55. MCR Symons, VK Thomas. J Chem Soc, Faraday Trans 1 77:1891–1897, 1981.
56. ID Kuntz, Jr. CJ Cheng. J Am Chem Soc 97:4852–4859, 1975.
57. MCR Symons, TA Shippey, PP. Rastogi. J Chem Soc, Faraday Trans, 1 76:2251–2258, 1980.
58. T Tarui. J Inorg Nucl Chem 37:1213–1215, 1975.
59. T Osakai, M Hoshino, M Izumi, M Kawakami, K Akasaka. J Phys Chem 104:12021–12027, 2000.
60. JR. Johnson, SD Christian, HE Affsprung. J Chem Soc (A) 1924–1928, 1967.
61. M Nakahara, C Kawai. Chem Lett 809–812, 1992.
62. T Osakai, A Tokura, H Ogawa, M Kawakami, K Akasaka. To be submitted.
63. TC Farrar, ED Becker. Pulse and Fourier Transform NMR, Introduction to Theory and Methods, New York: Academic Press, 1971, ch. 4.
64. DR Lide, ed. CRC Handbook of Chemistry and Physics. 80th ed. Boca Raton, CRC Press, 1999.
65. A Shimizu, Y Taniguchi. Bull Chem Soc Jpn 64:221–226, 1991.

66. JA. Riddick, WB. Bunger, Organic Solvents, New York: Wiley-Interscience, 1970.
67. R Motley, CE Meloan. Sepn Sci 3:279–284, 1968.
68. JJP Stewart. J Comput Chem 19:209–220, 1989.
69. M Gérin, J Fresco. Anal Chim Acta 67:155–164, 1978.
70. CJ Weinheimer, JM Lisy. J Chem Phys 105:2938–2941, 1996.
71. OM Cabarcos, JM Lisy. Chem Phys Lett 257:265–272, 1996.

5

Interfacial Potential and Distribution Equilibria Between Two Immiscible Electrolyte Solutions

LE QUOC HUNG National Center for Natural Science and Technology, Hanoi, Vietnam

I. INTRODUCTION

When a system consisting of two immiscible electrolyte solutions is in contact, depending on the standard Gibbs energy for transfer, noninteracting and interacting components and their products can, to different degrees, be transferred across the interface between the two phases, until a state of thermodynamic equilibrium in the system is established. The Galvani potential difference reaches a certain value in accordance with a definite concentration distribution for every component in the system.

Equilibrium concentration calculations based on the calculation of the Galvani potential difference between two phases was developed in the previous papers [1,2]. This chapter will systematize the theoretical distribution equilibrium calculation presented in Refs 1 and 2, evaluate how well the electrochemical concept is able to be applied to the study of the liquid – liquid extraction process, and establish the problem for the most general case where arbitrary interactions occur in the system.

II. FORMULATION OF THE GENERAL DISTRIBUTION EQUILIBRIUM PROBLEM

A. Assumptions

Let us consider a system consisting of two immiscible liquid phases α and β, with volumes V_α and V_β at temperature T. In the system there are I noninteracting components I ($i = 1, 2, \ldots, I$) and J interactions, with known equilibrium constants. For example, in the jth reaction, N_J reactants A_{nj} participate in a reaction as follows:

$$\nu_{1,j}A_{1,j} + \nu_{2,j}A_{2,j} + \cdots + \nu_{Nj,j}A_{Nj,j} \overset{kj}{\longleftrightarrow} \lambda_{1,j}B_{1,j} + \lambda_{2,j}B_{2,j} + \cdots + \lambda_{Lj,j}B_{Lj,j} \tag{1}$$

Briefly we can write

$$\sum_{n=1}^{N_j} \nu_{n,j}\, A_{n,j} \overset{k_j}{\longleftrightarrow} \sum_{l=1}^{L_j} \lambda_{\ell,j}\, B_{l,j} \tag{2}$$

where $\nu_{n,j}$, $\lambda_{l,j}$ are stoichiometric numbers of the reactant $A_{n,j}$ and of the product $B_{l,j}$; .k_j is the equilibrium constant of the jth reaction, defined as

$$k_j = \prod_{l=1}^{L_j} \alpha_{B_{l,j}}^{\lambda_{l,j}} \Big/ \prod_{n=1}^{N_j} \alpha_{A_{n,j}}^{\nu_{n,j}} \tag{3}$$

Here, $\alpha_{A_{n,j}}$ and $\alpha_{B_{n,j}}$ are the activities in phase α of the reactant $A_{n,j}$ and of product $B_{l,j}$ respectively. If the reaction (2) takes place in phase β we have

$$k_j' = \prod_{l=1}^{L_j} \alpha'^{\lambda_{l,j}}_{B_{l,j}} \Big/ \prod_{n=1}^{N_j} \alpha'^{\nu_{n,j}}_{A_{n,j}} \tag{4}$$

where $\alpha'_{A_{n,j}}$ and $\alpha'_{B_{n,j}}$ are activities of reactant $A_{n,j}$ and product $B_{l,j}$ in phase β, respectively. The system can be described by the scheme below:

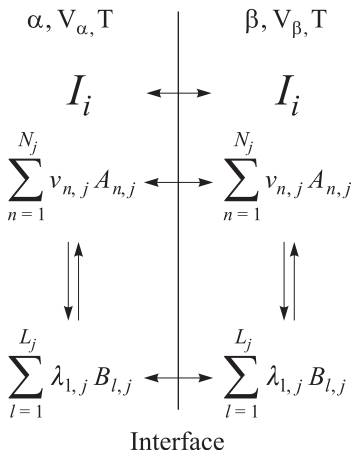

B. Unknowns

From the system described above we can establish a unique problem which contains the following unknowns:

—The first and the most important one is the Galvani potential difference or equilibrium potential between two phases $\Delta\varphi_{eq}$.
—Besides $\Delta\varphi_{eq}$, there are also unknowns corresponding to concentrations of all components in the system, i.e., $2I$ unknowns corresponding to the concentration of I noninteracting components in phases $\alpha(c_i)$ and $\alpha(c_i')$ with $i = 1, 2, \ldots, I$.

If N_j reactants participate in the jth reaction forming L_j products for J reactions occurring in the system, we have: $\sum_{j=1}^{J}(N_j + L_j)$ unknowns corresponding to the concentrations of the $\sum_{j=1}^{J}(N_j + L_j)$ reactants and products in phases $\alpha(c_{A_{n,j}} c_{B_{l,j}})$ and β $(c'_{A_{n,j}} c'_{B_{l,j}})$.

Thus, finally, the problem contains a total of unknowns:

$$2\,[I + \sum_{j=1}^{J} (N_j + L_j)] + 1 \tag{5}$$

In principle, in order to solve this equation we have to find the same number of independent equations.

C. Equations

1. Equations Based on the Electrochemical Potential Equilibrium Condition

In equilibrium the electrochemical potential $\tilde{\mu}_i$ of any component must be the same in both phases α and β:

$$\tilde{\mu}_i^{\alpha} = \tilde{\mu}_i^{\beta} \tag{6}$$

giving

$$\tilde{\mu}_i^{0,\alpha} + RT \ln a_i + z_i F \varphi^{\alpha} = \tilde{\mu}_i^{0,\beta} + RT \ln a_i' + z_i F \varphi^{\beta} \tag{7}$$

where $\tilde{\mu}_i^{0,\alpha}$ and $\tilde{\mu}_i^{0,\beta}$ are standard chemical potentials of the ith component in the phases α and β, respectively, and φ^{α} and $\varphi^{\beta}$are the electrical potentials of phases α and β, respectively; a_i and a_i' are the activities in phases α and β, z_i is the charge number of the ith component, and F is the Faraday constant.

From Eq. (7) we can calculate the concentration ratio of the ith component present in phases α and β to be

$$\alpha_i = \frac{c_i'}{c_i} = \frac{\gamma_i}{\gamma_i'} \exp\left[\frac{z_i F}{RT}\ \Delta\varphi\right] \exp\left[-\frac{\mu_i^{0,\beta} - \mu_i^{0,\alpha}}{RT}\right] \tag{8}$$

where $\Delta\varphi = \varphi^{\alpha} - \varphi^{\beta}$ is the potential difference between phases α and β, and γi and $\gamma i'$ are the activity coefficients of the ith component in phases α and β. Furthermore, we have

$$\tilde{\mu}_i^{0,\beta} - \tilde{\mu}_i^{0,\alpha} = \Delta G_{tr,\mathrm{i}}^{\circ} \tag{9}$$

where $\Delta G_{\mathrm{tr,i}}^{\circ}$ is the standard Gibbs energy for the transfer of the ith component from α to β. In the case of a neutral component ($z_i = 0$) we obtain from Eq. (8):

$$\alpha_i = \frac{c_i'}{c_i} = \frac{\gamma_i}{\gamma_i'} \exp\left[-\frac{\Delta G_{\mathrm{tr,i}}^{\circ}}{RT}\right] = D_i = \text{const.} \tag{10}$$

The distribution ratio of a neutral component does not depend on the potential difference at the interface and is called the distribution coefficient.

For an ionic species, Eq. (8) can be written in the form:

$$\alpha_i = \frac{c_i'}{c_i} = \frac{\gamma_i}{\gamma_i'} \exp\left[\frac{z_i F}{RT}\,(\Delta\varphi - \Delta\varphi_i^{\circ})\right] \tag{11}$$

The concentration ratio, depending on $\Delta\varphi$,

$$\Delta\varphi_i^{\circ} = \frac{\Delta G_{\mathrm{tr,i}}^{\circ}}{z_i F} \tag{12}$$

is called the standard Galvani potential difference between phases α and β corresponding to transfer of the ith ion.

The standard Galvani potential difference, which, on a purely thermodynamic basis, is inaccessible to measurement, can be calculated from extraction data [3,4] by using some additional thermodynamic assumptions, e.g., the TATB assumption [5]. This supposes that the standard Gibbs transfer energies of tetraphenylarsonium cation and tetraphenylborate anion between any pair of solvents are equal. A table of the standard Gibbs energies for transfer of ions from one solvent to the other can be constructed by using standard Gibbs energies of salts calculated from Eq. (12), as shown in [Refs.3,4,6–10], and recently in Ref. 11 (see Table 1). Osakai and Ebina reported the possibility for prediction of a standard transfer potentials by using nonBornian theory [12,13].

From the electrochemical potential equilibrium condition, we have a total of

TABLE 1 Standard Ion-Transfer Potential $\Delta\varphi_i^o$ (V) for Mutually Saturated Water Organic Solvent System at 25°C

Ion	Nitrobenzene	1,2-Dichloroethane	Dichloromethane
Li+	0.298	0.493	
Na+	0.355	0.490	
H+	0.337		
NH_4^+	0.280		
K+	0.241	0.499	
Rb+	0.201	0.445	
Cs+	0.159	0.36	
Acetylcholine	0.052		
$(CH_3)_4N^+$ (TMA)	0.037	0.182	0.195
$(C_2H_5)_4N^+$ (TEA)	−0.063	0.044	0.044
$(C_3H_7)_4N^+$ (TPrA)	−0.160	−0.091	−0.091
$(C_4H_9)_4N^+$ (TBA)	−0.270	−0.225	−0.230
$(C_5H_{11})_4N^+$		−0.360	−0.377
$(C_6H_5)_4As^+$ (TPAs)	−0.372	−0.364	
Crystal Violet	−0.410		
$(C_6H_{13})_4N^+$	−0.472	−0.494	−0.455
Mg^{2+}	0.370		
Ca^{2+}	0.354		
Sr^{2+}	0.348		
Ba^{2+}	0.320		
Cl^-	−0.395	−0.481	−0.481
Br^-	−0.335	−0.408	−0.408
NO_3^-	−0.270		
I^-	−0.195	−0.273	−0.273
SCN^-	−0.161		
BF_6^-	−0.091		
ClO_4^-	−0.091	−0.178	−0.221
2,4-Dinitrophenolate	−0.077		
PF_6^-	0.012		
Picrate	0.047	−0.069	−0.069
$(C_6H_5)_4B^-$ (TPB)	0.372	0.364	
Dipicrylaminate	0.414		
Dicarbonylcobaltate	0.520		

Source: Ref. 11.

$$n = I + \sum_{\mathrm{j}=1}^{J} (N_{\mathrm{j}} + L_{\mathrm{j}}) \tag{13}$$

equations in the form of Eq. (10) for neutral components and Eq. (11) for ionic components of all species present in the system.

2. Equations Obtained from Mass Conservation Law

Let us suppose that m_i and $m_{\mathrm{A_{n,j}}}$ are given amounts (in moles) of noninteracting components I and reactants $\mathrm{A_{n,j}}$ respectively. Using the mass conservation law we obtain $I + N_{\mathrm{j}}$ equations, including I equations for noninteracting components:

$$m_i = V_\alpha c_i + V_\beta c_i' \tag{14}$$

with $i = 1 \to I$ and $\sum_{\mathrm{j}=1}^{J} N_{\mathrm{j}}$ equations for reactants $\mathrm{A_{n,j}}$:

$$\begin{aligned} m_{A_{\mathrm{n,j}}} \;=\; & V_\alpha \left(c_{\mathrm{A_{n,j}}} + \sum_{\mathrm{j}=1}^{J} \sum_{\mathrm{l}=1}^{L_{\mathrm{j}}} \beta_{\mathrm{n,l,j}}\, c_{B_{\mathrm{l,j}}} \right) \\ & + V_\beta \left(c'_{\mathrm{A_{n,j}}} + \sum_{\mathrm{j}=1}^{J} \sum_{\mathrm{l}=1}^{L_{\mathrm{j}}} \beta_{\mathrm{n,l,j}}\, c'_{B_{\mathrm{l,j}}} \right) \end{aligned} \tag{15}$$

with j values from 1 to J, ℓ values from 1 to L_{j} and n values from 1 to N_{j}, where $\beta_{\mathrm{n,l,j}}$ is the stoichiometric number of reactants $\mathrm{A_{n,j}}$ in the product $\mathrm{B_{l,j}}$. In the case where a reactant takes part in some reaction (concurrent reaction), the number of equations obtained from the mass conservation law and the electrochemical potential equilibrium condition is reduced in accordance with a decrease in the number of unknowns because some of the $\mathrm{A_{n,j}}$ coincide.

3. Equations Based on Stoichiometric Numbers

Assuming that all products in the system have zero initial concentration, and using the stoichiometric number of each product of the jth reaction at equilibrium, we can write $(\mathrm{L_j} - 1)$ equations briefly as follows:

$$m_{B_{\mathrm{1,j}}} \;:\; m_{B_{\mathrm{2,j}}} \;:\ldots:\; m_{B_{L_{\mathrm{j}},j}} \;=\; \lambda_{\mathrm{1,j}} \;:\; \lambda_{\mathrm{2,j}} \;:\ldots:\; \lambda_{\mathrm{L_j,j}} \tag{16}$$

or

$$\begin{aligned} & (V_\alpha c_{\mathrm{B_{1,j}}} + V_\beta c'_{\mathrm{B_{1,j}}}) \;:\; (V_\alpha c_{\mathrm{B_{2,j}}} + V_\beta c'_{\mathrm{B_{2,j}}}) \;:\ldots:\; (V_\alpha c_{\mathrm{B_{L_j,j}}} + V_\beta c'_{\mathrm{B_{L_j,j}}}) \\ & = \lambda_{\mathrm{1,j}} \;:\; \lambda_{\mathrm{2,j}} \;:\ldots:\; \lambda_{\mathrm{L_j,j}} \end{aligned} \tag{17}$$

If J interactions occur in the system, we obtain from Eq. (17):

$$\sum_{\mathrm{j}=1}^{J} (L_{\mathrm{j}} - 1) \;=\; \sum_{\mathrm{j}=1}^{J} L_{\mathrm{j}} - J \quad \text{equations.} \tag{18}$$

In the case where a product can be formed by some reactions, the number of equations obtained from Eqs (10), (11), and (17) is decreased because some products coincide. For example, for the first reaction we have

$$m_{\mathrm{B_{1,1}}} \;:\; m_{\mathrm{B_{2,1}}} \;=\; \lambda_{1,1} \;:\; \lambda_{2,1} \tag{19}$$

and for the second:

$$m_{B_{1,2}} : m_{B_{2,2}} = \lambda_{1,2} : \lambda_{2,2} \tag{20}$$

If $B_{1,1}$ is identical to $B_{1,2}$ and denoted by B_1, we obtain, instead of Eqs (19) and (20), the equation:

$$m_{B_1} = \frac{\lambda_{1,1} m_{B_{2,1}}}{\lambda_{2,1}} + \frac{\lambda_{1,2} m_{B_{2,2}}}{\lambda_{2,2}} \tag{21}$$

4. Equations for Equilibrium Constants

If J interactions occur in the system, we obtain J equations describing these equilibria:

$$k_j = \prod_{l=1}^{L_j} (\gamma_{l,j} c_{B_{l,j}})^{\lambda_{l,j}} / \prod_{n=1}^{N_j} (\gamma_{n,j} c_{A_{n,j}})^{\nu_{n,j}} \tag{22}$$

with $j = 1 \rightarrow J$.

5. Equation for Electrical Neutrality

When equilibrium between two phases is established, the equilibrium potential difference at the interface is called the Galvani potential difference or equilibrium potential. With respect to the electrical neutrality of each phase, we obtain the last equation:

$$\sum_{i=1}^{I} z_i c_i + \sum_{j=1}^{J} \left(\sum_{n=1}^{N_j} z_{n,j} c_{A_{n,j}} + \sum_{l=1}^{L_j} z_{l,j} c_{B_{l,j}} \right) = 0 \tag{23}$$

where z_i, $z_{n,j}$, and z_{lj} are the charge numbers of noninteracting species, I_i, of reactants $A_{n,j}$ and of products B_{lj}, respectively.

This means that this system of equations, in which the numbers of equations and unknowns are the same [see Eq. (5)], can in principle be solved by various methods. The solution of the problem gives the values of equilibrium potential difference and concentration of every component in any form in each phase. It is then easy to calculate distribution coefficients of every component:

For a noninteracting component, $$d_i = c_i'/c_i; \tag{24}$$

For an interacting component: $$d_{A_{n,j}} = \frac{c'_{A_{n,j}} + \sum_{j=1}^{J} \sum_{l=1}^{L_j} \beta_{n,l,j} c'_{B_{l,j}}}{c_{A_{n,j}} + \sum_{j=1}^{J} \sum_{l=1}^{L_j} \beta_{n,l,zj} c_{B_{l,j}}} \tag{25}$$

III. SOLUTION

As shown in Section II, the equations obtained above have different forms. Generally, it is a nonlinear system of equations. In particular, when the number of reactions and their order are large, the nonlinear level of the equation system increases, its solution becomes more difficult, and the problem needs to be solved with the aid of a computer. In the

previous papers [1,2] the present author dealt with some cases where the problem could be solved by analytical or approximate numerical methods. We define Q as an algebraic total of the charge of all components in the considered phase α Equation (23) then becomes

$$Q = \sum_{\mathrm{i}=1}^{I} z_i c_i + \sum_{\mathrm{j}=1}^{J} \left(\sum_{\mathrm{n}=1}^{N_\mathrm{j}} z_{n,\mathrm{j}} c_{A_{\mathrm{n,j}}} + \sum_{\mathrm{l}=1}^{L_\mathrm{j}} z_{\mathrm{l,j}} c_{B_{\mathrm{l,j}}} \right) \tag{26}$$

where c_i, $c_{\mathrm{An,j}}$, $c_{\mathrm{Bi,j}}$ are functions of $\Delta\varphi$; obviously, Q is also a function of $\Delta\varphi$. For simplicity we assume that the activity coefficients of all components are equal to 1. The equation system, in principle, provides only a simple solution. The most suitable method for solving the problem is a repeating method in which $\Delta\varphi$ can be found as follows.

At the start, we choose $\Delta\varphi_0$ where $Q(\Delta\varphi_0) < 0$ and $\Delta\varphi_1$ where $Q(\Delta\varphi_1 > 0$, for sure $\Delta\varphi_0 = -1V$ and $\Delta\varphi_1 = +1V$ respectively. Next, the approximate value of $\Delta\varphi$ is averaged for $\Delta\varphi_1$ and $\Delta\varphi_0$:

$$\Delta\varphi_2 = \frac{\Delta\varphi_0 + \Delta\varphi_1}{2} \tag{27}$$

if $Q(\Delta\varphi_2) < 0$, then

$$\Delta\varphi 3 = \frac{\Delta\varphi_2 + \Delta\varphi_1}{2} \tag{28}$$

and $Q(\Delta\varphi_2) > 0$, we have

$$\Delta\varphi_3 = \frac{\Delta\varphi_2 + \Delta\varphi_0}{2} \tag{29}$$

or generally, if $Q(\Delta\varphi_{\mathrm{n}-1}) < 0$ and $Q(\Delta\varphi_{\mathrm{n}}) > 0$:

$$\Delta\varphi_{n+1} = \frac{\Delta\varphi_{\mathrm{n}-1} + \Delta\varphi_{\mathrm{n}}}{2} \tag{30}$$

The calculation is repeated to the expected precision when $|\Delta\varphi_{\mathrm{n}} - \Delta\varphi_{n-1}| < P_{\mathrm{err}}$; P_{err} is a given error of calculation of equilibrium potential. It is defined as $\mathrm{Abs}(\Delta\varphi_{\mathrm{n}} - \Delta\varphi_{\mathrm{n}} \to \infty)$. The last calculated value of $\Delta\varphi$ is an approximation of $\Delta\varphi_{\mathrm{eq}}$. The relationship between the error of calculated equilibrium potential and repeating number is described as follows:

$$P_{\mathrm{err}} = \frac{\mathrm{Abs}(\Delta\varphi_1 - \Delta\varphi_0)}{2^n} \tag{31}$$

where $\mathrm{Abs}(\Delta\varphi_1 - \Delta\varphi_0)$ is the absolute value of $(\Delta\varphi_1 - \Delta\varphi_0)$.

The number of repeats is independent of the composition of the system. The convergence of calculation of $\Delta\varphi$ dependent on the number of repeats is shown in Fig. 1. In this case with $\Delta\varphi_0 = 1V$ and $\Delta\varphi_1 = +1V$, the error for potential calculation P_{err} reaches $10^{-8}V$ after 21 repeats. Based on this procedure, a computer program entitled EXTRA.HH1 was written in Delphi 0.5 for general cases of noninteracting and interacting systems. All the results (tables of data or graphics) presented in this chapter are calculated from this software. The simplest program in Turbo Pascal for the case of noninteracting ions is shown in the appendix. The solution of the program provides:

- Equilibrium potential difference between two phases
- Concentration of every component in any existing form in each phase
- Influence of :
  —non-interaction ions
  —complex formation

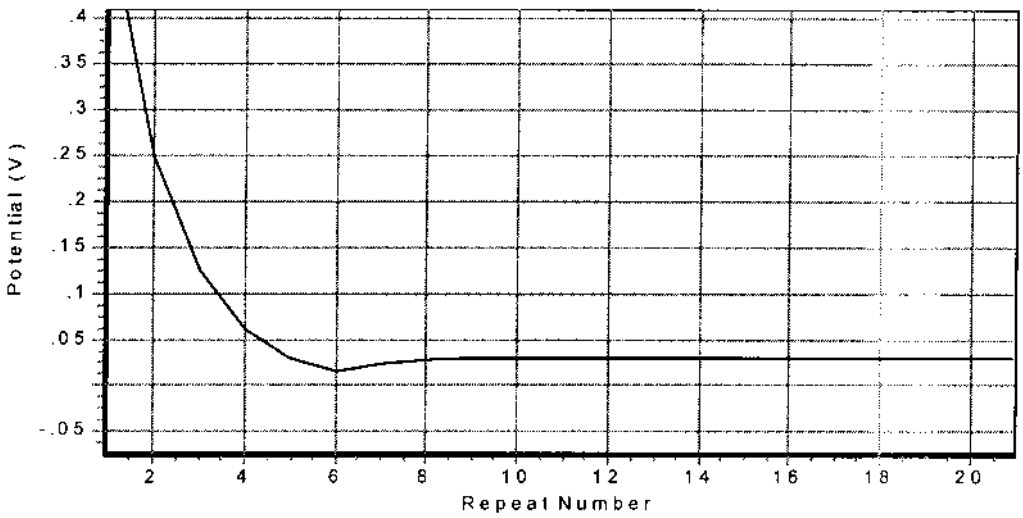

FIG. 1 Dependence of calculated potential on repeating number.

—ion association
—volume ratio of phase
—temperature
—solvents
on Galvani potential and distribution concentration of every component in the system.

- The shift of Galvani potential can be considered as a quantitative merit of those influences.

As illustrated in the following sections, from results obtained, it is also convenient to explain and estimate the properties of a liquid–liquid system.

IV. SOME SPECIAL CASES

For an electrolyte–electrolyte system, such as the water-nitrobenzene system, both phases are polar solvents where solutions can dissociate into ions.

A. Noninteracting System

Let us consider the system consisting of I noninteracting components I_i. As no interaction occurs in either phase, all equilibrium constants are equal to zero. From Eqs. (11) and (14) we have

$$m_i = V_\alpha c_i + V_\beta \alpha_i c_i \tag{32}$$

or

$$c_i = m_i/(V_\alpha + V_\beta \alpha_i) \tag{33}$$

Combining Eqs. (33) and (26) we have

$$Q = \sum_{i=1}^{I} z_i c_i = \sum_{i=1}^{I} z_i m_i / (V_\alpha + V_\beta \alpha_i) = 0 \tag{34}$$

or

$$\sum_{i=1}^{I} \frac{z_i m_i}{V_\alpha + V_\beta (\gamma_i / \gamma_{i'}) \exp[(z_i F / RT)(\Delta\varphi - \Delta\varphi_i^\circ)}} = 0 \tag{35}$$

In order to solve Eq. (35), we consider Q as a function of $\Delta\varphi$:

$$Q = \sum_{i=1}^{I} \frac{z_i m_i}{V_\alpha + V_\beta (\gamma_i / \gamma_{i'}) \exp[(z_i F / RT)(\Delta\varphi - \Delta\varphi_i^\circ)}} \tag{36}$$

Figure 2 shows how the concentration of every component in phase β and, as a consequence, the total charge Q, depends on $\Delta\varphi$ and is very useful for the understanding of electroextraction. Although the curve $Q - \Delta\varphi$ is different from curve $i - \Delta\varphi$, the former curve can be used for predicting properties of the polarization curve, when a linear potential difference is applied to the interface. The solution of Eq. (35) is $\Delta\varphi$ where $Q \to 0$. The $\Delta\varphi_{eq}$ is called the equilibrium potential.

1. System of Two Salts with a Common Cation

Let us consider the following system (see Table 2):

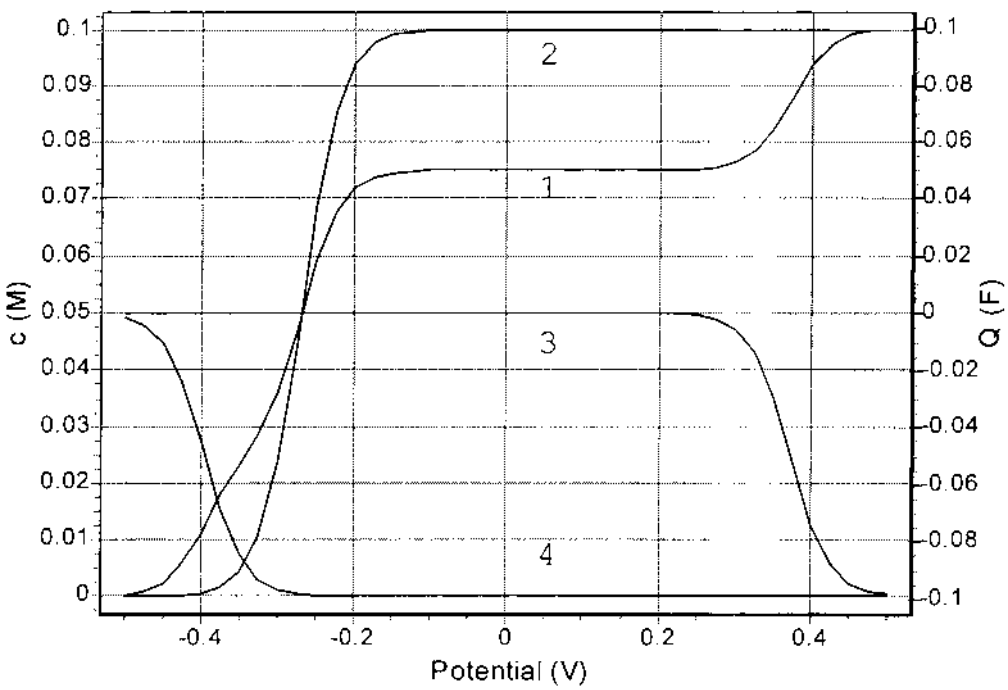

FIG. 2 Dependence of charge in every phase and concentration of ions in phase β on potential difference when $Q = 0$, $\Delta\varphi_{eq} = \Delta\varphi$; 1—$Q$; 2—$TBA^+$, 3—$TPB^-$, 4—$Cl^-$.

TABLE 2 Equilibrium Situation of System I

Ion	C_w	C_{NB}	d	% in NB
TBA^+	4.963×10^{-2}	5.037×10^{-2}	1.015	5.037×10^{1}
TPB^-	6.927×10^{-13}	5.000×10^{-2}	7.218×10^{10}	1.000×10^{2}
Cl^-	4.963×10^{-2}	3.748×10^{-4}	7.552×10^{-3}	7.495×10^{-1}

Equilibrium potential = 0.2696 V.

System I: 0.05 M TBACl in water (W) and 0.05 M tetrabutylammonium tetraphenylborate (TBATPB) in nitrobenzene (NB), with volume ratio $V_w/V_{nb=1}$.

The terms C_w, C_{NB}, d, and % in NB, in Table 2, are concentrations of the components in water, nitrobenzene, distribution coefficient, and percentage of ion in nitrobenzen, respectively.

From this table it was shown that in the equilibrium ($Q = 0$), $\Delta\varphi_{eq}$ equals -0.2696 V with 50.37 % of TBA^+, 0.7495% of Cl^-, and nearly 100% of TPB^- present in NB. Such a kind of system is characterized by a drastic change in the Q plot at the values close to zero. In order to shift the potential from -0.2696 to -0.220 V, a large amount of charge (0.0375 F) must be transfered through the interface. This charge is mainly contributed by the transfer of ≈ 0.03715 mol TBA^+ from W to NB, the rest by other ions. In this case, system I can be used for the interface of a reference electrode for a liquid–liquid membrane ion-selective electrode, as the presence of other ions has negligible influence on the equilibrium potential.

2. System of Ions with Large Difference in Standard Transfer Potential

We now consider a system (System II) of two salts, one of which is strongly soluble in water (NaCl) and the other (TBATPB) in NB. The standard transfer potential of all ions in the system is strongly negative or strongly positive.

System II: 0.05 M NaCl in water, 0.05 M TBATPB in NB with volume ratio $V_w/V_{nb=1}$.

As shown in Fig. 3 the curve Q versus potential has a wide plateau (from -0.125 to $+0.2$ V) whereas the Q values are close to zero. With this change in potential, only a negligible amount of charge (0.00076 F) is transferred through the interface, which behaves like an ideal polarization interface. The potential window for voltammetric measurement is wide. On the other hand, the equilibrium potential is sensitive to the presence of ions that have standard transfer potentials within the window. Therefore, system II cannot be used as a reference electrode.

For system II the equilibrium establishes at a potential of 0.0373 V; the distribution of concentrations of all components are shown in Table 3:

Table 3 indicates that, in equilibrium, depending on the standard transfer potential, the amount of ions transferred from one phase to another follow the order: $Cl^- < TPB^- < Na^+ < TBA^+$.

3. Influence of Ions with Small Standard Transfer Potential

In the system of KCl and TBATPB, the presence of ions, that can be easily transferred through the interface (standard transfer potential of the ion is close to zero) can strongly influence the galvani potential and the distribution equilibrium as well. Let us consider the system:

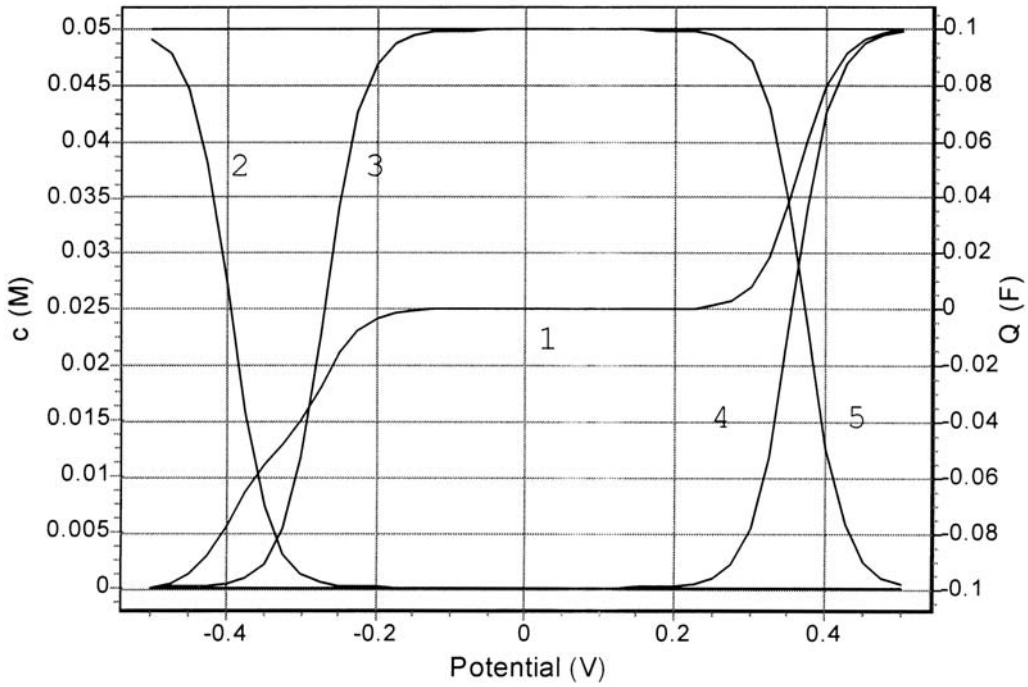

FIG. 3 Dependence of charge in every phase and concentration of ions in phase β on potential difference when $Q = 0$, $\Delta\varphi_{eq} = \Delta\varphi$: 1—Q; 2—Cl^-, 3—TBA^+, 4—Na^+, 5—TPB^-.

System III: 0.1 M KCl, 0.01 M tetraethylammonium chloride (TEACl) in water, 0.05 M TBATPB in NB, with volume ratio $V_w/V\text{nb} = 1$.

The dependence of Q and concentration of ions on the potential is shown in Fig. 4. Table 4 presents the equilibrium potential and concentration in both phases, and the distribution coefficient and percentage of all components in NB.

Figure 5 indicates clearly the role of so-called potential-determining ions. With the addition of TEA, the equilibrium potential changes linearly with the logarithm of concentration of C_{TEA} in the range from -5.5 to 0 with a slope of about 31.5 mV/decade of C_{TEA}. In equilibrium there is only 0.42% of TEA moved from W to NB. The transfer of TEA from W to NB accompanying Cl^- forces 3.4910^{-3} M TBA^+, 3.3×10^{-6} M K^+ and 7.9×10^{-8} M H^+ from NB to W.

On the other hand, the addition of HCl (Fig. 6) or of $CaCl_2$ (Fig. 7) with the same concentration range (from 10^{-8} to 1 M) has a negligible influence on the equilibrium.

TABLE 3 Equilibrium Situation of System II

Ion	C_W	C_{NB}	d	% in NB
Na	5.000×10^{-2}	2.098×10^{-7}	4.195×10^{-6}	4.195×10^{-4}
TBA	3.155×10^{-7}	5.000×10^{-2}	1.585×10^{5}	1.000×10^{2}
TPB	1.082×10^{-7}	5.000×10^{-2}	4.623×10^{5}	1.000×10^{2}
Cl	5.000×10^{-2}	2.419×10^{-9}	4.837×10^{8}	4.837×10^{-6}

Equilibrium potential = 0.0373 V.

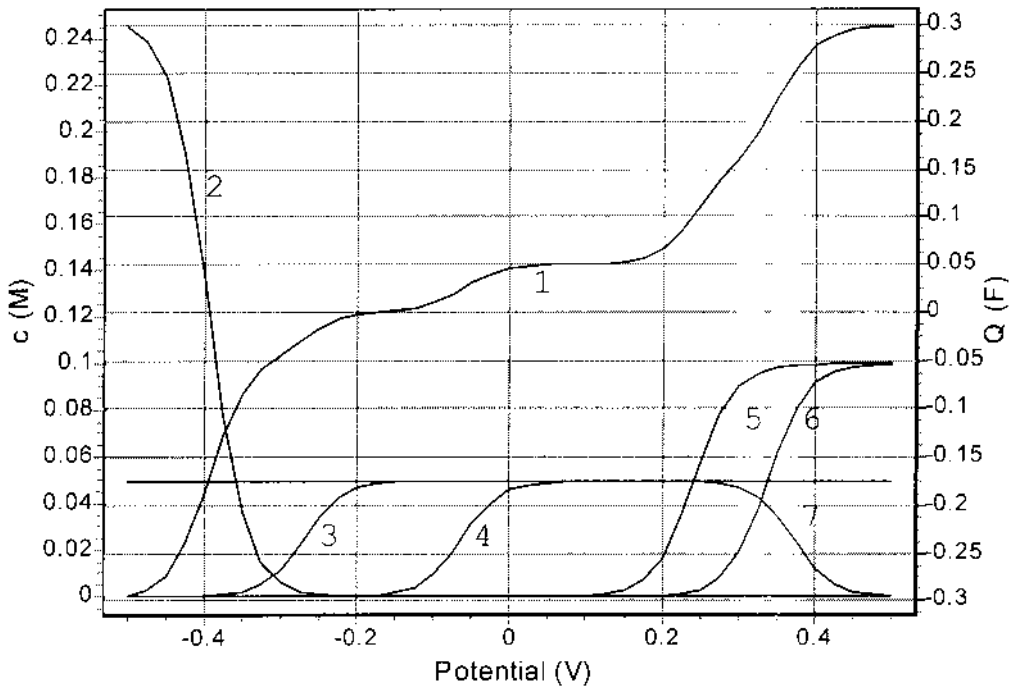

FIG. 4 Dependence of total charge (Q) and concentration of ions in nitrobenzene (NB) on applied potential difference in system III: 1—Q; 2—Cl^-; 3—TBA^+; 4—TEA^+; 5—K^+; 6—H^+; 7—TPB^-.

B. Interacting System

Influence of first-order interactions such as complex formation or ion-pair formation on equilibrium potential and distribution concentration has been shown [1,2,14,15].

1. Complex Formation

Complex formation between an ion with a neutral ligand plays an important role in biomembrane transport, liquid–liquid membranes, and ion-selective electrodes and in liquid–liquid extraction as well. For an example, we consider the system:

TABLE 4 Equilibrium Situation of System III

Ion	C_W	C_{NB}	d	% in NB
H^+	1.000×10^{-1}	3.072×10^{-10}	3.072×10^{-9}	3.072×10^{-7}
K^+	1.000×10^{-1}	1.295×10^{-8}	1.295×10^{-7}	1.295×10^{-5}
TEA^+	4.911×10^{-2}	8.873×10^{-4}	1.807×10^{-2}	1.775
TBA^+	8.540×10^{-4}	4.915×10^{-2}	5.755×10^{1}	9.829×10^{1}
TPB^-	3.927×10^{-11}	5.000×10^{-2}	1.273×10^{9}	1.000×10^{2}
Cl^-	2.500×10^{-1}	3.330×10^{-5}	1.332×10^{-4}	1.332×10^{-2}

Equilibrium potential = −0.1660 V.

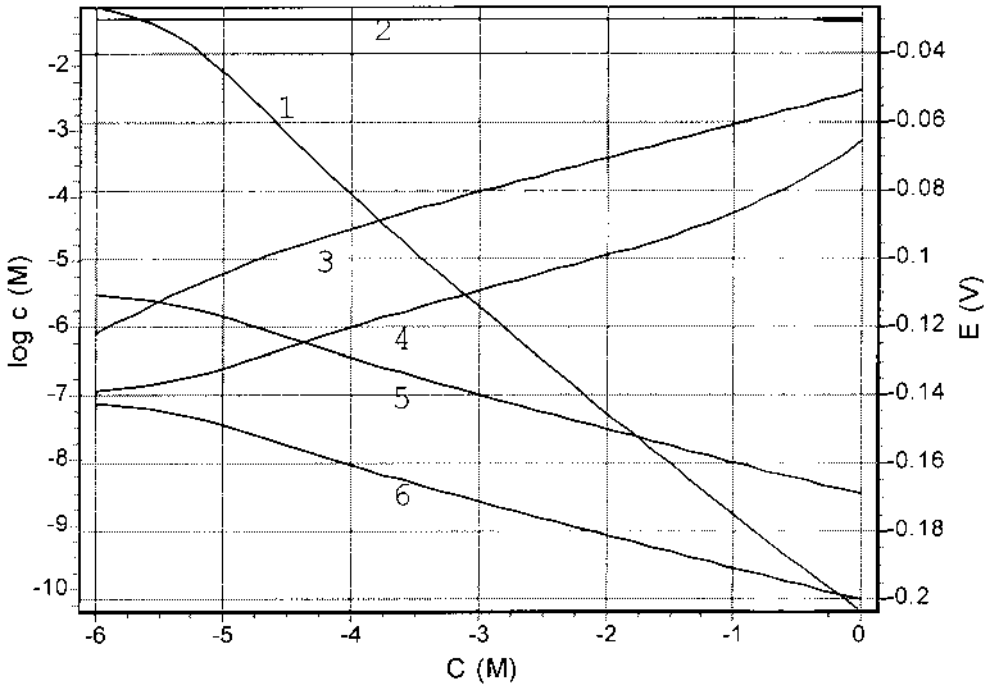

FIG. 5 Dependence of equilibrium potential (E) and the distribution ratio of ions in NB on the initial concentration of TEA in system III: 1—E; 2—TPB^-; 3—TEA^+; 4—Cl^-; 5—K^+; 6—H^+.

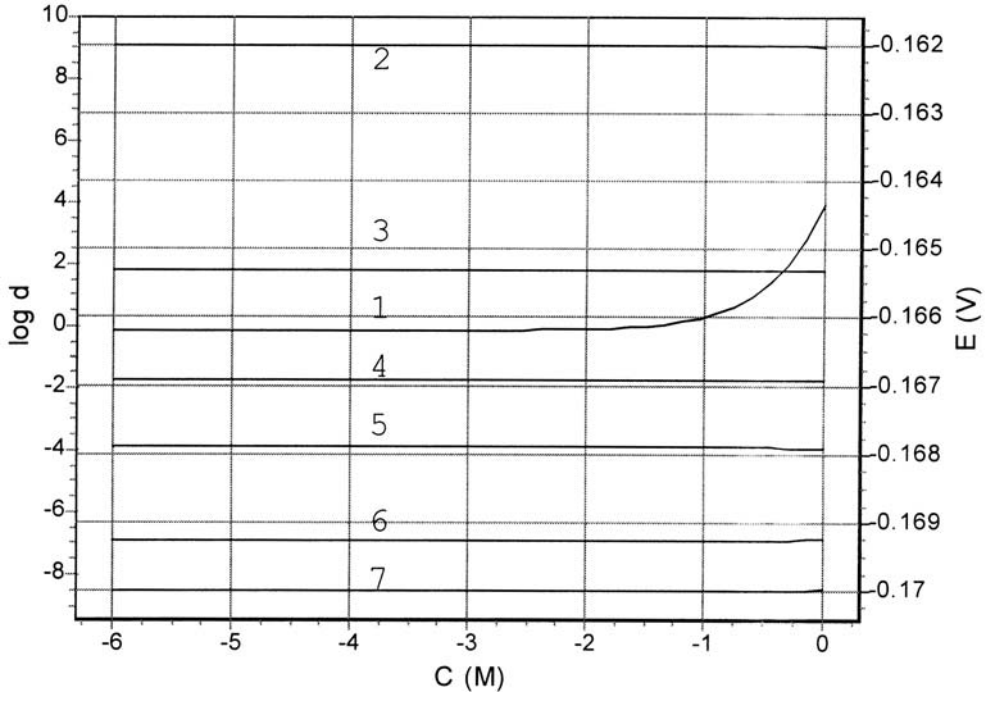

FIG. 6 Dependence of equilibrium potential (E) and the distribution coefficient of ions in NB on the initial concentration of HCl in system III: 1—E; 2—TPB^-; 3—TBA^+; 4—TEA^+; 5—Cl^-; 6—K^+; 7—H^+.

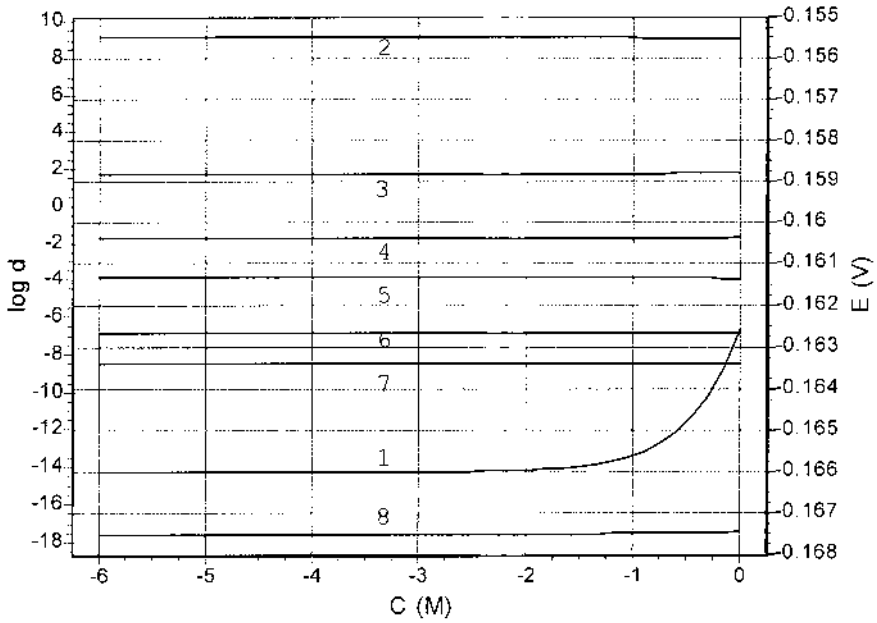

FIG. 7 Dependence of equilibrium potential (E) and the distribution coefficient of ions in NB on the initial concentration of $CaCl_2$; 1—E; 2—TPB^-; 3—TBA^+; 4—TEA^+; 5—Cl^-; 6—K^+; 7—H^+; 8—Ca^{2+}.

System IV: 0.1 M KCl, 0.1M HCl in water, 0.01 M dibenzo-18-crown-6, and 0.05 M TBATPB in NB, with a volume ratio $V_w/V_{nb} = 1$. We have the following reactions:

In W:

$$K^+ + X \overset{k_W}{\leftrightarrows} [KX]^+$$

Similarly, in NB:

$$K^+ + X \overset{k_{NB}}{\leftrightarrows} [KX]^+$$

where dibenzo-18-crown-6 is symbolized as X, and K_W and K_{NB} are equilibrium constants in W and NB, respectively.

For calculation of the equilibrium potential and distribution concentration of components we have to know all the parameters as mentioned in Section II. Here, we suppose that complex formation taking place mainly in NB with $K_{NB} = 5.01 \times 10^{-6}$ does not occur in W; let us accept that $K_W = 0.001$. It is also necessary to know the distribution coefficient of dibenzo-18-crown-6; therefore, we assume that dibenzo-18-crown-6 dissolves mainly in NB with $d_x = 1.8 \times 10^6$.

If we define:

$$B_{K+} = V_\alpha + V_\beta \alpha_{K+} \tag{37}$$

$$B_X = V_\alpha + V_\beta \alpha_X \tag{38}$$

$$B_{KX} = V_\alpha + V_\beta \alpha_K \alpha_X \tag{39}$$

where α_{K+} is calculated by Eq. (11) and α_X is a distribution coefficient of X, because the initial amount of K^+ or X in the system is equal to the total of free K^+ or X and $[KX]^+$ in the system, respectively, we have

$$m_{K+} = C_{K^+}B_{K^+} + C_{K^+}C_X B_{[KX]^+} \tag{40}$$

$$m_X = C_X B_X + C_{K^+}C_X B_{[KX]^+} \tag{41}$$

where m_{K^+}, and m_X are the initial amounts of K^+ and X in the system, respectively. From Eq. (40) we obtain:

$$C_{K+} = m_{K^+}/(B_{K^+} + C_X B_{[KX]^+}) \tag{42}$$

By substituting Eq. (42) into Eq. (41), we have a second-order equation:

$$D''_{KX]^+}C_X^2 + D_{KX]^+}C_X + D_{[KX]^+} = 0 \tag{43}$$

where:

$$D''_{[KX]^+} = B_X B_{[KX]^+} \tag{44}$$

$$D'_{[KX]^+} = B_X B_{[KX]^+} + B_{[KX]^+}\ (m_{K^+} - m_X) \tag{45}$$

$$D_{[KX]^+} = -m_X B_{K^+} \tag{46}$$

After solving Eq. (43) we find the concentration of X as a function of potential $\Delta\varphi$ [$C_X(\Delta\varphi)$] and by substituting C_X into Eq. (42) the dependence of concentration of K^+ on potential $C_{K^+}(\Delta\varphi)$ can be found as well. For noninteracting components, from Eq. (14) we have:

$$m_i = C_i(V_\alpha + V_\beta\alpha_i) \tag{47}$$

From Eq. (26) we obtain the last equation for electroneutrality. With the help of computer program EXTRA.HH1 this equation can be easily solved, giving the results presented in this section.

From Fig. 8 and Tables 5 and 6 it is indicated that, with addition of 0.01 M dibenzo-18-crown-6 to the system, the equilibrium potential strongly shifts from −0.027 to −0.162 V. The complex formation in NB facilitates removal of 7.263×10^{-4} M K^+ and 2.10×10^{-5} M Cl^- from W to NB and forces 7.00×10^{-4}M TBA^+ and 7.8×10^{-8} M H^+ from NB to water.

As shown in Fig. 9, the dependence of E on $\log K_{nb}$ is relatively linear when $\log K_{nb}$ varies from 3 to 8. The slope of curve E–$\log K_{nb}$ slightly depends on the concentration of dibenzo-18-crown-6 as follows:

With CKCl = 0.1M

$C_{\text{dibenzo-18-crown-6}} = 0.001$ M; slope of E–$\log K_{nb} = 27.6mV$

$C_{\text{dibenzo-18-crown-6}} = 0.01$ M; slope of E–$\log K_{nb} = 28.8mV$

$C_{\text{dibenzo-18-crown-6}} = 0.1$ M; slope of E–$\log K_{nb} = 29.1mV$

With $C_{\text{dibenzo-18-crown-6}}$ of 0.01 M, the slope of E–$\log K_{nb}$ is constant and equal to 28.8 mV with changes in KCl concentration from 0.01 to 0.1 M.

If complex-formation reactions occur in both phases, the second complex formation influences the equilibrium of the system only if $K_w > K_{nb}$ (see Fig. 10). Therefore, the calculation also provides the possibility for electrochemical determination of the equilibrium constant of complex-formation reactions.

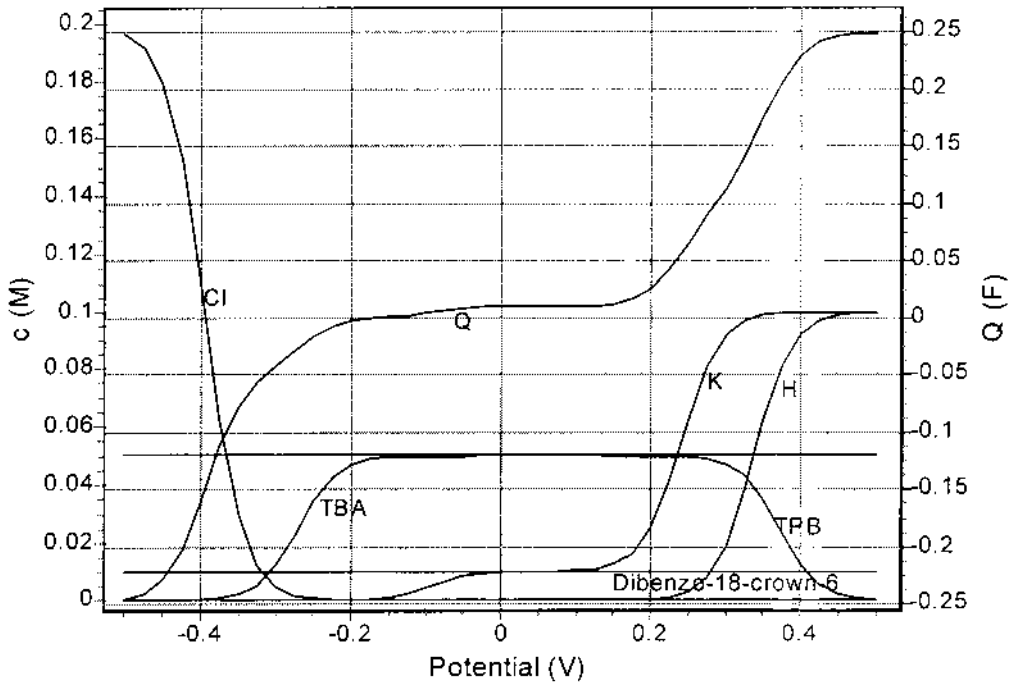

FIG. 8 Dependence of total charge (Q) and concentration of ions in NB on the potential in system IV: HQ; F$C1^-$; TBA^+; K^+; H^+; TPB^-; −dibenzo-18-crown-6.

Figure 11 indicates that the addition of HCl up to 1 M to the system of 0.1 M KCl/0.05 M TBATPB has no significant effect on the equilibrium. The equilibrium potential changes from 0.161 to 0.159 V, meanwhile KCl has a strong influence on the equilibrium of the system. If the equilibrium constant of the complex-formation reaction is 5.012×10^6, the addition of KCl in the concentration range from 10^{-6} M to 1 M to the system shifts the equilibrium potential to a negative value. The dependence of equilibrium potential (E) on the logarithm of KCl concentration is only relatively linear (see Fig. 12). With $\log C_{KCl}$ from −6.0 to −3.5, the slope of E–$\log C_{KCl}$ is ≈ 55.6 mV/decade of C_{KCl}. If the equilibrium constant of complex formation in NB is larger than 10^{10}, and the concentration of KCl is less than the concentration of X, the dependence of E on $\log C_{KCl}$ is

TABLE 5 Equilibrium Situation in System IV

Ion	C_w	C_{NB}	d	% in NB
K^+	9.927×10^{-2}	7.263×10^{-4}	7.316×10^{-3}	7.263×10^{-1}
Dibenzo-18-crown-6	5.077×10^{-9}	1.000×10^{-2}	1.970×10^{6}	1.000×10^{2}
H^+	1.000×10^{-1}	3.736×10^{-10}	3.736×10^{-9}	3.736×10^{-7}
TBA^+	7.044×10^{-4}	4.930×10^{-2}	6.998×10^{1}	9.859×10^{1}
TPB^-	4.776×10^{-11}	5.000×10^{-2}	1.047×10^{9}	1.000×10^{2}
Cl^-	2.000×10^{-1}	2.191×10^{-5}	1.095×10^{-4}	1.095×10^{-2}

Equilibrium potential = −0.1610 V.

TABLE 6 Equilibrium Situation in System IV in Absence of Dibenzo-18-Crown 6

Ion	C_w	C NB	d	% in NB
K^+	1.000×10^{-1}	3.360×10^{-6}	3.360×10^{-5}	3.360×10^{-3}
H^+	1.000×10^{-1}	7.974×10^{-8}	7.974×10^{-7}	7.974×10^{-5}
TBA^+	3.347×10^{-6}	5.000×10^{-2}	1.494×10^{4}	9.999×10^{1}
TPB^-	1.019×10^{-8}	5.000×10^{-2}	4.905×10^{6}	1.000×10^{2}
Cl^-	2.000×10^{-1}	1.026×10^{-7}	5.132×10^{-7}	5.132×10^{-5}

Equilibrium potential = −0.0233 V.

completely linearly with slope $\simeq$ 59 mV (Fig. 13). If the concentration of KCl is greater than the concentration of dibenzo-18-crown-6 the equilibrium potential reaches a constant value. Therefore, using the theoretical calculation, it is possible to choose a suitable ionophore for ion-selective electrodes and for the concentration range of determination of K^+.

The dependence of equilibrium potential (E) on the logarithm of concentration of dibenzo-18-crown-6 in system IV is relatively linear with slope = 54.2 mV when $K_{nb} = 5.012 \times 10^6$, (Fig. 14) and completely linear with slope = 59.3 mV when $K_{nb} > 5.012 \times 10^9$ (Fig. 15). Therefore, the calculation provides a possibility of determining the concentration of an ionophore by potentiometeric methods.

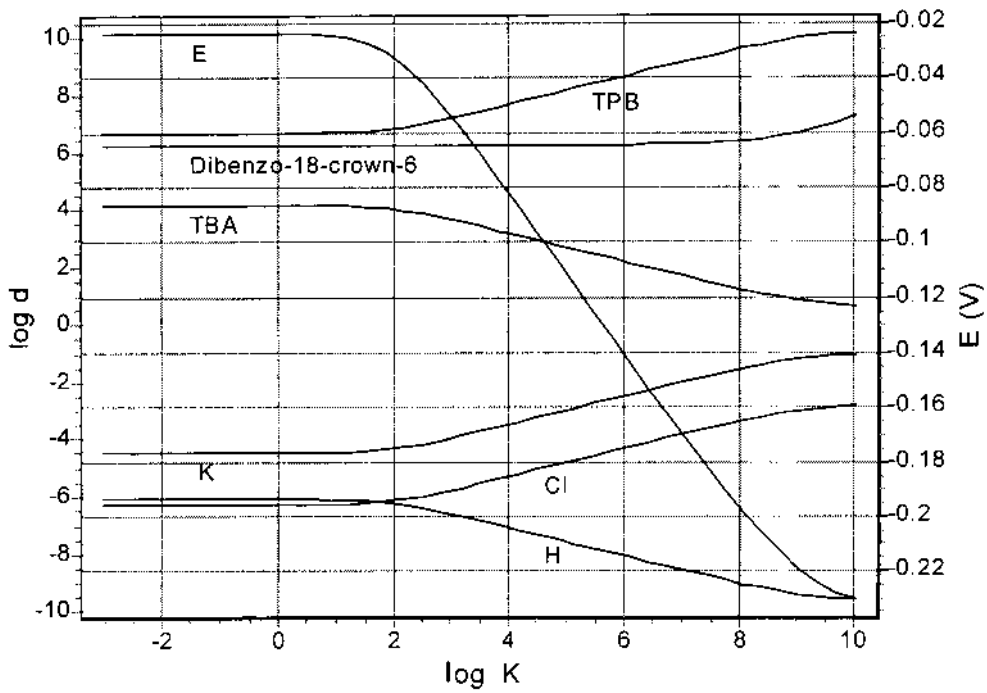

FIG. 9 Dependence of equilibrium potential (E) and the distribution coefficient of ions in NB on the equilibrium constant of complex formation K_{NB} in NB in system IV with assumption $K_w = 0.001$: E; TPB^-; dibenzo-18-crown-6; TBA^+; K^+; 6—Cl^-; 7—H^+.

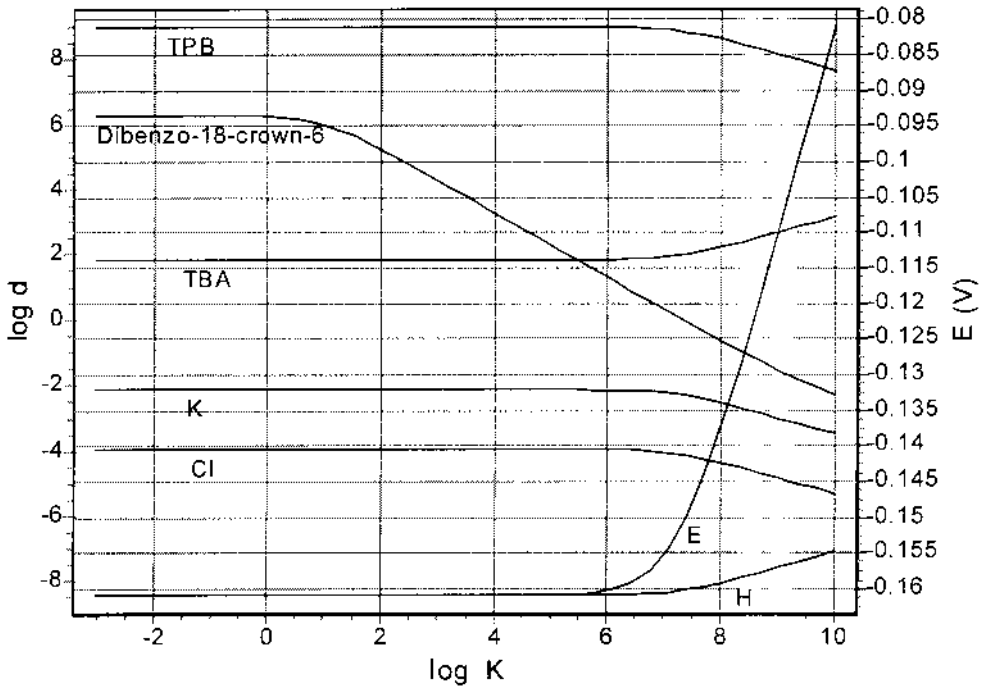

FIG. 10 Dependence of equilibrium potential (E) and the distribution coefficient of ions in NB on the logarithm of equilibrium constant of complex formation in water in system IV with assumption $K_{NB} = 5.012 \times 10^6$; E; TPB^-; dibenzo-18-crown-6, TBA^+; —K^+; Cl^-; H^+.

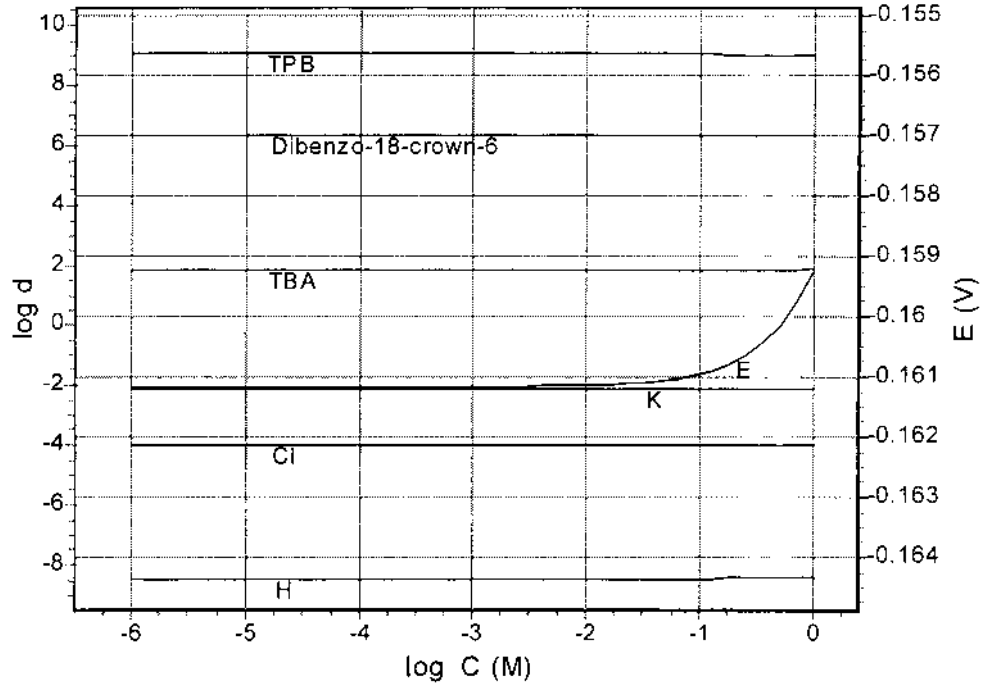

FIG. 11 Dependence of equilibrium potential (E) and the distribution coefficient of ions in NB on the concentration of HCl in system IV: E; TPB^-; dibenzo-18-crown-6; TBA^+; K^+; Cl^-; H^+.

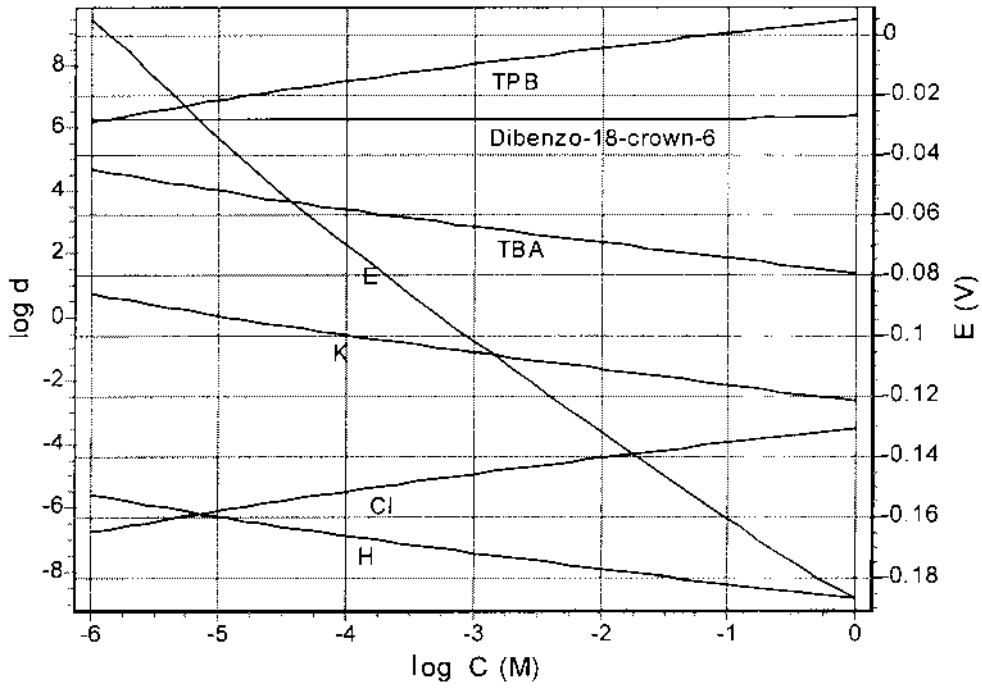

FIG. 12 Dependence of equilibrium potential (E) and the distribution coefficient of ions in NB on the concentration of KCl in system IV with assumption $K_{NB} = 5.012 \times 10^6$: E, TPB^-; dibenzo-18-crown-6; TBA^+; K^+; Cl^-; H^+.

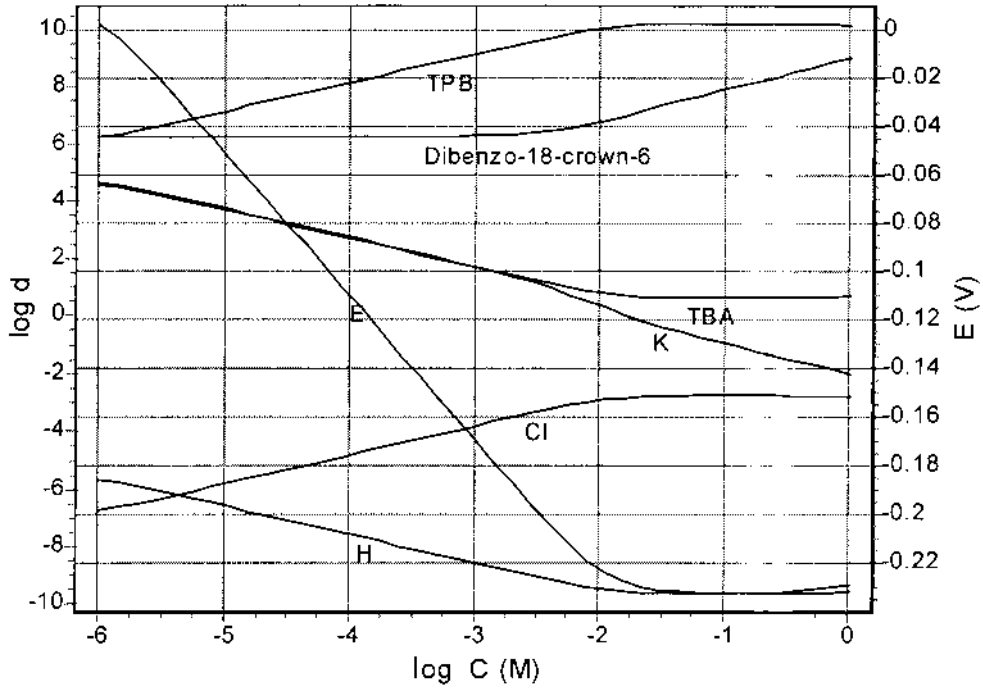

FIG. 13 Dependence of equilibrium potential (E) and the distribution coefficient of ions in NB on the concentration of KCl in system IV with assumption $K_{NB} = 5.012 \times 10^{10}$; > E; TPB^-; dibenzo-18-crown-6; TBA^+; K^+; Cl^-; H^+.

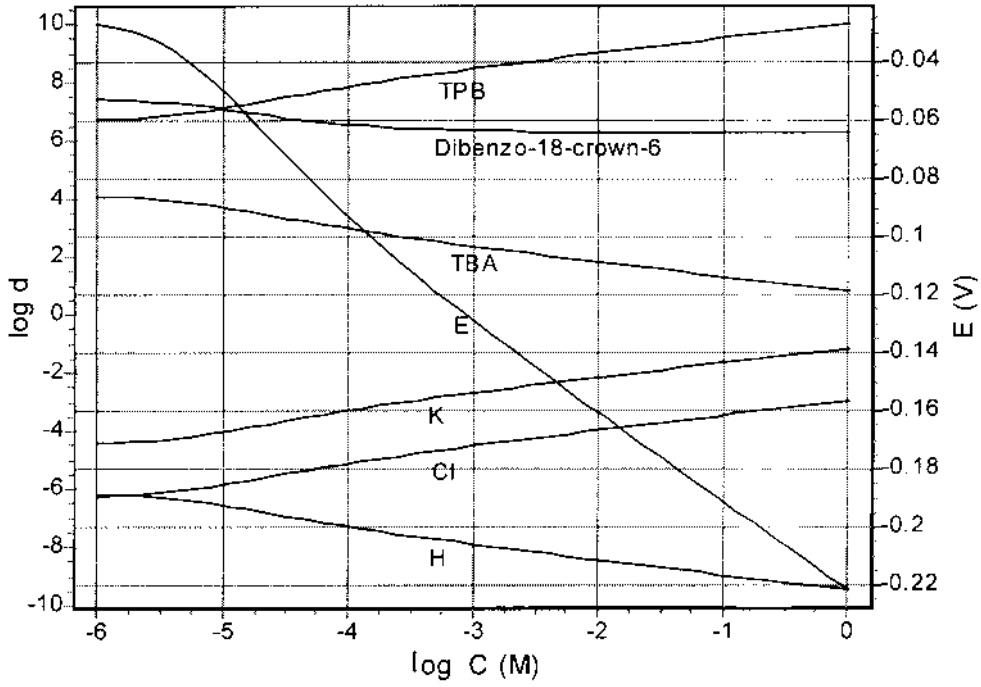

FIG. 14 Dependence of equilibrium potential (E) and the distribution coefficient of ions in NB on the concentration of dibenzo-18-crown-6 in system IV with assumption $K_{NB} = 5.012 \times 10^6$; E; TPB^-; dibenzo-18-crown-6; TBA^+; K^+; Cl^-; H^+.

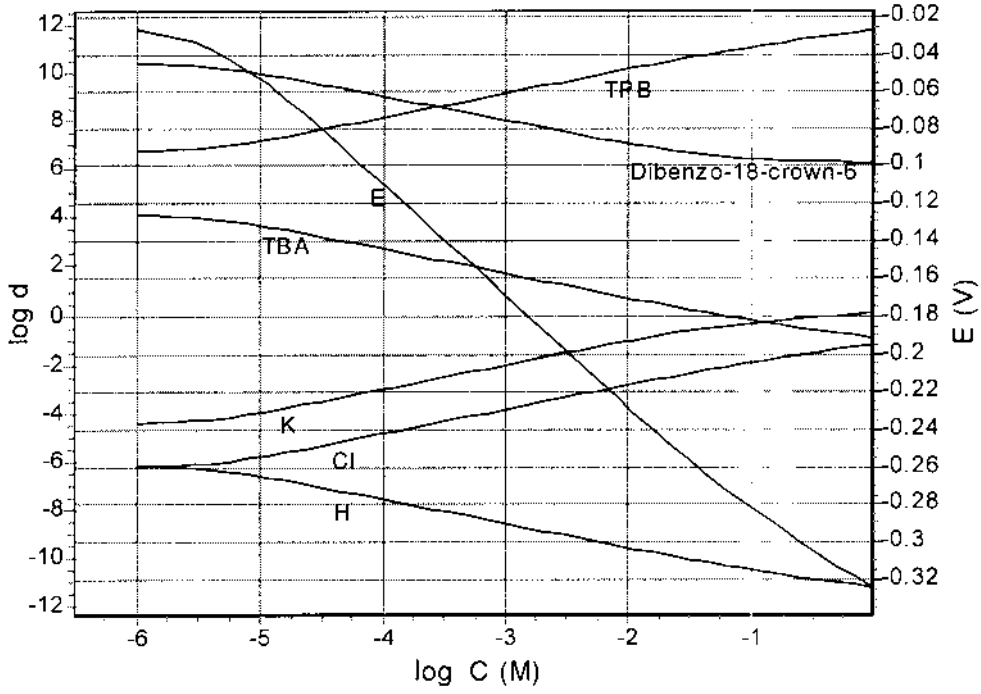

FIG. 15 Dependence of equilibrium potential (E) and the distribution coefficient of ions in NB on the concentration of dibenzo-18-crown-6 in system IV with assumption $K_{NB} = 5.012 \times 10^9$; E; TPB^-; dibenzo-18-crown-6; TBA^+; K^+; Cl^-; H^+.

2. Ion-Association

In most organic solvents, it is necessary to take into account ion-pair formation, especially in the case of solvents of low dielectric constant. Generally, the problem can be solved as shown in Section III. The same detailed solution was presented in Refs 1 and 2. The computer program EXTRA.HH1 was also used to solve this problem. Let us consider the system:

System V: 0.1 M KCl, 0.1 M NaCl in water, and 0.05 M TBATPB in NB, with volume ratio $V_w/V_{nb} = 1$.

With the assumption that $K_{nb} = 137$ [16], ion-pair formation in NB is too weak to have any effect on the equilibrium of the system. The ion-pair formation significantly influences the equilibrium of the system only when $K_{nb} >> 1000$, whereas the dependence of the equilibrium potential (E) on the logarithm of the equilibrium constant of ion-pair formation in NB is actually linear (Fig. 16).

3. Reactions Resulting in Several Products

As a more complicated case we consider, e.g., the system of the two following reactions in phase α:

$$\nu_{1,1}A_{1,1} + \nu_{2,1}A_{2,1} + \nu_{3,1}A_{3,1} \overset{k_1}{\leftrightarrow} \lambda_{1,1}B_{1.1} + \lambda_{2,1}B_{2,1} + \lambda_{3,1}B_1 \tag{48}$$

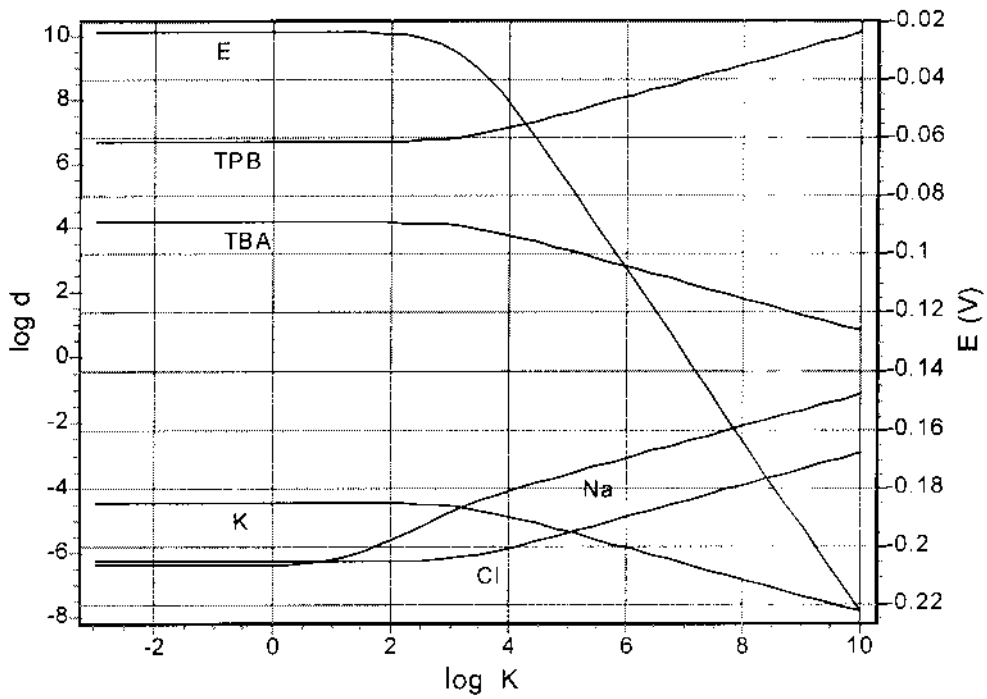

FIG. 16 Dependence of equilibrium potential (E) and the distribution coefficient of ions in NB on equilibrium constant of ion-pair formation in nitrobenzene in system V with assumption $K_w = 0.01$; E; TPB^-; TBA^+; K^+; Na^+; Cl^-.

$$\nu_{1,2}\mathrm{A}_{1,2} + \nu_{2,2}\mathrm{A}_{2,2} \overset{k_2}{\leftrightarrow} \lambda_{1,2}\mathrm{B}_{1.2} + \lambda_{2,2}\mathrm{B}_{2,2} \tag{49}$$

There are 10 components taking part in reactions (48 and 49) corresponding to 20 unknowns representing their concentrations in both phases. Including $\Delta\varphi$, we have a total of 21 unknowns, so we must find 21 independent equations. It is easy to write 10 equations corresponding to $\alpha_{\mathrm{A_{n,j}}}$ and $\alpha_{\mathrm{B_{l,j}}}$ [see Eqs (10) and (11)], with $j = 1, n = 1, 2, 3, l = 1, 2, 3, j = 2, n = 1, 2,$ and $\ell = 1, 2$. Five equations are obtained from Eq. (15). Because no component can take part in more than one reaction at a time, we have

$$m_{\mathrm{A_{n,j}}} = V_\alpha \left(c_{\mathrm{A_{n,j}}} + \sum_{\mathrm{l}=1}^{L_\mathrm{j}} \beta_{\mathrm{n,l,j}}\, c_{\mathrm{B_{l,j}}} \right) + V_\beta \left(c'_{\mathrm{A_{n,j}}} + \sum_{\mathrm{l}=1}^{L_\mathrm{j}} \beta_{\mathrm{n,l,j}}\, c'_{\mathrm{B_{l,j}}} \right) \tag{50}$$

On the basis of Eq. (17) we can briefly write three equations, for reaction (48):

$$(V_\alpha c_{\mathrm{B}_{1,1}} + V_\beta c'_{\mathrm{B}_{1,1}}) : (V_\alpha c_{\mathrm{B}_{2,1}} + V_\beta c'_{\mathrm{B}_{2,1}}) : (V_\alpha c_{\mathrm{B}_{3,1}} + V_\beta c'_{\beta_{3,1}}) = \lambda_{1,1} : \lambda_{2,1} : \lambda_{2,3} \tag{51}$$

and for reaction (49):

$$(V_\alpha c_{\mathrm{B}_{1,2}} + V_\beta c'_{\mathrm{B}_{1,2}}) : (V_\alpha c_{\mathrm{B}_{2,2}} + V_\beta c'_{\mathrm{B}_{2,2}}) = \lambda_{1,2} : \lambda_{2,2} \tag{52}$$

Two equations are obtained from Eq. (22):

$$k_1 = \frac{(\gamma_{\mathrm{B}_{1,1}} c_{\mathrm{B}_{1,1}})^{\lambda}_{1,1}\ (\gamma_{\mathrm{B}_{2,1}} c_{\mathrm{B}_{2,1}})^{\lambda_{2,1}} (\gamma_{\mathrm{B}_{3,1}} c_{B_{3,1}})^{\lambda_{3,1}}}{(\gamma_{\mathrm{A}_{1,1}} c_{\mathrm{A}_{1,1}})^{\nu_{1,1}} (\gamma_{\mathrm{A}_{2,1}} c_{\mathrm{A}_{2,1}})^{\nu_{2,1}} (\gamma_{\mathrm{A}_{3,1}} c_{\mathrm{A}_{3,1}})^{\nu_{3,1}}} \tag{53}$$

$$k_2 = \frac{(\gamma_{\mathrm{B}_{1,2}} c_{\mathrm{B}_{1,2}})^{\lambda_{1,2}} (\gamma_{\mathrm{B}_{2,2}} c_{\mathrm{B}_{2,2}})^{\lambda_{2,2}}}{(\gamma_{\mathrm{A}_{1,2}} c_{\mathrm{A}_{1,2}})^{\nu_{1,2}} (\gamma_{\mathrm{A}_{2,2}} c_{\mathrm{A}_{2,2}})^{\nu_{2,2}}} \tag{54}$$

and the remaining single equation [see Eq. (23)] is

$$\sum_{\mathrm{n}=1}^{3} z_{\mathrm{A_{n,1}}} c_{\mathrm{A_{n,1}}} + \sum_{\mathrm{l}=1}^{3} z_{\mathrm{B_{l,1}}} c_{\mathrm{B_{l,1}}} + \sum_{\mathrm{n}=1}^{2} z_{\mathrm{A_{n,2}}} c_{\mathrm{A_{n,2}}} + \sum_{\mathrm{l}=1}^{2} z_{\mathrm{B_{l,2}}} c_{\mathrm{B_{l,2}}} = 0 \tag{55}$$

The system of 21 independent equations for 21 unknowns can in principle be solved.

The case where $\mathrm{A}_{1,2}$ is identical to $\mathrm{A}_{1,1}$ and symbolized by A_1, implies that A_1 participates in two concurrent reactions (48) and (49). Obviously, two equations and two unknowns are rejected. Instead of two equations for $\alpha_{\mathrm{A}_{1,1}}$ and $\alpha_{\mathrm{A}_{1,2}}$, we can write a single equation:

$$\alpha_{\mathrm{A}_1} = \frac{c'_{\mathrm{A}_1}}{c_{\mathrm{A}_1}} = \frac{\gamma_{\mathrm{A}_1}}{\gamma'_{\mathrm{A}_1}} \exp\left[\frac{z_{\mathrm{A}_1} F}{RT} (\Delta\varphi - \Delta\varphi^{\mathrm{o}}_{\mathrm{A}_1}) \right] \tag{56}$$

Instead of two equations obtained from the law of mass conservation $\mathrm{A}_{1,1}$ and $\mathrm{A}_{1,2}$, we have an equation:

$$\begin{aligned} m_{\mathrm{A_{n,j}}} = {} & V_\alpha \left(c_{\mathrm{A}_{1,1}} + \sum_{\mathrm{l}=1}^{3} \beta_{1,1,1}\, c_{\mathrm{B}_{l,1}} \right) + \sum_{\mathrm{l}=1}^{2} \beta_{1,1,2}\, c_{\mathrm{B}_{1,2}} \Bigg) + \\ & V_\beta \left(c'_{\mathrm{A}_{1,1}} + \sum_{\mathrm{l}=1}^{3} \beta_{1,1,1}\, c'_{\mathrm{B}_{l,1}} \right) + \sum_{\mathrm{l}=1}^{2} \beta_{1,1,2}\, c'_{\mathrm{B}_{l,2}} \Bigg) \end{aligned} \tag{57}$$

where $\beta_{1,l,1}$ and $\beta_{1,l,2}$ are stoichiometric numbers of A_1 in products $B_{l,1}$ and $B_{l,2}$ respectively. The simplest case for

$$\begin{aligned} A_1 + A_2 &= A_1A_2 \\ A_1 + A_3 &= A_1A_3 \end{aligned} \tag{58}$$

was presented in Ref. 2 in detail. In the case where $B_{1,1}$ is identical to $B_{1,2}$ and called B_1, two unknowns representing concentrations and thus two equations can be removed. From the electrochemical potential equilibrium condition, instead of two equations for $\alpha_{B_{1,1}}$ and $\alpha_{B_{1,2}}$ we now have the equation:

$$\alpha_{B_1} = \frac{c'_{B_1}}{c_{B_1}} = \frac{\gamma_{B_1}}{\gamma'_{B_1}} \exp\left[\frac{z_{B_1}F}{RT}(\Delta\varphi - \Delta\varphi^{o}_{B_1})\right] \tag{59}$$

Instead of three equations arising from the stoichiometric number [see Eqns. (51) and (52)] we obtain two equations as follows:

$$(V_\alpha c_{B_1} + V_\beta c'_{B_1}) = \frac{\lambda_{1,1}}{\lambda_{2,1}}(V_\alpha c_{B_{2,1}} + V_\beta c'_{B_{2,1}}) + \frac{\lambda_{2,2}}{\lambda_{2,1}}(V_\alpha c_{B_{2,2}} + V_\beta c'_{B_{2,2}}) \tag{60}$$

and

$$(V_\alpha c_{B_{2,1}} + V_\beta c'_{B_{2,1}}) : (V_\alpha c_{B_{3,1}} + V_\beta c'_{B_{3,1}}) = \lambda_{B_{2,1}} : \lambda_{B_{3,1}} \tag{61}$$

without change in any other equation.

C. Influence of Volume Ratio

Kakuichi first dealt with a very important analysis of the distribution potential in small systems [17]. If theconcentration of NaCl in W and the concentration of TBATPB in NB are constants, a similar effect of volume ratio (V_{NB}/V_W) on the equilibrium potential and distribution ratio of TBA^+, TPB^-, Na^+, and Cl^- is shown (Fig. 17). When the size of droplets is too small, the surface of the double layer is large enough in comparison with its volume, the electroneutrality condition may not be obeyed, and unusual behaviour of the system can be found. As pointed out by Kakuichi the system mentioned is very important for understanding the processes taking place in a small droplet mixed in a water environment. This important system will be investigated in more detail later.

D. Influence of Temperature

If no interaction occurs in the system the equilibrium potential, logarithm of concentration, and distribution ratio of all the cations increase linearly while the logarithm of distribution ratio of all the anions decreases linearly with increasing logarithm of temperature (Fig. 18). In the case of interacting systems, the temperature dependence of interaction constants must be known.

E. Other Solvents

The calculation can be carried out for different solvent systems in conditions that the standard transfer potential of all components and the equilibrium constants of all interactions (if they occur) are given.

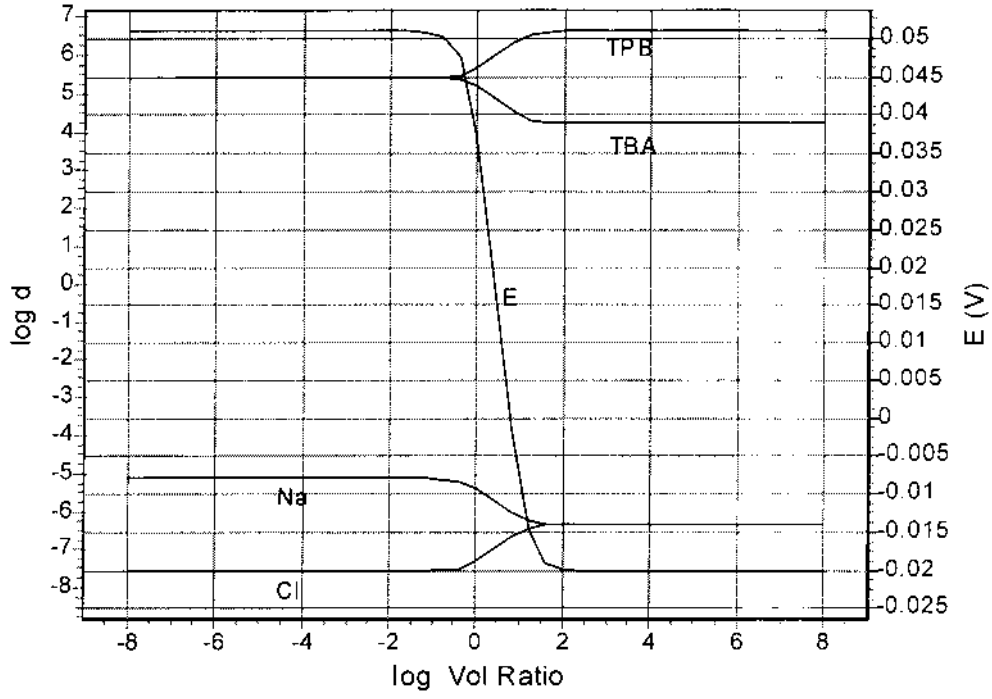

FIG. 17 Dependence of equilibrium potential (E) and the distribution coefficient of ions on volume ratio between NB and W phases in system II: E; TPB^-; TBA^+; K^+; Na^+; Cl^-.

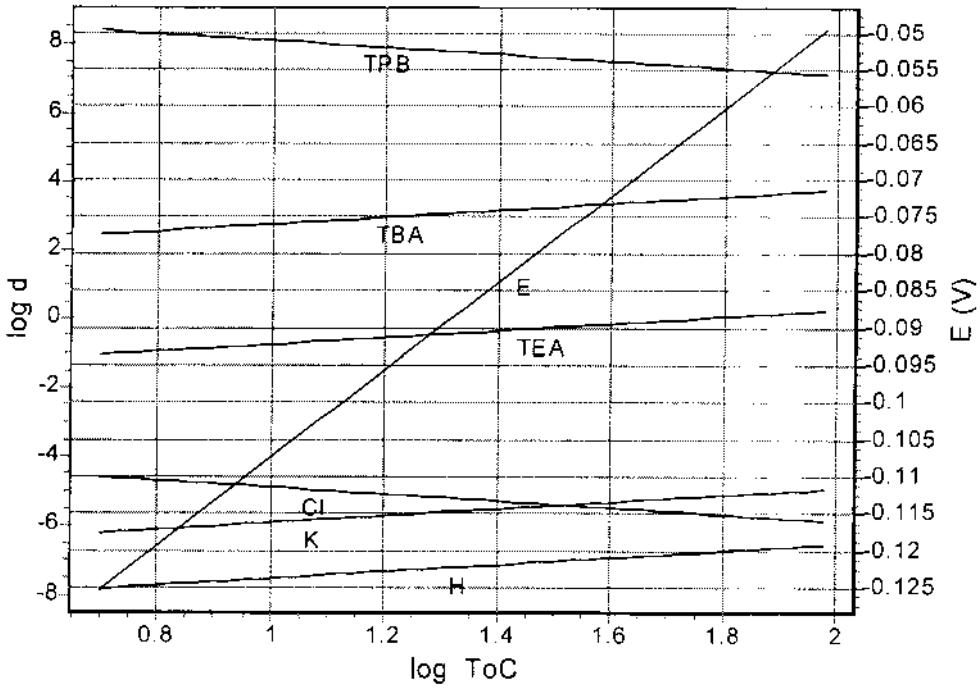

FIG. 18 Dependence of equilibrium potential (E) and the distribution coefficient of ions in NB on temperature in system III: E; TPB^-; TBA^+; TEA^+; Cl^-; K^+; H^+.

1. Dichloroethane as an Organic Solvent

For example, we consider the system VI of water/dichloroethane:

System VI: 0.05 M KCl, 0.01 M TEACl in water, and 0.05 M TBATPB in dichloroethane, with volume ratio $V_w/V_{dicchloroethane} = 1$.

From Table 7 and Fig. 19 it is indicated that the only difference between this system and the water/nitrobenzene system is an expansion of the potential scale because of the larger difference in standard transfer potential between ions present in the system.

2. An Electrolyte–Dielectric System

In this case, two solvents with very different dielectric constants form an extraction system, where ionic species are dissolved in the polar solvent, and a neutral component is dissolved in the dielectric solvent. The system is characterized by the following conditions:

$$\begin{aligned} \Delta\varphi_i^o &>> 0 \quad \text{if} \quad z_i > 0 \\ \Delta\varphi_i^o &<< 0 \quad \text{if} \quad z_i < 0 \\ D_i &>> 0 \quad \text{if} \quad z_i = 0 \end{aligned} \tag{62}$$

or

$$\begin{aligned} s_i^e &>> s_i^d \quad \text{if} \quad z_i \neq 0 \\ s_i^e &<< s_i^d \quad \text{if} \quad z_i = 0 \end{aligned} \tag{63}$$

where s_i^e and s_i^d are the solubilities of the ith component in the electrolyte and dielectric solvent, respectively.

In this case, the dissociation constant in the electrolyte and association constant in the dielectric solvent are very large. The calculation can be carried out in the same way as mentioned above. Under some circumstances, the problem becomes simpler, such as where some components are mainly present in only one of the phases.

V. ELECTROCHEMICAL APROACH OF LIQUID–LIQUID EXTRACTION

When no external electrical current is supplied to the system, the mass-transfer process across an interface is basically by extraction, including both the transport in the bulk of solutions and the interfacial kinetic steps. As mentioned in Section I, when thermodynamic equilibrium in the system is established, the Galvani potential difference reaches a certain value in accordance with the distribution equilibrium. The theoretical calculation for interfacial potential and equilibrium distribution presented in previous sections can be

TABLE 7 Equilibrium Situation in System VI

Ion	C_w	$C_{Dichloroethane}$	d	% in Dichloroethane
K	5.000×10^{-2}	1.186×10^{-11}	2.372×10^{-10}	2.372×10^{-8}
TEA	9.882×10^{-3}	1.175×10^{-4}	1.189×10^{-2}	1.175
TBA	1.175×10^{-4}	4.988×10^{-2}	4.244×10^{2}	9.976×10^{1}
Cl	6.000×10^{-2}	6.576×10^{-9}	1.096×10^{-7}	1.096×10^{-5}
TPB	2.284×10^{-9}	5.000×10^{-2}	2.189×10^{7}	1.000×10^{2}

Equilibrium potential = −0.0697 V.

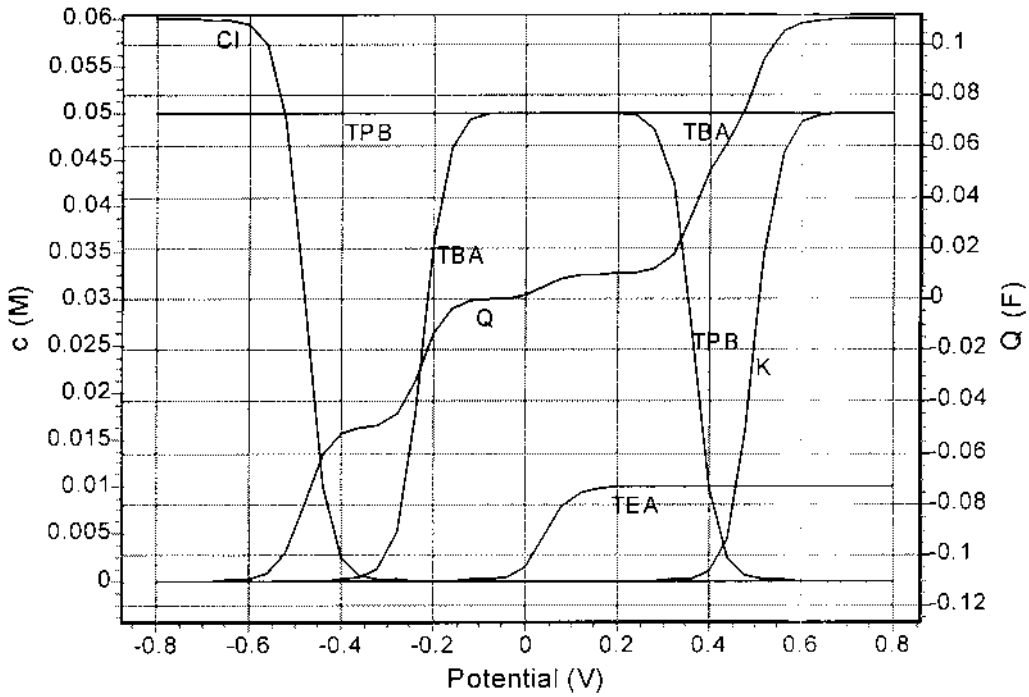

FIG. 19 Dependence of total charge (Q) and concentration of ions in dichloroethane on the potential in system IV: Q; Cl^-; TBA^+; TPB^-; TEA^+; K^+.

immediately applied to liquid–liquid extraction. A comparison between conventional calculation and the calculation based on an electrochemical approach is described by a scheme in Fig. 20.

If a certain potential, different from the equilibrium value, is applied to both sides of the interface, under potentiostatic conditions, electrical current through the interface can decrease to zero when equilibrium is established. The process is called electroextraction. The calculation as described in previous sections (see Figures 2–4, 8, and 19) can be used for a quantitative description of electroextraction.

VI. CONCLUSION

From the basic parameters: initial concentration of ions, their standard transfer potential, distribution coefficients for neutral components, equilibrium constants of reactions taking place in the system, volume of phases, and temperature, a unique general problem for the Galvani potential difference and distribution concentration of all components was established. A numerical solution to the problem with the help of computer program EXTRA.HH1 provided a good means for quantitative investigation of the liquid–liquid interface. It is also useful for the study of liquid–liquid extraction, electroextraction, voltammetry at interface of two immiscible electrolyte solutions (ITIES) [15,18], liquid–liquid membrane ion-selective electrodes, biomembrane transport, and other fields of science and engineering.

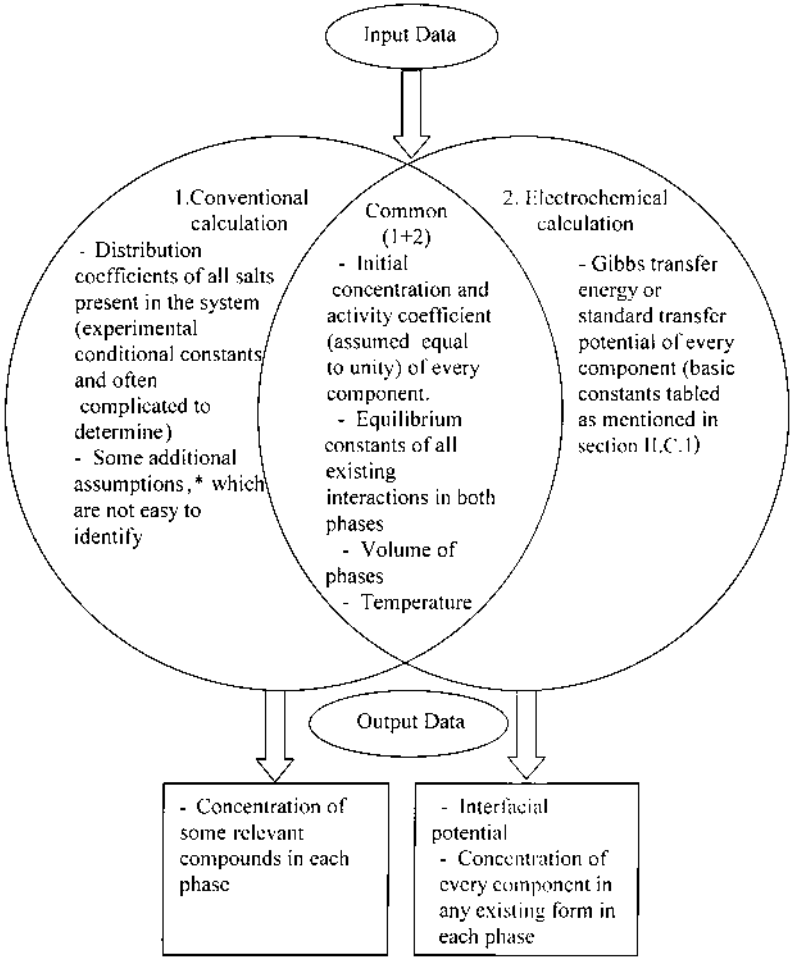

FIG. 20 Scheme for comparison between conventional calculation and the calculation based on electrochemical approach, where left and right ellipses are required input data for conventional and electrochemical calculations respectively; the overlap area is common required input data for both calculations.*Assumption about relative relationship between forecasted equilibrium concentrations of some components, e.g., $K = K_1/(C_A + CB)$, if $C_A >> C_B$, we have $K = K_1/C_{A,}$, where K and K_1 are constants, and C_A and C_B are concentrations of A and B, respectively.

ACKNOWLEDGMENTS

I am grateful to Professor A. G. Volkov for his interest in my manuscript and appreciate the fruitful discussions with Professor D. Britz. I would like to thank Mrs K. Melanie, Vu Thi Thu Ha, and Ms Tran Lan Huong for helping in this work. This work was supported by the National Foundation for Fundamental Scientific Research of Vietnam.

APPENDIX

```
Program Extraction;
Uses Crt, Dos;
var
  temp,dt1,dt2,S,dt : real;
  Temps : string;
  k,l : integer;
  Calpha, Cbeta, d : array[1..5] of real;
Const
  {KCl 0.1M,TEACl 0.01M,TBATPB 0.05M}
  NI = 5;
  ION : array [1..NI] of string = ('K','TEA','TBA','TPB','Cl');
  Zi : array [1..NI] of integer = (1, 1, 1, −1, −1);
  E0I : array [1..NI] of real = (0.242, −0.059, −0.248, 0.372, −0.395);
  m : array [1..NI] of real = (0.1, 0.01, 0.05, 0.05, 0.11);
  PErro = 0.00001;
  Valpha = 1.0;
  Vbeta = 1.0;
  ToC = 25.0;
Function RatioB_A(zz :integer;E0,E:real): real;
begin
  if ZZ<>0 then RatioB_A:= exp(2.303* ZZ*298/(0.0591*(273 + Toc))*(E-E0))
  else RatioB_A:= exp(2.303*E0* 298/(0.0591*(273 + Toc)));
end;
Function Q(E:real): real;
var
    Temp: real;
    i : integer;
begin
    temp:=0;
    for i:= 1 to NI do
    begin
          Calpha[i]:= m[i]/(Valpha + Vbeta*RatioB_A(ZI[i],E0I[i],E));
          Cbeta[i]:=Calpha[i]*RatioB_A(ZI[i],E0I[i],E);
       Temp:=temp + ZI[i]*Calpha[i];
  end;
  Q:=temp;
end;
Procedure cal(E:real);
var
    i : integer;
begin
    For i:= 1 to NI do
    Begin
       if m[i]=0 then d[i]:=0 else
       begin
          Calpha[i]:= m[i]/(Valpha + Vbeta*RatioB_A(ZI[i],E0I[i],E));
          Cbeta[i]:=Calpha[i]*RatioB_A(ZI[i],E0I[i],E);
          d[i]:=Cbeta[i]/Calpha[i] ;
       end;
    end;
end;
```

```
Procedure WriteResult;
var
  i : integer;
begin
  Clrscr;
  Writeln('solution of KCl 0.1 M,TEACl 0.01 M,TBATPB 0.05 M');
  Writeln('Ion amount(mol) ');
  For i:=1 to NI do writeln(ION[i], m[i]:3:4);
  Writeln('Volume of phase Water = ',VAlpha:3:2,' l');
  Writeln('Volume of Phase Nitrobenzene(NB) = ',Vbeta:3:2,' l');
  Writeln('Temperature(oC) : ',ToC :3:2);
  Writeln('Erro for potential calculation : ',PErro:3:6,' V');
  Writeln('Potential = ', dt:3:6);
  Writeln('Ion  Tran.Pot.(V) C in water C in NB  Dis Ratio % in NB');
  For i:= 1 to NI do
   writeln (ION[i],E0I[i]:12:4,Calpha[i]:12,Cbeta[i]:12,d[i]:12,100*(1-1/(1 + d[i])):12 );
end;
begin
dt1:=1;
dt2:=-1;
dt:=(dt1 + dt2)/2;
k:=0;
repeat
  inc(k);
  if Q(dt) > 0 then dt2 :=dt else dt1:=dt;
  dt:=(dt1 + dt2)/2;
until abs(dt2-dt1) < PErro;
cal(dt);
WriteResult;
Repeat Until KeyPressed;
end.
```

REFERENCES

1. LQ Hung. J Electroanal Chem 115:159–174, 1980.
2. LQ Hung. J Electroanal Chem 149:1–14, 1983.
3. J Rais. Collect Czech Chem Commun 36:3253–3562, 1971.
4. J Rais, P Selucky, M Kyrs. J Inorg Nucl Chem 38:1376–1378, 1976.
5. A J Parker. Chem Rev 69:1–32, 1969.
6. J Koryta. Ion-Select Electr Rev 5:131–164, 1983.
7. J Koryta, P Vanysek. In: H Gerischer, C W Tobias, eds. Advances in Electrochemistry and Electrochemical Engineering. Vol.12. New York: John Wiley, 1981, pp 113–176.
8. J Koryta. Electrochim Acta 29:445–452, 1984.
9. C Gavach, F Henry. J Electroanal Chem 54:361–370, 1974.
10. T Wandlowski, V Marecek, Z Samec. Electrochim Acta 15:1173–1175, 1990.
11. T Kakuichi. In: A G Volkov, D Deamer, eds. Liquid–Liquid Interface: Theory and Methods. Boca Raton, FL: CRC Press, 1996, pp 1–18.
12. T Osakai, K Ebina. J Phys Chem B 103:5691–5698, 1998.
13. T Osakai, K Ebina. In A G Volkov, ed. Liquid Interfaces in Chemical, Biological, and Pharmaceutical Applications. New York: Marcel Dekker, 2000, pp 23–49.
14. V S Markin, A G Volkov. J Colloid Interface Sci 131:382–392, 1989.

15. Z Koczorowski. In A G Volkov, ed. Liquid Interfaces in Chemical, Biological, and Pharmaceutical Applications. New York: Marcel Dekker, 2000, pp 1–22.
16. M Pivonkova, M Kyrs. J Inogr Nucl Chem 31:175–185, 1969.
17. T Kakuichi. Anal Chem 68:3658–3664, 1996.
18. E Makrlik, LQ Hung. J Electroanal Chem 158:277–284, 1983.

6

Use of Cyclodextrins or Porous Inorganic Supports to Improve Organic/Aqueous Interfacial Transfers

MARTINE URRUTIGOÏTY and PHILIPPE KALCK Ecole Nationale Supérieure des Ingénieurs en Arts Chimiques et Technologiques, Toulouse, France

I. INTRODUCTION

Homogeneous catalysts continue to attract great interest in the synthesis process, because by modifications of the coordination sphere of the metal center, through especially adapted ligands, it is possible to attain high selectivities. Some more recent goals concern the economy of atoms during the cascade of various steps to prepare elaborate structures [1] and the use of environmentally friendly solvents [2]. However, these catalysts need to be recycled with the maximum of efficiency, either in the major processes of petrochemistry for bulk products or also for high-value molecules even produced in batch reactors. Not only is it necessary to reduce the cost of the product in a major process, but also heavy metals should not be released into the environment, even in tiny traces. Water has been recognized as an elegant and economical medium to meet all these requirements [3]. Indeed, water-soluble catalysts have been designed so that the aqueous phase is usually in contact with the organic phase, which contains the substrate and the resulting products of the reactions, but also with a gaseous phase even though such catalysis continues to be called *biphasic*.

Interestingly, biphasic catalysis has gained considerable interest in academic research groups after the discovery of a very efficient water-soluble hydroformylation catalyst by Emile Kuntz [4] in Rhône Poulenc in 1975, and the development of the process by Ruhr Chemie in 1984 [5]. At present, the two industrial units in Oberhausen (Germany) produce 400,000 tonnes per year of *n*-butanal by hydroformylation of propene. The actual catalyst precursor is $[HRh(CO)(TPPTS)_3]$ in which the TPPTS ligand is the sodium salt of tris-(*m*-sulfonatophenyl)phosphine, which is highly soluble in water (1100 g L^{-1}) and insoluble in the classical organic solvents. Thus, the process combines homogeneous catalysis in the aqueous phase where the rhodium complex is in contact with propene, hydrogen, and carbon monoxide dissolved in water, and a rigorous heterogeneous sequence by which the products are immediately macroscopically separated from the aqueous phase as soon as they are formed in order to feed the organic phase.

Due to the great solubility in water of the ligand TPPTS and the rhodium complex $[HRh(CO)(TPPTS)_3]$, it has been considered from the beginning that the hydroformylation reaction was occurring in the bulk of the aqueous phase [6]. In addition, the presence

of cosolvents such as alcohols, which increase the solubility of propene in the aqueous phase, led Hablot et al. to support this assumption [7]. More recent studies, particularly kinetic measurements, carried out by the scientists who have developed the Ruhr Chemie process, have inferred such a hypothesis. The experimental data fit better with a model in which the reaction is considered at the boundary of the two gaseous and aqueous phases. However, it is necessary to have an accurate definition of the thickness of the interface and also the mass-transfer coefficients between all the reactants, such as propene, carbon monoxide, and hydrogen [8].

For heavier olefins it becomes necessary to consider an organic phase so that the system contains gaseous reactants (CO and H_2) in contact with the organic phase where they dissolve. The boundary region is certainly formed by the alkene and dissolved CO/H_2 in close vicinity with the catalyst in the aqueous phase. Such a situation is most often called a transfer phenomenon between the two liquid phases, but clearer definitions should clarify this general problem [8].

Many solutions have been proposed by a relatively reduced number of research groups. The objective of all of them is to increase the transfer coefficient between the two phases. However, several systems provide stronger drawbacks than benefits, so they can just be mentioned in perspective. For example, we can mention the use of some surfactants, which generate such stable emulsions that the separation between the two phases takes a very long time and is quite tedious [9]. Although some solutions have been proposed to circumvent this drawback [10,11], we have focused our attention on three main concepts that are the basis of an efficient contact enhancement between the reactants and the water-soluble catalyst.

II. SUPPORTED AQUEOUS PHASE CATALYSIS

Davis and his group developed in 1989 a new approach to the increase in the interfacial area by immobilizing the water-soluble coordination complex in a thin film of water maintained on a high surface-area hydrophilic solid [12–16]. It has been called "supported aqueous phase catalysis" and sometimes by its acronym "SAPC."

The inorganic support should present a high hydrophilicity and a very high specific surface area; it is a case, for instance, for silica or mesoporous glass beads. A general scheme is given in Fig. 1.

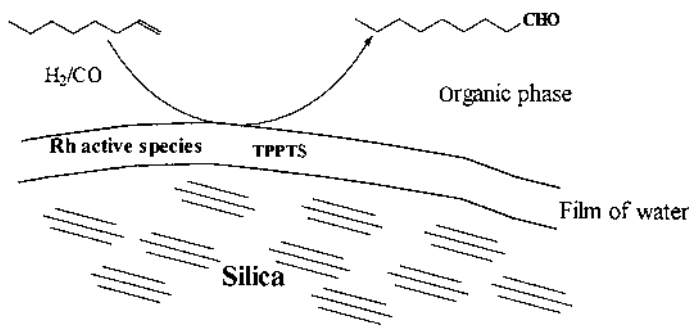

FIG. 1 Schematic view of the SAPC.

Generally, the support is impregnated with a catalyst precursor, such as $[HRh(CO)(TPPTS)_3]$, and eventually an excess of TPPTS, and the content of water is adjusted by addition of controlled amounts to complete those originally present on the support. At this stage, the catalyst appears as a dry yellow solid. Extensive experiments have been carried out to measure the loss of metal in the organic solution, and the analyses have shown that no rhodium was detectable with a sensitivity of 1 ppb [17]. Moreover, after one catalytic cycle the organic solution presents no activity in hydrogenation or hydroformylation reactions. It can be concluded that rhodium is not leached into the organic phase as either a soluble species or as a colloid.

In the early experiments [18] the hydrogenation or hydroformylation of oleyl alcohol into the corresponding saturated alcohol and aldehyde, all products being completely insoluble in water, was performed with success. The authors have considered that the reaction is occurring at the organic–aqueous film interface. Further experiments carried out by Horvàth have confirmed this interpretation [19]. Indeed, several olefins of different carbon chain length are functionalized at the same rate, more precisely at the same turnover frequencies (TOFs). Olefins with up to 17 carbon atoms can be transformed [14].

The water content of the support exerts a dramatic influence on the activity of such catalysts. Davis along with his group [12–16] and Horvàth [19] have observed that for poor levels of hydration, the activity remains low. This has been interpreted as being due to important restrictions to the mobility of the organometallic complex inside the pores. Raising the quantities of water increases the conversion whereas the normal/branched selectivity in aldehyde remains unaffected. For instance, with 2.9 wt % H_2O on a controlled-pore glass CPG-240 support a TOF of 2×10^{-4} s^{-1} was noted, and for 9 wt % H_2O the TOF was 2×10^{-2} s^{-1} [18]. Beyond this latter value the activity decreases. This phenomenon has been interpreted as being due to the progressive filling of the pores, which favors the mobility of the complex in water but reduces the contact between the organic reactants and the catalyst.

More recently, studies have been carried out by varying the nature of the supports and the size of the pores [20]. Starting from the catalyst precursor $[Rh_2(\mu\text{-}StBu)_2(CO)_2(TPPTS)_2]$ in the presence of a slight excess of free ligand in order to maintain a molar P/Rh=6 ratio, in such a way that the inactive species $[Rh_2(\mu\text{-}StBu)_2(CO)_4]$ does not form, the hydroformylation of oct-1-ene has been followed [21]. Sipernat Silica 22 (commercialized by DEGUSSA), characterized by a 100 μm mean granulometry, a 173 m^2 g^{-1} BET surface area, and a 45 nm mean pore diameter, has been used as a support. Different hydration rates for this silica, ranging from 1.3 to 47.2 wt % total water content, show that a poor conversion is obtained up to about 12.7%. Beyond this value the yields increase sharply up to 60% when the pores are fully filled with water (16%).

However, as shown in Table 1 and Fig. 2, the conversion still rises until a plateau is reached at about 20 wt % hydration. The curve shows an important zone of stability where the activity is maintained at 80–90% (yields in 18h). This area represents between 20 and 44% of water content [22]. When higher hydration rates are experimented with, water, is of course, no longer strongly retained on the support so that droplets are found in the organic solution when the stirring is stopped. Thus, some complexes leach from the support, decreasing the apparent efficiency of the SAPC. A bell curve has also been observed for the hydroformylation of methyl acrylate catalyzed by $[HRh(CO)(TPPTS)_3]$ on silica. A higher activity when going from the organosoluble triphenylphosphine analog to the water-soluble complex is characteristic of this substrate since such an increase was not obtained with propene. The polarity and polarization properties of methyl acrylate are presumably responsible for this optimal activity [23]. A thorough investigation of palla-

TABLE 1 Yields of the Hydroformylation Reaction of Oct-1-ene as a Function of the Hydration Rate

Water (%)	Yield (%)	Linear aldehyde	Branched aldehyde	TOF (h^{-1})
1.3	1.1	89.3	10.7	1.6
9.2	4.0	75.0	25.0	5.9
12.7	5.1	74.4	25.6	7.6
14.3	12.2	77.8	22.2	18.3
15.9	47.9	78.0	22.0	71.5
18.9	76.2	78.2	21.8	113.9
21.7	86.8	81.2	18.8	129.7
24.3	87.9	79.2	20.8	131.3
26.8	87.0	79.7	20.3	130.0
31.2	65.7	85.5	14.5	98.1
35.1	77.1	83.3	16.7	115.2
37.8	79.7	81.5	18.5	119.1
40.3	77.5	82.7	17.3	115.8
44.0	79.7	81.9	18.1	119.1
47.2	45.9	87.3	12.7	68.6

$P_T = 5$ bar; $T = 80°C$; $\Delta t = 18$ h; Catalyst = 0.024 mmol; P/Rh = 6; oct-1-ene = 25.6 mmol; toluene = 57 mL.

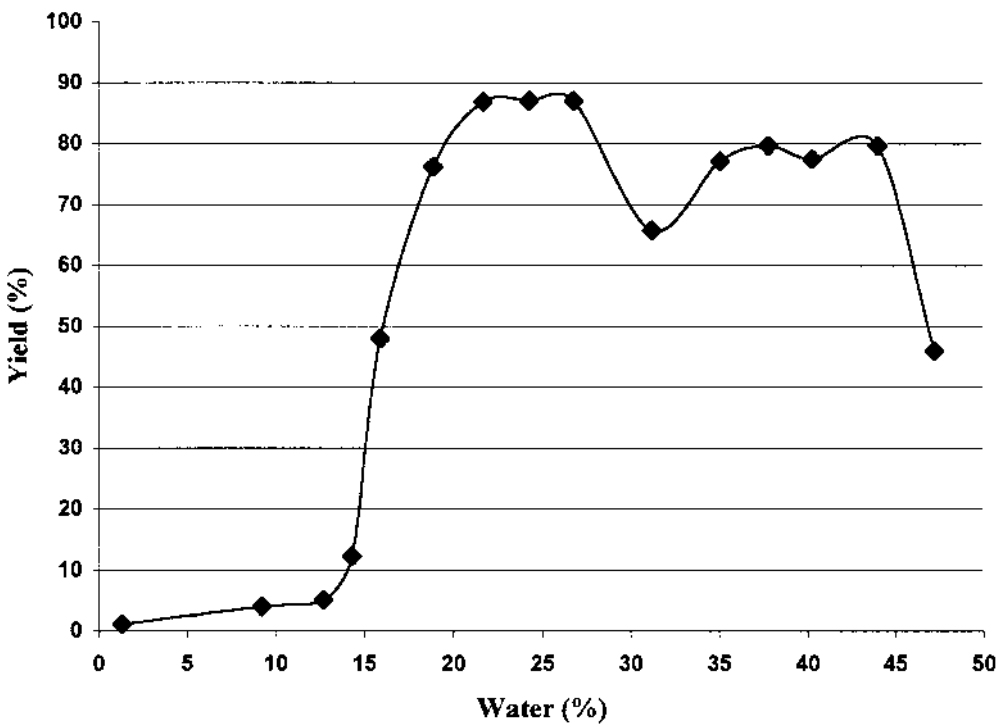

FIG. 2 Different hydration rates of Silica DS 22 [catalyst = 0.024 mmol; P/Rh = 6; oct-1-ene = 25.6 mmol; toluene = 57 mL; $T = 80°C$; P(H_2/CO) = bar, $\Delta t = 18$ h].

dium–TPPTS complexes has been carried out for the alkylation of allylic substrates, and the main influence of various parameters, such as the water content of the solid catalyst and the porosity of the silica support. The SAP catalysts show a sharp maximum of activity between 30 and 50% of water on the solid, and above 50% leaching of water has been noted, which explains the loss of activity. On the other hand, the porosity of silica does not present any significant influence and is not a working parameter [24].

Some other supports present the same behavior as for instance, as displayed in Fig. 3, S200 (from DEGUSSA), which is a silica with a 316 $m^2\ g^{-1}$ BET surface area and a 704 nm mean pore diameter, or an apatitic phosphate (86 $m^2\ g^{-1}$ and 8.3 nm).

In both cases, a stable area is observed after the volume of the pores is filled. In all the experiments the selectivity for the conversion of oct-1-ene into the linear aldehyde is more or less the same, the highest value being 87%. Two salient features are worthy of remark. Indeed, when catalysis is carried out in a pure biphasic system the linearity is generally close to 95–97% [25], whereas the organosoluble complex counterpart $[Rh_2(\mu\text{-}StBu)_2(CO)_2(PPh_3)_2]$ leads in toluene solutions to selectivities in linear aldehydes of $\simeq 75\%$ [26]. a general linearity of 80% means that the catalytic reaction occurs in a rich organic area, but is already influenced to some extent by water molecules. Thus, the interfacial surface plays an essential role in this catalysis. The second feature is related to the large domain of stability of the apatitic phosphate support [27]. Presumably, the sulfonate groups of the TPPTS ligand interact with the calcium atoms of the support, so that the rhodium complex with its solvation sphere is firmly retained. It is necessary to visualize the catalytic action in a volume where the sulfonate groups and the apatite surface are in an aqueous environment. The phenyl groups bonded to the phosphorus atoms and the rhodium metal should emerge in the organic phase to be in direct contact with the reactants. Moreover, solid-state NMR recorded directly after preparation of the SAP catalyst shows broad signals for adsorbed water on the support [28]. Several hours after catalysis this peak at $\simeq 5.5$ ppm becomes less intensive, whereas two additional sharp peaks appear near to 1.3 ppm. These two latter peaks have already been observed during the evolution of tricalcium phosphate gels or with triclinic octacalcium phosphate [28] and should correspond to water molecules in a fixed location. In our opinion, the solvation sphere of the complex and the extra TPPTS ligands should become increasingly organized with catalysis

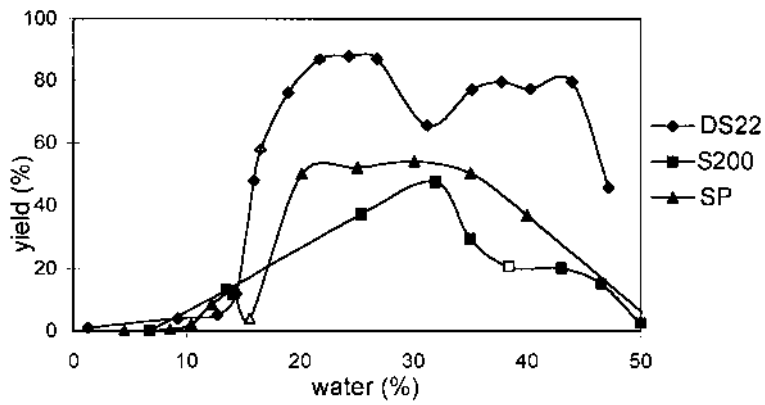

FIG. 3 Influence of the hydration rate on the conversion for the DS 22 ($\Delta t = 18$ h), S200 ($\Delta t = 3$ h) and SP ($\Delta t = 3$ h). The black squares correspond to the full filling of the pores [catalyst = 0.024 mmol; P/Rh = 6; oct-1-ene = 64 mmol; toluene = 57 mL; $T = 80°C$; $P(H_2/CO) = 5$ bar].

in such a way that the influx of the reactants (alkene, hydrogen, and carbon monoxide) is more efficient. On the curves in Fig. 3 the values for the filling of pores with water have been shown by empty squares or triangles. In particular, for the apatitic phosphate SP (synthetic phosphate) this value is 15.5. Thus, the plateau corresponds essentially to the external surface of the support. We still consider that the pores play an important role, because they can contain the extra TPPTS ligands, which are in equilibrium with the rhodium complex on the surface since this has proved necessary in order to prevent the irreversible deactivation into $[Rh_2(\mu\text{-StBu})_2(CO)_4]$.

Recent results have appeared related to the use of a new bio-support for SAPC. The authors report the first example of a palladium complex containing TPPTS supported on cellulose, a natural polysaccharide. The cellulose powder, which presents a specific surface area of 1.35 $m^2\ g^{-1}$ and 3 wt% water content with $[Pd(TPPTS)_3]$ formed in situ, is an efficient support for the Trost–Tsuji allylic alkylation reaction [29].

The concept of SAPc catalysis has been extended to the use of other solvents, such as diethylene glycol, which is compatible with the hydrophobic support and the organic solvent. Indeed, Wan and Davis have reported asymmetric hydrogenation using $[Ru(BINAPsulfonated)_2]$ in a film of ethylene glycol on a controlled-pore glass support [30,31]; the authors chose this solvent instead of water to prevent hydrolysis of the ruthenium species [30]. Thus, dehydronaproxen, a substituted acrylic acid, can be selectively hydrogenated into (*S*)-naproxen, known for its anti-inflammatory properties, with an enantiomeric excess of 96% in 100% yield (Scheme1).

This strategy has been employed in the Heck reaction for the C–C coupling of an aryl halide and an alkane in the presence of a base, and catalyzed by $[Pd(TPPTS)_n]$ [32] and $[Ni(TPPTS)_n]$ complexes [33].

III. INVERSE PHASE-TRANSFER AGENTS

Cyclodextrins can play the role of shuttles to transport an appropriate organic substrate. Harada has shown that they can act as counter phase-transfer agents, which function in the reverse manner of phase-transfer catalysts [34]. In fact, cyclodextrins, which are characterized by a high solubility in water but a poor solubility in a polar solvent, form inclusion complexes with a large variety of substrates, which leads to their transfer into the aqueous phase. Similarly, encapsulation of the product after catalysis allows it to be transferred into the organic phase according to the partition coefficients [35].

The first use of such agents has been reported, almost simultaneously, by Zahalka et al. [36] and Harada et al. [37]: they introduced a cyclodextrin into the $PdCl_2$–$CuCl_2$ catalyzed oxidation of terminal alkenes into the corresponding methyl ketones (Wacker-

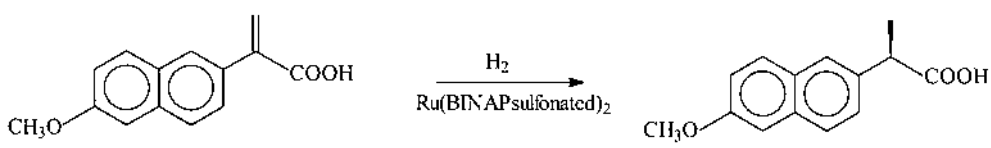

dehydronaproxen (S)-naproxen

SCHEME 1

type reaction). They observed, for instance, the oxidation of oct-1-ene into octan-2-one at 65°C for 10 h whereas in the absence of α-cyclodextrin (α-CD) no catalysis occurs [37]. Zahalka et al. were able to oxidize under mild conditions long-chain alkenes and noted that β-cyclodextrin (β-CD) gave an activity higher than that of α- or δ-cyclodextrin [36]. During the hydrogenation of arylketones [38] in the presence of a rhodium(I) precursor and β-CD, the catalytic reaction proceeds easily at room temperature to give the corresponding alkanes. However, α-CD has a negative effect on the hydrogenation reaction, presumably due to the absence of an inclusion complex between the ketone and the transfer agent. Thus, Anderson and al. [39] have reported the negative effect of α-CD in the hydroformylation reaction of hex-1-ene, catalyzed by a water-soluble complex bearing monosulfonated triphenylphosphine (TPPMS). Indeed, addition of α-CD reduces the rate of the catalytic reaction, the yield dropping to 55% with the same precursor and a fivefold amount of α-CD.

Whereas water-soluble rhodium complexes catalyze the biphasic hydrogenation of various unsaturated substrates but rapidly form colloids, the addition of β-CD has been shown to lead to efficient homogeneous catalytic systems [40]. For instance, in the absence of transfer agent, as reported by Larpent et al. [41], maleic acid is completely transformed in 83 h instead of a reaction time of 17 h with β-CD. Similarly, the hydrosilylation reaction of an alkene catalyzed by a platinum precursor can be notably accelerated by the presence of β-CD; the case of a Lamoreaux Pt^{II}/Pt^{IV} catalyst is more spectacular since the yield can reach 100% in 12 min, whereas no transformation of the substrate occurs in 24 h in the absence of β-CD [42].

Selective chemical modifications of the hydroxyl groups of the primary alcohol functions have been performed for many years [43,44]; the functionalization of the secondary alcohols has also been achieved [44]. Their modified complexation capacities have been recognized and for 20 years numerous papers have appeared on the modification of cyclodextrins, and this continues to attract a marked interest. It is worth to mentioning the strong accelerating effect provided by a permethylated (14 methyl functions in fact) β-CD bearing an additional imidazolylethyl substituent on a secondary alcohol in performing the hydrolysis of nitrophenyl acetate [45]. This permethylated material is usually called "dimethylated" β-cyclodextrin, (DM β-CD) and is now classically used in catalysis. Monflier and coworkers have demonstrated that the combination of $PdSO_4$, $CuSO_4$, a heteropoly acid, and such a cyclodextrin is an efficient catalytic system for performing the oxidation of a terminal alkene to the corresponding methyl ketone in a biphasic system [46,47]. The yield in 2-ketone is as high as 98%, although for the two terminal C_{14} and C_{16} olefins, isomerization to the corresponding internal alkenes can reach 6 and 10%, respectively. The authors have observed that the optimal size and shape for the alkene were achieved with dec-1-ene. Mechanistic investigations have shown that the DM β-CD presents simultaneously a higher solubility in water and a higher hydrophobicity of the cavity that hosts the substrate [48]. At low cyclodextrin concentration, the rate-determining step is the mass transfer between the aqueous and organic phases as illustrated in Fig. 4.

However, when a higher concentration of ketone is reached, the cyclodextrin is poisoned by this product and the catalytic activity decreases dramatically. Presumably, the inclusion of the 2-methyl ketone is preferred over that of the terminal alkene.

Extension to other functionalized cyclodextrins has been done by the introduction of 2-hydroxypropyl (or acetyl) and sulfonato- groups in place of the methyl substituents [49]. It can be concluded that the solubility of the inverse phase-transfer agent in each phase plays the main role in the mass transfer. In addition, the presence of intermolecular hydrogen bonds between the hydroxyl groups of the cyclodextrin and the carbonyl oxygen

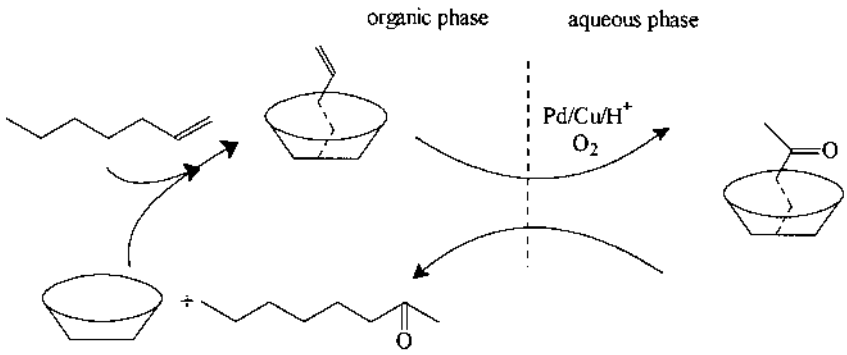

FIG. 4 Oxidation of terminal alkene in the presence of cyclodextrin.

atom of the ketone, which results from the catalytic oxidation, is responsible for the poisoning effect observed. The same phenomena have been shown to dominate the catalysis in the hydroformylation [50] and hydroxycarbonylation [51] of terminal alkenes. Particularly in the latter case, where carboxylic acids are produced, the presence of hydrogen bonds has been noted, even with permethylated β-CD.

Allylic substitutions catalyzed by a TPPTS containing a palladium(0) complex, generated in situ, have been also explored. For instance, addition of diethylamine to an allylic carbonate leads, with high efficiency, to the corresponding allyldiethylamine with simultaneous loss of CO_2 [52].

In catalysis the excess of a phosphine ligand is often necessary because it preserves the active species in the medium [2a]. However, it retards to some extent the co-ordination of the alkene to the metal center. Recent studies, performed by Monflier and coworkers, have shown that the water-soluble TPPTS ligand could reduce the rate of the reaction by another effect. Indeed, TPPTS can be included partially in the cyclodextrin hydrophobic cavity [53,54]; NMR measurements, observation by UV–visible spectroscopy and circular dichroism, as well as scanning tunneling microscopy are consistent with a 1:1 inclusion complex in which the phosphorus atom would be incorporated into the torus of the β-CD. NMR investigations carried out on (*m*-sulfonatophenyl)diphenylphosphine have shown that a phenyl group is incorporated [55]. Thus, the phosphorus ligand could modify the association constant of the alkene with the cyclodextrin so that the mass transfer between the two phases could be decreased.

The participation of the secondary alcoholic functions to the increase in association constant of the ketone recalls the basic catalysis of various esters in aqueous medium. Indeed, this hydrolysis is clearly assisted by β-CD and Tee et al. present a mechanism in which an ionized hydroxy group of the cyclodextrin acts as a nucleophile towards the "guest" ester [56]. In several cases the kinetics studies are consistent with a hydrolysis process in which a complex formed from the ester and two molecules of cyclodextrin is involved [57].

Such an example of a 2:1 complex is interesting because, for our part, we observed nonlinear effects during the hydroformylation of various heavy alkenes, which led us to propose the association of two cyclodextrin units in the interphase [58]. Experiments, carried out at 5 bar, 80°C, and in the conditions of a chemical regime for the stirring of the biphasic system, with the dinuclear $[Rh_2(\mu\text{-StBu})_2(CO)_2(TPPTS)_2]$ complex, show interesting trends.

Indeed, β-CD allows a 26% yield of aldehydes in 18 h for oct-1-ene, but the conversions become very poor for longer chain terminal alkenes: 6% for dec-1-ene, and 2.1,1.6, and 1.4% for the C_{12}, C_{14}, and C_{16} alkenes, respectively. However, DM β-CD not only allows yields higher than those of β-CD, but also for the heavier alkenes investigated: 59% for C_8, 51% for C_{10}, 30% for C_{12}, 8.3% for C_{14}, and 5.3% for C_{16}. Not only is DM β-CD more soluble than β-CD in water (590 and 18.5 gL^{-1}, respectively) and thus brings more alkene into the aqueous phase, but it is also more flexible so that it more easily incorporates longer chains. In addition, it is necessary that the included alkene presents its carbon–carbon double bond emerging from the torus.

The regioselectivity of the hydroformylation reaction is an informative parameter. Indeed, in a pure water/oct-1-ene biphasic system the $[Rh_2(\mu\text{-StBu})_2(CO)_2(TPPTS)_2]$ catalyst precursor leads to 98% of nonanal and 2% of 2-methyloctanal [25], whereas in a pure organic medium the analogous organosoluble complex $[Rh_2(\mu\text{-StBu})_2(CO)_2(PPh_3)_2]$ affords a linearity near to 75% [59]. Thus, for a classical run carried out with a catalyst/cyclodextrin/oct-1-ene molar ratio of 1: 10: 256 the linearity is 88.5%, clearly indicating that a purely non aqueous medium is present to provide the solvation sphere of the rhodium atom.

Moreover, the catalytic activity and the regioselectivity are affected by the amounts of cyclodextrin added as transfer agent.

As presented in Table 2, the conversion of oct-1-ene increases regularly with the concentration of β-CD in the medium until a constant value is obtained above 2.3 mmol when β-CD begins to precipitate.

Interesting information is provided when the TOF is divided by the molar quantity of β-CD and plotted versus the amounts of β-CD introduced to express the catalytic performance per mole of cyclodextrin. The expected straight line was not observed, as shown in Fig. 5.

A minimum near 1.5 mmol appears before the curve increases to a local optimum value of 3.5 $mmol^{-1}h^{-1}$ near 2.3 mmol. A further decrease in the curve then occurs, due to the precipitation of β-CD; the dashed line corresponds to the TOF calculated as a function of the 2.3 mmol of β-CD present in solution, thus showing that beyond roughly 3 mmol the organization around the cyclodextrin is more or less invariant. The minimum observed in the curve, and which corresponds to an inhibiting effect is consistent with a less accessible double bond. Presumably, this phenomenon does not correspond with modifications

TABLE 2 Effect of the Quantity of β-CD on the Yield and Linearity of the Hydroformylation Reaction of Oct-1-ene

β-CD (mmol)	Yield (%)	Linearity (%)	TOF (h^{-1})	TOF/β-CD ($h^{-1}/mmol^{-1}$
0	2	98	0.6	—
0.44	6	98	1.8	4.1
0.88	10.2	97	3.0	3.4
1.32	14.1	95	4.2	3.2
1.76	19.2	93	5.7	3.3
2.20	26.2	88.5	7.8	3.5
4.41	30.1	87.2	9.0	2.0

$P_T = 5$ bar; $T = 80°C$; $D\Delta t = 18$ h; catalyst = 0.25 mmol; P/Rh = 10 ; $H_2O = 40$ mL; oct-1-ene = 64 mmol.

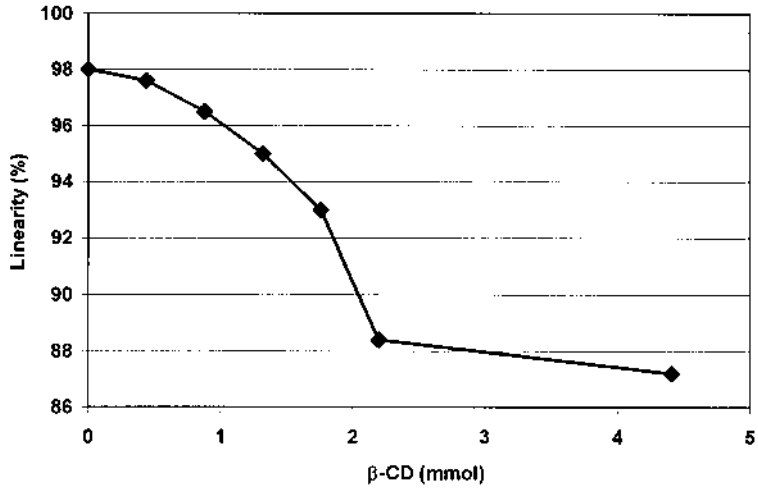

FIG. 5 Curve of TOF/β-CD as a function of the quantity of β-CD.

in the solvation sphere but rather is consistent with a peculiar arrangement of two β-CDs, maybe in a head-to-head manner [60,61] that encapsulates one molecule of oct-1-ene.

Figure 6 shows the linearity of the C_9 aldehyde produced versus the molar quantities of β-CD. This selectivity decreases dramatically for increasing amounts of transfer agent. Such a behavior is consistent with the effect of the steric hindrance of the host on to the C=C double bond, which should be increasingly included in the cavity, so that the hydride ligand bond to rhodium is preferentially transferred to the terminal carbon atom in a step where the rhodium–alkyl species is formed.

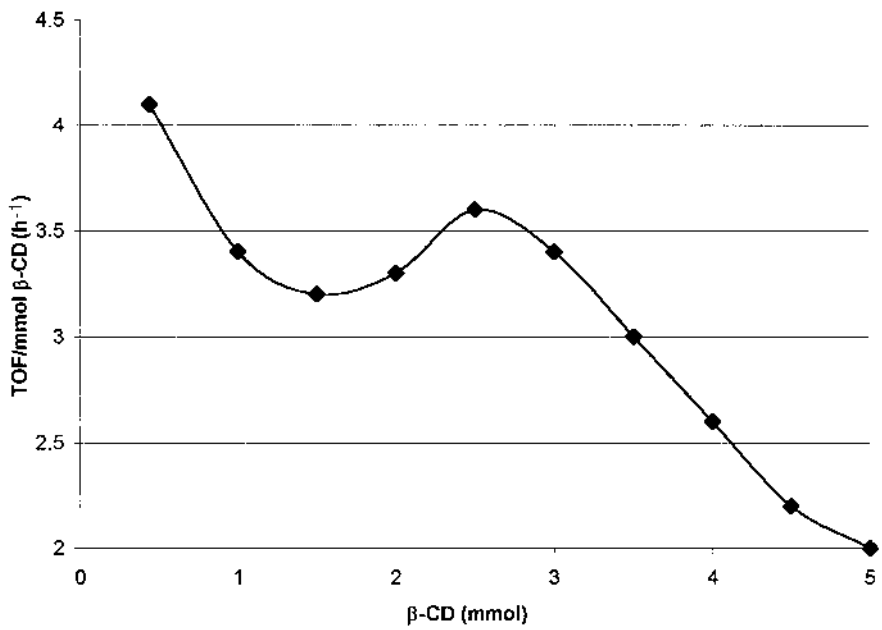

FIG. 6 Linearity variation as a function of the quantity of β-CD.

TABLE 3 Hydroformylation of Oct-1-ene with DM β-CD

DM-β-CD (mmol)	Yield (%)	Linearity (%)	TOF (h^{-1})	TOF/DM-β-CD ($h^{-1}/mmol^{-1}$)
0	2	98	0.6	—
0.38	13.0	91.9	3.9	9.0
0.76	25.5	91.4	7.6	8.8
1.52	45.2	90.2	13.5	7.8
2.29	59.1	88.7	17.7	6.8
3.05	71.2	87.4	21.3	6.0
3.81	81.6	85.0	24.4	5.7

$P_T = 5$ bar; $T = 80°C$; $\Delta t = 18$ h; catalyst = 0.25 mmol; P/Rh = 10; H_2O = 40 mL; oct-1-ene = 64 mmol.

Similarly, addition of DM β-CD to the biphasic catalytic system affords a linear increase in the conversion of oct-1-ene, dec-1-ene, and dodec-1-ene as shown in Tables 3–5.

However, whereas the linearity as a function of added DM β-CD does not vary significantly for the C_{10} and C_{12} alkenes (Figs 7 and 8), the inhibiting effect appears clearly for oct-1-ene. Presumably, this latter alkene has a too short chain length so it is more masked by the arrangement of two cyclodextrins, whereas nothing is observed for heavier alkenes.

The recycling of the catalyst has been examined just by reintroducing the aqueous phase containing the water-soluble rhodium complex and the permethylated β-CD, since usually a loss of activity occurs. Results are shown in Tables 6 and 7 for four successive runs carried out with either oct-1-ene or dec-1-ene.

For each recycling a higher yield is obtained, the linearity being more or less constant. In both cases the conversion raises significantly from 20 to 27 and 25%, respectively. In homogeneous conditions, a species more closed to the active species has never been observed starting from $[Rh_2(\mu\text{-StBu})_2(CO)_2(TPPTS)_2]$. Thus, the catalytic system should gradually adopt a higher level of organization, so that the transfer agent is globally more efficient thereby allowing the contact between the reactants. This local arrangement is not disrupted during the two-phase decantation or reintroduction of the reactants. Our hypothesis is that a catalyst/cyclodextrin/substrate/solvent system is formed and it associates the rhodium complex and the external part of the cyclodextrin in the water-rich area whereas the alkene stands in the organic-rich part. Such an organization supposes also that some water molecules are present at the interface in the organic phase, and in a symmetrical way that some alkene molecules belong to the aqueous phase in such a manner that no local discontinuity exists between the two phases. We prefer to envision an organization around the cyclodextrin in an interphase. In such a view the transfer agent should not only be efficient through the inclusion complex it can produce with alkene, but it also organizes a continuous variation of the solvent properties, so that the transfer is largely improved.

Further studies are on the way to evidence and model this level of organization.

IV. VARIOUS MODES TO MAINTAIN A COMPLEX IN THE INTERPHASE

In fact, the previous arrangement described with a cyclodextrin/catalyst couple and which improves the transfers is more efficient because it should maintain this system in the

TABLE 4 Hydroformylation of Dec-1-ene with DM β-CD

DM-β-CD (mmol)	Yield (%)	Linearity (%)	TOF (h^{-1})	TOF/DM-β-CD ($h^{-1}/mmol^{-1}$)
0	2	98	0.6	—
0.76	16.4	91.3	4.9	5.6
1.52	33.3	90.8	10.0	5.7
2.29	50.7	90.2	15.2	5.8
3.05	62.5	89.7	18.7	5.3
3.81	70.4	90.5	21.0	4.8

$P_T = 5$ bar; $T = 80°C$; $\Delta t = 18$ h; catalyst = 0.25 mmol; P/Rh = 10; $H_2O = 40$ mL; dec-1-ene = 64 mmol.

interphase. This concept has been proposed and developed for the first time by Chaudhari et al. [62]. Indeed, they observed a rate enhancement of 10 to 50 times that of a pure biphasic system by adding small amounts of PPh_3 to the complex $[Rh(H)(CO)(TPPTS)_3]$. In fact, an intermolecular exchange exists between the phosphine ligands so that a mixed species is obtained, maintained near the interface, thus increasing the concentration of the catalyst and its contact with the substrate in this region. NMR studies have allowed identification of the complex $[Rh(H)(CO)(PPh_3)_2(TPPTS)]$ [22]. Unfortunately, the exchange phenomenon shifts the equilibrium towards the complex $[Rh(H)(CO)(PPh_3)_3]$, which is responsible for a higher catalytic activity and for leaching of rhodium in the organic phase. A similar situation prevails for the complex $[Rh_2(\mu\text{-StBu})_2(CO)_2(TPPTS)_2]$ when a small concentration of PPh_3 is added; in this case too, the organosoluble $[Rh(H)(CO)(PPh_3)_3]$ complex is formed during the ligand exchange [22].

This concept has been extended to the hydroformylation of allyl alcohol in an aqueous phase and of the $[Rh(H)(CO)(PPh_3)_3]$ complex in toluene in the presence of small amounts of TPPTS, which increases notably the rate of the reaction [62].

Another approach to improve the transfer between the two phases by maintaining the catalyst in the interphase is to modify the ligand in such a way that micelles are formed. The first ligand containing surfactant groups was designed by Fell and Papadogianikis [63] who prepared several tris(sulfonatoalkylatedpyridyl)phosphines. Introduction of such a tenside ligand into the co-ordination sphere of rhodium was shown to afford an active catalyst for the hydroformylation of tetradec-1-ene when

TABLE 5 Hydroformylation of Dodec-1-ene with DM β-CD

DM-β-CD (g)	Yield (%)	Linearity (%)	TOF (h^{-1})	TOF/DM-β-CD ($h^{-1}/mmol^{-1}$)
0	1	97	0.3	—
0.76	8.5	92.6	2.5	2.9
1.52	17.9	93.3	5.4	3.1
2.29	31.4	93.2	9.4	3.6
3.05	41.2	92.3	12.3	3.5
3.81	52.1	91.5	15.6	3.6

$P_T = 5$ bar; $T = 80°C$; $\Delta t = 18$ h; catalyst = 0.25 mmol; P/Rh = 10; $H_2O = 40$ mL; dodec-1-ene = 64 mmol.

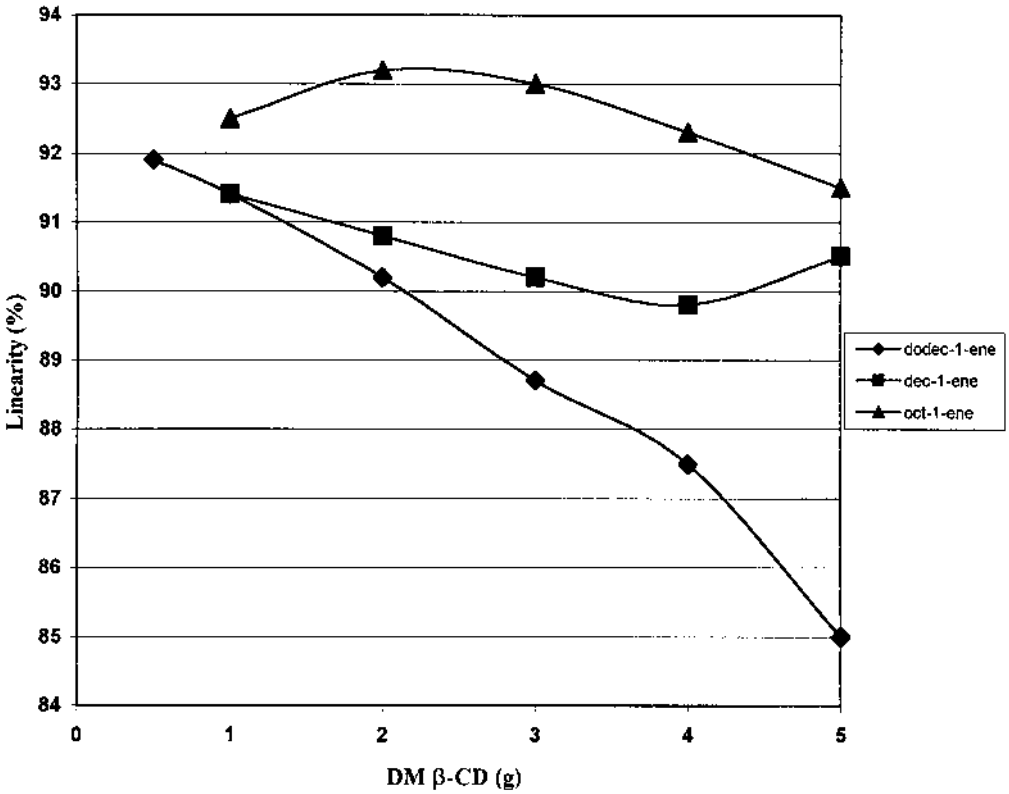

FIG. 7 Linearity variations of oct-1-ene, dec-1-ene, and dodec-1-ene, as functions of the quantity of DM β-CD.

$[Rh(H)(CO)(TPPTS)_3]$ is almost inactive. Many tenside ligands have been synthesized and examined in either a hydrogenation or hydroformylation reaction [64]. Hanson, in a recent review, points out the exact role of the amphiphilic water-soluble phosphines, which is to aggregate in water and to lead to great improvement of the reaction rates with poorly water-soluble substrates [65]. In the classical model of micelles the organosoluble tail of the phosphine is included in the core and the two Stern and Gouy–Chapman layers constitute in fact the interphase. Micellar systems have been extensively studied by Oehme, and the stabilization of spherical micelles, reverse micelles, and vesicles clearly established [66]. In addition to a considerable enhancement of the surface area, the variation in the dielectric constant as well as the lowering of the reaction transition state through direct interactions between the complex and polar head-groups play an important role in the rate enhancement. Amphiphilic diphosphines synthesized recently form, as well as the corresponding rhodium complexes, vesicles stable up to 90°C. Hydroformylation experiments have revealed that these systems are highly efficient since significant reaction rates and selectivities up to 99% in linear aldehydes were obtained. Moreover, no loss of activity was measured after four recycles [67].

The asymmetric hydrogenation of α-amino acids precursors has been particularly studied [68], but these micellar systems are also successful in Suzuki C–C coupling reactions [69] and in hydroformylation [70].

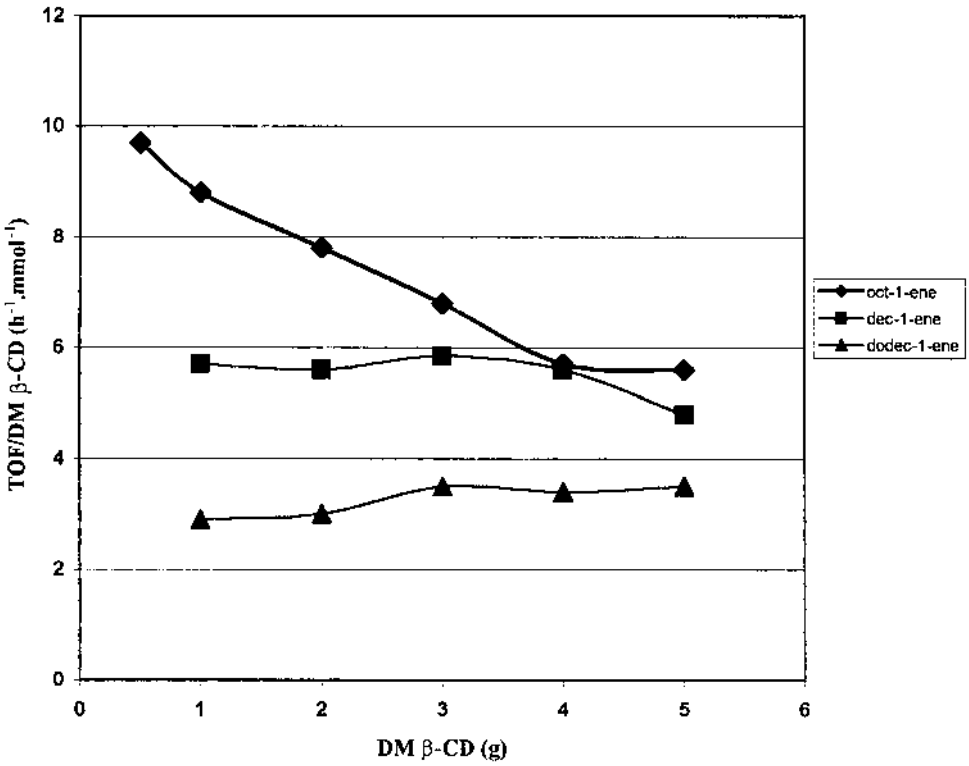

FIG. 8 Curve of TOF/DM β-CD as a function of the quantity of DM β-CD.

Phenylphosphines containing a tail terminated with a phosphanate group can advantageously co-ordinate to rhodium and provide efficient hydroformylation catalysts. Addition of methanol further increases the rate of the decantation step [71].

It is interesting to include in this category of interphase systems, the use of highly water-soluble protective agents, like polymers, surfactants, or ionic species, to stabilize colloidal metallic particles finely dispersed in water. Larpent and Patin have developed this original approach [72]. Ruthenium colloids can efficiently catalyze the oxidation, under room conditions, of cyclo-octane by *t*-butylhydroperoxide [73]. Recent results show that

TABLE 6 Recycling Results on Yield and Linearity for Hydroformylation of Oct-1-ene

Recycling	Yield (%)	Linearity (%)	TOF (h^{-1})
0	65.9	85.0	19.7
1	80.0	88.6	23.9
2	87.5	86.8	26.1
3	91.1	85.7	27.2

$P_T = 5$ bar; $T = 80°C$; $\Delta t = 18$ h; catalyst = 0.25 mmol; P/Rh = 10; $H_2O = 40$ mL; oct-1-ene = 64 mmol; DM β-CD = 3.05 mmol.

TABLE 7 Recycling Results on Yield and Linearity for Hydroformylation of Dec-1-ene

Recycling	Yield (%)	Linearity (%)	TOF (h^{-1})
0	65.5	89.7	19.6
1	69.1	89.3	20.6
2	73.0	88.8	21.8
3	84.7	87.6	25.3

$P_T = 5$ bar; $T = 80°C$; $\Delta t = 18$ h; catalyst = 0.25 mmol; P/Rh = 10; $H_2O = 40$ mL; dec-1-ene = 64 mmol; DM- β-CD = 3.05 mmol.

stable suspensions of colloidal rhodium prepared in the presence of hydroxyalkylammonium bromide surfactants can be recycled after the hydrogenation of various aromatic derivatives, without loss of activity [74].

Apparently, no colloids are formed when polyethylene glycol is added to rhodium trichloride hydrate to obtain a water-soluble rhodium polyethylene glycolate highly active in the hydroformylation of heavy alkenes such as dodec-1-ene [75]. Such a system does not require the presence of other ligands and works efficiently at 70–120 bar. Besides a hypothesis in which it is envisioned a migration of the catalyst into the organic phase, a model where the reaction takes place in the interphase, due to the presence of polyethylene glycol, is favored.

V. CONCLUSION AND PERSPECTIVES

This analysis of the literature has been essentially focused on the aqueous biphasic systems for which SAPC or cyclodextrins allow a good improvement of the transfer. Of course, the synthesis of new ligands continues to attract great attention. For instance, the development of functionalized phosphines presents prospects for their utilization in biphasic catalysis. Katti et al. discuss their approach in the design of water-soluble bi- or tri-dentate alkylphosphines to prepare complexes having the appropriate hydrophilic/lipophilic balance [76]. Other groups have adopted a similar strategy and we can quote dibenzofuran-based phosphines [77] or have an upsurge of interest for tris(hydroxymethyl)phosphine [78, 79] after the earlier work of Chatt et al. [80]. A new class of surfactants based on carbohydrates has been reported recently, and phosphines containing these alkylpolyglycosides could present interesting properties [81].

Fluorous containing ligands in fluorinated solvents can lead to homogeneous catalytic complexes at moderately high temperature and these separate at room temperature giving a two-phase system from which the catalysts is simply separated by decantation. Horvàth, who was the first to develop this concept [82], has reviewed recently the ''fluorous biphasic chemistry'' [83]. The combination of fluorinated ligands and supercritical carbon dioxide affords a particular efficiency to these systems [84,85].

Water-soluble polymer-bound catalysts represent an interesting alternative [86], in particular when they are attached to ''smart'' polymers, which can undergo a complete

change of solubility in a narrow temperature range [87], or to dendrimers with a subsequent separation by ultrafiltration [88].

Supercritical carbon dioxide ($scCO_2$) has been shown to be a powerful medium for performing catalysis and separating the products from the metallic center [89]. Good performances have been reported in hydrogenation reactions [90,91] in palladium-catalyzed carbon–carbon bond formation [92,93], and more recently in platinum-catalyzed enantioselective hydrogenation [94]. Darr and Poliakoff [95], with Jessop et al. [96], reviewed extensively the characteristic of co-ordination chemistry and catalysis in $scCO_2$.

Catalysis in ionic liquids is a burgeoning field of investigation and represents many potentialities for industrial applications, after the first demonstration by Chauvin and Olivier-Bourbigou at the Institut Français du Pétrole for the nickel-catalyzed dimerization of lower olefins [97]. This very promising catalysis has been reviewed recently by Sheldon [98].

However the literature is rich in many papers which show that new trends can be envisioned such as a combination of ionic liquids and $scCO_2$ [96], or association of cyclodextrins like rotaxanes [99].

In conclusion, biphasic catalysis is certainly a method that will allow attainment of fundamental requirements of modern chemistry.

REFERENCES

1. Ojima. Catalytic Asymetric Synthesis. 2nd ed. New York: Wiley-VCH, 2000.
2. (a) B Cornils, WA Herrmann. Applied Homogeneous Catalysis with Organometallic Compounds. Wienheim; VCH,1996; (b) F Joò, E Papp, A Kathò. Topics Catal 5:113–124, 1998; (c) RH Fish. Chem Eur J 5:1677–1680, 1999; (d) F Joò, G Laurenczy, L Nadasdi. J Elek Chem Commun 971–972,1999.
3. B Cornils, WA Herrmann. Aqueous Phase Organometallic Catalysis. Concepts and Applications, New York: Wiley-VCH,1998.
4. (a) Rhone Poulenc (EG Kuntz) FR Patents 2.349.562, 2.366.237,2.733.516, 1976; (b) EG Kuntz. Chemtech 570–575,1987.
5. (a) B Cornils, E Wiebus. Chemtech 33–38,1995; (b) B Cornils, EG Kuntz. J Organometal Chem 502:177–182, 1995.
6. RM Deshpande, SS Divekat, BM Bhanage, RV Chaudhari. J Mol Catal 75: L19, 1992.
7. I Hablot, J Jenck, G Casamatta, H Delmas. Chem Eng Sci 47:2689–2694, 1992.
8. O Wachsen, K Himmler, B Cornils. Catal Today 42:373–379, 1998.
9. J Gagnaire, A Cornet, A Bouchu, G Descotes, Y Queneau. Colloids Surfaces 172:125–138, 2000.
10. MS Goedhejt; BE Hanson, JNH Reek, PCJ Kamer, PWNM Van Leuwen. J Am Chem Soc 122:1650–1657, 2000.
11. SC Tsang, N Zhang, L Fellas, AM Steele. Catal Today 61:29–36, 2000.
12. JP Arhancet. ME Davis, JS Merola, BE Hanson. Nature 339:454–455, 1989.
13. JP Arhancet. ME Davis, JS Merola, BE Hanson, J Catal 121:327–339, 1990.
14. JP Arhancet. ME Davis, BE Hanson, J Catal 129:94–99, 1991.
15. JP Arhancet. ME Davis, BE Hanson, J Catal 129:99–104, 1991.
16. JP Arhancet. ME Davis, BE Hanson, Catal Lett 11:129–133, 1991.
17. ME Davis. Chemtech 498–502,1992.
18. ME Davis. In: B Cornils, WA Herrmann, eds. Aqueous Phase Organometallic Catalysis. Concepts and Applications. New York: Wiley-VCH, 1998, pp 241–251.
19. IT Horvàth. Catal Lett 6:43–48, 1990.

20. UJ Jauregui-Haza, M Dessoudeix, P Kalck, AM Wilhem, H Delmas. Catal Today 66:297–302, 2001.
21. P Kalck, L Miquel, M Dessoudeix. Catal Today 42:431–440, 1998.
22. P Kalck, M Dessoudeix. Coord Chem Rev 190–192: 1185–1198, 1999.
23. G Fremy, E Monflier, JF Carpentier, Y Castanet, A Mortreux. Angew Chem, Int Ed Engl 34:147–149, 1995.
24. S Dos Santos, Y Tong, F Quignard, A Choplin, D Sinou, JP Dutasta. Organometallics 17:78–89, 1998.
25. P Kalck, P Escaffre, F Serein-Spinau, A Thorez, B Besson, Y Colenille, R Perron. New J Chem 12:687–690, 1988.
26. Ph Kalck, JM Francès, PM Pfister, TG Southern, A Thorez. J Chem Soc, Chem Commun 510–511, 1983.
27. M Dessoudeix. ''Approche supramoléculaire de l'hydroformylation bisphasique des alcènes lourds''. PhD thesis, Université Paul Sabatier, Toulouse, France, 1999.
28. M Dessoudeix, UJ Jauregui-Haza, M Heughebaert, AM Wilhem, H Delmas, A Lebugle, P Kalck. Advanced Synthesis and Catalysis 344:406–412, 2002.
29. F Quignard, A Chopin. Chem Commun 21–211, 2000.
30. KT Wan, ME Davis. J Catal 148:1–6,1994.
31. KT Wan, ME Davis. Nature 370:449–452,1994.
32. L Tonks, MS Anson, K Ellgardt, AR Mirza, DF Thompson, JMJ Williams. Tetrahedron Lett 38:4319–4322, 1997.
33. BM Bhanage, F Zhao, M Shirai, M Arai. Catal Lett 54:195–198, 1998.
34. A Harada. J Syn Org Chem Jpn 48:517–521, 1990.
35. E Monflier, E Blouet, Y Barbaux, A Mortreux. Angew Chem, Int Ed Engl 34:2269–2271, 1995.
36. HA Zahalka, K Januskiewicz, H Alper. J Mol Catal 35:249–253,1986.
37. A Harada, Y Hu, S Takahashi. Chem Lett 2083–2084, 1986.
38. HA Zahalka, H Alper. Organometallics 5:1911–1913, 1986.
39. JR Anderson, EM Campi, WR Jackson. Catal Lett 9:55–58, 1991.
40. H Arzoumanian, D Nuel. CR Acad Sci Paris 2 (II c): 289–293, 1999.
41. C Larpent, R Dabard, H Patin. CR Acad Sci 304 (II): 1055–1059, 1987.
42. LN Lewis, CA Sumpter. J Mol Catal A: Chemical 104:293–297, 1996.
43. J Boger, RJ Corcoran, JM Lehn. Helv Chim Acta 61:2190–2218, 1978.
44. AP Croft, RA Bartsch. Tetrahedron 39:1417–1474, 1983.
45. H Ikeda, R Kojin, C Yoon, T Ikeda, F Toda. Tetrahedron Lett 29:311–312, 1998.
46. E Monflier, E Blouet, Y Barbaux, A Mortreux. Angew Chem, Int Ed Engl 33:2100–2102, 1994.
47. E Monflier, S Tilloy, G Fremy, Y Barbaux, A Mortreux. Tetrahedron Lett 36:387–388, 1995.
48. E Monflier, S Tilloy, E Blouet, Y Barbaux, A Mortreux. J Mol Catal A: Chemical 109:27–35, 1996.
49. S Tilloy, F Bertoux, A Mortreux, E Monflier. Catal Today 48:245–253, 1999.
50. E Monflier, G Fremy, Y Castanet, Y Castanet. Angew Chem, Int Ed Engl 34:2269–2271, 1993.
51. E Monflier, S Tilloy, F Bertoux, Y Castanet, A Mortreux. New J Chem 21:857–859, 1997.
52. H Bricout, L Caron, D Borman, E Monflier. Catal Today 66:355–361, 2001.
53. E Monflier, S Tilloy, C Meliet, A Mortreux, S Fourmentin, D Landy, G Surpateanu. New J Chem 23:469–472, 1999.
54. A Da Costa, E Monflier, D Landy, S Fourmentin, G Surpateanu. Surface Sci 470:275–283, 2001.
55. L Caron, C Christine, S Tilloy, E Monflier, D Landy, S Fourmentin, G Surpateanu. Supramol Chem 2001.
56. OS Tee, M Bozzi, JJ Hoeven, TA Gadosy. J Am Chem Soc 115:8990–8998, 1993.
57. OS Tee, XX Du. J Am Chem Soc 114:620–627, 1992.

58. M Dessoudeix, M Urrutigoïty, P Kalck. Eur J Inorg Chem 1797–1800, 2001.
59. P Kalck. In: A de Mejeire, H.tom Dieck, eds. Organometallics in Organic Synthesis. Aspects of a Modern Interdisciplinary Field. Heidelberg: Springer, 1987, pp 297–320.
60. PM Ivanov, D Salviaterra, C Jaime. J Org Chem 61:7012–7018, 1996.
61. J Velasco, P Guardado, C Carmona, MA Munoz, M Balon. J Chem Soc, Faraday Trans 94:1469–1476, 1998.
62. RV Chaudhari, BM Bhanage, RM Deshpande, H Delmas. Nature 373:501–503, 1995.
63. B Fell, G Papadogianikis. J Mol Catal 66:143–147, 1991.
64. G Papadogianikis, RA Sheldon. In: B Cornils, WA Herrman, ed. Aqueous Phase Organometallic Catalysis. Concepts and Applications. New York: Wiley-VCH, 1998, 123–134.
65. BE Hanson. Coord Chem Rev 185/186:795–807, 1999.
66. G Oehme. In: B Cornils, WA Herrman, ed. Aqueous Phase Organometallic Catalysis. Conceptual Applications. New York: Wiley-VCH, 1998, pp 193–206.
67. M Schreuder Goedheijt, BE Hanson, JNH Reek, PCJ Kamer, PWNM Van Leuwen. J Am Chem Soc 122:1650–1657, 2000.
68. G Oehme, I Grasset, S Ziegler, R Mersel, H Furhmann. Catal Today 42:459–463, 1998.
69. E Paetzold, G Oehme. J Mol Catal A: Chemical 152:69–74, 2000.
70. H Chen, Y Li, J Chen, BP Cheng, Y He, X Li. J Mol Catal A: Chemical 149:1–6, 1999.
71. S Bischoff, M Kant. Ind Eng Chem Res 39:4908–4913, 2000.
72. C Larpent, H Patin. J Mol Catal 44:191–195, 1988.
73. F Launay, A Roucoux, H Patin. Tetrahedron Lett 39:1353–1356, 1998.
74. J Schulz, A Roucoux, H Patin. Chem Commun 535–536, 1998.
75. T Bornman, HW Roesky, U Ritter. J Mol Catal A: Chemical 153:31–48, 2000.
76. KV Katti, H Gali, CJ Smith, DE Berning. Acc Chem Res 32:9–17, 1999.
77. AE Sollewijn Gelpke, JJN Veerman, M Schreuder Goedheijt, PCJ Kamer, PWNM Van Leuwen, H Hiemstra. Tetrahedron 55:6657–6670, 1999.
78. L Higham, AK Powell, MK Whittlesey, S Wocadlo, PT Wood. Chem Commun 1107–1108, 1998.
79. A Fukuoka, W Kosugi, F Morishita, M Hirano, L McCaffrey, W Henderson, S Komiya. Chem Commun 489–490, 1999.
80. J Chatt, GJ Leigh, RM Slade. J Chem Soc, Dalton Trans 2021–2024, 1973.
81. W Von Rybinski, K Hill. Angew Chem Int Ed Engl 37: 1328–1345, 1998.
82. IT Horvàth, J Ràbai. Science 266: 72–75, 1994.
83. IT Horvàth. Acc Chem Res 31:641–650, 1998.
84. MA Guillevic, AM Arif, IT Horvàth, JA Gladysz. Angew Chem, Int Ed Engl 36:1612–1615, 1997.
85. N Shezad, RS Oakes, AA Clifford, CM Rayner. Tetrahedron Lett 40:2221–2224, 1999.
86. M Beller, JGE Krauter. In: B Cornils, WA Herrman, ed. Aqueous Phase Organometallic Catalysis. Concepts and Applications. New York: Wiley-VCH, 1998, pp 577–581.
87. DE Bergbreiter, L Zhang, VM Mariagnaman. J Am Chem Soc 115:9295–9296, 1993.
88. CM Casado, B Gonzàles, I Cuadrado, B Alonso, M Moràn, J Losada. Angew Chem, Int Ed Engl 39:2135–2138, 2000.
89. S Kainz, D Koch, W Baummann, W Leitner. Angew Chem, Int Ed Engl 36:1628–1631, 1997.
90. BM Bhanage, Y Ikushima, M Shirai, M Arai. Chem Commun 1277–1278, 1999.
91. GB Jacobson, CT Lee, KP Johnston, W Tumas. J Am Chem Soc 121:11902–11903, 1999.
92. MA Carrol, AB Holmes. Chem Commun 1395–1396, 1998.
93. DK Morita, DR Pesiri, SA David, WH Glaze, W Tumas. Chem Commun 1397–1398, 1998.
94. R Wandeler, N Kunzlz, MS Scneider, T Mallat, A Baiker. Chem Commun 673–674, 2001.
95. JA Darr, M Poliakoff. Chem Rev 99:495–541, 1999.
96. PG Jessop, T Ikariya, R Noyori. Chem Rev 99:475–493, 1999.
97. Y Chauvin, H Olivier-Bourbigou. Chemtech 25:26–30, 1995.
98. R Sheldon. Chem Commun 2399–2407, 2001.
99. A Harada. Acc Chem Res 34:456–464, 2001.

7

Ultrathin Films: Their Use in Enhanced Oil Recovery and in Interfacial Catalysis

LU ZHANG, SUI ZHAO, and JIA-YONG YU Technical Institute of Physics and Chemistry, Chinese Academy of Sciences, Beijing, People's Republic of China

ANGELICA L. OTTOVÁ and H. TI TIEN Michigan State University, East Lansing, Michigan, U.S.A.

I. BACKGROUND

With the availability of thin-film systems at interfaces (planar lipid bilayer, liposomes, emulsions, and colloidal liquid/gas aphrons), a host of compounds can now be embedded in these systems for technology, including biotechnological applications, and for detecting their counterparts present in the environment. Concerning the interfaces, *aqueous solution* | *thin film* | *aqueous solution* and *aqueous solution* | *thin film* | *metal* systems are of particular interest from the viewpoint of practical uses. The reasons are as follows: first, an interface can be thought of as a structure so thin that it has no homogeneous interior. However, the kind of ultrathin films under discussion here are heterogeneous from their contacting phases. Second, an ultrathin film such as a planar lipid bilayer is a system whose interior is influenced by the proximity of its interfaces. In a sense we speak of two interconnecting membrane–solution interfaces or a *biface*, which is defined as any two coexisting membrane-liquid interfaces, through which material, charge, and/or energy transfer are possible. Thermodynamically speaking, it is an "open" system, similar to that of a living cell. These and other interfacial properties of thin films can be understood to a large extent in terms of the laws of interfacial chemistry and physics that govern them, in particular electrochemistry.

First, let us consider thin-film systems such as emulsions at interfaces. An emulsion is a quasi-stable suspension of fine drops of one liquid dispersed in another liquid. Emulsions, together with microemulsions, can be found in technology, and in almost every part of the petroleum production and recovery process: in reservoirs, produced at wellheads, in many parts of the refining process, and in transportation pipelines [1–4]. Understanding the chemistry involved in the stabilization of emulsions and in crude oil emulsions in particular is important both for economic and environmental reasons. The presence of water in oil (w/o) and oil in water (o/w) results in several costly byproducts, such as corrosion, scale, and dissolved metals. Water-in-crude oil emulsions are responsible for the enormous increase in the viscosity of the crude oils produced in reservoirs. Transportation of the viscous crude oil through pipelines is difficult and adds to the cost of production of the oil. With increasing

environmental regulations, the requirements for safe disposal of the produced water derived from the resolution of these emulsions are also increased. Past incidents have shown that the water-in-crude oil emulsions are responsible for the difficulty in effective cleaning up of the oil spillage by techniques such as burning, use of sorbants, use of dispersants, and pumping.

Emulsions are of great importance in enhanced oil recovery (EOR) techniques [1,5]. The stability of emulsions flowing through porous media affects oil recovery processes. In some cases, emulsions may be an unwelcome consequence of the process, but in other cases, the use of emulsions is critical and fundamental to the oil recovery process. The injection of alkaline solutions into a reservoir can improve oil recovery by several mechanisms. Among them emulsification and entrainment, and emulsification and entrapment have been proposed [6–8]. In general, processes that rely on the injection of surfactants or surfactant-forming materials into a reservoir rely heavily on emulsion technology.

Crude oil is found in reservoirs along with water or brine. During oil production, water is often coproduced. Water is also injected into the crude to wash out contaminants or is used as steam to improve fractionation. While contamination of water when processing crude oil frequently leads to emulsions of the o/w type, w/o emulsions are much more prevalent in the petroleum industry. Whenever these mixtures of oil and water pass through pipes with bends, valves, and chokes, emulsification of the aqueous phase into the crude oil occurs due to turbulence [9–12]. A desirable emulsion that must be carefully stabilized to assist one stage of an oil production process may be undesirable in another stage and necessitates a demulsification strategy [1]. For example, an in situ emulsion that is purposely created in a reservoir as part of an oil recovery process may change to a different, undesirable type of emulsion (w/o) when produced at the wellhead. This emulsion may have to be broken and reformulated as a new emulsion suitable for transportation by pipeline to a refinery.

Crude oil consists of a range of hydrocarbons (alkanes, naphthenes, and aromatic compounds) as well as phenols, carboxylic acids, and metals. A significant fraction of oxygen, sulfur, and nitrogen compounds, such as resins and asphaltenes, may be present as well. The carbon numbers of all these components range from 1 (methane) through 50 or more (asphaltenes). Asphaltenes are polyaromatic components that have a high molecular mass and also high sulfur, nitrogen, oxygen, and metal contents. In practical work, asphaltenes are usually defined operationally by using a standardized separation scheme. One such scheme defines asphaltenes as those components of a crude oil or bitumen that are soluble in toluene but insoluble in *n*-pentane. Resins are also polymeric, containing polyaromatic structures. They are differentiated by their solubility in light hydrocarbons such as pentane. This differentiation itself clearly indicates that the resins (soluble in pentane) are smaller on a molecular level compared to asphaltene (insoluble in pentane) molecules. There is no doubt that asphaltenes and resins comprise a major portion of the interfacially active components of the oil [10,11]. They can absorb on to the interface and improve the stability of crude oil emulsions. In addition, oil-soluble organic acids, and finely divided solids, such as carbonaceous materials, polymers, clays, or other minerals (elemental sulfur, iron sulfide, etc.), can also enhance emulsion stability [12,13].

In connection with crude oil research, the properties and mechanisms of emulsion stability in terms of thin liquid films formed at water–crude oil interface have been extensively discussed. We will summarize and review the literature in the next section.

II. ULTRATHIN FILMS AT INTERFACES

A thin film is a material of macroscopic thickness (visible to the naked eye); an ultrathin film is about 1% of the thickness of the wavelength of visible light in one dimension, and macroscopic in the other two dimensions. Thus, a bilayer lipid membrane (BLM) is an example of an ultrathin film; it is so thin that it has no homogeneous bulk phase. Similarly, liposomes and colloidal liquid/gas dispersions generated from surfactant solutions may also be so classified. In this connection many emulsions and foams fall into this category [2,6,14–17]. Although emulsions are not thermodynamically stable systems, in practice they can be quite stable and may resist explicit demulsification treatments. The stability of an emulsion is defined differently, depending on the application and, hence, depends on the stage of destabilization [13]. One finds four interrelated steps. The flocculation leads to aggregation of droplets, while the subsequent coalescence leads to an emulsion with a large variation in droplet size. The droplet or aggregate size is decisive for creaming or sedimentation rate, leading to a highly concentrated emulsion and finally to phase separation. In the petroleum industry, the stability of a crude oil emulsion is judged mostly from the point of view of coalescence. The coalescence process of emulsions occurs in three steps. The first step begins with movement of the droplets toward each other through the continuous phase. Subsequently, droplets deform as they approach one another, forming a thin, plane parallel film between them. Finally, this film thins to a critical thickness at which it becomes unstable and ruptures, and the two droplets unify to form a single larger droplet. The thinning of a thin liquid film and the strength of absorbed interfacial layers of surface-active components are the main two key factors in the coalescence process.

There are two kinds of interactions between two approaching droplets [14]. The first one, which we call thermodynamic interaction, is due to van der Waals', electrostatic, steric, and other similar forces. They are operative even when the particles are at rest, and are little or not at all affected by the motion. A convenient measure for this interaction is the "disjoining pressure," introduced by Derjaguin. The other interaction, hydrodynamic interaction, is caused by the presence of a second interface, which affects the drag force acting on a moving particle. It becomes sizable when the separation between the interfaces is of the order of the particle radius and increases rapidly with decreasing gap width. In the case of fluid particles, the hydrodynamic interactions are strongly affected by the deformation and the tangential mobility of the particle interfaces.

The thinning rate and stability of the thin liquid film is determined by the hydrodynamic and thermodynamic interactions between the two film interfaces. The first stage of film thinning, at a film thickness greater than 100 nm, is determined by the hydrodynamic interactions [15,18]. In this case, correlations between film stability and the rheological behavior of the single interface may be found. When the film has thinned to less than 100 nm, thermodynamic interactions begin to dominate. At least five major mechanisms can be clearly identified for emulsion stabilization [1,4,15–21]: (1) interfacial and thin film rheology, (2) steric repulsion, (3) electrical double layer repulsion, (4) long-range oscillatory structural forces, and (5) rigid, cross-linked network formation of the adsorbed interfacial layers.

A. Interfacial Rheology

Interfacial rheology deals with the shear and dilatational mechanical behavior of adsorbed and deposited layers of surfactants, proteins, polymers, and other mixtures at fluid–fluid interfaces and of monolayers at solid surfaces. The orientation of the adsorbed molecules,

molecular interaction and packing, formation of complexes, or structural transformations at the interface can result in a peculiar rheological behavior, which plays an important role in determining the coalescence behavior of the dispersed phase and in the structure and stability of colloidal liquid aphrons (CLAs) and colloidal gas aphrons (CGAs), as will be discussed in Section II.G.

Many experiments have been proposed for measuring the interfacial shear viscosity and elasticity and interfacial dilatational viscosity and elasticity at gas/liquid and liquid/liquid interfaces [22]. Interfacial shear viscosities of different oil/aqueous systems have been studied worldwide. Some experimental results indicate that low interfacial shear viscosities do not necessarily imply that an emulsion will be unstable [23]. The dilatational rheology is based on area changes due to an expansion or compression of a fluid surface and stress relaxation experiments. The experiment results show that the interfacial dilatational properties can be much higher than the interfacial shear properties for the same system [15,24–27]. This makes researchers believe that interfacial dilatational viscosity and elasticity may have a better relationship with the stability of the emulsion than with interfacial shear properties.

Wasan and his research group focused on the field of interfacial rheology during the past three decades [15]. They developed novel instruments, such as oscillatory deep-channel interfacial viscometer [20,21,28] and biconical bob oscillatory interfacial rheometer [29] for interfacial shear measurement and the maximum bubble-pressure method [15,29,30] and the controlled drop tensiometer [1,31] for interfacial dilatational measurement, to resolve complex interfacial flow behavior in dynamic stress conditions [1,15,27,32–35]. Their research has clearly demonstrated the importance of interfacial rheology in the coalescence process of emulsions and foams. In connection with the maximum bubble-pressure method, it has been used in the BLM system to access the properties of lipid bilayers formed from a variety of surfactants [17,28,36].

B. Thin-Film Rheology

The behavior of thin liquid films formed between coalescing drops and bubbles has attracted considerable attention in an attempt to understand the stabilizing mechanisms of emulsions and foams. It is now generally recognized that the drainage of this film plays a crucial role in determining the stability of the dispersion.

The approach of two droplets under the capillary pressure acting normal to the interface causes liquid to be squeezed out of the film into the bulk. This liquid flow results in the convective flux of surfactant in the sublayer. Therefore, the surfactant concentration at the interface is increased in the direction of that flow. The other fluxes associated with the drainage process shown include: (1) bulk flux in the droplet, (2) bulk flux in the film phase, and (3) interfacial diffusion flux caused by the concentration gradient at the interface [15,18,22,37–39].

The difference in concentration along the interface results in differences in the local values of interfacial tension, producing a force opposite to liquid flow (Marangoni–Gibbs effect) [40,41]. In addition, the surfactant monolayer may undergo dilating and shearing deformation that also produces interfacial stresses. The sum of the above stresses and the tangential bulk stress from the liquid in the droplet must counterbalance the tangential bulk stress from the film liquid that causes the interfacial flow.

In order to enhance coalescence in systems stabilized by the Marangoni–Gibbs effect, the interfacial activity of the surfactant must be high enough to account for the interfacial tension gradient created [39,41,42–44]. Some researchers found that the emul-

sion stabilized by the Marangoni–Gibbs effect becomes unstable when the interfacial shear viscosity and dynamic tension gradient is lowered [38,45–46]. Wasan and coworkers [15,18,47–49] found a direct correlation between the film rheological properties and the stability of foam and emulsion systems stabilized by low-molecular-weight surfactant, proteins, and macromolecules. In addition, they have demonstrated the important role film rheological properties play in the demulsification of water-in-crude oil emulsions. Their results show that there is a direct correlation between dynamic film tension or film elasticity and emulsion stability.

C. Steric Repulsion

Steric repulsion is a short-range interaction that is a result of strong interactions between solvent and material adsorbed at the droplet interface. The adsorbed species favor interaction with the solvent rather than lateral interaction with other adsorbed species [50]. Mackor and van der Waals modeled the adsorption of molecules on to a pair of adsorbing planes, and based on comparisons with experimental data, concluded that steric stabilization must be responsible for the stabilization of some dispersion systems [51,52]. This phenomenon is common with emulsion droplets stabilized by nonionic polymers.

The first systematic investigation of steric interactions in a liquid film sandwiched between two macroscopic liquid bodies was that of Andrews et al. [53], who applied an electric field across the film, leading to a compressional force on the film that consisted of glycerol mono-oleate chains in hydrocarbon oils. The films were formed in a 1 mm hole in a Fluon disk that was mounted between two bulk aqueous electrolyte solutions. Sonntag et al. [54] have studied aqueous films sandwiched between two hydrocarbon layers. The aqueous film containing the nonionic surfactant was formed between two approaching emulsion droplets that were projected in the dispersion medium at the ends of two capillaries. The film thickness and its change were determined by means of an interferometric method.

D. Electrical Double-Layer Repulsion

Two approaching emulsion droplets may be resisted by electrostatic forces. Electrostatic forces consist of Coulombic repulsion between two like charged objects and attractive van der Waals' forces. These two forces are accounted for by the Derjaguin, Landau, Verwey, and Overbeek (DLVO) theory. A third force, Born repulsion, occurs at very small separation distances when electron clouds overlap [1,6,20,21]. In emulsion systems an electrical double-layer may form around the disperse phase droplets. While electrical double-layer repulsion is certainly important in o/w emulsions, it does not play a large role in the stabilization of w/o emulsions due to the low dielectric constant of oil [55,56].

E. Long-Range (nonDLVO) Oscillatory Structural Forces

Lyklema and Mysels [44] were the first to suggest that micelles can contribute to the disjoining forces in foam films. Later on, stratification of both foam and emulsion films formed with ionic surfactants was observed and studied. Wasan [15] was the first to recognize that the stratification in thin liquid films was a manifestation of the long-range oscillatory structural forces, whose periodic distance was about their effective diameter of the particle. Wasan found that stepwise thinning due to micelle/particle organization into layers is a universal phenomenon in a variety of colloidal systems, involving

ionic and nonionic micelles, swollen micelles or microemulsions, globular proteins, and Brownian particles such as latex suspensions and silica hydrosols. The effects of micellar concentration and size, film area, electrolytes, temperature, and micellar polydispersity have been studied [15,18]. In addition, the researchers carried out a theoretical analysis of these forces using the statistical mechanics approach and Monte Carlo simulation [59]. At low particle concentrations, the long-range oscillatory structural force leads to an attractive depletion effect that gives rise to phase separation in colloidal dispersions. However, at high particle concentrations, the oscillatory structural force induces particle structural transitions inside the film and the formation of two-dimensional crystalline layers with hexagonal interplanar ordering that offers a new mechanism for stabilizing particle suspensions, foams, and emulsion. It is of interest to note that the current model of the structure of ionic micelles of synthetic surfactants in dilute aqueous solution is that of a rough-surfaced sphere or ellipsoid.

The detergent most commonly used in membrane biophysics studies is sodium dodecyl sulfate (SDS). It is a negatively charged surfactant with a 12-carbon chain length having a critical micellar concentration (CMC) of 8.1 mM. In biosystems, phospholipids are weak surfactants and have a very low CMC value because of their two long fatty acid chains. Due to their having a small head group with a large, bulky hydrocarbon part, phospholipids would ideally form elongated ellipsoidal structures. In fact, the ideal aggregate structure of phospholipids above their CMC are extended two-dimensional sheet structures, i.e., lipid bilayers. Phospholipids, however, solubilize very well in detergent micelles prepared from SDS. The CMC increased when increasing the molar ratio of methanol in the solution and reached 10 mM in pure methanol, indicating good solubility of phospholipids in this solvent. Naturally occurring phospholipids are thought to have CMC values in the range 0.01–10 nM. This is six orders of magnitude lower than the CMC values for common detergents used for membrane protein solubilization [16,60].

F. Rigid, Viscous Interfacial Film on Crude Oil

The formation of an interfacial layer consisting of surface-active material present in crude oil (asphaltenes and resins) may provide a physical barrier for droplet–droplet coalescence and improve the stability of emulsions. Numerous researchers have noted the presence of this rigid, viscous interfacial film in crude oil–water systems with these surface-active components present and have studied it [20,23–27,55,61–67]. The evidence is compelling that the primary mechanism of asphaltene stabilization of w/o emulsions is through the formation of a viscous, cross-linked three-dimensional network with high mechanical rigidity.

In 1960, Blair [59] and Dodd [68] published key studies on water-in-crude oil emulsions and their films (see [1–6] for references). Using a Cenco surface film balance to study the water–oil interface, Blair showed that the principal source of stability arises from the formation of a condensed and viscous interfacial film by adsorption of soluble material from the petroleum phase, such film presenting a barrier to coalescence of the dispersed droplets. This primary film may be augmented by secondary adsorption of large particles or micelles originally suspended in the petroleum. The classical picture of emulsion stabilization by an adsorbed monolayer yielding low interfacial tension values does not seem to be an accurate one in this case. It appears that a primary adsorbed layer is initially formed, almost certainly comprised of asphaltenes, and a secondary layer superimposes on this primary layer and is likely comprised of asphaltenes, wax particles, and possibly

inorganic particulates. Resins and polyaromatics may also be associated with the film as asphaltene-solvating species.

Dodd [68] measured the rheological properties of interfacial films in a semiquantitative manner by employing an interfacial shear rotational viscometer to study crude–water interfaces with NaCl, acid, and basic additives in the water phase. He concluded that the film must be comprised of naphthenic acids, naphthenic acid soaps, and naphthenic acid anions, in combination with resins, asphaltenes, and waxes. Furthermore, the acidic species must desorb from the interface under basic conditions and partition into the aqueous phase, rendering the interface considerably less rigid. Subsequent researchers have shown that acidic asphaltenes are more effective at emulsion stabilization than their neutral counterparts.

Strassner [69] explored the effects of pH on interfacial film properties and the stability of crude oil–water emulsions by using a pendant-drop technique and found a clear relationship between film rigidity and emulsion stability. He found that the interfacial films of crude oil emulsions contain organic acids and bases in widely differing amounts. Adding inorganic acids and bases strongly influences ionization of the organic acids and bases in the interfacial films, and radical changes in physical properties of the films (rigidity and mobility) occur with changes of pH in the aqueous phase. For most crude oil–brine emulsions, there exists an optimum pH range for which the adsorbed film exhibits minimum emulsion-stabilizing properties. The rigid interfacial films formed by asphaltenes are strongest in acid pH, intermediate in strength at neutral pH, and become very weak or are converted into mobile films in basic pH. The mobile films produced by resins are strongest in base and weakest in acid. The films formed with the remaining wax–oil fraction are insignificant. When the interfacial films were compressed, Strassner observed three types of film mobility:

1. Solid (or rigid) films that under compression form relatively insoluble skins and possess high interfacial shear viscosity.
2. Highly mobile (or liquid) films that pack under compression to give a momentary distortion of the drop, but rapidly redistribute and return the drop to a symmetrical shape when contraction is stopped.
3. Transition or nonmeasureable films that show no distortion under compression of the pendent drop and whose presence is indicated only by the lowering of interfacial tension.

Jones et al. [23] performed some critically important studies of crude oil film formation at oil–water interfaces utilizing experimental probes of interfacial tension, surface pressure, and interfacial rheology. Different crude oils exhibited radically different pressure–area curves as probed by a Langmuir film balance with a hydrophobic Wilhelmy plate. Four types of interfacial film behavior were observed: (1) compressible relaxing, (2) incompressible relaxing, (3) incompressible relaxing with phase transition, and (4) incompressible nonrelaxing. There is a strong correlation between emulsion stability and the existence of incompressible nonrelaxing films because these stable films act as a mechanical barrier to coalescence [2].

Sjöblom and his research team have probed the causes of emulsion stability in a series of North Sea crude oils and observed that emulsion stability correlates with asphaltene, wax, and resin/asphaltene ratio [11]. In their early work, they theorized that asphaltenes may aggregate through stacking interactions mediated by aromatic π-bond overlap to form lamellar structures that stabilize the emulsions. Moreover, they further observed

that the interfacially active fractions of crude oils, which give rise to emulsion stability, are rich in acidic functional groups.

The strongest films are formed under the most acidic conditions. Finally, the films least able to relax under reduced surface stress conditions were observed to form the most stable emulsions. They also found that components other than asphaltenes, such as alkanes (paraffin waxes), resins, and aged interfacially active components of relatively high H/C ratio (1:5), can also contribute to the stabilization of water-in-crude oil emulsions. They concluded that the state of solvation of asphaltenes in the oil phase plays an important role in their ability to stabilize emulsions, which may explain the indirect action of resins on emulsion stability. The temperature is also an important factor when it comes to the stability of crude oil emulsions, especially true when the wax content is relatively high. The most important factor influencing the water-in-crude oil emulsion stability at low temperature is the interaction at the water–oil interface between wax crystals and the heavy fractions of the crude.

Mohammed et al. [55] published a series of papers in which they probed the rheology, interfacial tension, surface pressure, and compressional modulus of crude oil–water interfaces with and without added demulsifiers under thermal and electrical fields. They observed that with short aging times of the crude oil–water interface, the interface rheology could be characterized as substantially viscous, but with very little elastic character. They demonstrated that thick viscoelastic films tended to accumulate in aged films and that some demulsifiers prevented such accumulations.

McLean and coworkers [19,56] have investigated the effects of crude oil solvency and resin-asphaltene interactions on the stability of water-in-crude oil emulsions. They showed that there were three main factors that control the solubility of asphaltenes in crude oil, their tendency to aggregate, and their tendency to adsorb at oil–water interfaces. These are (1) the ratio of resins to asphaltenes, (2) the concentration of the functional group contained in the resin and asphaltene fractions, and (3) the aromaticity ratios of the resins and the crude medium to the asphaltenes.

G. Thin-Film Systems from Surfactant Solutions

Orientation of surfactant molecules at the gas–liquid interface, defined as surfactant-stabilized gas microbubbles, and known as colloidal gas aphrons (CGAs), have been investigated since the 1980s. A closely related system at the liquid–liquid interface, known as colloidal liquid aphrons (CLAs), has also been characterized for a number of surfactants, in terms of stability, and for surfactant layers. Early work on both CGAs and CLAs has shown that they have considerable potential in the field of predispersed solvent extraction. Several studies have looked at the influence of a range of solvents, varying from nonpolar to mildly polar, and a variety of ionic and nonionic surfactants, on CLA size, stability, and phase volume ratio (PVR, volume ratio of the dispersed oil phase to the continuous aqueous phase). In addition, the effect of surfactant type, and stirring speed and time, on the formation of CGAs has also been considered. The results show that CLAs can be formulated with quite polar solvents (e.g., pentanol) and their stability increases as the hydrophilic–lipophilic balance (HLB) number of the nonionic surfactant increases [60].

The CLAs could also be formulated with PVRs as high as 20 without coalescence, which is markedly higher than with microemulsions, and seems to indicate that the liquid aphrons are stabilized by more than a surfactant monolayer. Further, it has been reported that CGAs could be formulated as foam with a half-life of 6 min, and that they could be used to separate dispersed CLAs effectively from a bulk solution. Also, recent advances in

emulsion and foam technology allow surfactants and polymers to be used for decontamination of subsurface soil, and for the removal of colloid-bound contaminants [45,70–72]. Moreover, these novel thin-film systems have been used in biocatalysis. For example, the immobilization of a fusion protein between plant cytochrome and its electron donor, using an o/w macroemulsion [73], as will be described in more detail later.

While both CGAs and CLAs' areas of application are potentially very broad, their most promising use appears to be in downstream separation in biotechnology (e.g., multiphase biocatalysis) where products are very dilute and occur in complex mixtures [67], and possibly in EOR. Thus, the applicability of conventional surfactant solutions, CGAs generated from surfactant solutions, and CLA suspensions will be described in the following subsections.

1. Colloidal Gas Aphrons

(a) Experimental Methods. In 1971, Sebba and coworkers envisaged CGAs as microbubbles (10–100 μm), composed of a gaseous inner core surrounded by a thin surfactant film [2,45,74]. The effects of CGA flow rate, amounts of CGA introduced into the system, surfactant concentration on the flotation efficiency, etc., all have been established. The experimental apparatus, as described by Sebba, consists of a rapidly spinning disk impeller and shaft within a Pyrex vessel. CGAs are created by intense stirring (usually over 5000 rpm) of a surfactant solution. The action of the impeller creates sufficient shearing forces to entrain significant volumes of gas within the liquid.

The experimental parameters of the generator, which could be varied, are as follows: temperature (26 to 375°C) and impeller speed (6000–11,500 rpm). Laboratory studies have been carried out to evaluate the relative suitability of cationic, anionic, and nonionic surfactants under various conditions (e.g., in removing naphthalene from the soil). Nonionic surfactants were found to be more efficient than ionic surfactants in removing naphthalene from a contaminated soil matrix in batch experiments [75]. The presence of surfactant reduced the volatilization of naphthalene. Micellar solubilization appears to be the primary mechanism of removal using both surfactant solutions and CGA suspensions. Increasing the concentration of the surfactant solution enhanced the percentage removal of naphthalene. Using a CGA suspension as a hushing medium may result in channeling and pore clogging in the soil matrix, thereby affecting the overall efficiency of the process. In this connection, Save and Pangarkar [76] described potential applications of CGAs in wastewater processing and bioseparations and reported the effects of various operating conditions, such as pH, power input, impeller location, surfactant type and its concentration, and viscosity of the liquid, on the half-life of the CGA generated. Further, the effects of various additives, such as polymers, enzymes, solvents, salts, etc., were also investigated. A procedure for predicting the drainage rate of CGA has been proposed.

(b) Applications. CGAs for flushing automatic transmission fluid from contaminated soil. Roy et al. [75] reported the use of CGAs to flush residual levels of a light nonaqueous phase liquid (e.g., automatic transmission fluid, ATF) from a contaminated soil. The performance of CGA suspensions was compared with that of conventional aqueous anionic surfactant solutions under both gravity stable (down flow) and gravity unstable (up flow) conditions. CGA suspensions were found to be more effective in washing ATF under both down-flow and up-flow modes. The displacement of ATF from the soil pores seems to be the mechanism of removal in the case of water floods. Increasing the surfactant concentration did not increase the removal rate correspondingly. The

pressure required in pumping the CGA suspension was much lower than that required for conventional surfactant solutions or water flood. In a related earlier study, Roy et al. [77] reported in situ surfactant flushing for decontamination of subsurface soil, using CGA suspensions generated from surfactant solutions. The efficiency of CGA suspensions in the removal of oily waste was compared with that of conventional surfactant solutions and water floods under different flow regimes. Results showed that CGA suspensions produced using sodium dodecyl sulfate had a recovery of waste material (56%) higher than that of conventional surfactant solutions (47%) or water flood (43%) in the down-flow (gravity-stable) mode. The efficiency of CGA suspensions was greater in the down-flow mode than in up-flow (gravity-unstable) or horizontal (gravity-neutral) modes, and increasing the surfactant concentration from 8 to 30 mM did not enhance the removal efficiency for either CGA suspensions or conventional surfactant solutions. CGA suspensions appeared to be better in removing the major chlorinated hydrocarbons present in the oily waste.

Simulation of soil washing with surfactants. Cheah et al. [78] have carried out a theoretical study of soil washing with surfactants and found that the surfactant enhanced mobilization and solubilization of organic compounds. Their model identifies the contributions of the various mechanisms—water displacement, surfactant mobilization, and dissolution—on the removal of organic contaminants from soil. Mobilization of the organic phase was described by a reduction in the residual oil saturation caused by decreased interfacial tension. Increased aqueous solubility of organic compounds due to solubilization by surfactant micelles was modeled assuming local equilibrium. Parameters for the model were obtained from experimental measurements and literature sources. In most cases, the predicted organic recoveries were found to agree well with experimental results. For the surfactant SDS, mobilization of organic contaminants was the main recovery mechanism for both waste liquids modeled. The results suggest that complete dissolution of a contaminant nonaqueous phase, rather than mobilization and subsequent vertical migration, may be difficult to achieve at the surfactant concentrations studied.

Production of finely divided tin powders. Using an apparatus similar in design to that described by Sebba, Riviello et al. [79] reported a novel production method for finely divided tin metal powders. As with CGA production, the action of the impeller creates sufficient shearing forces to entrain significant volumes of gas within the metal. When this gaseous incorporation is performed in an atmosphere that contains oxygen (air), oxidation of the tin lamellas of the CGA occurs. This reaction leads to a microcosmic structural collapse within the CGA system and discrete particle formation from the plateau border. This effect is not observed in a pure nitrogen atmosphere. The experimental parameters, which were varied in this investigation, were at temperatures of 260–375°C and at impeller speeds of 6000–11,500 rpm. Following the removal of the oxide layer from the particles, powder yield and mean particle size were determined. Powder mass yield increased with temperature, at the same time little change in the mean particle size of $\simeq 5$ (m was observed.

Separation of Cu(II) from an aqueous solution. Wang et al. [70] described a new method for separating heavy metal ions from dilute solution, and reported flotation of Cu(II) by CGAs. The effects of flow rate, amounts of CGAs introduced into the system, and surfactant concentration on the flotation efficiency have been investigated. The results show that the flotation efficiency at pH 5–6 has an optimum value for CGA flow rate and amount. When the pH is greater than 7, the flotation efficiency can be as high as 99% under optimum conditions.

Remediation of contaminated groundwater sources. Mosler and Hatton [80] reported the use of surfactants and polymers for the remediation of contaminated groundwater sources. This was achieved by mobilizing contaminants trapped in the soil matrix through reduction in interfacial tension or solubilization within micellar cores (for organics), by binding of metal ions with the charged surfaces of ionic micelles and polyelectrolytes, and by metal ion complexation with ligands solubilized within the micelles or attached to polymer backbones. According to the authors, similarly, control of end-of-pipe waste can also be attained using surfactants and polymers through the removal of colloid-bound contaminants, as the colloids are separated from the aqueous discharge stream by ultrafiltration.

2. Colloidal Liquid Aphrons

Besides CGAs described in the preceding subsections, there are the CLAs, which are surfactant-stabilized solvent droplets. According to Sebba [2,45] the structure of polyaphron phases resemble a biliquid foam while the individual CLAs, when dispersed in a continuous aqueous phase, consist of spherical, micrometer-sized oil droplets surrounded by a thin, aqueous "soapy-shell." Lye and Stuckey [81] investigated the structure and stability of CLAs using a variety of experimental techniques, i.e., cryo-TEM, DSC, and light scattering. Their results allowed quantitative comparison of CLA stability when dispersed under various conditions and of the influence of including various concentrations of lipase or erythromycin-A in the aphron formulation. Based on these results, Lye and Stuckey have proposed a mechanism for the breakdown of dispersed CLA structure, which involves destabilization and loss of the "soapy-shell" followed by coalescence of the oil cores of the aphrons. However, according to these authors direct evidence for the structure of the surfactant-laden interfaces responsible for the stabilization of aphrons is still required if the structural model proposed by Sebba is to be fully confirmed.

(a) Applications. Interfacial catalysis using CLAs. Lamb et al. [73] reported the use of a novel immobilization technique utilizing an o/w macroemulsion, i.e., CLA. They immobilized six different enzymes of different molecular weights. All enzymes were immobilized to a greater or lesser extent, with greater than 70% of β-galactosidase and 90% of α-amylase effectively being immobilized over a wide range of pH values (4–10). It was found that in most cases the pH had little effect on the degree of immobilization. The method of immobilization appeared to be related to the hydrophobicity and adiabatic compressibility of the enzyme, and its molecular weight. These enzymes also exhibited improved activity, after immobilization, while the values of the Michaelis–Menten constant were altered [16]. The major factor affecting loss of activity of the immobilized enzymes was found to be the anionic surfactant, SDS, used in the polyaphron preparation. However, SDS also appeared to enhance activity by altering protein conformation.

Erythromycin extraction. Lye and Stuckey [81] reported the equilibrium partitioning of a microbial secondary metabolite, erythromycin, using both CLAs [formulated from 1% (w/v) Softanol 120 (alcohol ethoxylate type, Honeywill & Stein) in decanol and 0.5% (w/v) SDS in water] and surfactant-containing, two-phase systems. The equilibrium partitioning of erythromycin was found to be strongly influenced by the extraction pH, and exhibited a marked change on either side of the pK_a of the molecule. A modified form of the Henderson–Hasselbach equation [16] could be used as a simple design equation to predict the equilibrium partition coefficient, as a function of pH. For extraction experi-

ments with dispersed CLAs where pH > p_a, erythromycin values as high as 150 could be obtained and the erythromycin could be concentrated by factors of up to 100. Experiments were also carried out in surfactant-containing, two-phase systems to determine the effect of individual surfactants used for CLA formulation on erythromycin partitioning. For extraction at pH 10 neither the Softanol (a nonionic surfactant) nor SDS (an anionic surfactant) had any influence on the equilibrium erythromycin partition coefficients. For stripping at pH 7, however, it was found that recovery of erythromycin from the organic phase decreased with increasing concentration of SDS, although again the Softanol had no influence on the equilibrium. The effect of SDS was attributed to a specific electrostatic interaction between individual erythromycin and SDS molecules under stripping conditions. The concentration factors achievable in the two-phase systems were considerably less than those for the predispersed solvent extraction (PDSE) experiments. The physical properties of the two-phase systems, i.e., density, viscosity, interfacial tension, etc., and the equilibrium distribution of the surfactants were also determined in relation to subsequent studies on the kinetics of erythromycin extraction.

Biocatalysis. The diverse substrate specificity of the cytochrome P450 (P450; CYP) enzyme superfamily offers the opportunity to develop enzymic systems for environmental detoxification and biotransformations of drugs, pesticides, and fine chemicals, Concerning these, Lamb and Stuckey [51] reported on the immobilization of a fusion protein between plant cytochrome P450–71B1 (CYP71B1) and its electron donor, plant NADPH cytochrome P450 reductase, using an o/w macroemulsion (i.e., CLA), which contained a proportion of internal organic phase. The efficiency of P450 immobilization was greater than 85%, and in this state enzymatic activity could be measured for more than 24 h at 15°C. Chlortoluron, a recalcitrant herbicide pollutant in the environment, was shown to be metabolized, with the major metabolite (N-monodemethylated chlortoluron) being separated from the substrate due to partitioning into the aqueous phase. The turnovers exhibited superactivity compared with those obtained using free enzyme located in membranes prepared following heterologous expression in *Saccharomyces cerevisiae* and *Escherichia coli*. The authors also discussed the potential to exploit the unprecedented catalytic diversity of the P450 superfamily in biocatalysis.

Multiphase catalysis. CLAs provide very large interfacial areas, and thus could enhance mass transfer in multiphase biocatalytic processes. Interphase mass transfer of a sparingly soluble solute is often the rate-limiting step in such processes. Srivastava et al. [67] have characterized the mass transfer properties of CLA dispersions during transfer of heptanoic acid from water to limonene. The interfacial area per unit volume (a), the film mass transfer coefficient [$K(L)$], and volumetric mass transfer coefficient [$K(L)a$] values were determined in a stirred-tank reactor. These results were used, along with a literature correlation, to estimate the mass transfer coefficient of the surfactant-stabilized shell surrounding the CLA. As a result, the range of $K(L)a$ values obtained using CLA was about an order of magnitude greater than that obtained using a conventional dispersion. The concentration of the aqueous-phase surfactant used to form the CLA strongly affected the mean diameter of the CLA; however, the concentration of the nonpolar-phase surfactant had little effect. These results suggest that CLAs have considerable potential for multiphase biocatalytic applications.

Predispersed solvent extraction (PDSE) of phenol. Wang et al. [82] reported the use of CLAs generated using kerosene as a solvent, tributyl phosphate as an extractant, sodium dodecylbenzene sulfhate as surfactant in the aqueous phase, and Tween-80 in the oil phase. The PDSE process is more suitable for extraction of dilute solutions. It

has also been discovered that according to the authors, the PDSE process has a great advantage over the traditional single-stage extraction process.

Preparation of TiO_2. Using stable CLAs, Shi et al. [74] investigated the extraction and phase behaviors of tri-octyl phosphinic oxide (TOPO [or tri-alkyl phosphinic oxide TRPO])–kerosene/H_2SO_4–Ti(IV) systems. They found that, under favorable hydrolysis conditions, a porous spherical TiO_2 was obtained after the hydrolysis of Ti(IV) in the inner organic phase loaded with Ti(IV).

Enzymic activities of polyion–protein and lipid–protein assemblies. Through layer-by-layer alternate adsorption, Ariga et al. [83] reported the preparation of nanosized enzyme reactors where the enzymes are sandwiched between molecular films of polyions or lipids. Two kinds of enzymes, lactate dehydrogenase (LDH) and alcohol dehydrogenase (ADH), were assembled with the polycation, poly(diallyldimethylammonium chloride—PDDA—an artificial cationic lipid). The assembling behavior was analyzed by a quartz crystal microbalance (QCM) with nanogram precision that revealed that the polyion, the lipid membrane, and the enzyme layers could be repeatedly and reproducibly assembled. The catalytic activity of the films obtained was spectrophotometrically examined. The activity of the LDH on a lipid-surface film was apparently greater than that of the LDH on a polyion-surface film. According to the authors, this difference might originate from the difference in the surface nature of the films. Michaelis–Menten analysis [16] suggested that the concentration increase in an anionic substrate in the vicinity of the cationic lipid surface led to the enhanced enzymic activity. The surface morphology of the film was investigated using atomic force microscopy (AFM). The lipid-surface film apparently has a rough surface, while a relatively smooth surface morphology was observed for the polyion-surface film. This difference in the surface morphology might affect the activity of the immobilized enzymes. Many functional molecules such as polyions, proteins, colloidal particles, dyes, and lipid membranes, can be assembled as thin films using the technique described by Ariga et al. [83].

III. EXPERIMENTAL METHODS IN EOR

Many methods have been used to characterize emulsified systems. The NMR technique [84] gives valuable insight into structures occurring in the continuous phase of the crude oil emulsion and how this association affects stability. It also can give the information on droplet sizes and size distributions as a nonintrusive method. Time-domain dielectric spectroscopy method [57] is very sensitive for monitoring flocculation processes in emulsions. When equipped with an external high-voltage unit, this method can be utilized to follow the coalescence in different emulsion systems as a very convenient technique for the on-line analysis of emulsions. The ultrasonic techniques [58] are used to determine the droplet sizes and the concentrations of both the dispersed and continuous phases. An obvious advantage of the technique is its applicability to optically opaque media.

The thin film formed between two approaching droplets is considered as a model emulsion system. The thinning of these films and their resistance to rupture is considered to be of great significance in understanding the behavior of emulsions. In our studies, we employed an electrical method to measure the film lifetime and thickness of model oils and crude oils. Through this, we probed the important roles that petroleum acids and asphaltenes play in the stability of crude oil emulsions.

1. Apparatus

The apparatus used in our study of thin liquid films is shown diagrammatically in Fig. 1 [16, 17, 85, 86]. There is a hole (0.5 mm in diameter) in the side of the Teflon chamber, which separates two aqueous solutions. The oil phase containing film-forming substances is introduced into the hole with the aid of a small syringe (ATP Inc., MI, USA). The film capacitance (C_m) and resistance (R_m) were measured by a Multi-Function Analyzer (Sino-Jinke Electronics Co. Ltd, Tianjin, China). The thickness of thin liquid films, according to the parallel-plate formula, is given by

$$d_m = 8.85\varepsilon A/C_m \tag{1}$$

where C_m is the film capacitance (in μF), A is the film area (in cm^2), ε is the relative dielectric constant, and d_m is the thickness of the film (in Å). In our study, the method of cyclic voltammetry is used [16, 17, 60, 85, 86]. The scan amplitude is 100 mV, the scan rate is 100 mV/s, the scan period is 8 s, and the input resistor is 10^9 ohm. The values of specific capacitance can be used to estimate the hydrocarbon thickness, t_m, of membranes using Eq. (1). The polar layers of the lipid bilayer can be represented as a large capacitor in series with a smaller one (the hydrophobic core of the membrane), and t_m is therefore equal to the thickness of the hydrocarbon layer of the BLM.

2. Materials

In our study the crude oil came from Shengli Oil Field (Shandong, China). The oil had an acid number of 2.98 mg KOH/g crude oil, a density of 0.9518 g/mL at 25°C, a weight percent of 32.5% for resin, and a weight percent of 4.2% for asphaltenes. In our experiments the crude oil and its fractions used were classified in following categories: (1) crude oil, (2) crude oil with asphaltenes removed (deasphaltenes oil), (3) crude oil with petroleum acids removed (deacids oil), and (4) crude oil with both asphaltenes and petroleum acids removed (deasphaltenes and deacids oil). They were treated as described by Shaw and Stapp [61].

The chemicals used in this study, such as sodium hydroxide, sodium chloride, n-decane and oleic acid, are all analytical reagents. The surfactant, petroleum sulfonates LH,

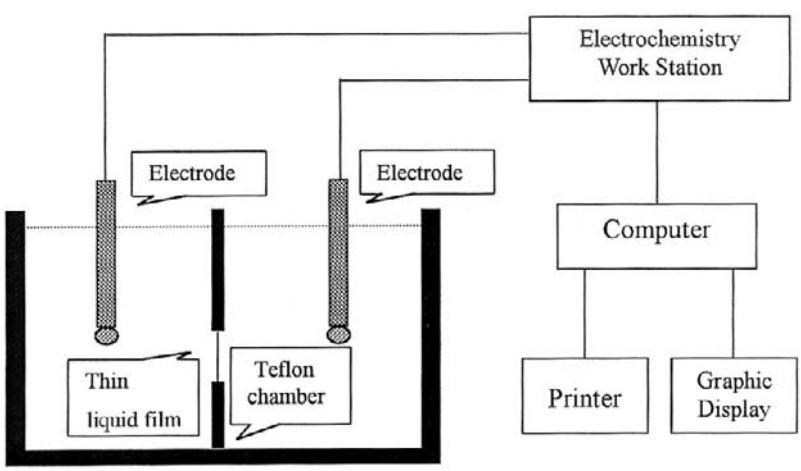

FIG. 1 Schematic diagram of the thin liquid film apparatus.

was obtained from Yumen Petroleum Chemical Plant as an 80 wt % active solution. Double-distilled water was used in the preparation of the aqueous solutions. All experiments were performed at $25 \pm 0.5^{\circ}C$.

A. Correlation Between Film Lifetime and Dynamic Interfacial Tension

During our study, the formation of thin liquid film is similar to that of a BLM [75]. When the oil is introduced into the hole, the thin liquid film (with a thickness of several hundred angstrom units) was soon formed after drainage by gravity. After this, the pressure gradient between the Plateau–Gibbs border and film area and the van der Waals' attractive interactions make the film thin, while the interfacial gradient (Marangoni–Gibbs effect), the steric interactions, the electrostatic interactions, and the formation of ordered long-range structures in the thin film keep it stable. When the oil phase consists of hydrocarbons, the liquid film will keep in stability because of the high interfacial gradient. When the surfactant molecules absorbed on to the oil–aqueous interface have the ability of greatly reducing interfacial tension, the film will thin to a certain smaller thickness or rupture.

Figures 2 and 3 show the effect of dynamic interfacial tension (IFT) on the film lifetimes of decane/petroleum sulfonate systems. We use the value of dynamic interfacial tension at a certain time (here it is 30 min, i.e., IFT_{30min}) and the time to obtain a certain value of dynamic interfacial tension (here it is 0.5 mN/m, i.e., $T_{0.5mN/m}$) to characterize the different interfacial behavior. The results show that the film lifetime decreases with

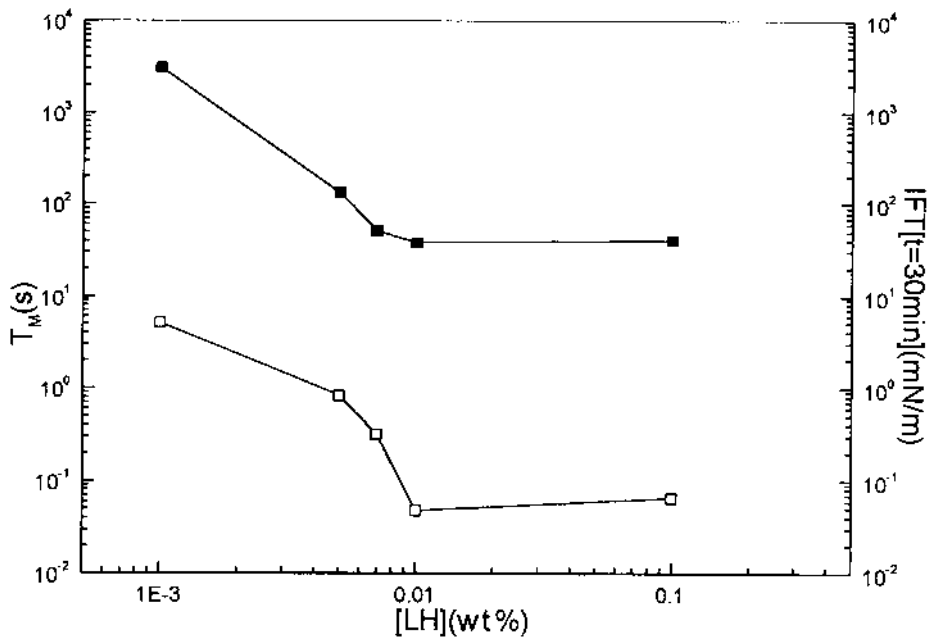

FIG. 2 Effect of LH (in aqueous phase) concentration on film lifetimes and transient values of dynamic IFTs. Oil phase; decane; aqueous phase: 1.0% NaCl + petroleum sulfonate. ■, Film lifetime; □, $IFT_{30\ min}$.

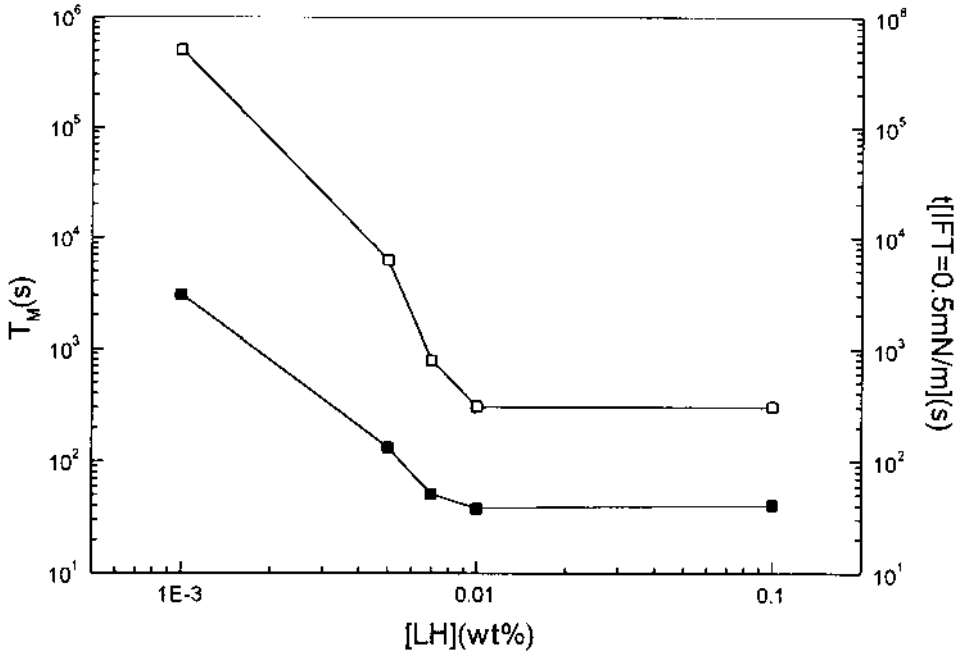

FIG. 3 Effect of LH (in aqueous phase) concentration on film lifetimes and times to obtain certain values of dynamic IFTs. Oil phase: decane; aqueous phase: 1.0% NaCl + petroleum sulfonate. ■, Film lifetimes; □, $T_{0.5\ mN/m}$.

increasing concentration of petroleum sulfonate. This tendency is very similar to the change in IFT_{30min} and $T_{0.5mN/m}$ with increasing concentration of petroleum sulfonate.

We repeated the experiments above when the petroleum sulfonate is soluble in decane. The results are shown in Figs 4 and 5. We can see that the film lifetime, the IFT_{2min}, and the $T_{0.05mN/m}$ have almost the same change with the increasing concentration of petroleum sulfonate in decane.

Figures 6 and 7 show the effect of NaCl concentration on the film lifetimes and dynamic interfacial tensions of decane/petroleum sulfonate systems. The results show that the lifetime decreases with increasing NaCl concentration. At the same time, the IFT_{80min} and $T_{0.5mN/m}$ also decrease with increasing of NaCl concentration.

The results from Figs 2 through 7 imply that there is a direct correlation between the film lifetime and dynamic interfacial tension in our experimental systems. The low interfacial tension obtained by adding petroleum sulfonate plays an important role in film thinning and rupture processes in w/o emulsions stabilized by the interfacial tension gradient.

B. Drainage–Rupture Character of the Thin Liquid Film in Crude Oil EOR Systems

Figure 8 shows the formation of a thin liquid film in a crude oil/alkali system. When the crude oil is contacted with an alkaline solution, the film capacitance increases and reaches a stable value after several minutes. This implies that the film has another thinning mechanism after the gravity drainage.

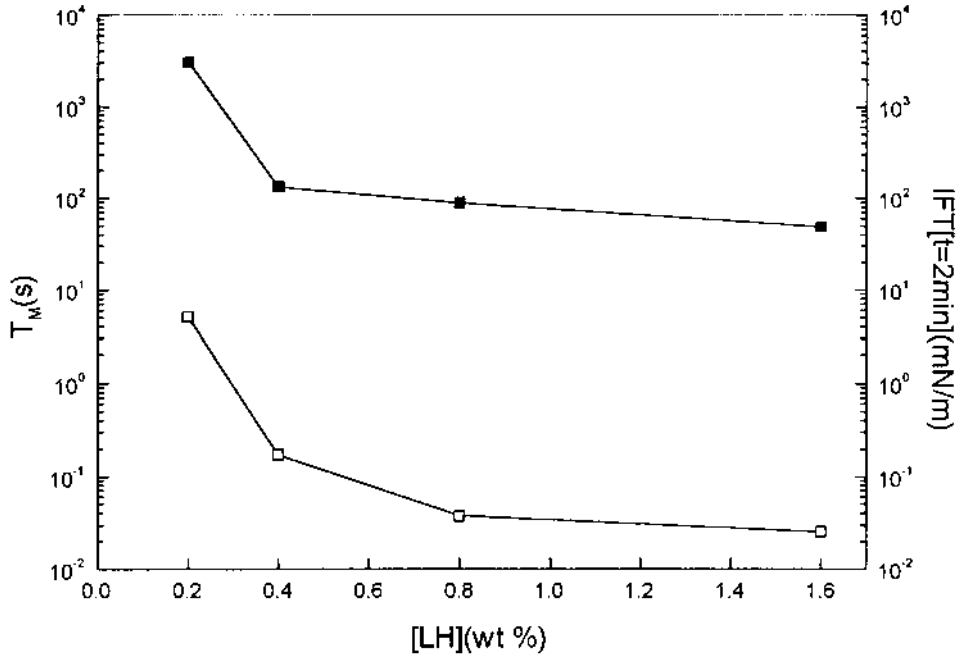

FIG. 4 Effect of LH (in oil phase) concentration on film lifetimes and transient values of dynamic IFTs. Aqueous phase: 1.0% NaCl; oil phase: petroleum sulfonate in decane. ■, Film lifetime; □, $IFT_{2\ min}$.

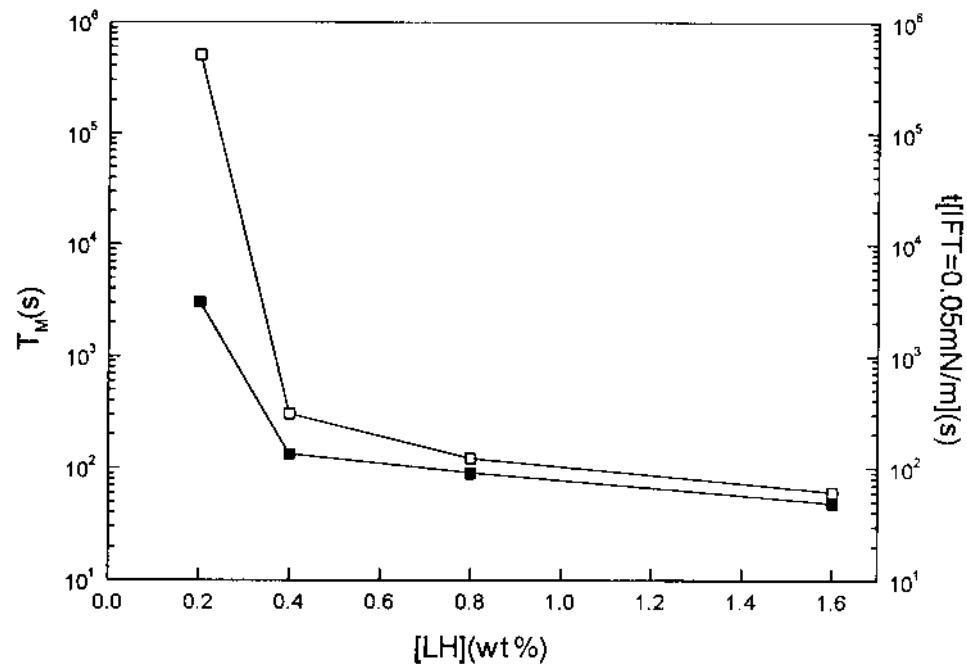

FIG. 5 Effect of LH (in oil phase) concentration on film lifetimes and times to obtain certain values of dynamic IFTs. Aqueous phase: 1.0% NaCl; oil phase: petroleum sulfonate in decane. ■, Film lifetime; □, $T_{0.05\ mN/m}$.

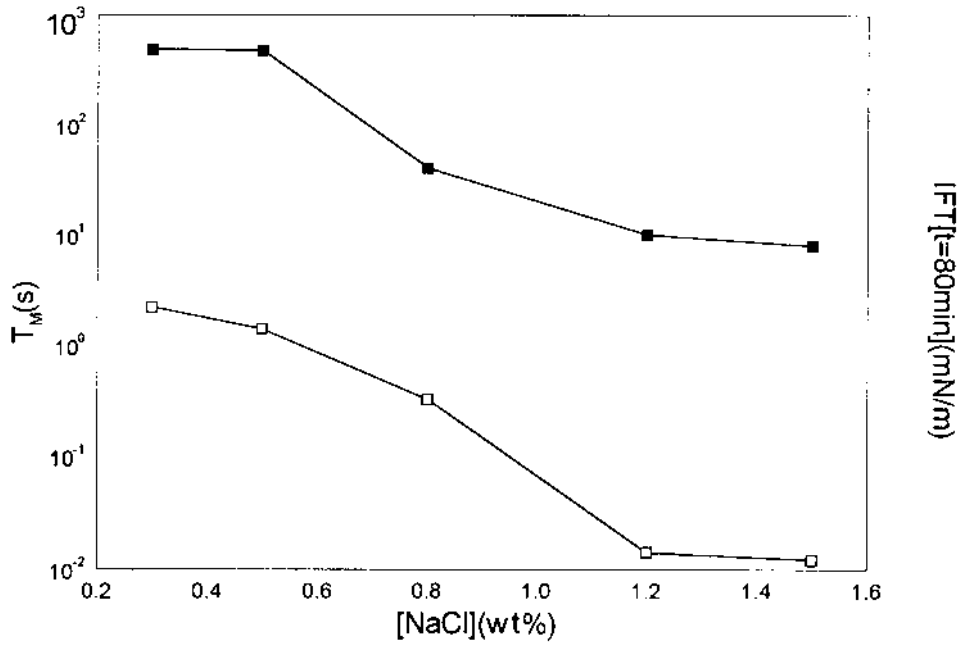

FIG. 6 Effect of NaCl concentration on film lifetimes and transient values of dynamic IFTs. Oil phase: decane; aqueous phase: NaCl + 0.005% petroleum sulfonate. ■, Film lifetime; □, $IFT_{80\ min}$.

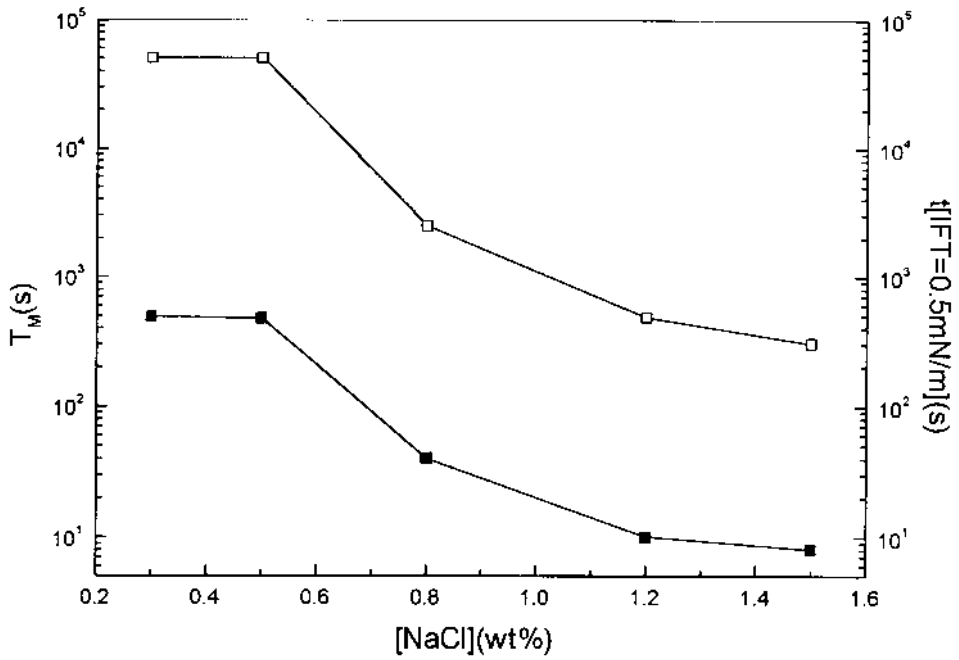

FIG. 7 Effect of NaCl concentration on film lifetimes and times to obtain certain values of dynamic IFTs. Oil phase: decane, aqueous phase: NaCl + petroleum sulfonate. ■, Film lifetime; □, $T_{0.5\ mN/m}$.

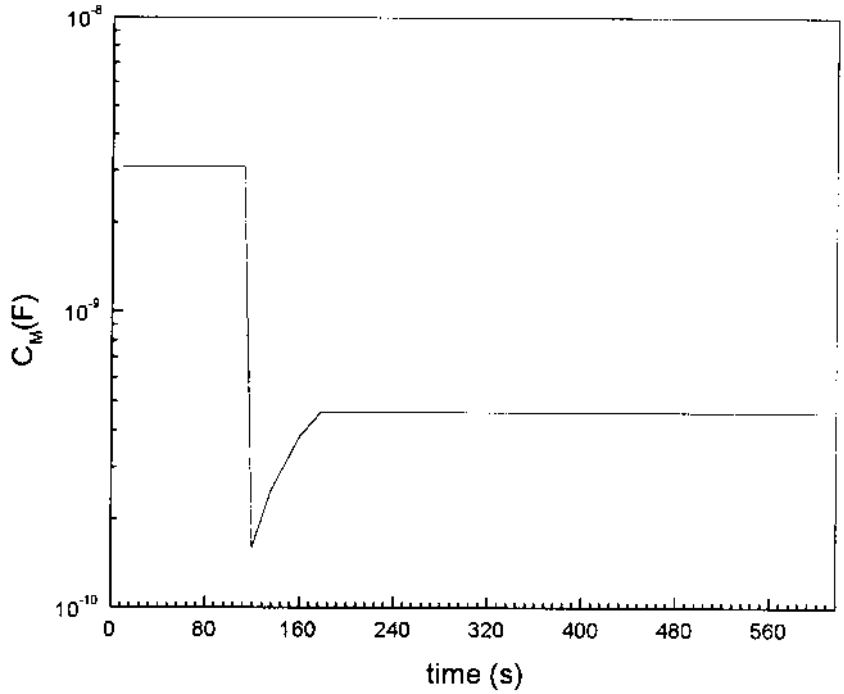

FIG. 8 Film capacitance of crude oil/alkali system as a function of time. Oil phase: 30% Shengli crude oil/*n*-C_{10}; aqueous phase: 0.25 mol/L NaOH.

There exist natural surface-active substances in crude oil, such as petroleum acids and asphaltenes. The ionized acids formed by the reaction between the petroleum acids and the alkali can decrease the interfacial tension [1,5–7] and accelerate the thinning and breakdown of the film. At the same time, the asphaltenes can adsorb on to the interface and improve the stability of the film. When the film thickness is small enough ($<$ 100 nm), it can keep this value for a long time because of the stabilization of the asphaltenes in the oil. In our study, almost all crude oil/alkali systems have this drainage process, and the crude oil/brine systems do not show it. So we can conclude that the drainage is correlated with the components, which have the interactions with alkaline solutions.

We have studied the mechanisms of rupture of a thin film in crude oil/EOR systems (with or without demulsifier). The results we obtained show that there are three kinds of mechanisms of film rupture. Figure 9 shows the first kind of mechanisms of film rupture in crude oil/EOR systems. The character of the mechanism is that the film keeps thinning to a critical film thickness and ruptures. The film ruptures in this kind of mechanism when the aqueous solution has surfactants that can greatly decrease the interfacial tension and the oil phase has no components that can improve the stability of the film, such as the asphaltenes.

Figure 10 shows the second kind of mechanism of film rupture in crude oil/EOR systems. The character of the mechanism is that the film keeps a certain film thickness for a period of time, then suddenly ruptures within 30 s. This may be explained in terms of the formation and quick development of local structural defects (''black hole'') [60,62].

Figure 11 shows the third kind of mechanism of film rupture in crude oil/EOR systems. The mechanism is characterized in that the film ruptures in ''steps.'' An explanation for this is the formation of ordered long-range structures in the film [16,18,85].

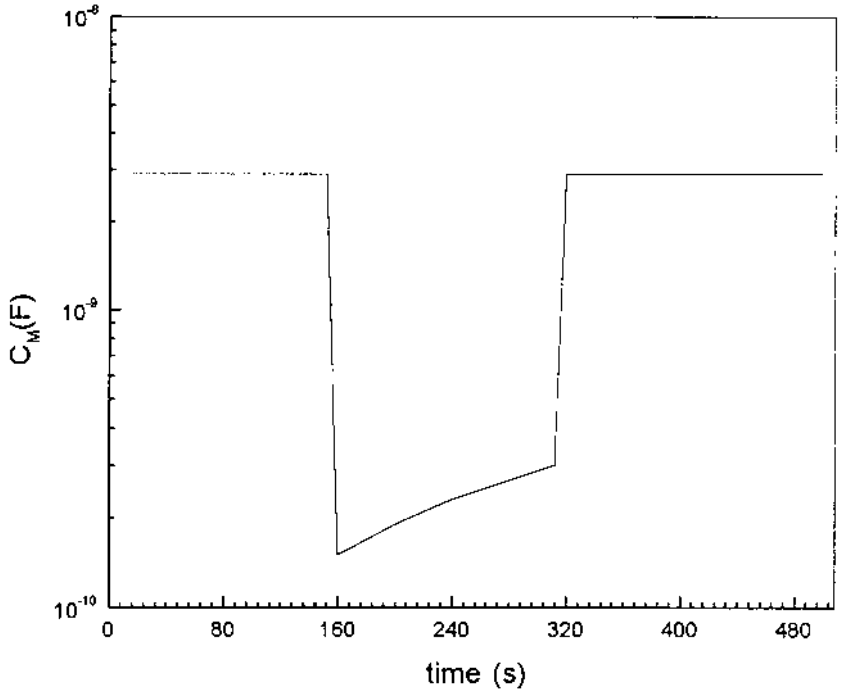

FIG. 9 Film capacitance of crude oil/EOR system as a function of time: the first kind of mechanism of film rupture. Oil phase: 30% Shengli deasphaltene oil/*n*-C_{10}; aqueous phase: 0.1 mol/L NaOH + 0.15 mol/L NaCl + 5 ppm demulsifier.

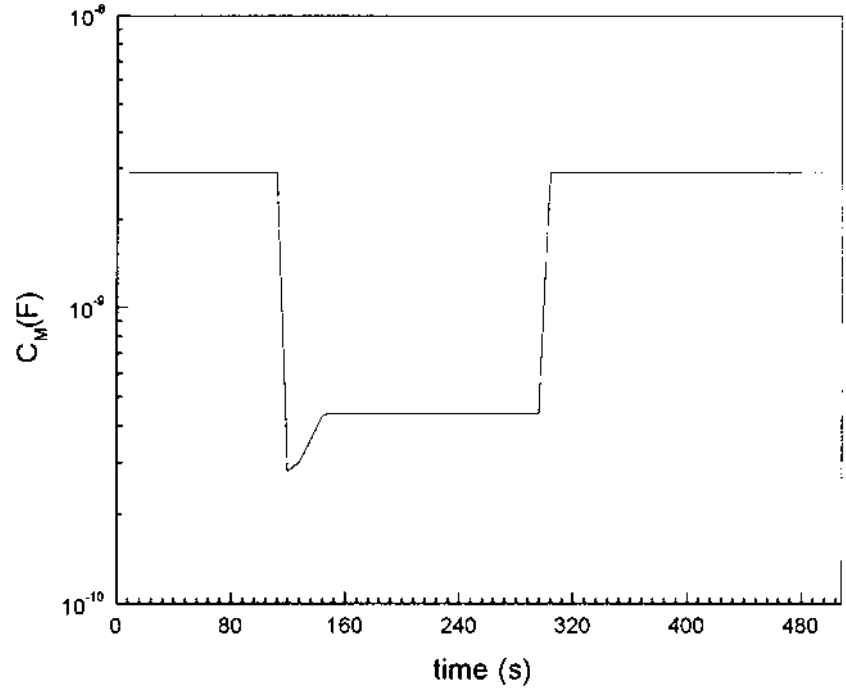

FIG. 10 Film capacitance of crude oil/EOR system as a function of time: the second kind of mechanism of film rupture. Oil phase: 30% Shengli deasphaltene and depetroleum acids oil/*n*-C_{10}; aqueous phase: 0.1 mol/L NaOH + 0.15 mol/L NaCl + 100 ppm demulsifier.

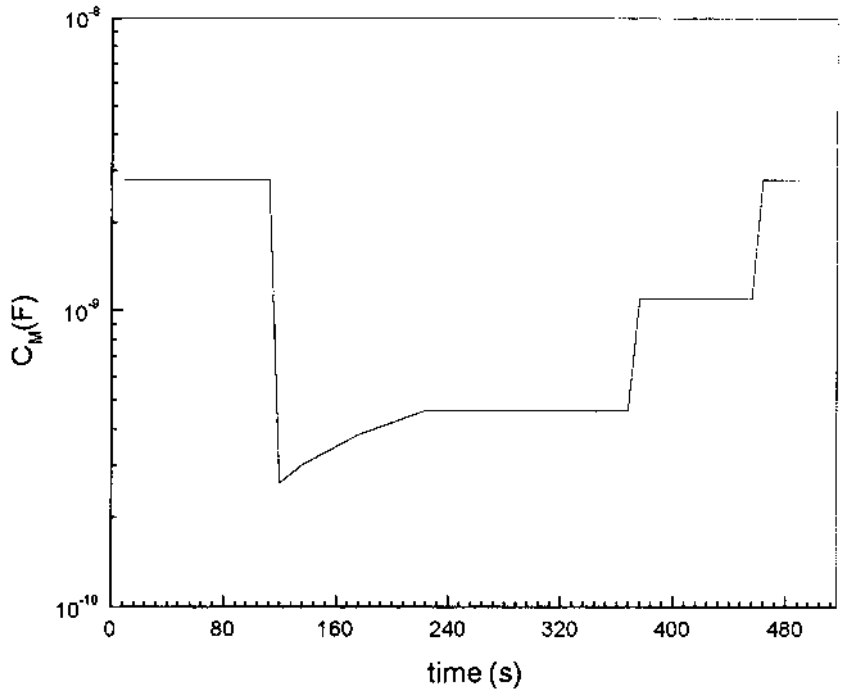

FIG. 11 Film capacitance of crude oil/EOR system as a function of time: the third kind of mechanisms of film rupture. Oil phase: 30% Shengli crude oil/*n*-C_{10}; aqueous phase: 0.0025 mol/L NaOH + 0.02% petroleum sulfonate (PS).

C. The Film Capacitance

We can see from Tables 1 and 2 that the alkali concentrations have no influence on the film capacitance of model oil systems. The sodium oleate formed by the reaction between the oleic acid and the alkali has a strong trend to partition into the aqueous solution, so it moves from the interface very quickly and has no effect on the interface. This may explain the results in Tables 1 and 2. The results in Table 3 show that the film capacitance of crude oil systems decreases with increasing alkali concentration below 0.06% NaOH.

TABLE 1 Effect of Alkali Concentration on Film Capacitance in Modeling Oil (7.5 mmol/L Oleic Acid)/Alkali Systems

Oil phase	Aqueous phase	C_M (10^{-10} F)
Oleic acid/*n*-decane	0.1% NaOH	1.4
Oleic acid/*n*-decane	0.2% NaOH	1.6
Oleic acid/*n*-decane	0.3% NaOH	1.2
Oleic acid/*n*-decane	0.4% NaOH	1.3
Oleic acid/*n*-decane	0.5% NaOH	1.4
Oleic acid/*n*-decane	1.0% NaOH	1.4
Oleic acid/*n*-decane	1.5% NaOH	1.3

TABLE 2 Effect of Alkali Concentration on Film Capacitance in Modeling Oil (15 mmol/L Oleic Acid)/Alkali Systems

Oil phase	Aqueous phase	$C_m/(10^{-10}\,F)$
Oleic acid/*n*-decane	0.1% NaOH	1.5
Oleic acid/*n*-decane	0.2% NaOH	1.4
Oleic acid/*n*-decane	0.3% NaOH	1.3
Oleic acid/*n*-decane	0.4% NaOH	1.3
Oleic acid/*n*-decane	0.5% NaOH	1.3
Oleic acid/*n*-decane	1.0% NaOH	1.3
Oleic acid/*n*-decane	1.5% NaOH	1.4

D. The Film Lifetime

1. The Effect of Physicochemical Conditions on Film Lifetime

We can see from Tables 4 and 5 that the physicochemical conditions have great influence on the film lifetimes in 30% Shengli crude oil/alkali systems. When the alkali concentration is low or the ionic strength is small, the film lifetimes are short. When the alkali concentration is high or the ionic strength is high, the film lifetimes are long.

2. Effect of Concentrations of Crude Oil on Lifetimes in Crude Oil/Alkali Systems

Table 6 shows that the concentrations of crude oil have great effect on the lifetimes in crude oil/alkali systems. The lifetime is very short at 5% crude oil/*n*-decane. Below or above this concentration, the lifetimes are long. We can explain these phenomena as follows: when the concentration of crude oil is below 5%, the interfacial tension is very high because of the low concentration of the petroleum acids, so the film lifetime is long. When the concentration of crude oil is above 5%, the concentration of asphaltenes is high enough to form a strong interfacial film and the film lifetime is also long. Only at 5% crude

TABLE 3 Effect of Alkali Concentration on Film Capacitance in 30% Shengli Crude Oil/Alkali Systems

Oil phase	Aqueous phase	$C_m\,(10^{-10}F)$
Shengli crude oil/*n*-decane	Distilled water	1.2
Shengli crude oil/*n*-decane	0.01% NaOH	1.8
Shengli crude oil/*n*-decane	0.06% NaOH	3.4
Shengli crude oil/*n*-decane	0.1% NaOH	3.6
Shengli crude oil/*n*-decane	0.2% NaOH	3.1
Shengli crude oil/*n*-decane	0.3% NaOH	3.8
Shengli crude oil/*n*-decane	0.4% NaOH	3.3
Shengli crude oil/*n*-decane	0.5% NaOH	3.3
Shengli crude oil/*n*-decane	1.0% NaOH	3.4
Shengli crude oil/*n*-decane	1.5% NaOH	3.3

TABLE 4 Effect of Alkali Concentration on Film Lifetimes in 30% Shengli Crude Oil/Alkali Systems

Oil phase	Aqueous phase ($[Na^+] = 0.25$ mol/L)	T_m (s)
Shengli crude oil/*n*-decane	0.0001 mol/L NaOH	190
Shengli crude oil/*n*-decane	0.0005 mol/L NaOH	299
Shengli crude oil/*n*-decane	0.001 mol/L NaOH	> 1000
Shengli crude oil/*n*-decane	0.005 mol/L NaOH	> 1000
Shengli crude oil/*n*-decane	0.01 mol/L NaOH	> 1000
Shengli crude oil/*n*-decane	0.05 mol/L NaOH	> 1000
Shengli crude oil/*n*-decane	0.1mol/L NaOH	> 1000

TABLE 5 Effect of Ionic Strength on Film Lifetimes in 30% Shengli Crude Oil/Alkali Systems

Oil phase	Aqueous phase ([NaOH] = 0.005 mol/L)	T_m (*s*)
Shengli crude oil/*n*-decane	$[Na^+] = 0.005$ mol/L	< 10
Shengli crude oil/*n*-decane	$[Na^+] = 0.01$ mol/L	> 1000
Shengli crude oil/*n*-decane	$[Na^+] = 0.05$ mol/L	> 1000
Shengli crude oil/*n*-decane	$[Na^+] = 0.1$ mol/L	> 1000
Shengli crude oil/*n*-decane	$[Na^+] = 0.25$ mol/L	> 1000

TABLE 6 Effect of Concentrations of Crude Oil on Film Lifetimes in Crude Oil/Alkali Systems

Oil phase	Aqueous phase	T_m (s)
n-decane	0.075 mol/L NaOH	> 1000
1% Shengli crude oil/*n*-decane	0.075 mol/L NaOH	> 1000
5% Shengli crude oil/*n*-decane	0.075 mol/L NaOH	98
10% Shengli crude oil/*n*-decane	0.075 mol/L NaOH	> 1000
20% Shengli crude oil/*n*-decane	0.075 mol/L NaOH	> 1000
Shengli crude oil/*n*-decane	0.075 mol/L NaOH	> 1000
40% Shengli crude oil/*n*-decane	0.075 mol/L NaOH	> 1000
50% Shengli crude oil/*n*-decane	0.075 mol/L NaOH	> 1000
60% Shengli crude oil/*n*-decane	0.075 mol/L NaOH	> 1000
70% Shengli crude oil/*n*-decane	0.075 mol/L NaOH	> 1000

oil, the concentration of the petroleum acids is high enough to decrease the interfacial tension, but the asphaltenes cannot form a stable interfacial film because of their low concentration. From the results in Section III.E, we can see that the film lifetime in crude oil/alkali systems is shorter than that in deacids and deasphaltenes oil/alkali systems. This may also imply that the petroleum acids have a stronger influence than the asphaltenes on the film strength in this kind of crude oil in our study.

3. Effect of Added Surfactant on Film Lifetimes in Crude Oil/Alkali Systems

The results in Table 7 show that the film lifetimes become shorter with increasing concentration of petroleum sulfonate (LH). The role LH plays in this case is similar to that of petroleum acids.

E. Effect of Surface-Active Components on Film Lifetimes in Crude Oil/EOR Systems

The results in Table 8 show that the film lifetime in deasphaltene oil systems is shorter than that in crude oil systems at low concentration of surfactants. When the concentration of surfactant increases, the film lifetimes of the two kinds of oil become close. The results in Figs 12 and 13 show that the film lifetimes of different oils are very different for the same alkaline–demulsifier system.

IV. SUMMARY AND CONCLUSIONS

In this chapter, we report the influence of surface-active compounds on the stability of crude oil emulsions using the apparatus designed for bilayer lipid membrane studies. The electrical method we employed to measure the film lifetime and thickness of model oils and crude oils seems to be a convenient technique for monitoring the coalescence processes in emulsions. The results obtained show that the natural surface-active substances in crude oil, such as petroleum acids and asphaltenes, have a great effect on the film strength. The ionized acids formed by the reaction between the petroleum acids and the alkali can decrease the interfacial tension and accelerate the thinning and breakdown of the thin liquid film. The asphaltenes can adsorb on to the interface and improve the stability of the film. The order of stability of the films between different oils and alkaline solutions is as follows: crude oil with asphaltenes removed < crude oil < crude oil with both asphaltenes and petroleum-acids removed (iv) < crude oil with petroleum acids removed. In addition,

TABLE 7 Effect of Petroleum Sulfonate (LH) on Film Lifetimes in 30% Crude Oil/Alkali Systems

Oil phase	Aqueous phase	$T_m(s)$
Shengli crude oil/*n*-decane	0.05 mol/L NaOH	> 1000
Shengli crude oil/*n*-decane	0.05 mol/L NaOH + 0.005% LH	> 1000
Shengli crude oil/*n*-decane	0.05 mol/L NaOH + 0.01% LH	> 1000
Shengli crude oil/*n*-decane	0.05 mol/L NaOH + 0.05% LH	218
Shengli crude oil/*n*-decane	0.05 mol/L NaOH + 0.1% LH	131

TABLE 8 Effect of Asphaltenes on Film Lifetimes in Crude Oil/EOR Systems

Oil phase	Aqueous phase	T_m (*s*)
30% Shengli crude oil/*n*-decane	0.05 mol/L NaOH + 0.01% LH	> 1000
30% Deasphaltenes oil/*n*-decane	0.05 mol/L NaOH + 0.01% LH	178
30% Shengli crude oil/*n*-decane	0.05 mol/L NaOH + 0.1% LH	131
30% Deasphaltenes oil/*n*-decane	0.05 mol/L NaOH + 0.1% LH	112

we have observed three kinds of mechanism of film rupture and found stratification phenomena in crude oil/EOR systems.

Additionally, we have reviewed the current research on colloidal dispersions in terms of two thin-film systems generated from surfactant solutions. The aqueous phase surfactant forms a bilayer that encapsulates and stabilizes the solvent droplets. These novel gas–liquid and liquid–liquid macroemulsions appear to have high potential in technology and in interfacial catalysis.

ACKNOWLEDGMENT

Financial support by the National Key Basic Research Development Program "Fundamental Studies of the Extensively Enhanced Petroleum Recovery" (Project Grant number G19990225) is gratefully acknowledged.

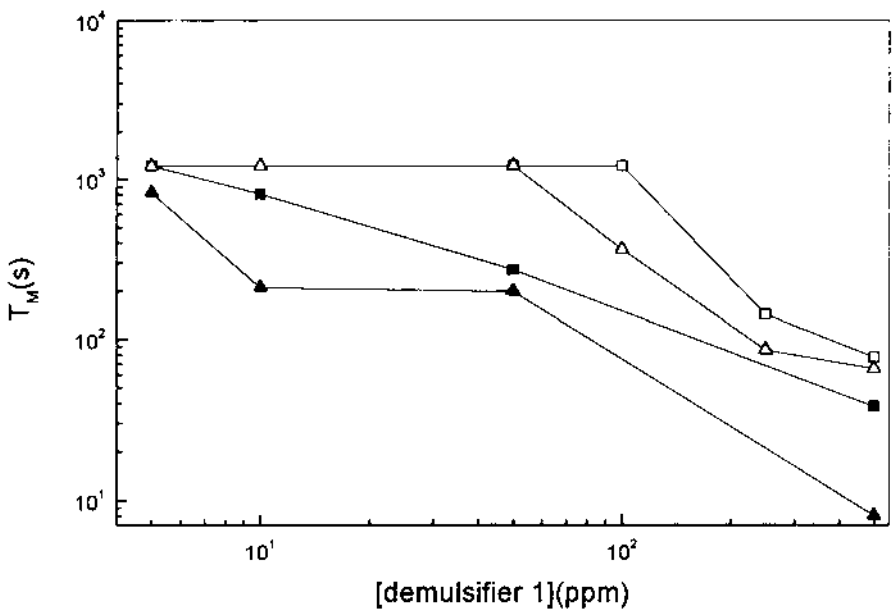

FIG. 12 Effect of surface-active components on the film lifetimes in crude oil/EOR systems. Aqueous phase: 0.1 mol/L NaOH + 0.1 mol/L NaCl + demulsifier 1. Oil phase: ■, Shengli crude oil; □, deacids oil; ▲, deasphaltenes oil; △, deashaltenes and deacids oil.

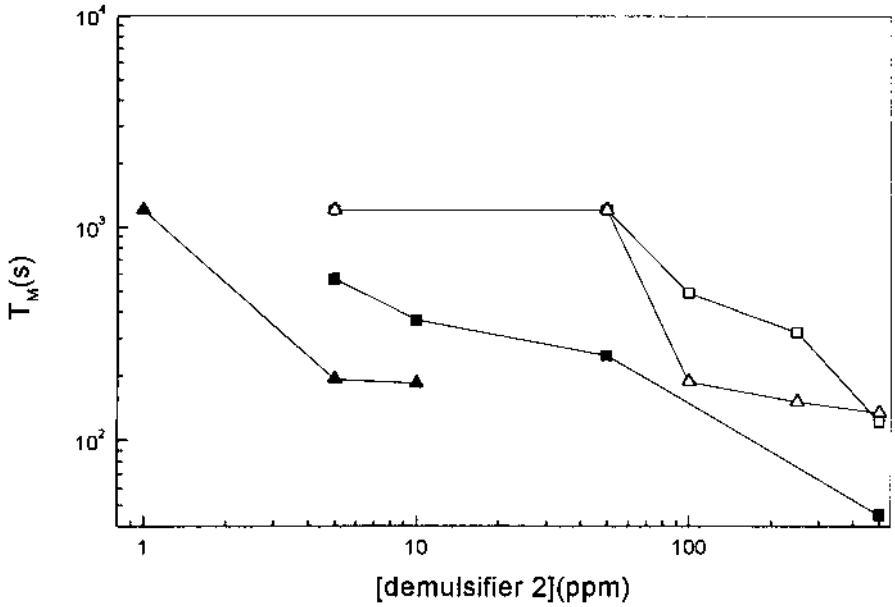

FIG. 13 Effect of surface-active components on the film lifetimes in crude oil/EOR systems. Aqueous phase: 0.1 mol/L NaOH + 0.1 mol/L NaCl + demulsifier 2. Oil phase; ■, Shengli crude oil; □, deacids iol; ▲, deasphaltenes oil; △, deasphaltenes and deacids oil.

REFERENCES

1. LL Schramm, ed. Emulsions: Fundamentals and Applications in the Petroleum Industry. Advances in Chemistry Series 231. Washington, DC: American Chemical Society, 1992.
2. F Sebba. Sep Purif Meth 14: 127–148, 1985.
3. DP Rimmer, AA Gregoli, JA Hamshar, E Yildirim. In: LL Schramm, ed. Emulsions: Fundamentals and Applications in the Petroleum Industry. Advances in Chemistry Series 231. Washington, DC: American Chemical Society, 1992, pp 295–317.
4. LL Schramm, SM Kutay. In: LL Schramm, ed. Surfactants: Fundamentals and Applications in the Petroleum Industry. Cambridge, New York: Cambridge University Press, 2000, pp 79–97.
5. DT Wasan, SM Shah, M Chan, K Sampath, R Shah., In: RL Berg, ed. Chemistry of Oil Recovery. ACS Symposium Series 91, Washington, DC: American Chemical Society, 1979, pp 115–146.
6. D Exerowa, PM Kruglyakov. Foam and Foam Films. Amsterdam: Elsevier, 1998, pp 1–796; CE Johnson. J Petrol Technol 1976: 85–106.
7. TP Castor, RS Somerton, JF Kelly. In: DO Shah, ed. Surface Phenomena in Enhanced Oil Recovery. New York: Plenum Press, 1981, pp 249–262.
8. G Leopold. In: LL Schramm, ed. Emulsions: Fundamentals and Applications in the Petroleum Industry. Advances in Chemistry Series 231, Washington, DC: American Chemical Society, 1992, pp 341–366.
9. KJ Lissant. In: DO Shah, RS Schechter, eds. Improved Oil Recovery by Surfactant and Polymer Flooding. New York: Academic Press, 1977, pp 93–113.
10. KG Nordli, J Sjöblom, J Kizing, P Stenius. Colloids Surfaces 57:83–89, 1991.
11. J Sjöblom, MY Li, AA Christ, T Gu., Colloids Surfaces 66:55–61, 1992.
12. FS Manning, RE Thompson. Oilfield Processing. vol. 2: Crude Oil. Tulsa, OK: Pennwell, 1995, pp 149–200.

13. SE Friberg. In: J Sjöblom, ed. Emulsions: A Fundamental and Practical Approach. NATO ASI Series C: 363. Dordrecht: Kluwer Academic, 1992, pp 1–36.
14. IB Ivanov, ed. Thin Liquid Film. New York: Marcel Dekker, 1988, pp 379–409.
15. DT Wasan. In: KL Mittal, P Kumar, eds. Emulsions, Foams, and Thin Films. New York: Marcel Dekker, 2000, pp 1–37.
16. HT Tien, AL Ottova. Membrane Biophysics: As Viewed from Experimental Bilayer Lipid Membranes (Planar Lipid Bilayers and Spherical Liposomes). Amsterdam, New York: Elsevier, 2000, pp 1–648.
17. HT Tien. Bilayer Lipid Membranes: Theory and Practice. New York: Marcel Dekker, 1974.
18. PJ Breen, DT Wasan, YH Kim, AD Nikolov, CS Shetty. In: J Sjöblom, ed. Emulsions and Emulsion Stability. Surfactant Science Series 61. New York: Marcel Dekker, 1996, pp 237–258.
19. JD McLean, PM Spiecker, AP Sullivan, PK Kilpatrick. In: OC Mullins, EY Sheu, eds. Structures and Dynamics of Asphaltenes. New York: Plenum Press, 1998, pp 377–398.
20. M Kerker. In: M Kerker, ed. Surface Chemistry and Colloids. vol. 7, MTP International Review of Science, London: Butterworth, 1972, ch. 1 and 2.
21. AW Adamson. The Physical Chemistry of Surfaces. 2nd ed. New York: John Wiley, 1967.
22. AK Malhotra, DT Wasan. In: IB Ivanov, ed. Thin Liquid Film. New York: Marcel Dekker, 1988, pp 829–846.
23. TJ Jones, EL Neustadter, KP Whittingham. J Can Petrol Tech 17:100–132, 1978.
24. ASC Lawrence, W Killner. J Inst Petrol 34: 821–862, 1948.
25. F Sebba. J Colloid Interface Sci 35: 643–684, 1971.
26. L Ting, DT Wasan, K Miyano, SQ Xu. J Colloid Interface Sci 102:248–266, 1984.
27. K Miyano. Jpn J Appl Phys 24:1379–1388, 1985.
28. SG Davison. In: SG Davison, ed. Progress in Surface Science. vols 4, 8, 19, 23, 30, 41, 47, 49. New York: Pergamon Press, 1973, 1985, 1986, 1989, 1992, 1994, 1995,.
29. R Nagarajan, SL Chung, DT Wasan. J Colloid Interface Sci 204:53–73, 1998.
30. RL Kao, DA Edwards, DT Wasan, E Chen. J Colloid Interface Sci 48:247–257, 1992.
31. DT Wasan, V Mohan. In: DO Shah, RS Schechter, eds. Improved Oil Recovery by Surfactant and Polymer Flooding. New York: Academic Press, 1977, pp 161–185.
32. Z Zapryaanov, AK Malhotra, N Aderangi, DT Wasan. Int J Multiphase Flow 9:105–119, 1983.
33. S Hartland, SAK Jeelani. Colloids Surfaces A 88:289–302, 1994.
34. YH Kim, DT Wasan, PJ Breen. Colloids Surfaces A 95:235–249, 1995.
35. T Hirato, K Koyama, T Tanaka, Y Awakura, H Majima. Materi Trans 52:257–272, 1991.
36. KL Mittal, DO Shah. In: KL Mittal, DO Shah, eds. Surfactants in Solution. vols. 8, 11. New York: Plenum Press, 1986, 1991.
37. D Tambe, J Paulis, MM Sharma. J Colloid Interface Sci 171:463–486, 1995.
38. A Bhardwaj, S Hartland. Ind Eng Chem Res 33:1271–1289, 1994.
39. JM Soos, K Koczo, DT Wasan. Rev Sci Instrum 65:3555–3576, 1994.
40. YH Kim, K Koczo, DT Wasan. J Colloid Interface Sci 187:29–38, 1997.
41. AD Nikolov, DT Wasan. Colloids Surfaces A 375:123–124, 1997.
42. YH Kim, AD Nikolov, DT Wasan, H Diaz-Arauzo, CS Shetty. J Disp Sci Technol 17:33–48, 1996.
43. AK Malhotra, DT Wasan. Chem Eng Commun 48:35–56, 1986.
44. J Lyklema, KJ Mysels. J Am Chem Soc 87:2539–2557, 1965.
45. F Sebba. Sepn Purif Meth 14:127–148, 1985.
46. K Koczo, AD Nikolov, DT Wasan, RP Borwankar, A Gonsalves. J Colloid Interface Sci 178:694 -719, 1996.
47. W Xu, AD Nikolov, DT Wasan. AIChE J 43:3215–3222, 1997.
48. DT Wasan, AD Nikolov, XL Chu. In: DO Shah, ed. Micelles, Microemulsions and Monolayers: Science and Technology. New York: Marcel Dekker, 1998, pp 127–148.
49. XL Chu, AD Nikolov, DT Wasan. J Chem Phys 103:6653–6674, 1995.
50. S Friberg, C Solans. Langmuir 2:121–128, 1986.

51. EL Mackor, JH van der Waals. J Colloid Science 7:535–550, 1952.
52. TF Tadros. In: IB Ivanov, ed. Thin Liquid Film. New York: Marcel Dekker, 1988, pp 331–358.
53. DM Andrews, ED Manev, DA Haydon. Spec Disc Faraday Soc 1:46–52, 1970.
54. H Sonntag, B Unterberger, Z Zinontowsky. Colloid Polym Sci 257:286–290, 1979.
55. RA Mohammed, AI Bailey, PF Luckham, SE Taylor. Colloids Surfaces A 91:129–134, 1994.
56. JD McLean, PK Kilpatrick. J Colloid Interface Sci 196:23–29, 1997.
57. J Sjöblom, H Førdedal, T Skodvin. In: J Sjöblom, ed. Emulsions and Emulsion Stability. Surfactant Science Series 61. New York: Marcel Dekker, 1996, pp 393–436.
58. KE Froysa, O Nesse. In: J Sjöblom, ed. Emulsions and Emulsion Stability. Surfactant Science Series 61. New York: Marcel Dekker, 1996, pp 437–447.
59. CM Blair. Chem Ind 5:538–547, 1960.
60. HT Tien, AL Ottova. J Membr Sci 189:83–117, 2001.
61. JE Shaw, PR Stapp. US Patent 4494604, 1985; JE Shaw, PR Stapp, J Colloid Interface Sci 107:231–236, 1985.
62. YA Chizmadzhev, VF Pastushenko. In: IB Ivanov, ed. Thin Liquid Film. New York: Marcel Dekker, 1988, pp 1059–1079.
63. TF Yen. In: JW Bunger, NC Li, eds. Advances in Chemistry Series 195. Chemistry of Asphaltenes, Washington, DC: American Chemical Society, 1979, pp 39–52.
64. DA Storm, EY Sheu. In: TF Yen, GV Chilingarian, eds. Developments in Petroleum Science. vol. 40. Amsterdam, New York: Elsevier, 1994, Vol. 40, pp 245–254.
65. S Puskas, J Balazs, A Farkas, I Regdon, O Berkesi, I Dekany. Colloids Surfaces A Physicochem Eng Aspects 113:279–293, 1996.
66. YH Kim. J Ind Eng Chem 5:22–31, 1999.
67. P Srivastava, O Hahr, R Buchholz, RM Worden. Biotechnol Bioeng 70:525–532, 2000.
68. CG Dodd. J Phys Chem 64:544–550, 1960.
69. JE Strassner. J Petrol Tech 20:303–312, 1968.
70. YD Wang, HZ Wen, YY Huang, YY Dai. J Chem Eng Jpn 34:1127–1130, 2001.
71. K Matsushita, AH Mollah, DC Stuckey, C Delcerro, AI Bailey. Colloids Surfaces 69:65–72, 1992.
72. P Jauregi, GR Mitchell, J Varley, AICHE J 46:24–36, 2000.
73. SB Lamb, DC Lamb, SL Kelly, DC Stuckey. FEBS Lett 431:343–346, 1998.
74. JH Shi, GH Gu, X Fu, MY Wang, ZS Hu. Colloids Surfaces A: Physicochem Eng Aspects 194:207–212, 2001.
75. D Roy, S Kongara, KT Valsaraj. J Hazard Mater 42:247–263, 1995.
76. SV Save, VG Pangarkar. Chem Eng Commun 127:35–54, 1994.
77. D Roy, RR Kommalapati, KT Valsaraj, WD Constant. Water Res 29:589–595, 1995.
78. EPS Cheah, DD Reible, KT Valsaraj, WD Constant, BW Walsh, LJ Thibodeaux. J Hazard Mater 59:107–122, 1998.
79. AE Riviello, D Young, F Sebba, Powder Technol 78:19–24, 1994.
80. R Mosler, TA Hatton. Curr Opin Colloid Interface Sci 1:540–547, 1996.
81. GJ Lye, DC Stuckey. Colloid Surfaces A 131:119–136, 1998.
82. YD Wang, M Chen, LL Xu, YY Dai. Chinese J Chem Eng 8:103–107, 2000.
83. K Ariga, Y Sasaki, H Horiguchi, N Horiuchi, J Kikuchi. Defect and Diffus Forum 191:35–59, 2001.
84. O Söderman, B Balinov. In: J Sjöblom, ed. Emulsions and Emulsion Stability. Surfactant Science Series 61, New York: Marcel Dekker, 1996, pp 369–385.
85. A Ottova-Leitmannova, HT Tien. Progr Surface Sci 41:337–445, 1992.
86. HT Tien, AL Ottova. Colloids Surfaces A: Physicochem Eng Aspects 149:217–233, 1999.

8
Phase Transfer Catalysis

MIECZYSŁAW MĄKOSZA Institute of Organic Chemistry, Polish Academy of Sciences, Warsaw, Poland

MICHAŁ FEDORYŃSKI Faculty of Chemistry, Warsaw University of Technology, Warsaw, Poland

I. INTRODUCTION

For a reaction to proceed it is necessary that the reacting species: molecules, ions, etc., can enter intimate contact. It is, therefore, a natural tendency to carry out chemical reactions in homogeneous media—in solvents able to dissolve, at least partially, the reacting partners.

In many cases, formation of homogeneous media for a reaction encounters serious difficulties, particularly when ionic reactants are to react with nonpolar organic compounds. For such and many other cases, phase transfer catalysis (PTC) offers a simple and efficient solution to these problems.

PTC is a general methodology applicable to a great variety of reactions in which inorganic and organic anions and also carbenes and other active species react with organic compounds. Contrary to the common tendency to carry out chemical reactions in homogeneous media, according to the PTC concept reactions are performed in heterogeneous two phase systems—one phase being a reservoir of reacting anions or base for generation of organic anions, whereas organic reactants and catalysts—source of lipophilic cations—are located in the second, organic phase. The reacting anions are continuously introduced into the organic phase in the form of lipophilic ion pairs with lipophilic cations supplied by the catalyst. Most often tetra-alkylammonium (TAA) cations serve this purpose.

A two-phase system in which PTC operates offers numerous advantages over traditional methodologies, which use homogeneous media, and finds extremely wide application in laboratory organic synthesis and industrial processes. Detailed descriptions of the concept, mechanistic features, and wide field of application can be found in numerous monographs [1–6] and review papers [7,8].

PTC originated from the observation reported by Jarrousse in 1951 that phenylacetonitrile can be efficiently alkylated with ethyl chloride in the presence of 50% aqueous NaOH and $\simeq 20\%$ molar of benzyltriethylammonium chloride [9]. In this short note it was also stated that the reaction is less efficient with ethyl bromide and does not proceed with ethyl iodide.

On the basis of this observation, which in that time contradicted the common knowledge and rules of organic chemistry, in 1960 we elaborated an efficient and highly economic industrial process for manufacturing 2-phenylbutyronitrile [10] and subsequently developed a general method for catalytic generation and reactions of carbanions [11] and

dichlorocarbene 12], using aqueous NaOH and TAA salts in a two phase system (1965–1969). Subsequently, reactions of inorganic anions (CN^-, MnO_4^-, etc.) catalyzed by lipophilic TAA salts in two-phase systems were reported by Starks, who coined the term phase transfer catalysis [13].

II. BASIC PRINCIPLES OF PHASE TRANSFER CATALYSIS

The basic principle of PTC, the methodology of which differs from commonly used techniques of organic synthesis, is that the reactions are performed in heterogeneous two-phase systems in which there is a negligible mutual solubility of the phases. In such systems the catalyst, a source of lipophilic cations, located in the organic phase, introduces continuously the reacting anionic species in the form of lipophilic ion pairs into the organic phase. Reactions for which PTC methodology is applicable can be divided into two major groups:

1. Reacting anions are available in the form of sodium or potassium salts, for instance, NaCN, KN_3, $KMnO_4$, CH_3COONa, etc., so the lipophilic cations of the catalyst simply transfer these anions into the organic phase in the form of lipophilic ion pairs, produced via continuous ion exchange.
2. Reacting anions shall be generated in situ from the corresponding precursors: e.g., CH, OH, NH, and SH acids under the action of a base located in the inorganic phase. Here, the catalyst participates in the formation and transport of the reacting anions into the organic phase.

Numerous important industrial processes of organic synthesis are carried out in heterogeneous systems, mostly gas–solid or liquid–solid. In general, such processes proceed via adsorption of reacting molecules on the solid surface, chemical transformations in the adsorbed state, and release (desorption) of the products from the surface to the bulk of the gas or liquid phase.

PTC operates in a different way: organic reactants, neat or in organic solvents, are located in liquid organic phase whereas inorganic salts or base—as aqueous solutions or in solid state—form the inorganic phase. The catalyst is dissolved in the organic phase and introduces continuously the reacting species into the organic phase. Thus, in fact phase transfer (PT)-catalyzed reactions, although carried out in heterogeneous systems, proceed to a substantial extent in homogeneous solutions. PT-catalyzed reactions are executed in systems comprising two mutually immiscible phases. Two types of such system are used: liquid–liquid and liquid–solid. In the liquid–liquid systems the organic reactants, neat or in an organic solvent, form an organic phase that is in contact with a mutually immiscible aqueous solution of salts containing the desired anions or with an aqueous solution of a base, most often a concentrated aqueous solution of sodium or potassium hydroxide. The catalyst transfers the inorganic anions from the aqueous solution, or organic anions generated via deprotonation of the appropriate precursors, into the organic phase. In the liquid–solid systems, solid, powdered inorganic salts or base (K_2CO_3, NaOH, etc.) are suspended in the organic phase, and the catalyst transfers the inorganic anions from the surface of the solid salts, or the organic anions generated on the surface of the solid base, into the organic phase.

Besides the mentioned earlier TAA salts typically used as PT catalysts—source of lipophilic cations—other lipophilic, stable organic cations such as trialkylsulfonium, tetraalkylphosphonium, or arsonium, etc., can also function as PT catalysts. Another category of PT catalysts consists of neutral organic molecules able to form relatively stable

complexes or solvates with, e.g. Na^+ or K^+ cations, thus producing lipophilic cationic species able to introduce anions into nonpolar organic phase. Typically, crown ethers and cryptands are used for this purpose [14] (see the representative structures in Figs 1a and 1b, respectively), but ethers of polyethylene glycols (Fig. 1c) or even some solvents: HMPT, DMSO, or DMF, can behave similarly.

The most important feature of PT-catalyzed reactions is that the concentration of the reacting anions in the organic phase cannot exceed the concentration of the catalyst—usually 1% molar of the educts. For this reason most of the PT-catalyzed reactions can be carried out without any organic solvent, provided that the organic starting materials are liquids, which hence can serve as solvents for the reacting species. The reacting anions in the organic phase are not in the form of the commonly used Li^+, Na^+, or K^+ but as TAA salts, in which partial covalent bonding and co-ordination between anions and cations are negligible. As a consequence these anions are in a very active form; hence, rate constants of the reactions are usually high, and, in spite of the relatively low concentration of the reacting species, the overall rates of PT-catalyzed processes are satisfactory, particularly because the low concentration of the reacting anions is compensated by the high concentration of the second reactant, especially when used neat. The effectiveness of the PT-catalyzed reactions is a function of activity of the reacting species and also their concentration in the organic phase. Assuming that all the catalyst, a TAA salt, is located in the organic phase, the concentration of the reacting species can be only a fraction of that of the catalyst. This fraction, when inorganic anions are reacting species, is determined by ion-exchange equilibrium (1a) which, for the case of nucleophilic substitution in haloalkanes, being a typical example of the reactions of the first group, is an integral part of the overall process presented in Eq. (1), where Q^+ denotes a lipophilic TAA cation.

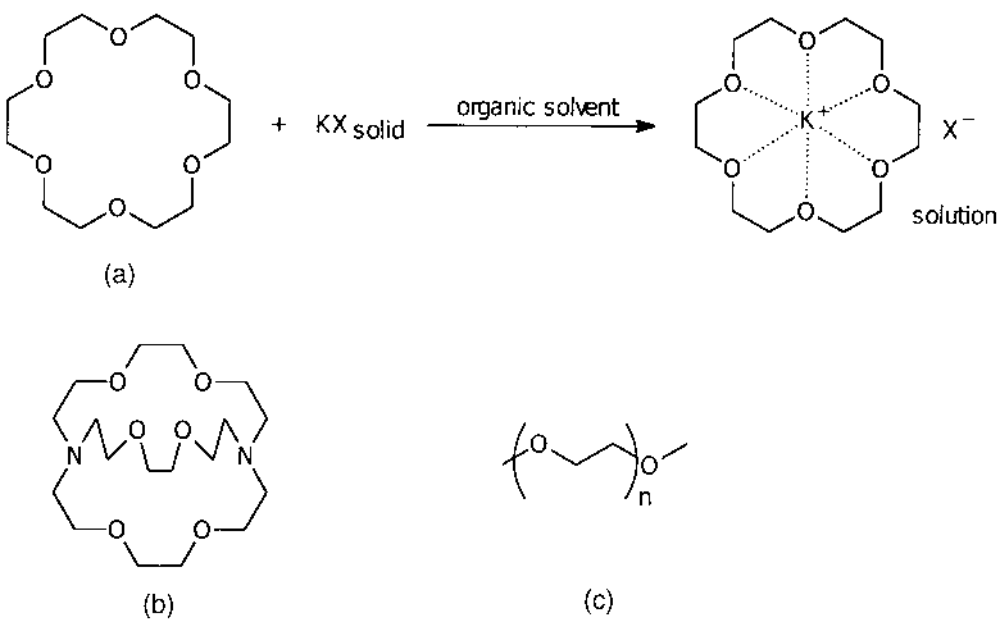

FIG. 1 Representative structures of compounds able to complex alkali metal cations.

$$Q^+X^-_{org} + Na^+Y^-_{aq} \rightleftharpoons Q^+Y^-_{org} + Na^+X^-_{aq} \quad (1a)$$

$$R - X_{org} + Q^+Y^-_{org} \longrightarrow R - Y_{org} + Q^+X^-_{org} \quad (1b)$$

Thus, the observed rate of the substitution in PT-catalyzed reactions is determined by the rate constants of the chemical reaction and the concentration of Y^- in the organic phase, the latter depends on the ion exchange equilibrium (1a) presented in a simplified version in eq. (2):

$$X^-_{org} + Y^-_{aq} \rightleftharpoons X^-_{aq} + Y^-_{org} \quad (2)$$

The position of the crucial equilibrium (2) is determined by relation of the energies of solvation and hydration of the anions X^- and Y^- in the organic and aqueous phases. Since for inorganic anions the energy of hydration is usually much higher, this is the factor governing the equilibrium (2); thus, ions of high hydration energy (having high charge density) stay preferentially in the aqueous phase. As a consequence,

$$OH^-, F^-, Cl^-, CN^-, Br^-, I^-, ClO_4^-, SCN^- \quad (3)$$

the concentration of the right located anion in the organic phase will always be much higher than its left located partner. It is therefore evident that PTC can operate efficiently when anions produced during the reaction [X^-, Eq. (1b)] are more hydrophilic [located left in (3)] than those introduced into the reaction (Y^-), otherwise the concentration of the Y^- anions in the organic phase, according to the equilibrium (1a) or (2) become negligible, and the catalytic process is hindered or does not occur at all. This can be exemplified with PT-catalyzed cyanation of various alkyl halides. The process is efficient with alkyl chlorides, less efficient with alkyl bromides, and does not proceed with alkyl iodides; thus, obviously it is not governed by the intrinsic activity of alkyl halides but by the concentration of Q^+CN^- in the organic phase, which in turn is determinated by the ion-exchange equilibrium, as shown in Eq. (2), where Y^- is CN^- and X^- is Cl^-, Br^-, or I^-. In the case of I^- anions the equilibrium concentration of Q^+CN^- in the organic phase is negligible.

In the PT-catalyzed processes in liquid–liquid systems inorganic anions are transferred from the aqueous to the organic phase in a hydrated form, so the hydration shell modifies their activity. The degree of hydration of the transferred anions and, as a consequence, their activity may be controlled to some extent by the concentration of the inorganic salt in the aqueous phase [15]. On the other hand, in the PT-catalyzed reactions in liquid–solid systems the anions are transferred into the organic phase in anhydrous, very active form; thus, these conditions should be particularly convenient for reactions of less active alkyl halides and anions of low nucleophilicity. However, due to the much less efficient exchange between a solution and the solid phase than between two liquid phases and also formation of the new solid phase of the produced salts, which can cover the surface of the solid phase of the educt and hinder this exchange, the use of starting salts in liquid–solid PT-catalyzed system is much less efficient than in the liquid–liquid system.

PTC is a particularly attractive methodology in applications for reactions of organic anions: carbanions, alkoxides etc. In such reactions the organic anion precursors are located in the organic phase and the reacting anions are generated in situ and subsequently introduced into the organic phase in the form of lipophilic ion pairs with the catalyst cations. These ion pairs are produced continuously via interaction of the precursor with a base located in the aqueous (inorganic) phase. Thus, the overall equilibrium process for carbanions is shown in Eq. (4):

$$\rangle C\!-\!H_{org} + Q^+X^-_{org} + Na^+OH^-_{aq} \rightleftharpoons \rangle C^-Q^+_{org} + Na^+X^-_{aq} + H_2O_{aq} \quad (4)$$

This equilibrium embraces two main processes: deprotonation of the carbanion precursor and the formation of lipophilic ion pairs with the cation of the catalyst. One of the possible pathways for this process consists in initial inorganic ion exchange producing Q^+OH^-—a strong base soluble in the organic phase—followed by deprotonation of the carbanion precursor in the organic phase [12]:

$$Q^+X^-_{org} + Na^+OH^-_{aq} \rightleftharpoons Q^+OH^-_{org} + Na^+X^-_{aq} \quad (5a)$$

$$\rangle C\!-\!H_{org} + Q^+OH^-_{org} \rightleftharpoons \rangle C^-Q^+_{org} + H_2O_{org} \longrightarrow H_2O_{aq} \quad (5b)$$

The high hydrophilicity of hydroxide anions, and thus the unfavorable position of the ion exchange equilibrium (5a), and numerous other observations, contradict this pathway. It is presently generally accepted that in the majority of cases the reaction does not proceed as in Eq. (5) and that Eq. (4) is composed of two processes: deprotonation of the carbanion precursor at the phase boundary (interfacial region) followed by ion exchange with the catalyst proceeding with carbanions located at the phase boundary [1,3,7]:

$$\rangle C\!-\!H_{org} + Na^+OH^-_{aq} \rightleftharpoons \rangle C^-Na^+_{int} + H_2O_{aq} \quad (6a)$$

$$\rangle C^-Na^+_{int} + Q^+X^-_{org} \rightleftharpoons \rangle C^-Q^+_{org} + Na^+X^-_{aq} \quad (6b)$$

where subscript "int" denotes the interfacial region.

The degree of deprotonation of the carbanion precursor at the phase boundary—the acid–base equilibrium (6a)—is a function of its acidity. Since the lipophilic ion pairs formed via ion exchange [eq. (6b)] depart from the phase boundary, a component of equilibrium (6a) leaves the equilibrium site; thus, the equilibrium is shifted to the right. Due to this effect a plethora of organic compounds of low acidity: carbanion precursors, alcohols, N–H acids, etc., of pK_a values up to 24 can be efficiently converted into the corresponding anions, which being transferred into the organic phase subsequently enter the desired reactions. Taking into account the value of pK_a of water $\sim$ 15.7, a significant hyperbasic effect is observed in these systems expanding greatly the applicability of NaOH as the base in PT-catalyzed, base-promoted reactions. It should be stressed that thanks to this hyperbasic effect aqueous NaOH can be used for generation and reactions of a large range of carbanions and other organic anions instead of commonly used strong bases such as $NaNH_2$, NaH, *t*-BuOK, etc.

For the PT-catalyzed generation of organic anions in liquid–solid systems the most common bases are anhydrous K_2CO_3, powdered NaOH or KOH, or mixtures of these hydroxides with K_2CO_3. There are also a few reports on the application of NaH for this purpose. Examples can be found in Ref. 4. In all such cases, deprotonation of the anion precursors, Y–H, takes place on the surface of the solid phase, producing K^+ or Na^+ salts of Y^- in the adsorbed state. Ion exchange with Q^+X^- assures continuous introduction of Y^- into the solution in the form of lipophilic ion pairs Q^+Y^-:

$$Y - H + |K_2CO_3| \rightleftharpoons Y^-|K^+KHCO_3| \quad (7a)$$

$$Y^-|K^+KHCO_3| + Q^+X^-_{org} \rightleftharpoons Q^+Y^-_{org} + |KX| + |KHCO_3| \quad (7b)$$

where | | indicates a solid phase.

Further presentation of selected typical examples of applications of PTC in organic synthesis will disclose scope, limitation, and particularly practical advantages of this methodology of general application in laboratory organic synthesis and as a basis of efficient, economic, and environmentally benign manufacturing of chemical products.

III. PRACTICAL APPLICATIONS OF PHASE TRANSFER CATALYSIS

A. Reactions of Anions Available as Salts of Inorganic Anions

Amongst numerous practically important reactions belonging to this group there are: nucleophilic substitution of nucleofugal groups in aliphatic and aromatic systems, addition of anions to electron-deficient C=O, C=N– and C=C bonds, oxidation, reduction, etc.

Cyanation of alkyl halides can be considered the most important typical example of the nucleophilic substitution, for which PTC methodology is successfully applied [13]:

$$R - X + NaCN \longrightarrow R - CN + NaX \quad (8)$$

PT-catalyzed cyanation proceeds efficiently only with alkyl chlorides; alkyl bromides are less efficient whereas iodides are not suitable because Br^- produced and particularly I^- ions are more lipophilic than CN^- and they exert a strong inhibition effect. In such reactions, as for instance cyanation of alkyl halides, there is an important practical problem connected with the necessity to use an excess of NaCN to assure complete conversion of the starting halide into nitrile. Thus, when the reaction is carried out in the traditional way in a solvent system dissolving both reactants, after the reaction is complete, excess of NaCN should be regenerated or detoxified and disposed. The advantage of the PT-catalyzed process carried out in a system comprising two immiscible phases, is that upon separation of the organic phase containing practically pure product, excess of NaCN remaining in the aqueous phase can be readily used for cyanation of the next portion of alkyl halide. By this simple way a counter-current process can be mimicked [16]. Thus, application of PTC for the cyanation reaction assures high yields and purity of the product, elimination of organic solvents, a very simple procedure, and what is particularly important, elimination of the majority of industrial wastes. These advantages of PTC are observed in most other cases of substitution reactions for which this technique can be used.

Replacement of halogen, sulfonate, or sulfate substituents with a variety of inorganic anions such as azide, cyanate, halogen, thiocyanate, etc., via PTC is presently a common process for organic synthesis widely used in industry:

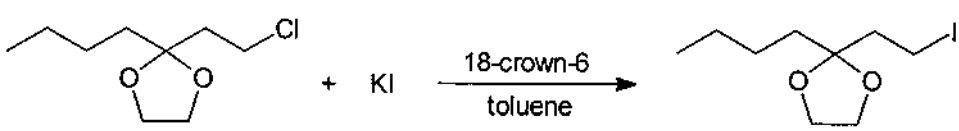

(9)

74% (Ref. 17)

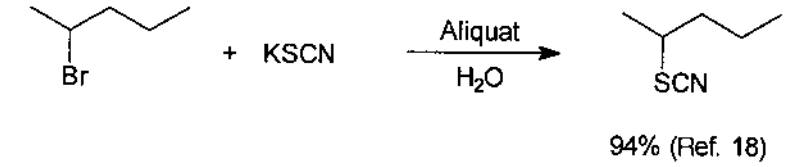

(10)

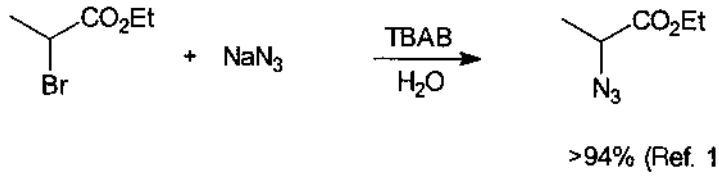

(11)

The major limitation of PTC in aliphatic nucleophilic substitution reactions is connected with unfavorable ion-exchange equilibria, particularly when the reacting anions, such as fluoride ions, have high hydration energy. For the reactions of such anions, use of PTC in a liquid–liquid system is impractical because, due to the unfavorable exchange equilibrium, they are transferred into the organic phase to a negligible extent. Moreover, from an aqueous solution they are transferred in highly hydrated form and thus are of low activity, and hydrolysis is often a competing reaction. Nevertheless a liquid–liquid PTC system can be used for synthesis of alkyl fluorides from alkyl sulfonates and KF [20]. However, for PTC reactions of such anions the liquid–solid system is much preferred and often assures good results [21]. Unfortunately, due to the harsh conditions and high basicity of fluoride anions these reactions are often accompanied by base-induced β-elimination of the starting alkyl halide and decomposition of the TAA catalyst via Hofmann-type degradation. These problems in PT-catalyzed fluorination of alkyl halides can be partially solved using triphenyltin halide as cocatalyst [22]. Thus, when catalytic amounts of Q^+X^- and triphenyltin fluoride are added to a suspension of KF in an aprotic solvent a soluble TAA salt of the complex hypervalent $Ph_3SnF_2^-$ anionisformed.Theanionisamild, p racticallynonbasicsourceoffluorideanion; thus, thesubstitutionproceedssatisfactorilyaccor dingtoEq.(12) :

$$\begin{aligned} Q^+X^-_{org} + Ph_3SnF_{org} + KF_{solid} &\rightleftharpoons Q^+Ph_3SnF_2{}^-{}_{org} + KX_{solid} \\ R - X_{org} + Q^+Ph_3SnF_2{}^-{}_{org} &\longrightarrow R - F_{org} + Q^+X^-_{org} + Ph_3SnF_{org} \end{aligned} \tag{12}$$

Ph_3SnF produced during the substitution process forms another hypervalent complex anion, so the tin compound and TAA cation used together are acting as catalysts.

PTC in liquid–solid systems is often used for the synthesis and manufacturing of esters via the reaction of solid sodium or potassium salts of carboxylic acids with alkyl halides. Liquid–liquid systems are also applied for this purpose:

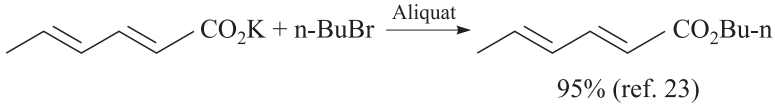

(13)

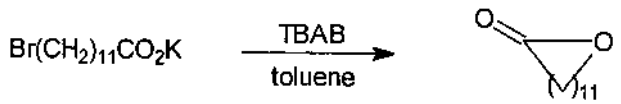

(14)

95% (Ref. 24)

The latter example shows that PTC mimicks a high-dilution technique, since even when small amounts of the solvent (toluene) was used, formation of the cyclic lactone was the major process. This was because the concentration of the reacting anions introduced continuously into the organic phase by the catalyst was very low; hence, intramolecular reaction was favored.

Nucleophilic additions of inorganic anions to carbonyl groups also proceed efficiently under PTC conditions. Syntheses of acyl azides, acyl cyanides, cyanohydrin derivatives, and the Reissert compounds belong to this category of reactions:

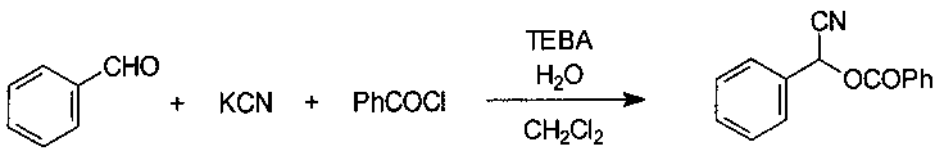

(15)

74% (Ref. 25)

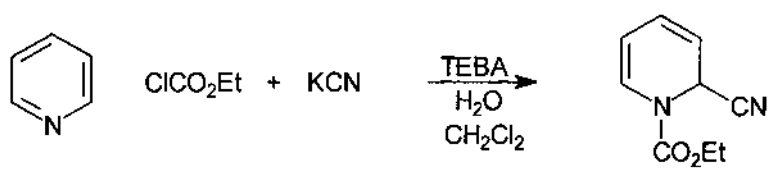

(16)

92% (Ref. 26)

Synthesis of the dinitrile of methylsuccinic acid exemplifies the PTC addition of inorganic anions to electron-deficient C=C bonds in a liquid–solid system:

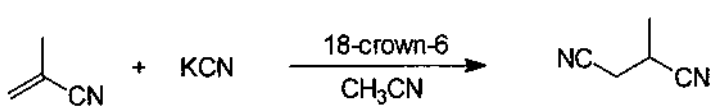

(17)

92% (Ref. 27)

Oxidation of organic compounds with anionic oxidants is efficiently executed using PTC methodology. In particular, $KMnO_4$ is well suited for this technique because, due to the high lipophilicity of MnO_4^- anions, they are readily transferred into a nonpolar organic phase in the form of TAA salts:

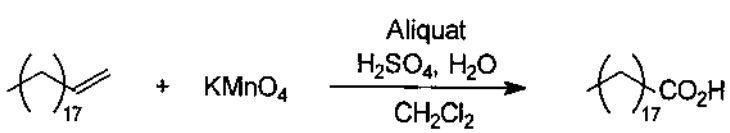

(18)

75–77% (Ref. 28)

Of particular value is the PTC oxidation with hydrogen peroxide in the presence of cocatalysts such as oxygen derivatives of V, W, Mo, etc. In such systems, alkenes are oxidized to oxiranes, alcohols to carbonyl compounds or carboxylic acids, etc.

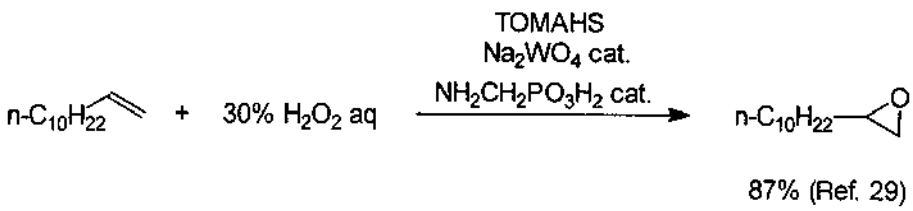

(19)

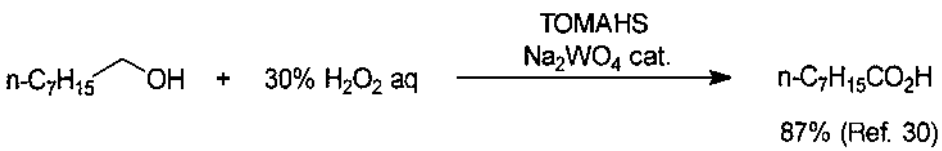

(20)

In this variant of PT-catalyzed oxidation two catalytic processes operate consecutively. In the aqueous phase a complex tungstate anion containing a H_2O_2 molecule is formed and, via interfacial ion exchange with the PT catalyst, is transferred into the organic phase in the form of a lipophilic ion pair with the TAA cation. In the organic phase, metal-catalyzed oxidation with this complex anion takes place with liberation of the complex anion containing H_2O. The ion pair of the TAA cation with this anion enters ion exchange in the interfacial region with more lipophilic complex anions containing H_2O_2 and this double catalytic process proceeds further. Thus, the key feature of PTC in this case is preferential introduction of the complex tungstate anion containing H_2O_2, produced via continuous ion exchange due to its higher lipophilicity, over the analogous complex anion containing H_2O. Since these anions are of rather low lipophilicity, highly lipophilic trioctylmethylammonium cations in the form of bisulfate should be used as PT catalyst. This method assures high selectivity and yields of the final products and operational simplicity. Use of H_2O_2 as oxidant, which is inexpensive and environmentally friendly, fulfills all the requirements for a modern (green) industrial process. For a recent review of H_2O_2 oxidations in PT-catalyzed systems see Ref. 31.

Among inorganic anions used as reducing agents, BH_4^- occupies a dominant position. This anion is sufficiently stable in an aqueous solution of its sodium salt and can be transferred into a nonpolar solvent by typical PT catalysts – lipophilic TAA salts. The use of PTC facilitates reduction of carbonyl compounds insoluble in hydroxylic solvents. In some cases even reduction of an ester group is possible under these conditions:

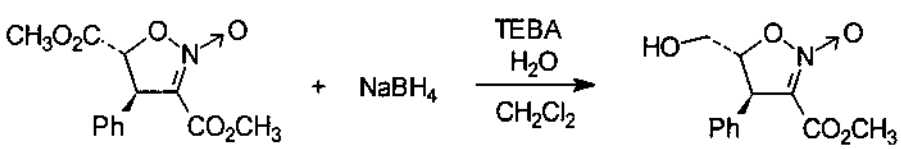

(21)

75% (Ref. 32)

Reduction of conjugated double bonds in α,β-unsaturated aldehydes and ketones proceeds with high selectivity by the use of sodium dithionite under PTC conditions:

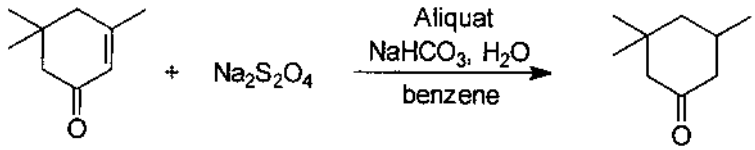

84% (Ref. 33) (22)

B. Phase Transfer Catalyzed Reactions Carried Out in Presence of Bases

This is a large group of processes that proceed with participation of, e.g., carbanions, oxygen, nitrogen, and sulfur derived anions generated in situ in two-phase systems. The first reported examples of the application of PTC in organic synthesis and industry were alkylations of carbanions of arylacetonitriles in the presence of aqueous NaOH [11]. These reactions were thoroughly studied, because many pharmaceuticals contain the arylacetic acid framework. High yields of monoalkylated products are as a rule obtained by alkylation with primary alkyl bromides:

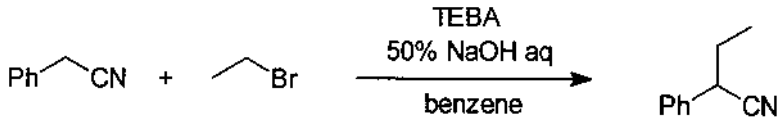

78–84% (Ref. 34) (23)

In the case of methylenic carbanions there is an important problem of selectivity of mono- versus di-alkylation, exemplified by the alkylation of phenylacetonitrile:

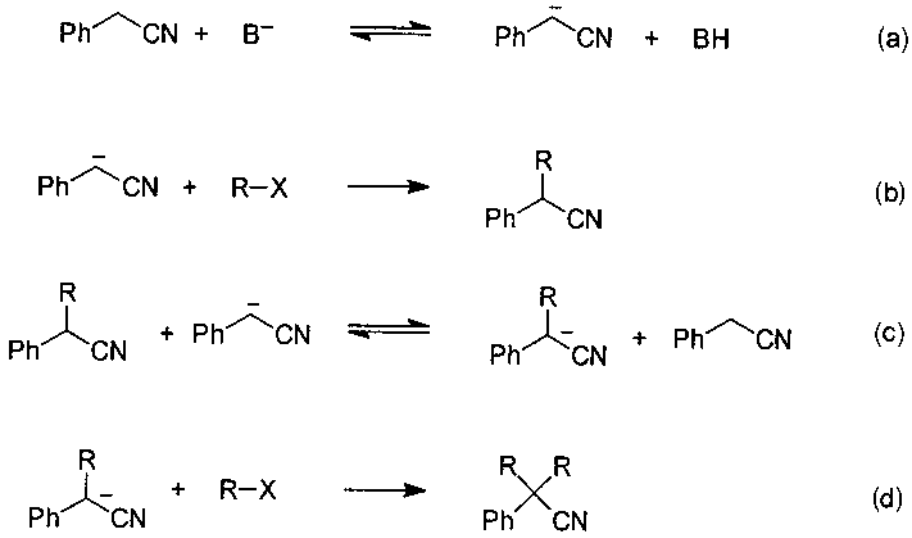

(24)

When R = alkyl, the alkylated products are usually weaker CH acids so equilibrium (*24c*) is shifted to the left; thus, the concentration of the methinic carbanion is low. On the other hand, these carbanions are more nucleophilic than methylenic ones and react faster with

alkyl halide and thus the dialkylation proceeds to some extent. However, under PTC conditions, the concentration of carbanions in the organic phase cannot exceed that of the catalyst, so they are always in the presence of a great excess of the carbanion precursors. For this reason the concentration of carbanions produced from less acidic precursors is negligible and the alkylation process is reasonably selective in the sense of monoalkylation [35].

For dialkylation or introduction of a secondary alkyl group the use of aqueous 60% KOH and tetrabutylammonium bromide (TBAB) as a catalyst is recommended:

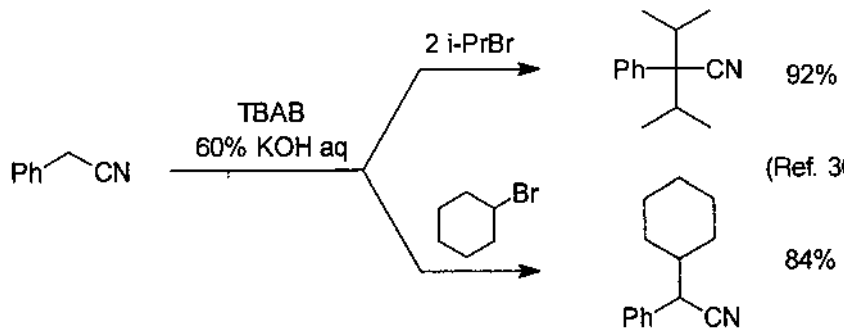

(25)

Alkylation of arylacetonitriles proceeds efficiently with a variety of substituted haloalkanes such as haloethers, esters, and nitriles of haloalkanoic acids, haloamines, etc. The reaction with dihaloalkanes can give cyclic and chain products:

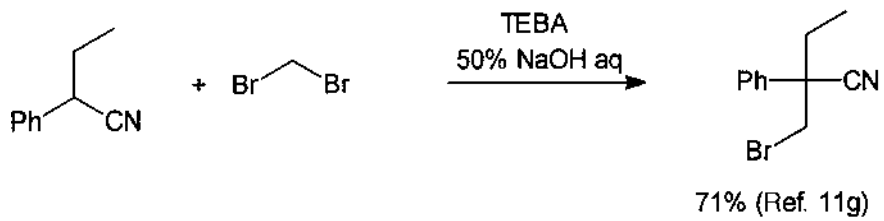

(26)

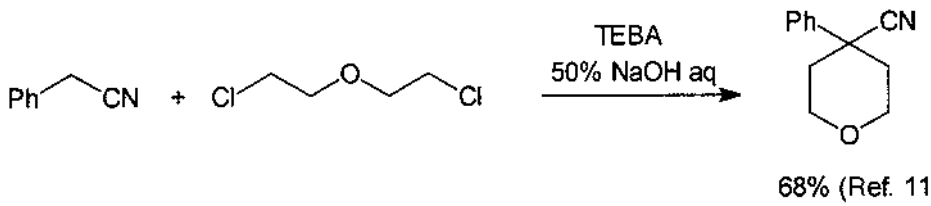

(27)

At present, PTC is a common methodology for alkylation of a large variety of carbanions of nitriles, esters, ketones, sulfones, acidic hydrocarbons, aldehydes, etc. The upper limit of the pK_a value for C—H acids able to form carbanions and undergo alkylation under PTC conditions is around 24. In the alkylation of carbanions with alkyl iodides often the inhibitory effect of iodide anions is observed, similarly as in the case of reactions of inorganic anions. For more detailed discussion see Section IV.C.

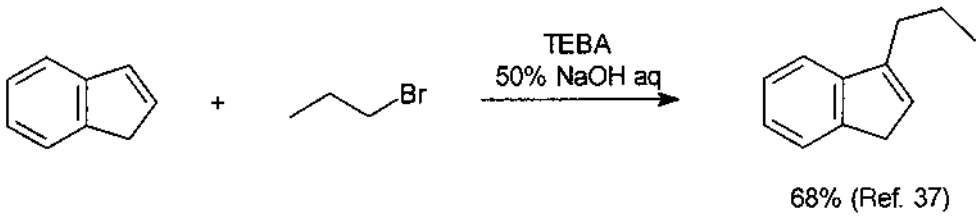

68% (Ref. 37)

(28)

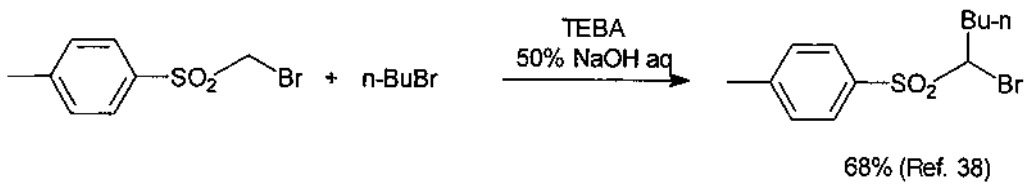

68% (Ref. 38)

(29)

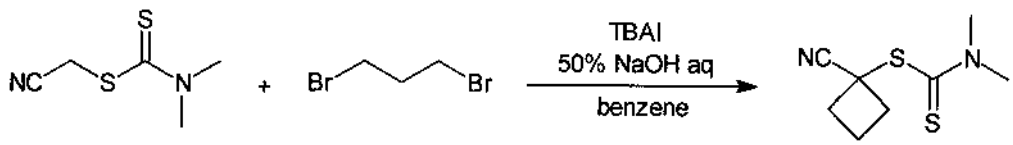

93% (Ref. 39)

(30)

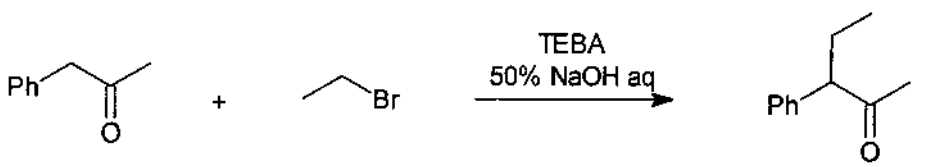

90% (Ref. 40)

(31)

For compounds of higher C–H acidity such as alkyl cyanoacetate, malonate, etc., a liquid–solid PTC system, in which anhydrous K_2CO_3 is used as a base, is particularly advantageous:

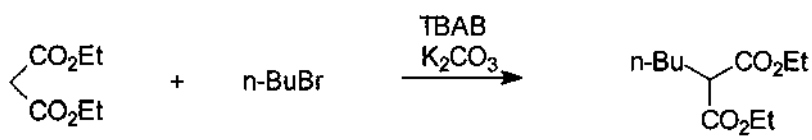

(32)

93% (Ref. 41)

Numerous other reactions of carbanions are efficiently executed in two-phase systems using concentrated aqueous NaOH and PT catalysts for deprotonation of the carbanion precursors. These conditions are particularly suitable for synthesis of oxiranes via condensation of aldehydes and ketones with carbanions of, e.g., α-chloronitriles, sulfones, and esters of α-chlorocarboxylic acids, known as the Darzens reaction, or with sulfonium

ylides. Since in the ylides the negative charge is compensated by the onium center, most reactions of ylides carried out in two-phase systems can proceed without PT catalysts:

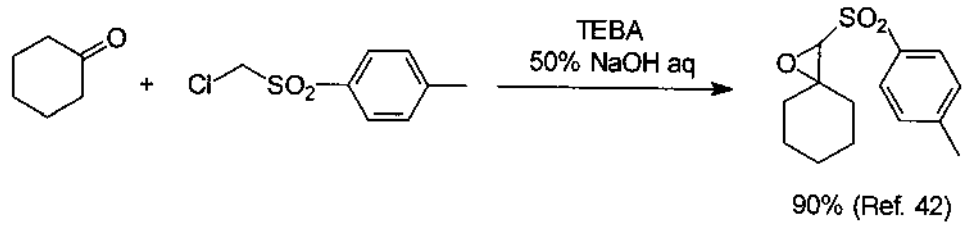

90% (Ref. 42)

(33)

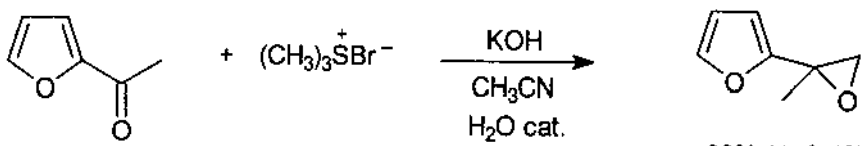

98% (Ref. 43) (34)

Similarly, PT-catalyzed condensation of α-chlorocarbanions, or of sulfonium and ammonium ylides, with electron-deficient alkenes, which proceeds via Michael-type addition followed by intramolecular substitution, is the most efficient procedure for synthesis of substituted cyclopropanes:

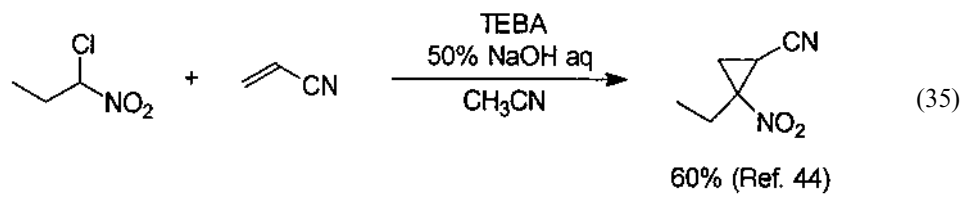

60% (Ref. 44) (35)

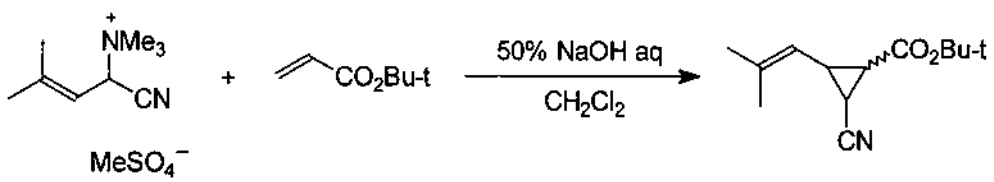

82% (Ref. 45)

(36)

Additions of PT-generated carbanions to electrophilic alkenes or carbonyl groups, followed by rapid reaction of the adduct anion with an internal electrophilic center, are often used in multistep, one-pot syntheses of interesting structures:

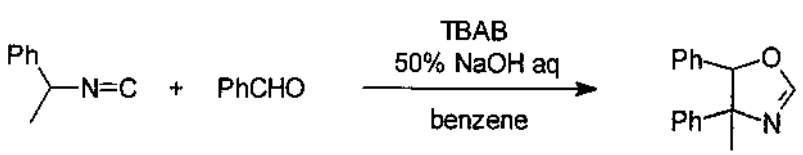

93% (Ref. 46) (37)

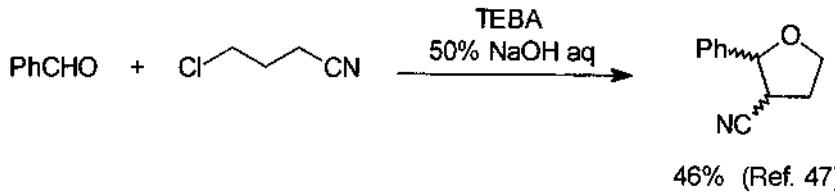

46% (Ref. 47) (38)

PTC-generated carbanions of 2-phenylalkanenitriles can add to acetylene and its derivatives with the formation of C-vinylated products:

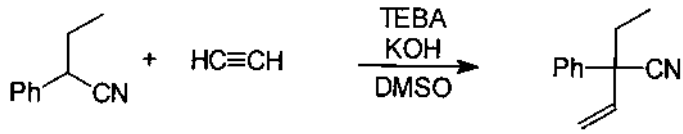

59–63% (Ref. 48) (39)

Addition of such carbanions to chloroacetylene results in the introduction of an ethynyl substituent. The reaction consists in addition of PT-generated carbanions to chloroacetylene produced in situ via PT-catalyzed β-elimination of HCl from vinylidene chloride, followed by β-elimination of HCl from the initial adduct. The reaction should be carried out in ethyl ether, which forms a nonexplosive complex with chloroacetylene:

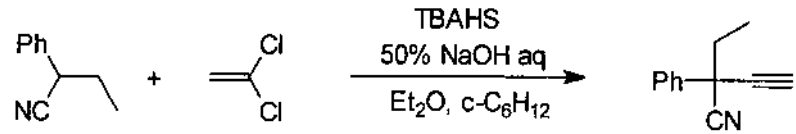

83% (Ref. 49) (40)

In a similar way, arylacetonitrile derivatives can be dichlorovinylated with trichloroethylene, under PTC conditions:

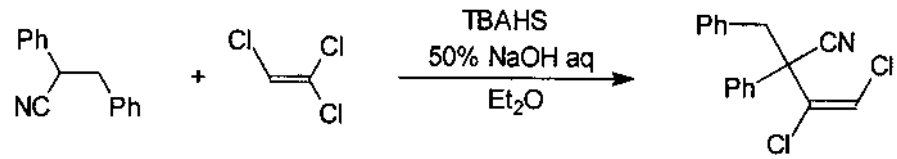

76% (Ref. 50) (41)

Nucleophilic substitution of halogen atoms in highly electrophilic arenes (most often nitroarenes) by carbanions proceeds efficiently under PTC conditions. However, the catalytic process operates only with methynic carbanions, when the products do not possess an acidic hydrogen atom. In the case of methylenic carbanions, introduction of nitroaryl substituents gives products that are much stronger C–H acids; thus, they are immediately converted into nitrobenzylic carbanions which, associated with the lipophilic TAA cations of the catalyst, stay in the organic phase. The low nucleophilic activity of these carbanions prevents their further reactions. In this situation the catalytic process is arrested.

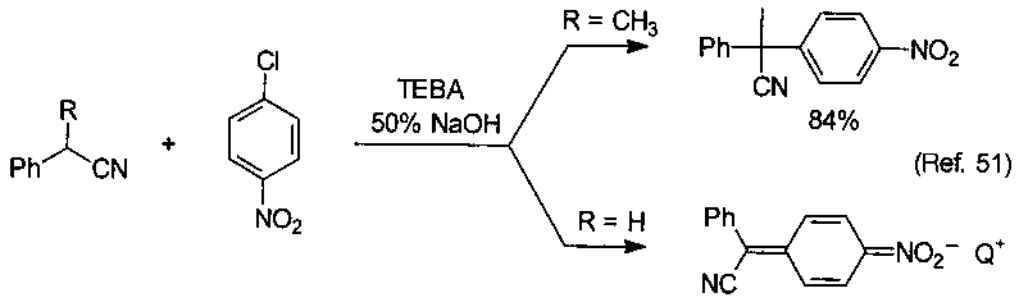

(42)

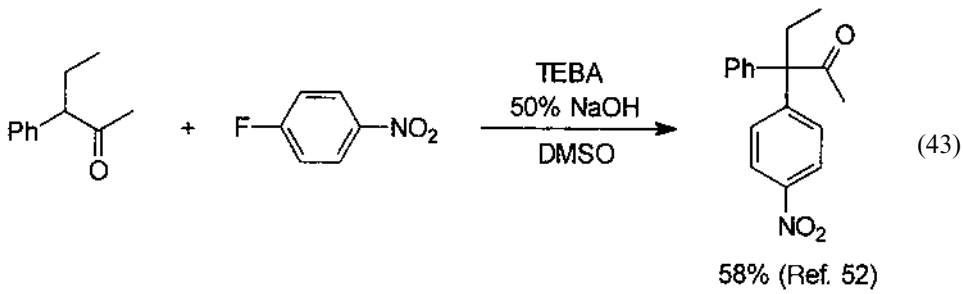

(43)

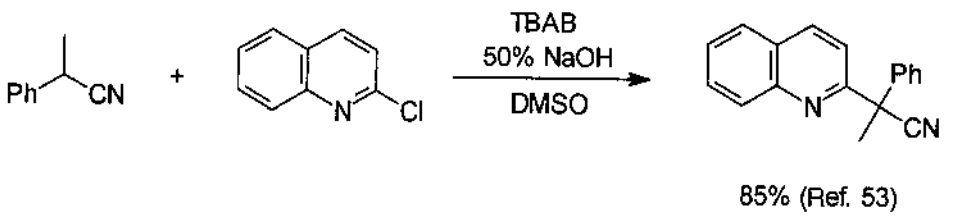

(44)

The high effectiveness of PT-catalyzed nucleophilic substitution of halogen atoms in nitroarenes by carbanions is probably connected with the existence of reacting anions in the organic phase in the form of TAA salts and low concentrations of the reacting species. In this situation eventual competing processes in the organic phase are suppressed.

Two-phase liquid–solid or liquid-liquid systems are often used for generation of phosphonium ylides from alkyltriphenylphosphonium salts and the subsequent reactions with aldehydes to produce alkenes (the Wittig reaction). Usually, the PT catalyst is not necessary for these reactions:

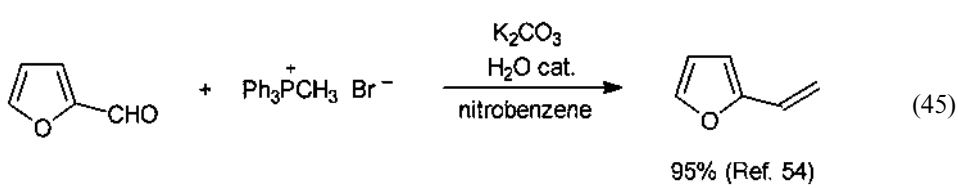

(45)

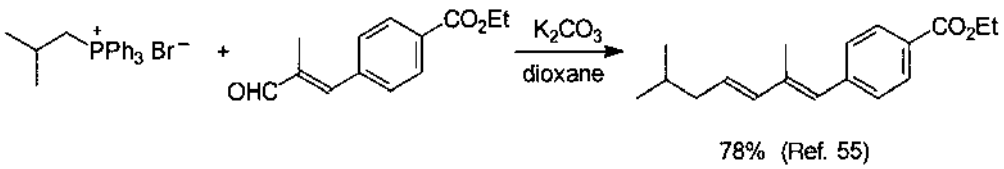

(46)

Carbanions (and some heteroanions), generated under PT-catalyzed conditions, enter a variety of reactions with compounds possessing electrophilic centers on sulfur, chlorine, or oxygen atoms. Of particular interest is direct thioalkylation of carbanions with organic thiocyanates. In this process, hydrophilic cyanide anions formed during the reaction are preferentially transferred to the aqueous phase; therefore, they do not hamper the PT catalyzed process:

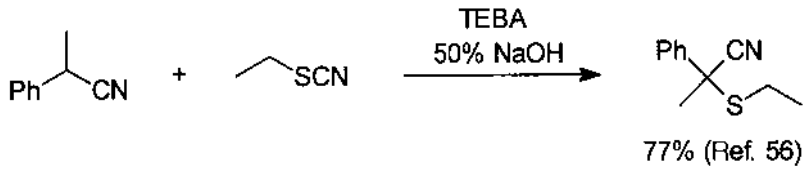

(47)

PTC has been used for the reactions of carbanions with carbon tetrachloride, hexachloroethane etc. (for review, see Ref. 57). These processes consist in nucleophilic attack of the carbanions on the halogen atom (halophilic reaction) and result in halogenation:

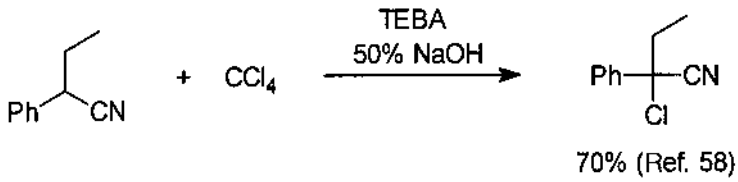

(48)

The product of PTC halogenation of carbanions with perhaloalkanes often enter further reactions:

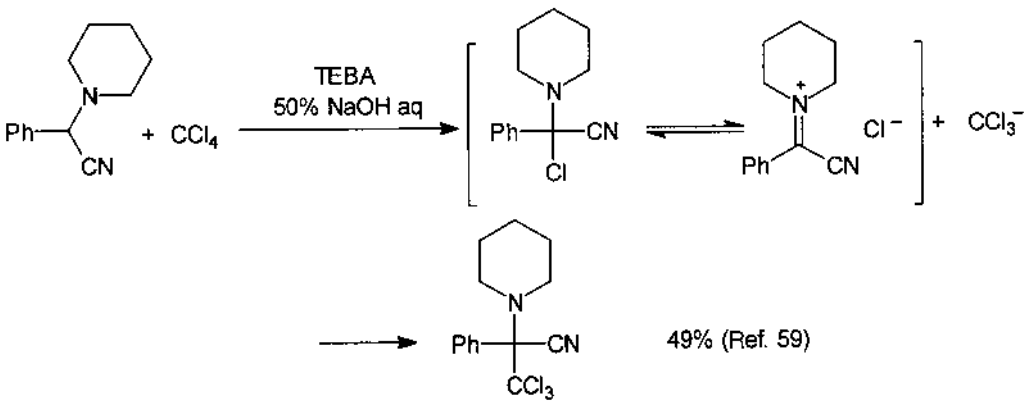

(49)

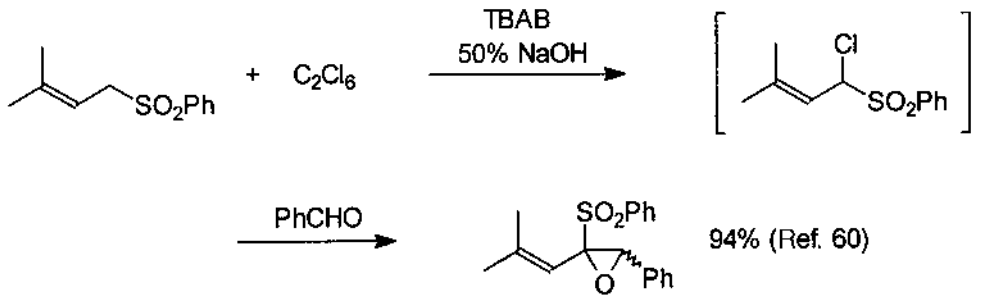

(50)

These examples illustrate specific features of PT-catalyzed systems, in which, thanks to low concentrations of the reacting species and proper relations of reaction rates, interesting multistep consecutive reactions proceed with good selectivity.

PTC has been used efficiently for chlorination of dialkylphosphite and subsequent phosphorylation of secondary amines, *O*-alkylhydroxylamines, alcohols, etc. (Atherton–Todd reaction) via halophilic reaction with carbon tetrachloride:

$$(EtO)_2P(O)H + CCl_4 + 2\ Et_2NH \xrightarrow[CH_2Cl_2]{\text{TEBA, 20\% NaOH}} (EtO)_2P(O)NEt_2 \quad (51)$$

86% (Ref. 61)

Generation and alkylation or other reactions of, e.g., organic oxygen, nitrogen, or sulfur anions are efficiently carried out using PTC methodology. The kind of base and system used depends on the acidity of the precursors. Phenols are readily *O*-alkylated in the presence of potassium carbonate in liquid–solid systems, whereas for aliphatic alcohols use of stronger bases such as concentrated aqueous NaOH is necessary:

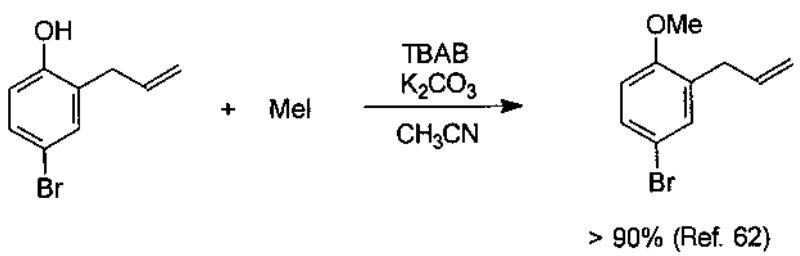

(52)

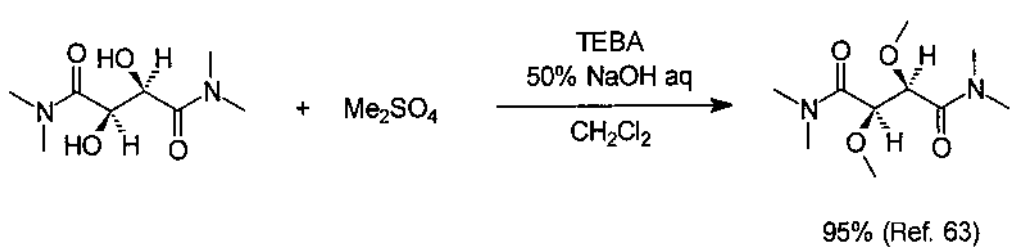

(53)

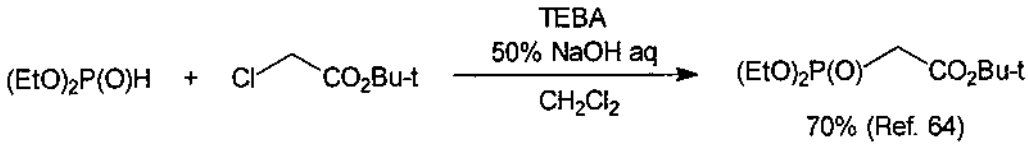

(54)

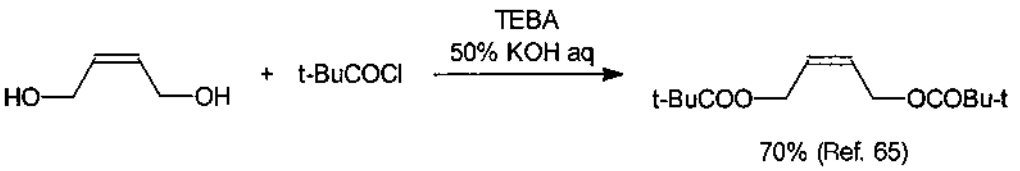

(55)

N-alkylation of nitrogen heterocycles, such as pyrroles, indoles, pyrazoles, etc., an important process for organic synthesis and industry, proceeds under the PTC conditions usually with high yields:

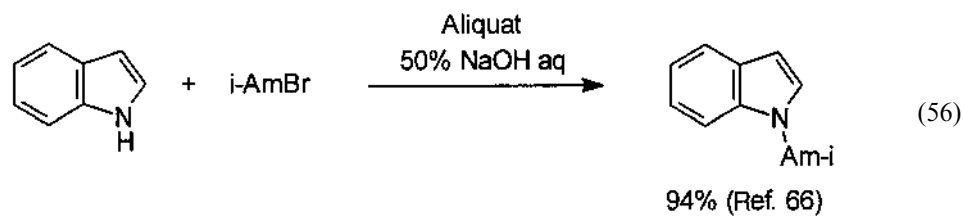

(56)

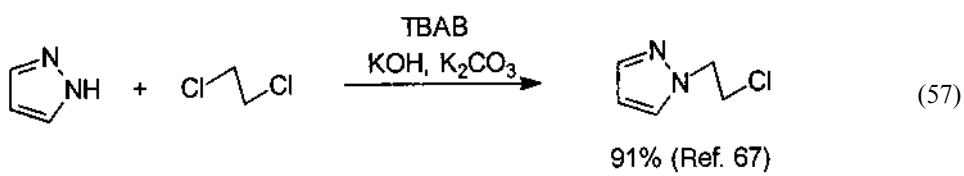

(57)

N-alkylation of other relatively strong NH acids such as sulfonamides, imides, or cyanamide as well as less acidic diarylamines, amides, etc., also belongs to this category of processes.

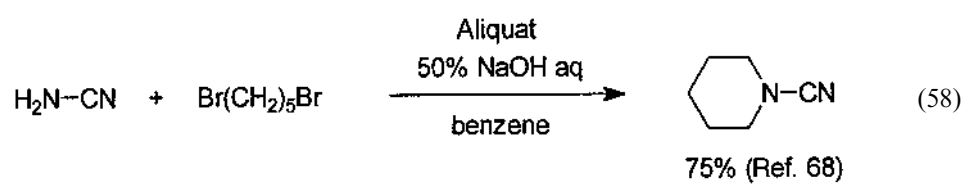

(58)

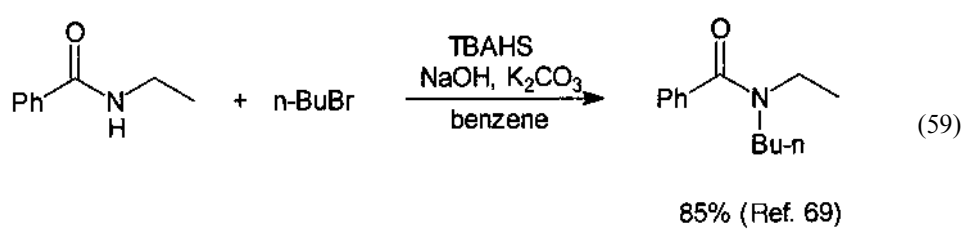

(59)

C. Generation and Reactions of Carbenes

A very important and large field of application of PTC is generation of dihalocarbenes via α-elimination and their reactions with a variety of partners. Thus, when chloroform and an alkene is treated with concentrated aqueous NaOH in the presence of a PT catalyst, rapid formation of dichlorocyclopropane takes place [12]:

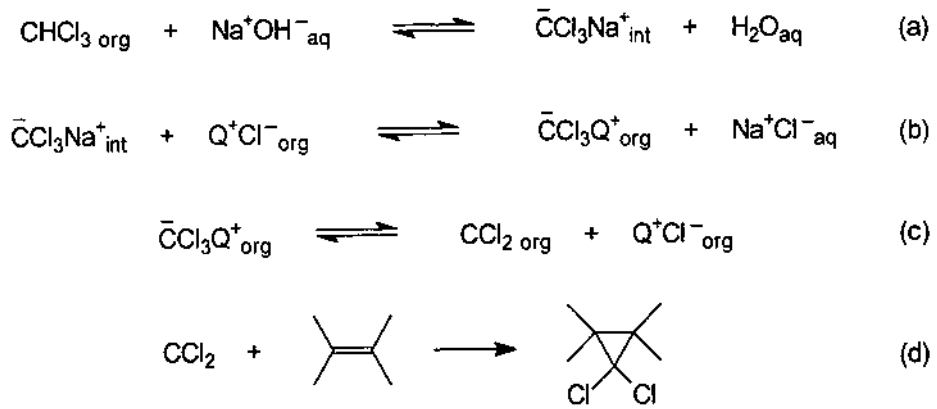

(60)

Usually, yields of dichlorocyclopropanes are high whereas hydrolysis of the dichlorocarbene is not a significant process in spite of its known very high rate of reaction with water or OH^- anions. This and other observations of reactions of dichlorocarbene generated under PTC conditions confirm the mechanistic picture presented in Section II.

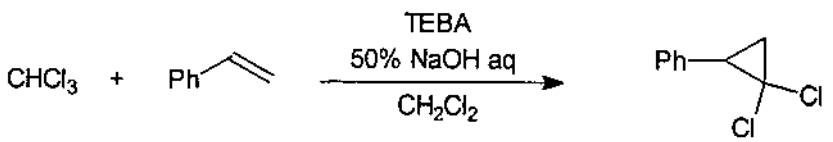

(61)

86–88% (Ref. 70)

It should be stressed that this methodology is of general use for generation of other dihalocarbenes via α-elimination of hydrogen halide from haloforms, and many other carbenes which can be generated via base-induced α-eliminations:

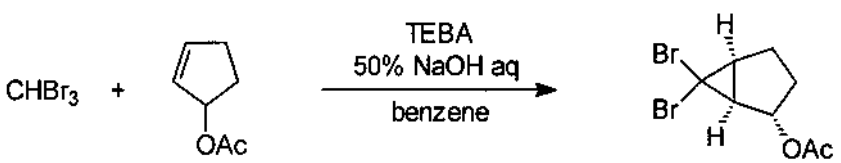

(62)

81% (Ref. 71)

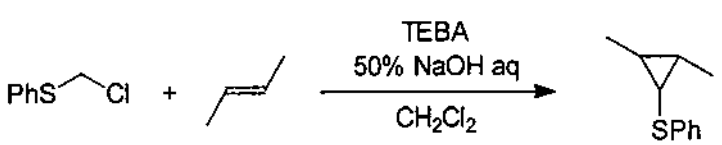

(63)

79% (Ref. 72)

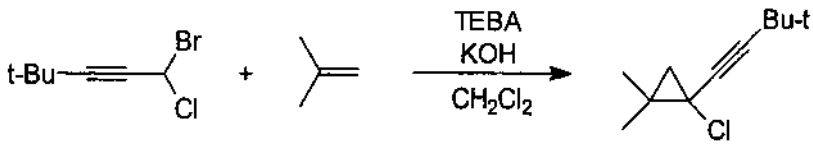

64% (Ref. 73) (64)

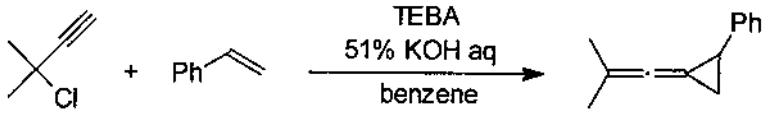

61% (Ref. 74) (65)

Besides addition to double bonds to give dihalocyclopropane derivatives—the most important reaction of dihalocarbenes—many other reactions of these active electrophilic species can be performed using PTC methodology, such as insertion into C–H bond, reactions with primary and secondary amines and with many other nucleophiles:

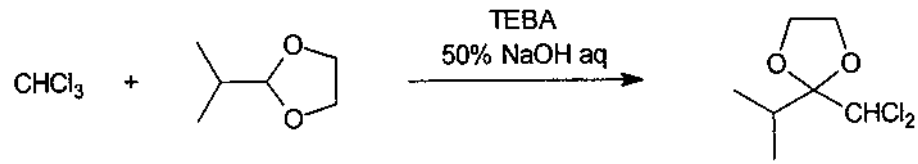

67% (Ref. 75) (66)

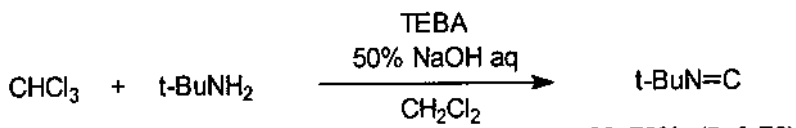

66–73% (Ref. 76) (67)

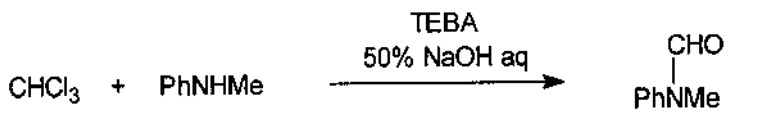

78% (Ref. 77) (68)

Difluorocarbene is the only dihalocarbene, which, being generated via PT-catalyzed α-elimination from chlorodifluoromethane in a two-phase system does not enter the cycloaddition reaction to alkenes. This is because of the instability of the chlorodifluoromethyl anion, which due to its very short lifetime cannot be transferred from the interfacial region, where it is formed, into the organic phase. Therefore, difluorocarbene is generated in the interfacial region and undergoes fast hydrolysis.

It was shown that difluorocarbene can be generated in the PT-catalyzed system via halophilic reaction of tribromomethyl [78] or dibromomethyl [79] carbanions with dibromodifluoromethane. In this process, the short-lived bromodifluoromethyl carbanion and consequently difluorocarbene are generated inside the organic phase; thus, the latter can

react efficiently with alkenes to produce *gem*-difluorocyclopropane derivatives. This method is limited to highly nucleophilic alkenes, but because of its simplicity it can be recommended as a method of choice in these cases.

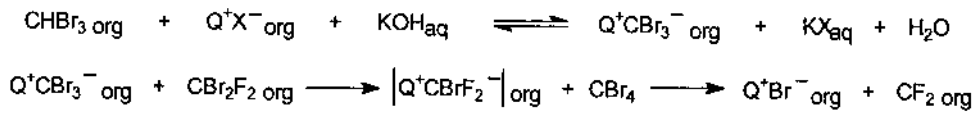

(69)

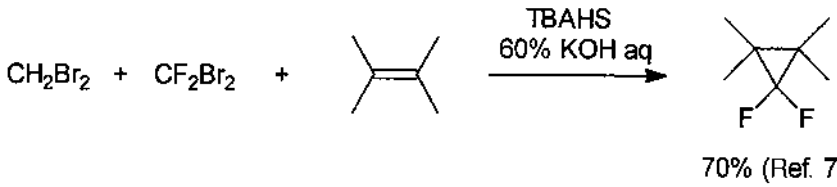

70% (Ref. 79)

(70)

D. Base-Induced β-Elimination

Elimination of hydrogen halide from haloalkanes to produce alkenes is an important process in organic synthesis and industry. Realization of this reaction under PTC conditions requires continuous transfer of base (OH^- anions) into the organic phase:

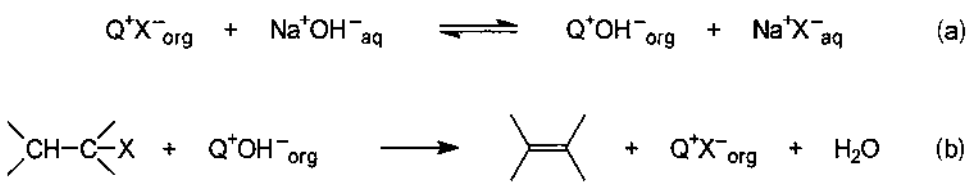

(71)

Since the equilibrium (71a) is shifted to the left, the concentration of OH^- anions in the organic phase is thus low, and PTC is only a moderately efficient methodology for β-elimination. Nevertheless, there are many examples of successful applications of PTC for practical realization of this process. The effectiveness of PTC for β-elimination reactions becomes much higher when cocatalysts are used. The cocatalysts, mostly alcohols or phenols such as benzyl alcohol, 2,2,2-trifluoroethanol, or mesitol, are deprotonated at the interface and the alkoxide anions produced, introduced into the organic phase by the lipophilic cation of the catalyst, act there as basic agents [80]:

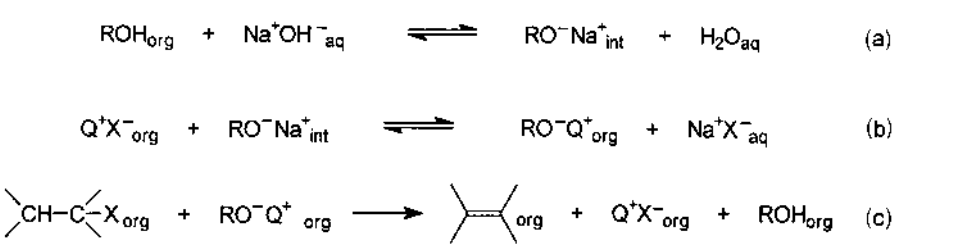

(72)

β-Elimination of hydrogen halide, induced by organic anions, generated in PT catalyzed systems, is often a first step of many synthetically useful reactions. Ring open-

ing of 1,1,2-trihalocyclopropanes with formation of acetylene derivatives serves as an example.

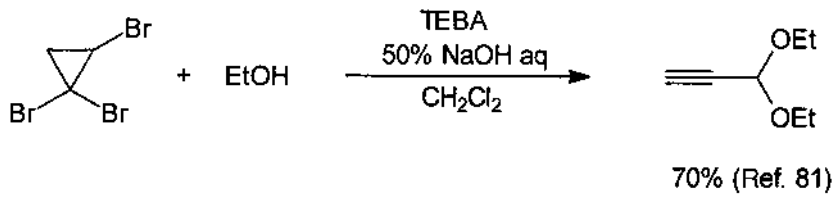

(73)

E. Phase Transfer Catalysis in Organometallic Chemistry

PTC has found wide application in organometallic chemistry and reactions catalyzed by organometallic compounds and complexes. There are many reviews on this subject [82] and we will only mention briefly the main types of reactions.

1. PT-Catalyzed Synthesis of Organometallic Compounds and Complexes

Some organometallic compounds and complexes are efficiently synthesized using PTC methodology:

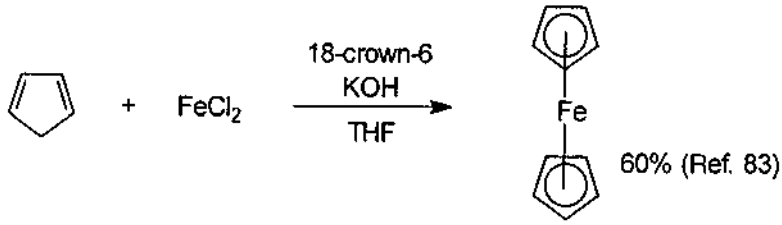

(74)

Ligand exchange in a variety of organometallic complexes of VI, VII, and VIII group metals can be often substantially improved when executed using PTC methodology:

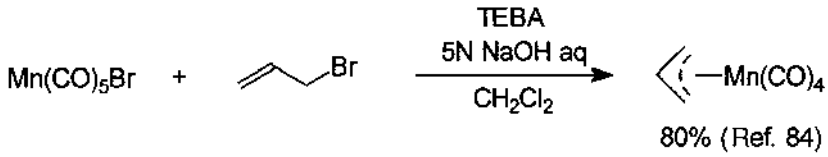

(75)

Complexation of organic compounds with organometallic moieties can modify substantially their properties, thus allowing the desired transformations to proceed. A variety of such transformations with organometallic complexes or organometallic compounds can be executed under PTC conditions. For instance, nucleophilic substitution of the halogen in halobenzenes usually requires harsh conditions. Conversion of these arenes into chromium tricarbonyl complexes facilitates these reactions. PTC is a method of choice for the execution of such a process with inorganic anions, alkoxides, etc.

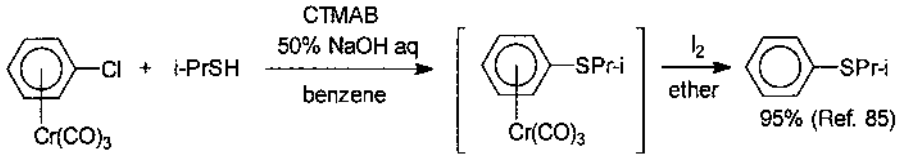

(76)

2. PTC Reduction and Hydrogenation with CO and H_2 Using Metal Carbonyls or Complexes

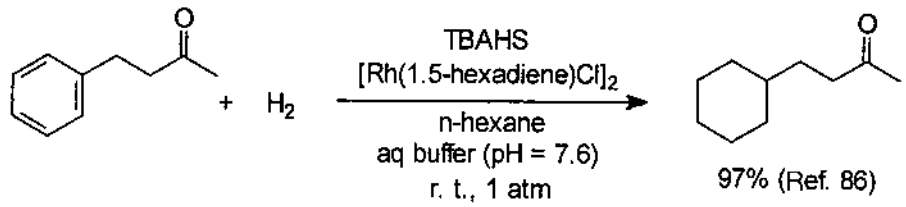

(77)

In these reactions, the TAA salt, in a two-phase system, provides a vehicle for contact of the hydrogenation catalyst and the organic substrate.

3. PTC and Metal Complexes Catalyzed Carbonylation of Organic Halides

Carbonylation of organic halides catalyzed by transition metals is a general and efficient method for manufacturing carboxylic acids. PTC offers particularly convenient conditions for this reaction:

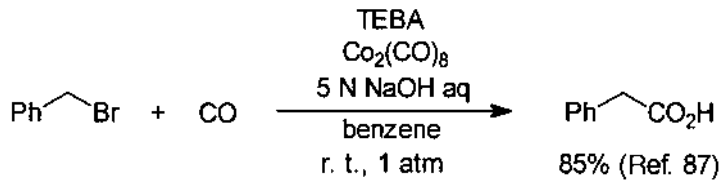

(78)

The main advantage of PTC methodology in these reactions is due to the fact that the product, a carboxylate anion, is constantly removed from the organic phase into the aqueous phase, assuring a high turnover of the organometallic catalyst and also high selectivity of the monocarboxylation of dihalo- or polyhalo-molecules.

4. PTC in the Heck and Related Reactions

Of great value for organic synthesis are the Pd-catalyzed processes of vinylation of aryl halides (Heck reaction), and ethynylation of aryl or vinyl halides, etc. Although these reactions are successfully executed in a homogeneous medium, in many cases use of PTC in heterogeneous systems give significant advantages as far as yields, selectivities and procedures are concerned:

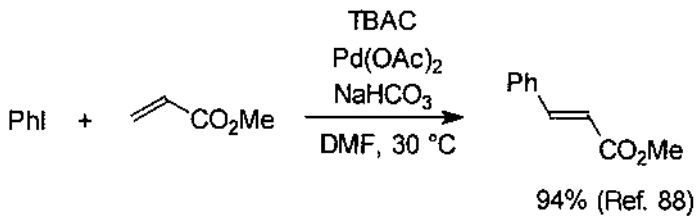

(79)

F. Enantioselective Phase Transfer Catalyzed Reactions

In many PT-catalyzed reactions new chiral centers are formed; thus, it would be of great interest to realize enantioselective syntheses promoted by optically active catalysts. Since optically active tertiary amines, e.g., alkaloids are readily available such possibilities appeared very attractive. A long-lasting search for such reactions gave at the beginning mostly negative results (for reviews see Refs 6 and 89). Only recently was this problem successfully solved by use of proper chiral TAA salts (for recent reviews see Ref. 90).

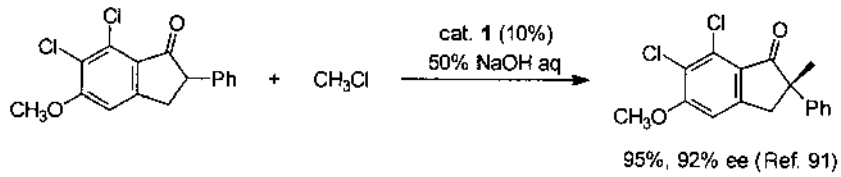

95%, 92% ee (Ref. 91) (80)

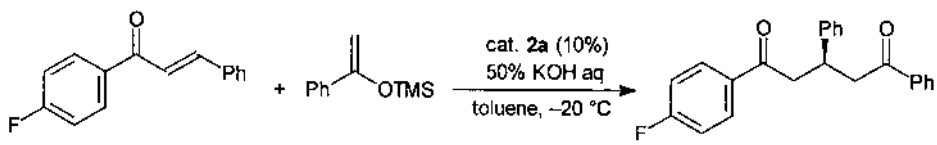

85%, 95% ee (Ref. 92) (81)

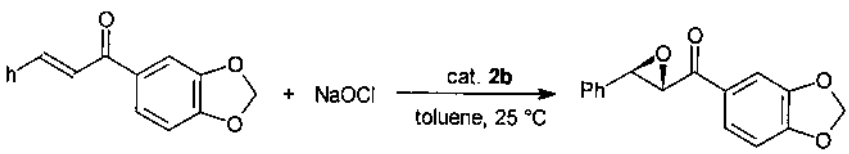

76% , 92% ee (Ref. 93) (82)

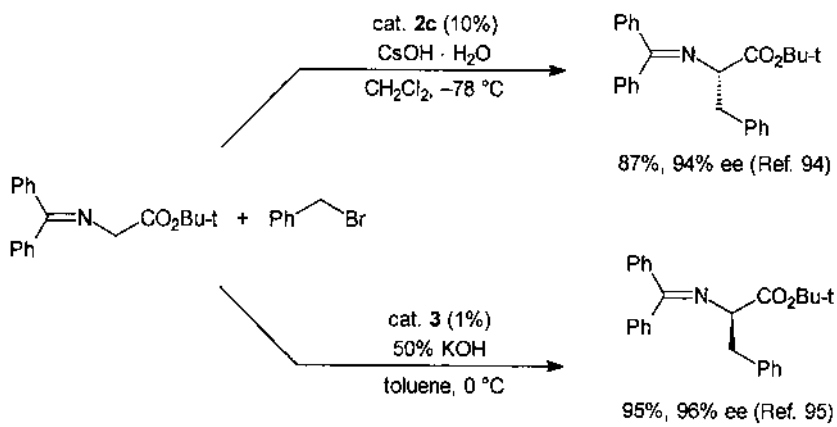

87%, 94% ee (Ref. 94)

95%, 96% ee (Ref. 95) (83)

The catalysts used in Eqs. (80–83) are represented by Structures **1–3**:

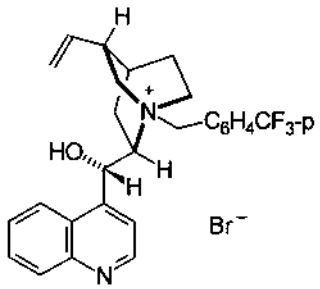

1

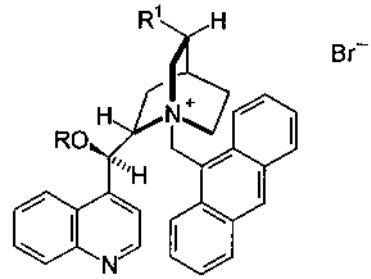

2, **a**: R = OH, R^1 = ethyl
b: R = benzyl, R^1 = vinyl
c: R = allyl, R^1 = vinyl

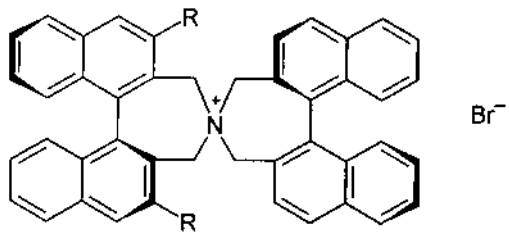

3, R = β-naphthyl

IV. ROLE OF INTERFACIAL AND TRANSPORT PROCESSES IN PHASE TRANSFER CATALYSIS

PT-catalyzed reactions proceed in heterogeneous systems formed by two mutually immiscible phases; thus, it is necessary to identify the site where the lipophilic ion pairs are formed. In these systems, transport processes, which bring together the reacting species, are of crucial importance. Since two systems—liquid–liquid and liquid–solid are used for PT-catalyzed reactions in which anions available as such (mostly inorganic) and generated in situ from the anion precursors and base are participating—there are four general cases which, due to their specific features should be discussed separately.

A. Phase Transfer Catalyzed Reactions of Inorganic Anions in Liquid–Liquid Systems

This large and important group of reactions is most conveniently discussed using the example of nucleophilic substitution with cyanide anions:

$$R - X + NaCN \longrightarrow R - CN + NaX \tag{84}$$

Stirring of neat alkyl chloride with a solution of sodium cyanide in water does not result in the substitution reaction, because the reaction partners: alkyl halide and cyanide anion, are located in mutually immiscible phases and cannot enter into an intimate contact. Addition of a small quantity of a lipophilic TAA salt to such a system promotes the reaction via continuous introduction of cyanide anions into the organic phase in the form of Q^+CN^-. The simplest mechanistic picture of this catalytic action is presented in Eq. (85):

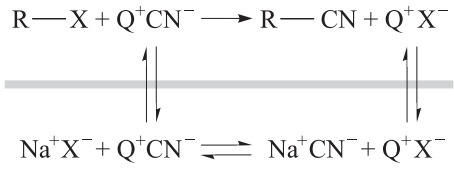

(85)

According to this picture the lipophilic ion pairs with cyanide anions are formed via migration of Q^+X^- into the aqueous phase, where the crucial ion exchange takes place. Highly hydrophilic TAA salts, insoluble in the organic phase, are obviously unable to act as PT catalysts; however, this picture suggests also that highly lipophilic TAA salts, insoluble in water, thus unable to effect ion exchange there, should be inactive as PT catalysts. Since this is not the case—the effectiveness of catalytic action of highly lipophilic TAA salt is well documented [4,5]—it is evident that migration of a TAA salt into the aqueous phase is not required for ion exchange; thus, it evidently occurs at the phase boundary.

The phase boundary between these liquid phases should be rather termed the interfacial region and defined as a region of contact of two mutually immiscible phases where, due to the molecular motion, there is a gradient of concentration of components of these phases as shown in Fig. 2.

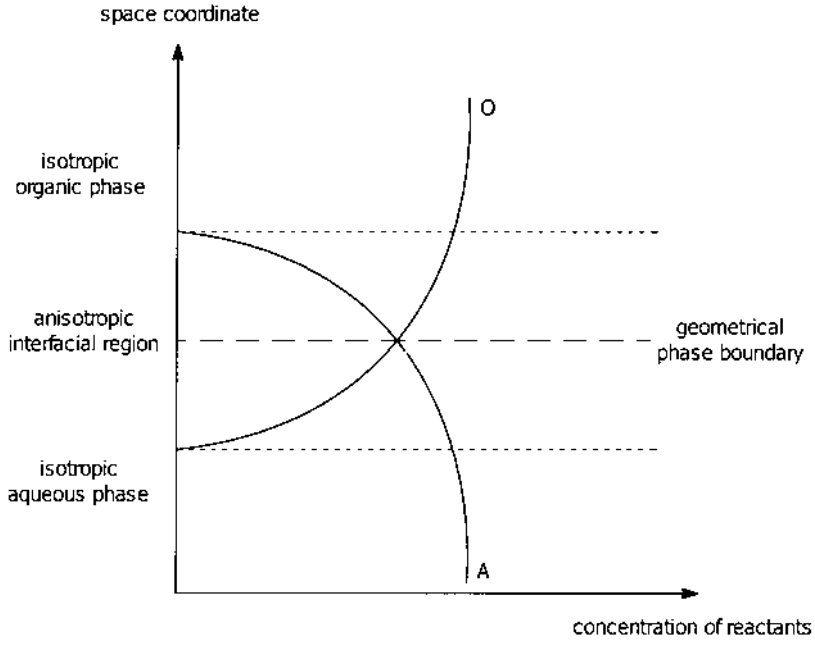

FIG. 2 Representation of the interfacial region between two mutually immiscible phases, in which there is a gradient of concentrations. Curves O and A represent concentrations of components of organic and aqueous phases, respectively.

Although in this region there is contact between an alkyl halide and cyanide anions, because of its very small volume and rather moderate rate constant of the reaction that proceeds via covalent bond breaking, the observed rate of substitution in this region is negligible.

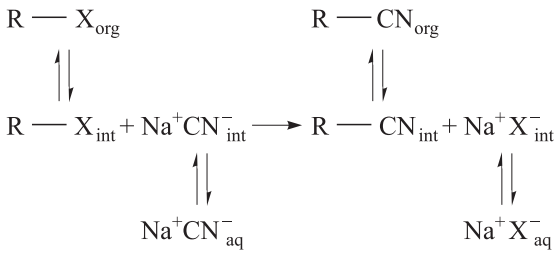

(86)

On the other hand, the ion exchange, which proceeds at a diffusion-controlled rate, assures fast formation of lipophilic ion pairs Q^+X^- which migrate subsequently into the organic phase where the substitution takes place. This mechanism of PTC can be pictured in general form:

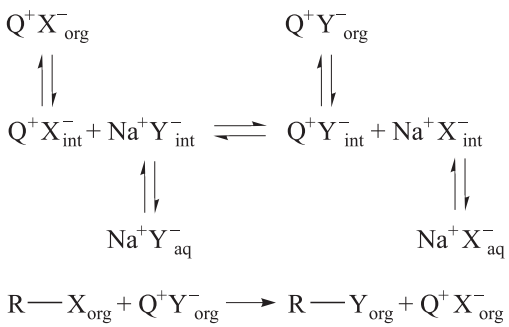

(87)

As has been mentioned the ion-exchange equilibrium is governed by the differences in energies of solvation and hydration of ions, more precisely the difference in the free energy, ΔG, of these ions, in both phases. The observed rate of the PT-catalyzed reaction, which is the most important characteristics of the process, $v = k[\text{R–X}][Y^-]$, depends on the rate constant of the reaction in the organic phase and concentrations of the reacting species there. In the case when the organic phase in the two -phase system, in which PTC operates, is formed by the neat organic reactant, the picture is somewhat simplified. In such systems the overall rate is controlled by the rate constant and concentration of Y^-. The former parameter depends inter alia on the chemical activity of Y^- and can be tuned to some extent by changing the degree of hydration (number of water molecules that enter with each Y^- into the organic phase) [15]. This number, and hence activity of Y^-, can be modified by changing the activity of water, i.e., the concentration of inorganic solutes, in the aqueous phase.

More complicated is the question of concentration of Y^- in the organic phase. At the first approximation one can suppose that it is constant, being determined by the ion-exchange equilibrium; thus, typical PT-catalyzed reactions should follow zero-order kinetics. However, as the reaction proceeds, the concentration of X^- and Y^- anions in the aqueous phase changes, affecting the equilibrium concentration of Q^+Y^- in the organic phase. Also, the organic reactant in the organic phase becomes diluted by the product and hence its concentration becomes lower. Moreover, the observed rate of PT-

catalyzed reactions depends not only on the rate of the chemical reaction in the organic phase but also on the rate at which ion-exchange equilibrium is established between the two phases. Without entering into mechanistic questions one can analyze two extreme cases: where the rate constant of the chemical reaction has a low or moderate value so that the overall rate is determined by the rate of the reaction in the organic phase and follows zero-order kinetics. One can consider that such reactions are in the kinetic region. On the other hand, when the rate constant of the chemical reaction in the organic phase is very high, ion exchange between the phases and transport of the ion pairs become slower than the rate of the chemical reaction and the rates of these processes determine the observed reaction rate. Such processes are in a diffusion-controlled region.

The ion-exchange process between two phases is a combination of a few processes: diffusion of the components from the bulk of both phases into the interfacial region, ion exchange in this region, and diffusion of the ion pairs formed back to the bulk of the phases. The rate of these processes depends mostly on mobility of the ion pairs and size of the interfacial region (more precisely its relation to the volume of the phases), but also viscosity, temperature, etc. The size of the interfacial region depends mostly on the intensity of stirring; a typical relationship between the observed rate of PT-catalyzed reactions and speed of stirring is presented in Fig. 3 [96].

Of course, there is no simple relationship between speed of stirring and size of interfacial area; thus, a curve as in Fig. 3 is only an example of a trend and has no exact meaning.

An important feature of PTC is that the reaction systems are kept constantly dispersed by vigorous stirring; thus, continuous interfacial ion exchange and transport of ion pairs is assured. However, all measurements of equilibrium concentration of reacting ion pairs in the organic phase are executed, for technical reasons, on coalescence and separation of the phases after equilibration is attained during vigorous stirring. There are many observations that the effectiveness of PTC reactions is often higher than that expected on the basis of the measured equilibrium concentration of the reacting anions. Calculations made on the basis of assumption of surface activity of TAA salts indicate that in highly dispersed systems (as during vigorous stirring) concentrations of TAA salts of carbanions or other anions can be different from that measured on coalescence. This peculiar result of calculations was experimentally verified [97].

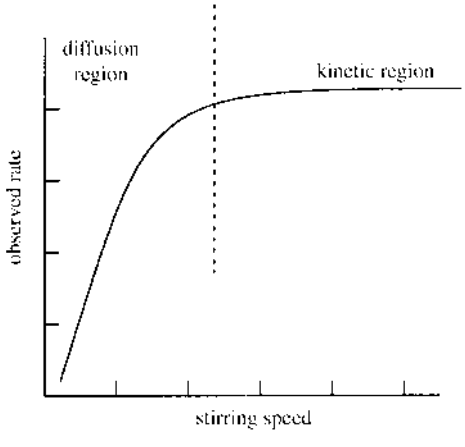

FIG. 3 Typical relationship between the observed rate of PT-catalyzed reactions and speed of stirring.

B. Phase Transfer Catalyzed Reactions of Inorganic Anions in Liquid–Solid Systems

The origin of the liquid–solid system was an observation that crown ethers, e.g., dibenzo-18-crown-6, are able to form relatively stable complexes with sodium or potassium cations and by this way solubilize inorganic salts in nonpolar or moderately polar solvents [98]. Inorganic anions in such solutions are not hydrated and only weakly solvated and hence exhibit very high chemical activity. Use of such solubilized inorganic salts in chemical reactions was termed "reactions of naked anions" [21]. An important improvement in this field was due to an observation that crown ethers can promote such reactions when used in quantities much lower than stoichiometric, thereby acting as catalysts. This catalytic action consists in continuous transfer of the anions into the organic phase in the form of lipophilic ion pairs with complexed potassium cations as in typical PT-catalyzed processes in liquid–liquid systems. However, the ion exchange between liquid and solid phases is more complicated because, contrary to the liquid–liquid systems, the interfacial region of mutual mixibility of the phases is absent. One can therefore suppose that continuous formation of the lipophilic ion pairs proceeds via adsorption of the free crown ether on the surface of the solid phase, complexation of the K^+ cations, and desorption of the lipophilic ion pair so the catalytic process proceeds as shown in Eq. (88a–c). On the other hand, it appears that direct ion exchange on the solid surface is also possible, Eq. (88d). This concept is supported by the observations that PTC reactions of inorganic anions in liquid–solid systems are catalyzed by lipophilic TAA salts.

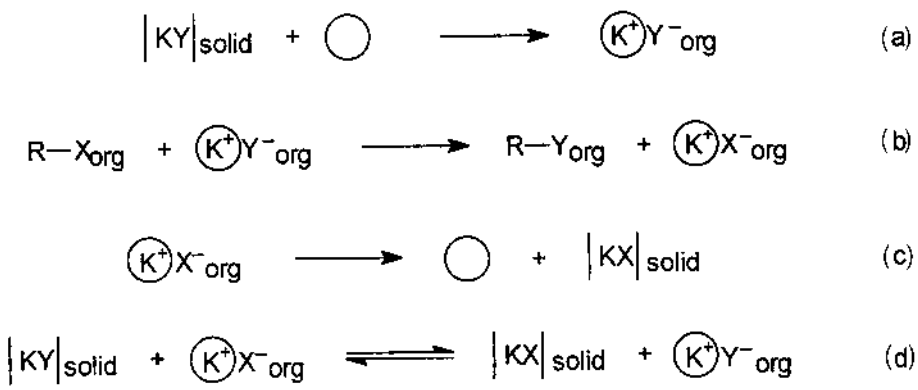

(88)

Contrary to the liquid–liquid system in which there is a rather free ion exchange equilibrium in the interfacial region and its position is governed by differences in energies of solvation and hydration, ion exchange in the liquid–solid system is much hindered by mechanical factors. Since such systems contain one liquid and two solid phases—the educt and that formed in the reaction—the ratio of ions in the organic phase should be a function of differences in solvation energies of solutes X^- and Y^- and energies of the crystalline lattices of KY and KX. However, due to mechanical difficulties in equilibration, and also to the covering of the surface of educt with a solid phase of KX, this simple picture does not reflect the real situation. This is particularly evident when taking into account an observation that the PT-catalyzed reactions in liquid–solid systems are often sensitive to the presence of small quantities of water. In many cases, when strictly anhydrous salts in meticulously dried solvents are used, PTC reactions in solid–liquid systems are hindered because of the very inefficient ion exchange. Only on addition of water in amounts below 1% can the catalytic process become efficient. On the basis of these observations a concept

of the ω-phase, which is formed by minute quantities of water on the surface of solid salt and facilitates ion-exchange processes, was formulated [99]. The most reasonable explanation of these observations appears to be that minute quantities of water in the system facilitate the exchange because they destroy the crystalline lattice on the surface of solid salts; thus, the situation is similar to the exchange in liquid–liquid systems.

Differentiation between the alternative exchange pathways [Eqs (88a,c) and (88d)], namely, via decomplexation–complexation of cations with crown ethers [Eq. (88a,c)] and via exchange of anions associated with lipophilic complexed cations, both proceeding via adsorption-desorption, is not a simple task. Since lipophilic TAA salts are equally efficient catalysts in liquid–solid PTC system as crown ethers one can suppose that both of these pathways are operating concurrently.

C. Phase Transfer Catalyzed Reactions of Anions Generated In Situ in Liquid–Liquid Systems

These reactions are mechanistically much more complicated than PT-catalyzed reactions of anions available as such, because there is an initial step of deprotonation of the anion precursors. For discussion of the mechanistic features of such processes, alkylation of carbanions in the presence of concentrated aqueous NaOH will be used as a model reaction.

The simplest hypothetical pathway of formation of the ion pairs of carbanions with TAA cations in such system appears to be the ion exchange of the TAA halide with aqueous NaOH to produce Q^+OH^-, which acts as a base in the organic phase [12]:

$$Q^+X^-_{org} + NaOH_{aq} \rightleftharpoons Q^+OH^-_{org} + NaX_{aq} \tag{89a}$$

$$\diagup\!\!\diagdown CH_{org} + Q^+OH^-_{org} \rightleftharpoons \diagup\!\!\diagdown C^-Q^+_{org} + H_2O_{org \rightarrow aq} \tag{89b}$$

$$R{-}X_{org} + \diagup\!\!\diagdown C^-Q^+_{org} \longrightarrow \diagup\!\!\diagdown C{-}R_{org} + Q^+X^-_{org} \tag{89c}$$

This process is in its first part analogous to the extraction mechanism of PT-catalyzed reactions of inorganic anions in liquid–liquid systems discussed in Section IV.A. However, due to the high hydrophilicity of hydroxide anions the ion-exchange equilibrium [Eq. (89a)] is shifted to the left and the concentration of Q^+OH^- in the organic phase is negligible and should decrease continuously because X^- anions are produced during the reaction. Since the position of the ion exchange equilibrium is unfavorable for Q^+OH^- and because of other observations it appears that this extractive mechanism does not operate and hence an alternative mechanism was proposed according to which deprotonation of CH acids takes place in the interfacial region in the direct reaction of the carbanion precursor with NaOH [7]. The carbanions generated at the interface cannot migrate into the aqueous phase because of a strong salt-out effect of the concentrated aqueous NaOH, nor into the organic phase because sodium cations are unable to leave the aqueous phase to move with carbanions into the organic phase. In the interfacial region, carbanions are hardly accessible for nonpolar reagents, show low activity, and, what is the most important, due to the very small volume of the region, their concentration averaged for the organic phase is negligible. In the presence of a TAA salt the ion exchange takes place to produce lipophilic ion pairs which migrate

into the organic phase whereas NaX enters the aqueous phase. In spite of low activity and concentration of the carbanions in the interfacial region, the ion exchange, which is diffusion controlled, proceeds at a good rate and assures the concentration of carbanions in the organic phase being a substantial fraction of that of the catalyst. Applying the definition of the interfacial region as in Section IV.A and Fig. 2 the generation of carbanions and the ion exchange responsible for formation of the lipophilic ion pairs of the carbanions with TAA cations can be presented as in Eq. (90):

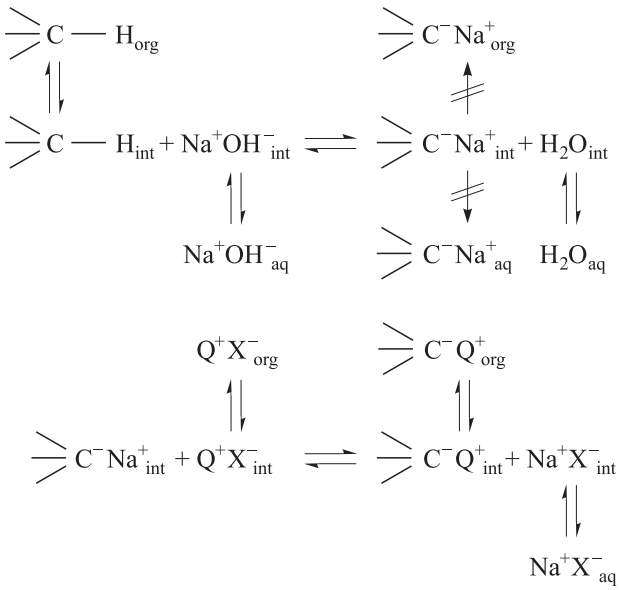

(90)

One should remember that in the interfacial region there is also ion exchange:

$$Q^+X^-_{int} + Na^+OH^-_{int} \rightleftharpoons Q^+OH^-_{int} + Na^+X^-_{int} \tag{91}$$

Although the ion pair Q^+OH^- does not migrate to the organic phase, the lipophilic ion pairs $\rightarrow C^-Q^+$ can be formed also in a direct reaction:

$$\rightarrow C{-}H_{int} + Q^+OH^-_{int} \rightleftharpoons \rightarrow C^-Q^+ + H_2O \tag{92}$$

An important specific feature of PTC reactions is the inhibitory effect of some inorganic anions, particularly iodide anions, on the catalytic process. Because of that, alkyl iodides, which are the most active alkylating agents, do not react efficiently under PTC conditions. For the PTC reactions of inorganic anions these phenomena are simply rationalized on the basis of the ion-exchange equilibrium (93), where Y^- are anions reacting in the organic phase in PTC reactions.

$$Q^+I^-_{org} + Na^+Y^-_{aq} \rightleftharpoons Q^+Y^-_{org} + Na^+I^-_{aq} \tag{93}$$

This equilibrium, governed by the hydration energies of the participating anions, is shifted to the left for the majority of Y^- because of the low hydration energy of iodide anions. As a consequence, only a small fraction of the TAA cations of the catalyst in the organic phase is acompanied by Y^- anions and thus their concentration is negligible.

This rationalization is not sufficient for PTC reactions of carbanions carried out in the presence of concentrated solutions of NaOH, because carbanions are, as a rule, more lipophilic than iodide anions. Decrease of the equilibrium concentration of carbanions in

the PTC systems by iodide anions is connected with inhibition of the interfacial deprotonation of the carbanion precursors. Iodide anions, due to their low hydration energy, occupy mostly the interfacial region between the organic phase and concentrated NaOH solution where the deprotonation takes place. One can assume that the fraction of the surface occupied by the carbanions and iodide anions in the equilibrated systems is a function of acidity of the carbanion precursors; thus, the inhibitory effect of iodide anions on PTC reactions of carbanions depends on the acidity of the carbanion precursors [100].

Since deprotonation is a fast process, differentiation between two mechanisms, i.e., extractive [Eq. (89)] and interfacial [Eq. (90)], is not a simple task. It can be based on two criteria: experimental verification that extraction of hydroxide anions into the organic phase is not necessary for the reaction to proceed and that indeed carbanions are formed in the interfacial region in the absence of the TAA salts. It should be, however, stressed that operation of one of these mechanisms can depend on the particular case and that both of them can operate concurrently. The best system for clarification of the first criterion are reactions of trihalomethyl carbanions and dihalocarbenes. It is well established that dihalocarbenes react rapidly with water and hydroxide anions. In fact, according to the established mechanism, alkaline hydrolysis of chloroform in aqueous NaOH proceeds via a multistep reaction [101]:

$$\begin{aligned} CHCl_3 + OH^- &\overset{\text{fast}}{\rightleftharpoons} \overline{C}Cl_3 + H_2O \\ \overline{C}Cl_3 &\overset{\text{slow}}{\rightleftharpoons} CCl_2 + Cl^- \\ CCl_2 &\xrightarrow[OH^-, H_2O]{\text{fast}} CO + HCO_2^- + Cl^- \end{aligned} \tag{94}$$

Because of these relationships between rates shown in Eq. (94) all traditional methodologies of generation and reactions of dihalocarbenes require strictly anhydrous conditions: flame dried glassware, meticulously dried solvents, etc. [102]. In spite of that, PTC generation and reactions of dihalocarbenes proceed very efficiently, with a negligible degree of hydrolysis of the carbenes despite the fact that the reactions are carried out in the presence of a great excess of aqueous NaOH [12]. These results indicate that in the PTC systems there is very limited contact between dihalocarbenes and water and hydroxide anions, and can be convincingly rationalized in terms of the interfacial mechanism. Thus, in the two-phase system—chloroform with alkene (the carbene acceptor) and concentrated aqueous NaOH—deprotonation of chloroform in the interfacial region produces trichloromethyl anions as sodium salts, which enter ion exchange with the TAA salt to produce lipophilic ion pairs. These ion pairs enter the organic phase where they dissociate reversibly to produce dichlorocarbene, which in turn add to alkene giving a *gem*-dichlorocyclopropane derivative. Thus, the carbene is in fact formed in an anhydrous medium that does not contain hydroxide anions or water and hence its hydrolysis is minimal.

Trichloromethyl carbanions can dissociate into dichlorocarbenes also into the interfacial region where they hydrolyze, giving chloride and formate anions. However, in the system with and without the catalyst this hydrolysis is a slow process because the chloride anions produced, being less hydrophilic than hydroxide anions, occupy preferentially the interfacial region, thus shifting equilibrium (95) to the left:

$$\overline{C}Cl_3 \rightleftharpoons CCl_2 + Cl^- \tag{95}$$

This picture is supported by two independent observations. Addition of PTC-generated dichlorocarbene to alkenes is accompanied by a small degree of hydrolysis. This hydrolysis, contrary to expectations based on a stoichiometry approach, proceeds mostly at the beginning of the reaction, when there is a great excess of alkene over generated dichlorocarbene, not at the end, when excess of alkene is negligible [103]. It means that when chloride anions are present in the system in small quantities, hydrolysis of carbene is the dominant process, whereas accumulation of chloride anions produced during the formation and hydrolysis of carbene prevent its further hydrolysis. Indeed, when sodium hydroxide saturated with sodium chloride was used for generation of dichlorocarbene hydrolysis was substantially diminished.

Generation of dichlorocarbene in the interfacial region is independently confirmed by the observation that trialkylamines, e.g., triethylamine or tributylamine, are efficient PT catalysts for the generation and reactions of dihalocarbenes [104]. It was shown that trialkylamines, being very active nucleophiles, react with carbene in the interfacial region to produce ammonium ylides, which enter the organic phase where they act as a base, deprotonating chloroform and thereby producing carbene in the organic phase [105]:

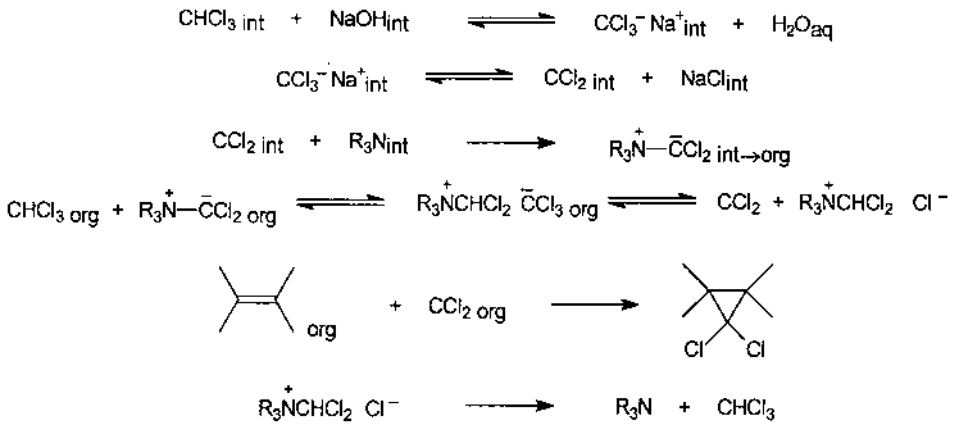

(96)

Another piece of experimental evidence against an extraction mechanism for PTC generation and reaction of dichlorocarbene is the observation that attempts to use ion-pair extraction methodology, namely, executing the process in a two-phase system, viz., chloroform and concentrated aqueous NaOH in the presence of an equimolar amount of tetrabutylammonium hydrogen sulfate, which assures transfer of Q^+OH^- into the organic phase, result in dominant, rapid hydrolysis of dichlorocarbene. Its addition to alkene, producing *gem*-dichlorocyclopropane, was in such an experiment a minor reaction.

Without PT catalysts, carbanions generated in the interfacial region in the two-phase system C–H acid–concentrated aqueous NaOH do not react with organic electrophilic partners, e.g., alkyl halides, because their concentration in the organic phase is negligible whereas in the interfacial region they are hardly accessible and in low quantities. The first reason—negligible concentration of the carbanions in the organic phase was verified experimentally by direct measurement of carbanions and sodium cations concentration.

Since in the interfacial region carbanions are of low activity and low quantity, they can react only with very active electrophiles. Thus, formation of lipophilic ion pairs via ion exchange with TAA salts, which is a diffusion-controlled process, proceeds efficiently as a step in the PTC reactions. The carbanions in the interfacial region can also react with other very active electrophiles such as aldehydes. Since addition of carbanions to aldehydes is a reversible process, completion of the reaction in the interfacial region requires further rapid

transformation of the initial aldol-type adducts into stable products. For example, when the Reissert compound and benzaldehyde in a small amount of acetonitrile are stirred with concentrated aqueous NaOH, rapid formation of 1-isoquinolylphenylcarbinol benzoate takes place:

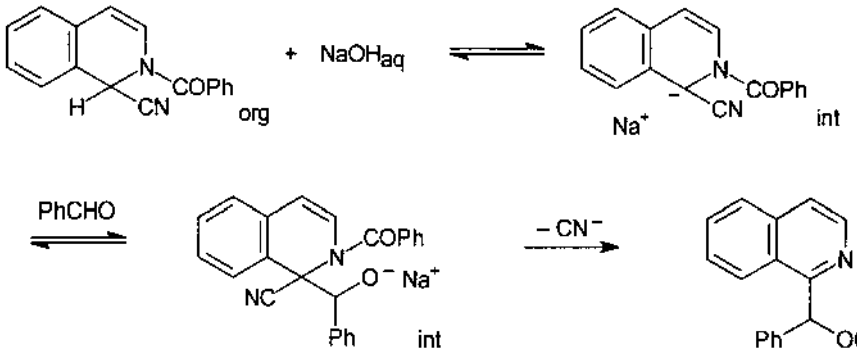

(97)

89% (Ref. 106)

Similarly, carbanions of α-halonitriles generated at the interface with concentrated aqueous NaOH react with benzaldehyde to produce the corresponding chlorohydrine anions, which, being in the interfacial region, undergo rapid intramolecular substitution giving cyano-oxiranes [107]. This reaction is discussed in more detail on pp. 193–194.

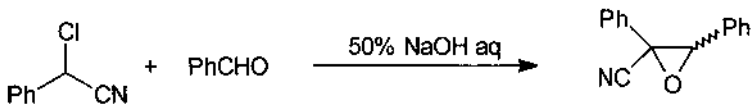

(98)

(Ref. 107)

A very convincing piece of evidence for the interfacial generation and reaction of carbanions provides addition of trichloromethyl carbanions to *N*-alkylpyridinium salts when the latter in chloroform solution are stirred with concentrated aqueous NaOH. Treatment of a solution of *N*-alkylpyridinium salt in chloroform with concentrated aqueous NaOH results in fast addition of trichloromethyl anions in positions 2 and 4 of the pyridinium ring, giving the corresponding adduct in high yield. On the other hand, treatment of these salts in toluene or chlorobenzene with concentrated aqueous NaOH results in rapid decomposition, obviously via formation of unstable adducts of hydroxide anions. These results exclude formation of Q^+OH^- type ion pairs as a path for generation of trichloromethyl anions [108].

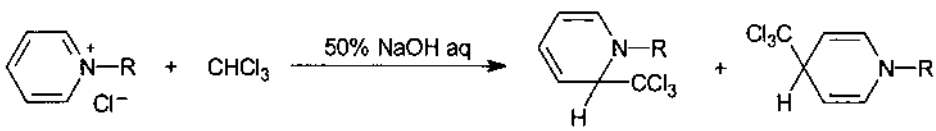

(99)

R = Ph_2CH, 92%

Even alkylation of carbanions can proceed in the interfacial region, provided that highly active alkylating agents are used. Thus, vigorous stirring of phenylacetonitrile and alkyl iodide with aqueous NaOH at slightly elevated temperature resulted in formation of the alkylated products, whereas corresponding alkyl bromides do not react under these conditions [109]:

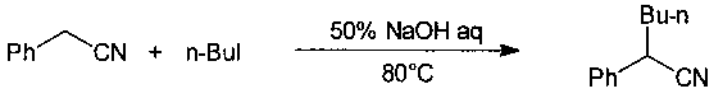

70% (Ref. 109) (100)

It should be stressed that, on the other hand, the catalytic process proceeds efficiently with alkyl bromides whereas PT-catalyzed alkylation with alkyl iodides is inhibited by the iodide ions produced during the reaction. The interfacial alkylation of phenylacetonitrile with alkyl iodides is limited by the rate of transfer of iodide anions from the interface to the aqueous phase.

The carbanions generated by deprotonation at the phase boundary are located in the interfacial region, which is essentially an anisotropic medium; thus, they should have preferential space orientation. In such a situation the stereochemical course of some reactions should be different from analogous reactions proceeding in isotropic solution.

Indeed, the Darzens condensation of phenylchloroacetonitrile with benzaldehyde proceeds efficiently under PTC conditions, giving predominantly the *trans* isomer of 2,3-diphenyl-2-cyanooxirane, whereas this reaction executed without PT catalyst, thus in the interfacial region, produced a mixture of *cis* and *trans* isomers in which the former was the major component [107]:

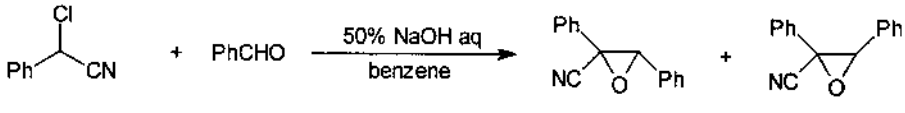

with TEBA	92	:	8
without TEBA	32	:	68

(101)

Cyclization of the intermediate isomeric chlorohydrine anions is slower than reversible addition of the carbanions to the carbonyl group: hence, there is an equilibrium between diastereomeric (erythro and threo) chlorohydrine anions. Thus, the ratio of *cis* and *trans* stereoisomers is governed by the energies of the isomeric transition states of the cyclization reaction. In the catalytic process, which occurs in the isotropic homogeneous phase, the transition state **I** is energetically preferred due to smaller steric interaction, leading to the *trans* isomer. At the interface, additional stabilization of the isomeric transition state **II** results in preferential formation of the *cis* isomer:

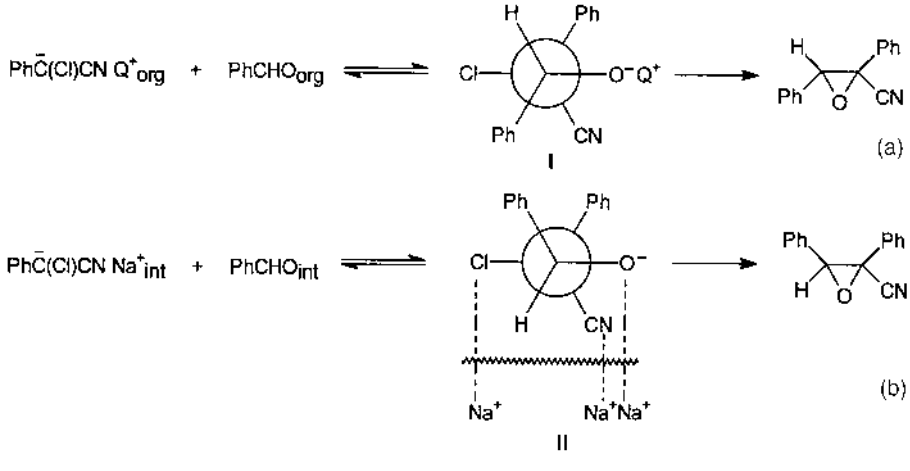

(102)

The picture of the interfacial process presented in Eq. (102b) is somewhat oversimplified; the process occurs in the anisotropic interfacial region in which additional stabilization of **II** is due to the gradient of concentration of Na^+ cations.

Similar effects operate in the two-phase reaction of phenylchloroacetonitrile with acrylonitrile, which gives dicyanophenylcyclopropane (*cis* and *trans* isomers). The interfacial process results in preferential formation of the *cis* isomer [110]:

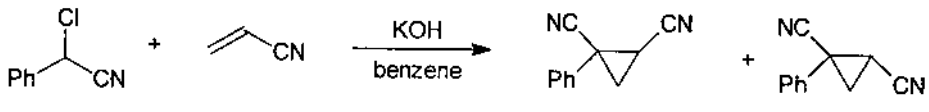

(103)

with TEBA	51	:	49
without TEBA	90	:	10

The kinetic picture of PT-catalyzed reactions of carbanions, e.g., alkylation, is very complicated because the observed rate is a superposition of chemical and transport processes: deprotonation, formation of ion pairs via ion exchange in the interfacial region, reactions of carbanions with alkyl halides in the organic phase, transport of the ion pairs from and to the interfacial region, etc., Because of that, numerous kinetic studies of PT-catalyzed alkylation of carbanions—although providing valuable practical data on the processes studied under particular conditions—do not contribute to an understanding of the general mechanistic picture, and determined thermodynamic characteristics of such processes are often meaningless. In a few papers reporting kinetic studies of PT-catalyzed alkylation and interfacial processes, executed with proper precision, convincing evidence for interfacial generation of carbanions is given. For instance, detailed studies of the rate of PTC ethylation of phenylacetonitrile revealed inter alia that it increases continuously with increasing of rate of stirring—confirming the crucial role of interfacial processes [111)]. The kinetics of interfacial alkylation of phenylacetonitrile was thoroughly studied [112].

Thus, a number of independent criteria confirm that the crucial step of PTC reactions of carbanions, namely, deprotonation of the carbanion precursors, takes place in the interfacial region. This process is facilitated by the TAA salts because ion pairs produced by the carbanions with TAA cations migrate from the interfacial region to the bulk of the organic phase. When TAA salts are absent, the carbanions stay in the adsorbed state, able to react only with very active electrophiles.

D. Phase Transfer Catalyzed Reactions of Anions Generated In Situ in Liquid–Solid Systems

Use of solid anhydrous potassium carbonate for generation of carbanions and other organic anions in liquid-solid PT catalyzed systems offers particular advantages. Contrary to common opinion anhydrous K_2CO_3 is a relative strong base; simultaneously it does not promote side reactions such as hydrolysis. Thanks to those properties it can be used for many purposes when more aggressive reagents, e.g., NaOH or KOH, are useless.

In the liquid–solid PT-catalyzed systems stronger bases, e.g., solid NaOH, KOH, or NaH, can also be used. Since finely grinded alkali hydroxides exert a tendency for agglomeration, particularly by water generated in the deprotonation reaction, further reactions are thus mechanically hindered; for practical reasons mixtures of powdered K_2CO_3 and

grinded NaOH are recommended. Mechanistic features of the operation of PTC in these liquid–solid systems are similar to those with K_2CO_3. The proton abstraction from the carbanion precursors takes place at the solid surface, producing carbanions in the adsorbed state. Further ion exchange with the catalyst Q^+X^- dissolved in the organic phase proceeds at the surface, producing soluble $\rightarrow C^-Q^+$ ion pairs and depositing a new solid phase of NaX. This new phase can decrease the accessibility of the basic surface.

The eventual alternative extraction mechanism in such systems can be excluded on the basis of experimental observations and also a priori reasoning. Thus, when a suspension of K_2CO_3 in a moderately polar solvent, e.g., acetonitrile, is treated with a TAA salt no basic anions are transferred into the organic solution. Since strongly basic carbonate dianions are much less lipophilic than bicarbonate anions, which are much weaker bases, and only the latter ions could eventually enter the organic solution, transfer of these could not be the pathway for deprotonation of the carbanion precursors.

Also in a carbanion precursor/K_2CO_3 system there is no transfer of basicity (potassium salt of the carbanion) to the organic phase. Only when the carbanion precursor is treated with K_2CO_3 in the presence of a PT catalyst–TAA salt, carbanions are transferred into the organic phase. Their concentration in the organic phase is a fraction of the concentration of the TAA salt. On this basis the following picture can be proposed:

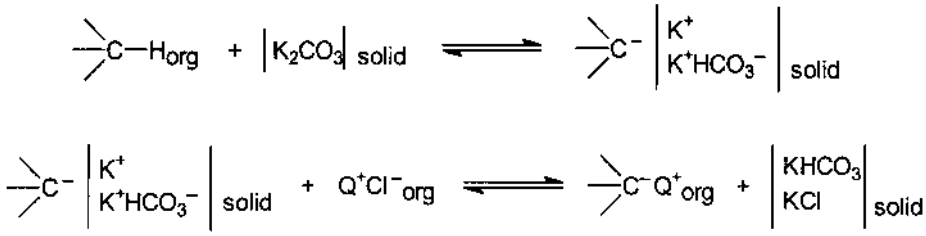

(104)

V. SUMMARY

In this chapter the general concept of PTC, its basic mechanistic features, especially the role of interfacial processes, some typical examples, and major benefits and advantages are presented. It should be stressed that the scope of application of this methodology is much larger—it can be used for many processes that were not mentioned here. Particular attention was directed to the role of interfacial processes in PT-catalyzed reactions. There is a large variety of systems in which organic reactions can be performed: homogeneous, pseudohomogeneous, and heterogeneous—in the latter two, interfacial processes are of crucial importance. Among these systems PTC occupies a special position because it comprises specific features of interfacial heterogeneous processes with reactions proceeding in homogeneous systems—combining advantages offered by both these otherwise different types of systems. In this connection it is necessary to understand relations between PTC and other systems such as micellar catalysis and reactions in microemulsions in which processes at liquid–liquid interfaces are of crucial importance. Although there is apparent similarity between these processes the basic principle of operation, mechanistic features, and field of application differ substantially.

The basic feature of PTC—catalytic action of TAA salts, which are often surface-active agents and a strong influence on the size of the interfacial region (degree of disper-

sion of phases) in the effectiveness of PTC reactions suggests that there is a strong similarity or even analogy of PTC with micellar catalysis and reactions in microemulsions. In spite of these apparent similarities the basic principles of operation of these systems are different. Since both of these systems, micellar catalysis and reactions in microemulsions, are subjects of separate chapters in this volume only principal differences in the way of operation between these systems and PTC will be shown here.

Micellar catalysis in reactions of nonpolar organic compounds with ionic reactants is based on dissolution of the organic compounds in aqueous solutions containing surface-active agents, e.g., alkyltrimethylammonium salts, in a concentration exceeding the critical micelle concentration. In such systems the organic compounds are located inside the cationic micelles and thus their reactions with inorganic anions are facilitated. Since the concentration of the reacting anions at the surface of the cationic micelles (in the so-called Stern layer) is higher than in the bulk of the solution, such processes are accelerated [113].

Microemulsions are thermodynamically stable systems in which organic nonpolar solvents are dispersed in water (oil in water) or vice versa (water in oil), stabilized by surfactants [114]. Due to the very small size of droplets (10–20 nm) the systems appear as homogeneous and the ratio of the interfacial area to volume of the bulk phase is very large. Such systems behave as solvents able to dissolve inorganic salts and organic nonpolar compounds. Although in such solutions the reactants, i.e., inorganic salts and organic compounds, are located correspondingly in aqueous and organic phase, thanks to the extremely large interfacial area chemical reactions between these partners proceed at a good rate [115]. Interestingly, a typical PT catalyst accelerates reactions in microemulsions [116].

This very short description of the basic principles of micellar catalysis and reactions in microemulsions indicate that contrary to PTC conditions in these systems one cannot work with high concentration of the reactants. There are also substantial limitations concerning the kind of reacting species that could be generated and introduced into the reaction in such systems. There is no question that isolation of products of chemical reactions carried out in these systems is more complicated than related reactions executed using PTC. Thus, in spite of very interesting new possibilities created by these phenomena only PTC can be considered as a general methodology of organic synthesis of great practical value.

The catalytic action of lipophilic TAA salts—PT catalysts consists in continuous interfacial formation of lipophilic ion pairs with inorganic or organic anions and transfer of them into an organic phase where further processes take place. In such systems most of the reactions can be carried out without organic solvents or in highly concentrated solutions. Thanks to that, PTC is of great practical value in organic synthesis and have found wide application in the chemical industry.

In conclusion, the basic features of PTC should be summarized:

Since in PTC reactions concentration of the reacting anions in the organic phase cannot exceed that of the catalyst, in a great majority of cases they can be carried out without an organic solvent. Indeed, when the starting materials and products are liquid they can act as solvents for the reacting species when used neat and form the organic phase, into which the reacting anions are introduced by the catalyst. Taking into account that the catalyst is used in $\simeq 1\%$ molar amounts, the reactions proceed in a diluted system with respect to the reacting anions, although no solvent is used. Since anions associated with TAA cations exhibit high activity and since the concentration of the partner reacting with the anions (when it is used neat) is high, the reactions proceed at good rates. Due to this situation, PTC reactions usually proceed in high yields and selectivity, whereas unde-

sired side-products are produced in low quantities. Use of this methodology instead of traditional technologies for the industrial process of organic synthesis assures significant economical advantages and provides substantial benefits for the environment.

In order to exemplify the benefits and advantages of the PTC methodology over traditional techniques direct comparison is made of the alkylation of phenylacetonitrile, the first industrial application of this technique.

Traditional technologies for this transformation are multistep processes. First, the starting nitrile dissolved in a strictly anhydrous solvent (e.g., toluene) is treated with a strong a base such as $NaNH_2$ or NaH to produce an intermediate carbanion in the form of its salt with Na^+. This preformed sodium derivative (carbanion) treated with an appropriate alkyl halide gives the final product:

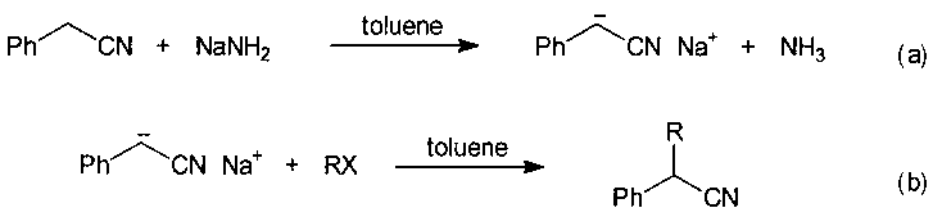

(105)

Isolation of the product needs treatment of the mixture with water and removal of the solvent, which should be subsequently regenerated. The overall process needs large investment—because large quantities of anhydrous solvents are used—and safety requirements due to work with $NaNH_2$ or NaH. The necessity of recovering solvents consumes much energy and large quantities of wastes are produced. Moreover, selectivity of the reaction in the sense of monoalkylation is low under these conditions; thus, the product is contaminated, and ultimate yield is not very high.

The same process executed using PTC technology consists of vigorous stirring of neat $PhCH_2CN$ and R–X with 50% aqueous NaOH and $\simeq$ 1% molar catalyst, a TAA salt:

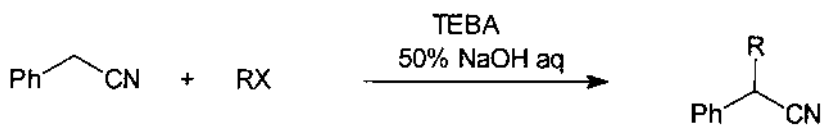

(106)

It proceeds with moderate exothermic effect and on completion the product is isolated just by simple separation of the phases, eventually on slight dilution of the aqueous phase with water. This methodology needs much less investment, consumes much less energy, and wastes are produced to a much less extent, particularly taking into account that, due to the high selectivity of the process, the yields of the final products are usually much higher than when traditional methodology is used.

One should stress that the first industrial application of this "green" technology for alkylation of phenylacetonitrile was in a Polish pharmaceutical factory in the early 1960s; it was subsequently used in many other companies.

At present, there are hundreds of industrial applications of PTC for a variety of processes of organic synthesis. These technologies always require less investment, consume less energy, and generate much less industrial waste as compared to the traditional ones. It is obvious that all measures that save energy and investment offer directly or indirectly substantial benefits to the environment. Of great importance is the direct effect—genera-

tion of a smaller volume of waste. The major advantages of PTC in industrial applications are listed below:

- Elimination of organic solvents
- Elimination of dangerous, inconvenient, and expensive reactants such as NaH, $NaNH_2$, *t*-BuOK, R_2NLi, etc., and use of NaOH, KOH, K_2CO_3
- High reactivity and selectivity of the active species
- High yields and purity of products
- Simplicity of the procedure
- Low investment cost
- Low energy consumption
- Possibility of mimicking counter-current process
- Minimization of industrial wastes

These numerous and important advantages of PTC are easily recognized in the examples given. One should stress that when a new synthetic process is developed, the possibility of applying PTC should be considered first. Due to the specific features of PTC and its advantages presented above it should be considered as a most efficient and general green technology [117].

ABBREVIATIONS AND ACRONYMS

Aliquat	methyltrioctylammonium chloride (technical grade); commercial names: Aliquat 336, Adogen 464
TAA	tetraalkylammonium
TBAB	tetrabutylammonium bromide
TBAC	tetrabutylammonium chloride
TBAHS	tetrabutylammonium hydrogensulfate
TBAI	tetrabutylammonium iodide
TEBA	benzyltriethylammonium chloride
TOMAHS	methyltrioctylammonium hydrogensulfate

REFERENCES

1. EV Dehmlow, SS Dehmlow. Phase Transfer Catalysis. 3rd ed. Weinheim: Verlag Chemie, 1993.
2. CM Starks, CL Liotta, M Halpern. Phase Transfer Catalysis: Fundamentals, Applications and Industrial Perspectives. New York: Chapman & Hall, 1994.
3. Y Sasson, R Neumann, eds. Handbook of Phase Transfer Catalysis. London: Blackie Academic & Professional, 1997.
4. WE Keller. Phase-Transfer Reactions, Fluka Compendium. Stuttgart, New York: Georg Thieme Verlag, vol. I, 1986; vol. II, 1987; vol. III, 1992.
5. RA Jones. Quaternary Ammonium Salts: Their Use in Phase-Transfer Catalysis. Academic Press, 2001.
6. Y Goldberg. Phase Transfer Catalysis, Selected Problems and Applications. Switzerland: Gordon & Breach Science, 1992.
7. M Mąkosza. Pure Appl Chem 43:439–462, 1975.
8. M Mąkosza, M Fedoryński. Adv Catal 35:375–422, 1987.
9. J Jarrousse. C R Hebd Seances Acad Sci Ser C 232:1424–1426, 1951.

10. T Urbański, C Bełżecki, J Lange, M Mąkosza, A Piotrowski, B Serafinowa, H Wojnowska. Polish Patent: 46030, 1962.
11. M Mąkosza, B Serafinowa. (a) Roczn Chem 39:1223–1231, 1965; Chem Abstr 64:12595h, 1966. (b) Roczn Chem 39:1401–1408, 1965; Chem Abstr 64:17474g, 1966. (c) Roczn Chem 39:1595–1602, 1965; Chem Abstr 64:17475c, 1966. (d) Roczn Chem 39:1799–1803, 1965; Chem Abstr 64:17475e, 1966. (e) Roczn Chem 39:1805–1810, 1965; Chem Abstr 64:17475g, 1966. (f) Roczn Chem 40:1647–1655, 1966; Chem Abstr 66:94792x, 1967. (g) Roczn Chem 40:1839–1848, 1966; Chem Abstr 66:115435a, 1967.
12. M Mąkosza, M Wawrzyniewicz. Tetrahedron Lett 4659–4662, 1969.
13. CM Starks. J Am Chem Soc 93:195–199, 1971.
14. F Montanari, S Quici, S Banfi. In: DR Reinhoudt, ed. vol. 10. Comprehensive Supramolecular Chemistry. Oxford: Elsevier, 1996, pp 389–416.
15. D Albanese, D Landini, A Maia, M Penso. Ind Eng Chem Res 40:2396–2401, 2001.
16. M Mąkosza, M Cieślak, E Grochowski, A Grembowicz, D Anioł. Przemysł Chem 57:299–302, 1978; Chem Abstr 89:108568t, 1978.
17. J Royer, H-P Husson. J Org Chem 50:670–673, 1985.
18. WP Reeves, MR White, RG Hilbrich, LL Biegert. Synth Commun 6:509–514, 1976.
19. Y Nakajima, R Kinishi, J Oda, Y Inouye. Bull Chem Soc Jpn 50:2025–2027, 1977.
20. D Landini, F Montanari, F Rolla. Synthesis 428–430, 1974.
21. CL Liotta, HP Harris, J Am Chem Soc 96:2250–2252, 1974.
22. M Mąkosza, R Bujok. Tetrahedron Lett 43:2761–2764, 2002.
23. P Vinczer, L Nowak, C Szantay. Org Prep Proc Int 24:349–351, 1992.
24. Y Kimura, SL Regen. J Org Chem 48:1533–1534, 1983.
25. MD Rozwadowska. Tetrahedron 41:3135–3140, 1985.
26. JV Cooney, GW Mushrush, R Hazlett. Org Prep Proc Int 17:60–62, 1985.
27. FL Cook, CW Bowers, CL Liotta. J Org Chem 39:3416–3418, 1974.
28. DG Lee, SE Lamb, VS Chang. Org Synth Coll VII: 397–400, 1990.
29. K Sato, M Aoki, M Ogawa, T Hashimoto, R Noyori. J Org Chem 61:8310–8311, 1996; K Sato, M Aoki, M Ogawa, T Hashimoto, D Panyella, R Noyori. Bull Chem Soc Jpn 70:905–915, 1997.
30. K Sato, M Aoki, J Takagi, R Noyori. J Am Chem Soc 119:12386–12387, 1997.
31. For review see: S Schrader, EV Dehmlow. Org Prep Proc Int 32:123–152, 2000.
32. J-M Melot, F Texier-Boullet, A Foucaud. Synthesis 558–560, 1988.
33. F Camps, J Coll, J Guitart. Tetrahedron 42:4603–4609, 1986.
34. M Mąkosza, A Jończyk. Org Synth Coll VI: 897–900, 1988.
35. M Mąkosza. Tetrahedron 24:175–181, 1968.
36. M Fedoryński, E Widecka. In preparation.
37. M Mąkosza. Tetrahedron Lett 4621–4624, 1966.
38. A Jończyk, K Bańko, M Mąkosza. J Org Chem 40:266–267, 1975.
39. Y Masuyama, Y Ueno, M Okawara. Tetrahedron Lett: 2967–2970, 1976; M Yanagawa, O Moriya, Y Watanabe, Y Ueno, T Endo. Bull Chem Soc Jpn 61:2203–2204, 1988.
40. A Jończyk, B Serafin, M Mąkosza. Tetrahedron Lett 1351–1352, 1971; A Jończyk, B Serafin, M Mąkosza. Roczn Chem 45:1027–1039, 1971; Chem Abstr 75:109997e, 1971.
41. M Fedoryński, K Wojciechowski, Z Matacz, M Mąkosza. J Org Chem 43:4682–4684, 1978.
42. J Goliński, M Mąkosza. Synthesis 823–825, 1978.
43. H Bouda, ME Borredon, M Delmas, A Gaset. Synth Commun 17:503–513, 1987.
44. GA Russel, M Mąkosza, J Hershberger. J Org Chem 44:1195–1199, 1979.
45. A Jończyk, A Konarska. Synlett 1085–1087, 1999.
46. M Umiński, M Jawdosiuk. Polish J Chem 57:67–73, 1983; Chem Abstr 101:7073p, 1984.
47. M Mąkosza, J Przyborowski, R Klajn, A Kwast. Synlett 1773–1774, 2000.
48. M Mąkosza, J Czyżewski, M Jawdosiuk. Org Synth Coll VI: 940–943, 1988.
49. A Jończyk, T Kuliński, M Czupryniak, P Balcerzak. Synlett 639–641, 1991.
50. A Jończyk, AH Gierczak. Synthesis 962–964, 1998.

51. M Mąkosza. Tetrahedron Lett 673–676, 1969; M Mąkosza. In: ME Halpern, ed. Phase Transfer Catalysis, Mechanisms and Syntheses. ACS Symposium Series 659, Washington, DC: American Chemical Society, 1996 pp 41–51.
52. M Jawdosiuk, I Kmiotek-Skarzynska. Polish J Chem 53:2259–2266, 1979; Chem Abstr 93:132191t, 1980.
53. M Jawdosiuk, M Ludwikow, B Bednarska. Polish J Chem 53:805–810, 1979; Chem Abstr 91:107397r, 1979.
54. J Arekion, M Delmas, A Gaset. Biomass 3:59–65, 1983; Chem Abstr 98:89955j, 1983.
55. GV Kryshtal, GM Zhdankina, EP Serebryakov. Izv Akad Nauk Ser Khim 2126–2129, 1993; Chem Abstr 123:256282f, 1995.
56. M Mąkosza, M Fedoryński. Synthesis 274–276, 1974.
57. E Abele, E Lukevics. Org Prep Proc Int 31:359–377, 1999.
58. A Jonczyk, A Kwast, M Mąkosza. J Org Chem 44:1192–1194, 1979.
59. M Mąkosza, A Kwast, E Kwast, A Jonczyk. J Org Chem 50:3722–3727, 1985.
60. A Jonczyk, T Radwan-Pytlewski. Chem Lett 1557–1560, 1983.
61. A Zwierzak. Synthesis 507–509, 1975.
62. W Lasek, M Mąkosza. Synthesis 780–782, 1993.
63. D Seebach, H-O Kalinowski, W Langer, G Crass, E-M Wilka. Org Synth Coll VII: 41–50, 1990.
64. W Ye, X Liao. Synthesis 986–988, 1985.
65. C Malanga, R Pagliai, R Menicagli. Synth Commun 20:2821–2826, 1990.
66. V Bocchi, G Casnati, A Dossena, F Villani. Synthesis 414–416, 1976.
67. D Bogdal, K Jaskot. Synth Commun 30:3341–3352, 2000.
68. A Jonczyk, Z Ochal, M Mąkosza. Synthesis 882–883, 1978.
69. A Koziara, S Zawadzki, A Zwierzak. Synthesis 527–529, 1979.
70. I Crossland. Org Synth Coll VII: 12–15, 1990.
71. MG Banwell, JE Harvey, DCR Hockless, AW Wu. J Org Chem 65:4241–4250, 2000.
72. G Boche, DR Schneider. Tetrahedron Lett 4247–4248, 1975.
73. KN Shavrin, IV Krylova, IB Shvedova, GP Okonnishnikova, E Dolgy, OM Nefedov. J Chem Soc, Perkin Trans 2 1875–1881, 1991.
74. T Sasaki, S Eguchi, T Ogawa. J Org Chem 39:1927–1930, 1974.
75. K Steinbeck. Chem Ber 112:2402–2412, 1979.
76. GW Gokel, RP Widera, WP Weber. Org Synth Coll VI: 232–235, 1988.
77. M Mąkosza, A Kacprowicz. Roczn Chem 49:1627–1631, 1975; Chem Abstr 84:43265s, 1976.
78. P Balcerzak, A Jonczyk. J Chem Res (S) 200–201, 1994.
79. P Balcerzak, M Fedoryński, A Jonczyk. J Chem Soc, Chem Commun 826–827, 1991.
80. M Mąkosza, W Lasek. Tetrahedron 47:2843–2850, 1991; M Mąkosza, A Chesnokov. Tetrahedron 56:3553–3558, 2000.
81. LK Sydnes, E Bakstad. Acta Chem Scand 50:446–453, 1996; LK Sydnes. Eur J Org Chem 3511–3518, 2000.
82. L Cassar. Ann NY Acad Sci 333:208–224, 1980; H Alper. Adv Organomet Chem 19:183–211, 1981; H Alper. Fundam Res Homogen Catal 4:79–95, 1984; EV Dehmlow. In: B Cornils, WA Herrmann, eds. Aqueous-Phase Organometallic Catalysis, Concepts and Applications. Weinheim: Wiley-VCH, 1998, pp 207–221; Y. Goldberg. Phase Transfer Catalysis, Selected Problems and Applications. Gordon & Breach Science, 1992, pp 127–259.
83. M Salisova, H Alper. Angew Chem, Int Ed Engl 18:792, 1979.
84. DH Gibson, W-L Hsu, D-S Lin. J Organomet Chem 172: C7-C12, 1979.
85. A Alemagna, P Del Buttero, C Gorini, D Landini, E Licandro, S Maiorana. J Org Chem 48:605–607, 1983.
86. KR Januszkiewicz, H Alper. Organometallics 2:1055–1057, 1983.
87. H Alper, H Des Abbayes. J Organomet Chem 134: C11-C14, 1977.
88. T Jeffery. J Chem Soc, Chem Commun 1287–1289, 1984.
89. JT Rao, TB Rao. J Indian Inst Sci 74:373–400, 1994; Chem Abstr 123:55043e, 1995.

90. A Nelson. Angew Chem Int Ed Engl 38:1583–1585, 1999; MJ O'Donnell. In: I Ojima, ed. Catalytic Asymmetric Synthesis, 2nd ed. Weinheim: Wiley-VCH, 2000, pp 727–755; MJ O'Donnell. Aldrichim Acta 34:3–15, 2001; K Kacprzak, J Gawroński. Synthesis 961–998, 2001. PI Dalko, L Moisan. Angew Chem Int Ed Engl 40:3726–3734, 2001.
91. U-H Dolling, P Davis, EJJ Grabowski. J Am Chem Soc 106:446–447, 1984.
92. F-Y Zhang, EJ Corey. Org Lett 3:639–641, 2001.
93. B Lygo, DCM To. Tetrahedron Lett 42:1343–1346, 2001.
94. EJ Corey, F Xu, MC Noe. J Am Chem Soc 119:12414–12415, 1997.
95. T Ooi, M Kameda, K Maruoka. J Am Chem Soc 121:6519–6520, 1999.
96. CM Starks, RM Owens. J Am Chem Soc 95:3613–3617, 1973.
97. W Lasek, M Mąkosza. J Phys Org Chem 6:412–420, 1993.
98. DJ Sam, HE Simmons. J Am Chem Soc 96:2252–2253, 1974.
99. CL Liotta, EM Burgess, CC Ray, ED Black, BE Fair. In: CM Starks, ed. Phase Transfer Catalysis: New Chemistry, Catalysts and Applications, ACS Symposium Series 326. Washington, DC: American Chemical Society, 1987, pp 15–23.
100. M Mąkosza, A Chesnokov. In preparation.
101. J Hine. Divalent Carbon, New York: Roland Press Co., 1964.
102. WE Parham, EE Schweizer. Org Reactions 13:55–90, 1963.
103. M Fedoryński. Generation and some reactions of trihalomethyl anions—dihalocarbene precursors. PhD dissertation, Warsaw University of Technology, Poland, 1974.
104. K Isagawa, Y Kimura, S Kwon. J Org Chem 39:3171–3172, 1974.
105. M Mąkosza, A Kacprowicz, M Fedoryński. Tetrahedron Lett 2119–2122, 1975.
106. A Jonczyk. Bull Acad Pol Sci Ser, Sci Chim 22:849–853, 1974; Chem Abstr 82: 139936w, 1975.
107. A Jonczyk, A Kwast, M Mąkosza. J Chem Soc, Chem Commun 902–903, 1977.
108. M Mąkosza, I Krylova. Tetrahedron 55:6395–6402, 1999.
109. M Mąkosza, E Bialecka. Tetrahedron Lett 183–186, 1977.
110. A Jonczyk, A Kwast, M Mąkosza. Tetrahedron Lett 541–544, 1979.
111. R Solaro, S D'Antone, E Chiellini. J Org Chem 45:4179–4183, 1980.
112. CS Sawarkar, VA Juvekar. Ind Eng Sci Res 35:2581–2589, 1996.
113. JH Fendler, EJ Fendler. Catalysis in Micellar and Macromolecular Systems. New York: Academic Press, 1975.
114. P Kumar, KL Mittal, eds. Handbook of Microemulsion Science and Technology. New York: Marcel Dekker, 1999.
115. R Schomaecker. J Chem Res (M) 810–833, 1991; FM Menger, AR Elrington. J Am Chem Soc 113:9621–9624, 1991.
116. M Häger, K Holmberg. Tetrahedron Lett 41:1245–1248, 2000.
117. M Mąkosza. Pure Appl Chem 72:1399–1403, 2000.

9

Liquid–Liquid Phase Transfer Catalysis: Basic Principles and Synthetic Applications

DOMENICO ALBANESE Università degli Studi di Milano, Milan, Italy

I. INTRODUCTION

Phase transfer catalysis (PTC) [1] was first introduced in the 1960s as a powerful tool to carry out reactions efficiently between reagents dissolved in mutually insoluble aqueous and organic phases. These reactions used to be performed by dissolving the inorganic anion in a protic organic medium, thus strongly reducing reactivity as a result of anion solvation and selectivity, as a result of solvolytic side reactions. The introduction of dipolar aprotic solvents such as dimethylformamide (DMF) or dimethylsulfoxide (DMSO) produced an enhanced reactivity by decreasing anion solvation [2]. However, their use is not devoid of drawbacks related to their cost, problematic removal, and environmental incompatibility.

As a consequence of its simplicity PTC soon received widespread attention by academic and industrial chemists and is now an established procedure for many industrial applications, e.g., in the pharmaceutical and agrochemical industries, as well as in monomer synthesis and polymer modification.

This chapter will focus on the basic principles of phase transfer catalysis with major attention devoted to catalysis at liquid interfaces, the topic of this book; therefore, important aspects of PTC such as solid–liquid PTC or gas–liquid PTC will only be touched on.

In the last part of this chapter a restricted selection of new relevant applications of liquid–liquid PTC are also presented in order better to illustrate the scope and generality of this methodology.

II. GENERAL PRINCIPLES

The important role played by PTC in organic synthesis is best evidenced by the constant high number of patents and references appearing in the literature over the last few years.

Reactions are carried out in a heterogeneous two-phase system in which one phase provides anions or a base for their generation, whereas the second phase contains organic reactants and PTC catalyst. Ionic reagents may be dissolved in the aqueous phase (liquid–liquid, LL-PTC) or used in the form of powdered solids (solid–liquid, SL-PTC) suspended in the organic medium.

Under PTC conditions the reacting anions are brought into the organic phase, where the reaction occurs, by catalytic amounts of lipophilic transport agents, usually a quatern-

ary ammonium or phosphonium salt. In the absence of the latter, the reaction proceeds at a very low rate, if at all.

In the simple case of the aliphatic nucleophilic substitution of alkyl halides R-X in an aqueous–organic two-phase system in the presence of catalytic amounts of a quaternary onium salt Q^+X^- and an excess of a metal salt M^+Y^-, the catalyst transfers the reacting anion Y^- into the organic phase as lipophilic and unsolvated and therefore a very reactive, ion pair Q^+Y^- (Scheme 1).

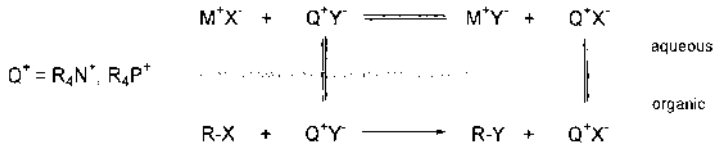

SCHEME 1

In order for an efficient process to be developed the leaving group X^- should then be returned to the aqueous phase.

Ion pairs are defined as pairs of oppositely charged ions held together by Coulomb attraction without formation of a covalent bond, in equilibrium with free anions:

$$[Q^+Y^-] \rightleftharpoons [Q^+] + [Y^-] \tag{1}$$

Ion pairs behave as single entities in determining conductivity, kinetic behavior, and osmotic properties. They do not conduct electricity, therefore it is possible to measure the amount of free ions present by conductivity measurements. Moreover, the dissociation constants of ion pairs are tabulated for many solvents. Generally, at low concentration, free ions are absent in solvents with dielectric constants ε lower than 15, whereas they are the main species in solvents with ε higher than 40. A borderline behavior is found in between.

Various factors such as partition and structure of the catalyst, reactivity of ion pairs in low-polarity organic medium, and hydration of anions are of paramount importance for the outcome of the PTC process.

The simple case of nucleophilic displacement as depicted in scheme 1 is regulated by several equilibria. The most important are the extraction equilibria [Eq. (2)–(4)] related to the capability of aqueous anions X^-_{aq}, Y^-_{aq} to be extracted into the organic phase as ion pairs $[Q^+X^-]_{org}$, $[Q^+Y^-]_{org}$.

$$[Q^+X^-]_{org} + M^+_{aq} + Y^-_{aq} \rightleftharpoons [Q^+Y^-]_{org} + M^+_{aq} + X^-_{aq} \tag{2}$$

$$Q^+_{aq} + X^-_{aq} \rightleftharpoons [Q^+X^-]_{org} \tag{3}$$

$$Q^+_{aq} + Y^-_{aq} \rightleftharpoons [Q^+Y^-]_{org} \tag{4}$$

The stoichiometric extraction constants E_{QX} (eq. 5) and E_{QY} (eq. 6) are thus defined as:

$$E_{QX} = \frac{[Q^+X^-]_{org}}{[Q^+]_{aq}[X^-]_{aq}} \tag{5}$$

$$E_{QY} = \frac{[Q^+Y^-]_{org}}{[Q^+]_{aq}[Y^-]_{aq}} \tag{6}$$

For precise determinations, activities should be used instead of concentrations, in such cases thermodynamic extraction constants are obtained. However, for practical purposes activities can normally be ignored.

In addition to the influence due to concentrations of anion and cation in the aqueous phase, the extraction equilibria [Eq. (5) and (6)] are influenced by a number of factors such as the pH of the aqueous phase, dissociation or association of ion pairs, and the possible formation of associated ions, e.g., $Q^+HX_2^-$, through extraction of an uncharged species HX. In particular the pH of the aqueous phase determines the actual anion [Eq. (7)] or cation concentrations if the latter ion is a protonated base [Eq. (8)].

$$X^- + H_3O^+ \rightleftharpoons HX + H_2O \tag{7}$$

$$BH^+ + H_2O \rightleftharpoons B + H_3O^+ \tag{8}$$

In a typical nucleophilic displacement (Scheme 1) a competitive extraction of two anions occurs and the selectivity coefficient $K_{sel\,(Y/X)}$ provides a valuable indication of the feasibility of a given reaction:

$$K_{sel\,(Y/X)} = \frac{E_{QY}}{E_{QX}} = \frac{[Q^+Y^-]_{org}}{[Q^+X^-]_{org}} \cdot \frac{[X^-]_{aq}}{[Y^-]_{aq}} \tag{9}$$

If E_{QY} and E_{QX} are known it is possible to calculate $K_{sel\,(Y/X)}$ and therefore the actual concentration of Q^+Y^- in the organic phase in competition with Q^+X^-, derived from the leaving group X^-, at any given concentration of X^-, Y^-, or catalyst during the reaction. Assuming that concentrations can be used instead of activities, Q^+ is lipophilic enough to be present in the organic phase only, and the influence of other factors is negligible, the amount of Q^+ associated with Y^- or X^- in the organic phase may be calculated.

Although in most cases satisfactory predictions can be obtained, it is worth noting that the influence of side processes cannot always be ignored.

A. Influence of the Onium Cation

The lipophilicity and consequently the extraction capability of quaternary onium salts increases with the number of carbon atoms in chains bonded to the cationic center. As a general rule, in a given homologous series, the logarithm of the extraction constant of an ammonium cation increases by 0.54 unit per carbon atom. This general trend proved to be independent of the anion and the aprotic nonpolar solvent and applies to symmetrical as well as nonsymmetrical ammonium salts [3]. However, the lipophilicity of an onium salt is not only correlated to its number of carbon atoms. For example, $BnEt_3N^+Cl^-$ (TEBA) is mainly partitioned in the aqueous phase, showing how the benzyl group is much less lipophilic than the corresponding aliphatic straight chain containing the same number of carbon atoms, i.e., a *n*-heptyl group, and exhibits a similar behavior to butyl and propyl groups.

B. Influence of the Onium Anion

The possibility of developing an efficient phase-transfer process under liquid–liquid conditions relies on the selective extraction of a quaternary salt from an aqueous into an organic phase. The hydration sphere, electronegativity, and volume and structure of anions play a fundamental role in determining the relative ease of their extraction into

the organic phase. The extraction constants of a series of tetrabutylammonium salts in water–chloroform or water–dichloromethane are reported in Table 1 [4]. Although they are influenced by other factors involved such as the cation, the solvent, and the ionic strength of the aqueous phase, the following scale of relative extraction capabilities can be drawn, which is independent of all other factors:

$$\text{Picrate} \gg ClO_4^- > I^- > TsO^- > NO_3^- > Br^- > PhCOO^- > PhO^- \cong Cl^-$$

$$\cong CN^- > HSO_4^- > HCO_3^- > AcO^- > F^- \cong OH^- \cong SO_4^{2-} \cong CO_3^{2-} > PO_4^{3-}$$

The order found can be ascribed mainly to differences in solvation energies of anions in organic solvents and water and applies to ammonium as well as alkyltriphenyl [5] or tetraphenyl phosphonium salts [6], at least in dilute solutions.

Selectivity coefficients $K_{\text{sel}(Y/X)}$ were measured for a series of anions relative to chloride in a number of solvents and for several quaternary cations by measuring the potential developed by anion-exchange membrane electrodes Q^+Y^- in the presence of a foreign anion X^- [7]. From these values it is possible to calculate $K_{\text{sel}\,(Y/X)}$ by Eq. (10) for any given anion pair whose $K_{\text{sel}(Y/Cl)}$, are known:

$$\log K_{\text{sel}(Y/X)} = \log\left[K_{\text{sel}(Y/Cl)} - K_{\text{sel}(X/Cl)}\right] \tag{10}$$

It is, therefore, possible to predict which anion is preferentially extracted into the organic phase by selectivity coefficients $K_{\text{sel}(Y/X)}$.

Multiply charged anions are less liphophilic than the corresponding anions of lower charge; therefore, they are extracted into the organic phase with greater difficulty. A typical case is represented by tetrabutylammonium hydrogensulfate ($Bu_4N^+HSO_4^-$), which is used for the preparation of a wide variety of tetrabutylammonium salts and in many synthetic applications. In fact, when treated with an equimolar amount of bases such as NaOH or $NaHCO_3$, it is converted into the sulfate anion (SO_4^{2-}), which remains quantitatively in the aqueous phase; the desired ion pair is thus selectively extracted into the organic phase [8]. For example, tetra-alkyl onium fluorides (Q^+F^-), hydrogendifluorides ($Q^+HF_2^-$), and dihydrogen trifluorides ($Q^+H_2F_3^-$) have been prepared by equilibrating an organic solution of $(Bu_4N^+)_2SO_4^{2-}$, obtained by neutralization of $Bu_4N^+HSO_4^-$, with

TABLE 1 Extraction Constants E_{QX} of Tetrabutylammonium Salts in Aqueous Organic Two-Phase System

Anion	$CHCl_3$–H_2O	CH_2Cl_2–H_2O
OH^-	—	0.0005
HSO_4^-	—	0.06
Cl^-	0.78	0.35
Br^-	19.5	17
I^-	1023	2188
ClO_4^-	3020	43700
PhO^-	0.93	—
2, 4, 6-$(NO_2)_3$-$C_6H_2O^-$	810,000	4,800,000
p-CH_3-C_6H_4-SO_3^-	214	—

Source: Ref. 4.

an aqueous solution of KF or KHF_2. After a single equilibration, quantitative yields of fluorides and polyfluorides can be obtained [9].

Although the high extraction constants of anions such as I^- and TsO^- make them useful nucleophiles in PTC processes, the same are detrimental in cases where they are leaving groups in nucleophilic displacements. In fact, when released during the reaction, they remain preferentially in the organic phase thereby decelerating then stopping the PTC reaction.

It can be concluded that a high nucleofugacity of the leaving group cannot ensure an efficient nucleophilic displacement under PTC conditions if not paired with a high hydrophilicity that secures its removal from the organic phase where the reaction occurs. For this reason, methanesulfonates, chlorides, or bromides provide better results than those for I^- and TsO^- when used as starting materials in nucleophilic displacements under PTC conditions.

The extraction of hydrophilic and basic anions such as OH^- is possible with highly lipophilic cations only. For example, the E_{QX} of $(C_7H_{15})_4N^+OH^-$ in benzene/water is $\cong 1$. However, this is 10^4 times lower than the E_{QX} of common ions such as Cl^-; therefore, even the presence of a very low amount of foreign anions in aqueous solution reduces to a negligible level the portion of the ammonium cation extracted into the organic phase as $(C_7H_{15})_4N^+OH^-$.

1. Anion Hydration

Liquid–liquid PTC is the most widely used protocol for carrying out phase transfer catalyzed reactions. Under liquid–liquid PTC conditions the anions X^- associated with quaternary cations Q^+ as ion pairs $[Q^+X^-]$ are extracted from the aqueous to the organic phase specifically solvated by a limited amount n of water molecules (Table 2).

The extent of anion hydration mainly depends on its polarizability and electronegativity, solvent and cation generally showing a negligible effect. Hard anions such as

TABLE 2 Anionic Reactivity Under LL-PTC and Anhydrous Conditions[a]

X^-	Hydration number n $(Q^+X^-\cdot nH_2O)$[b]	1000 k ($M^{-1}s^{-1}$) LL-PTC	1000 k ($M^{-1}s^{-1}$) $PhCl_{anhyd}$	$k_{PhCl\ anhyd}/k_{LL\text{-}PTC}$	Wet PhCl	$DMSO_{anhyd}$
F^-	8.5[c]	—	2.3	—	—	—
F^-	0	—	1890[c,d]	822[e]	—	—
Cl^-	3.4	1.8	19.7	11	2.2	3.6
Br^-	2.1	3.2	8.1	2.5	3.3	2.3
I^-	1.0	2.8	3.0	1.1	2.7	0.5
N_3^-	3.0	19.1	70.4	4	19.6	13.5
CN^-	5.0	11.7	86.7	8	13.3	33.8
PhO^-	4.0[f]	8.7	650	75	—	—
PhS^-	2.7[f]	971	3640	3.7	—	—

[a] *Source*: Ref. 11.
[b] $C_{16}H_{33}P^+Bu_3$ or $hexyl_4N^+$.
[c] *Source*: Ref. 12.
[d] Extrapolated by plotting $\log k$ vs. n.
[e] $k_{n=0}/k_{n=8.5}$.
[f] *Source*: Ref. 13.

OH^- and F^- have the greatest hydration numbers, whereas n is low with soft anions such as I^- [10].

The hydration shell, specific for each anion, reduces the rate of the chemical reaction in the organic phase. The nucleophilicity of a representative series of organic and inorganic anions has been tested in a typical bimolecular nucleophilic substitution in a chlorobenzene–water two-phase system in the presence of catalytic amounts of quaternary onium salt (Scheme 2) [11].

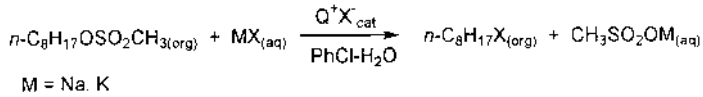

SCHEME 2

Under these conditions the extraction of the reacting anion and leaving group release to the aqueous phase are fast processes and the rate-determining step is the reaction in the organic phase. The narrow reactivity scale and sequence found $N_3^- > CN^- > Br^- \cong I^- > Cl^-$ are anomalous when compared with the anion reactivity, both in protic ($N_3^- \cong I^- > CN^- > Br^- > Cl^-$) and dipolar aprotic solvents ($CN^- > N_3^- > Cl^- > Br^- > I^-$).

A comparison with the same reaction carried out under homogeneous conditions in anhydrous chlorobenzene (Scheme 3) shows an increase in rate constants with all anions tested (Table 2) [11].

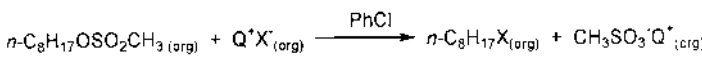

SCHEME 3

Relevant enhancements were found for highly hydrated anions such Cl^-, CN^-, and PhO^-, whereas the same were of low entity in the case of anions with lower n, suggesting that this behavior is related to the removal of the anion hydration sphere.

Moreover, addition of the small amount of water required to regenerate the hydration sphere of the anions in the organic phase (wet PhCl) restored the rate constants obtained under PTC conditions. This is a clear demonstration that the specific solvation of anions in the organic phase is responsible for the particular nucleophilicity scale of anions in PTC conditions. On the other hand, it is also a proof that the reaction takes place in the organic phase.

In homogeneous anhydrous solution the second-order rate constants decrease on changing from chlorobenzene to DMSO with smaller variations for anions with dispersed charge and larger for high charge density anions.

The rates depend on the polarity of the solvent both under PTC and anhydrous homogeneous conditions. A small increase is observed under PTC conditions by reducing solvent polarity, whereas a greater effect is observed under homogeneous conditions (Table 3) [11].

It is worth noting that the reactivity found under anhydrous homogeneous conditions can be reproduced under LL-PTC conditions by using concentrated aqueous alkaline solutions instead of water. In fact, 50% aqueous NaOH and 60% aqueous KOH are capable of extracting anions into the organic phase in an essentially anhydrous state and their reactivity is consequently increased to that observed under anhydrous conditions

(Table 4) [14,15]. The dehydrating effect is specific for such concentrated alkaline solutions and progressively disappears on dilution so that 30% aqueous NaOH no longer exhibits any dehydrating effect.

In aqueous NaOH–organic two-phase systems only negligible amounts of side products derived from the nucleophilic substitution by hydroxide anion have been found. This is in agreement with the unfavorable extraction constant of the hydroxide anion with respect to other anions.

The anion-specific hydration also plays a fundamental role in determining the selectivity coefficient values. In fact, the increase in concentration of the aqueous NaOH from 15 to 50% always produces a change in anion extractability into the organic phase. Reactions of anions with $K_{sel\,(X/Cl)} > 1$ are those most favored by 50% aqueous NaOH due to a higher partition of the reacting X^- in the organic phase, combined with enhanced anion activation derived from its dehydration. On the other hand, the reduced extractability of anions with $K_{sel\,(X/Cl)} < 1$ is largely overcome by the dramatic increase in reactivity [16].

The effect of specific solvation is noteworthy in the modification of the basic properties of high charge densities, and hence more hydrated, anions such as OH^- and F^-.

The basicity of OH^- in the Hofmann elimination of $hexyl_4N^+OH^- \cdot nH_2O$, carried out in a chlorobenzene–aqueous two–phase system, increases by a factor of 1.1×10^4, reducing n from 11 to 3.5 on passing from 15 to 50% aqueous NaOH (Scheme 4) [17].

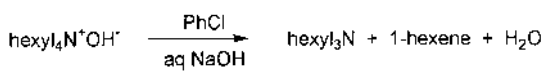

SCHEME 4

Any attempt to reduce the water content further leads to very fast decomposition to trihexylamine and 1-hexene; however, the basicity enhancement is extrapolated to be more than 10^9 in the hypothetical case of anhydrous hydroxide.

The differences found are comparable with those found in reactions promoted by $OH^-(H_2O)_n$ ($n = 0$–3; 5000 times) in the gas phase [18]. These results indicate that the reactivity of the gas phase can be approached in the condensed phase by using bulky quaternary onium salts in weakly polar nonhydrogen-bonding organic solvents.

TABLE 3 Solvent Effect on Reaction Rate of n-$C_8H_{17}OMs$ with Bromide Ion[a] at 60°C

	PTC conditions		Homogeneous conditions	
Organic solvent	$k \times 10^3$ ($M^{-1}s^{-1}$)[b]	k_{rel}	$k \times 10^3$ ($M^{-1}s^{-1}$)[b]	k_{rel}
Cyclohexane	5.5	3.4	40.5	9.0
Toluene	3.7	2.3	10.7	2.4
Chlorobenzene	3.2	2.0	8.1	1.8
Benzonitrile	1.6	1.0	4.5	1.0
DMSO	—	—	2.3	0.5
MeOH	—	—	0.2	0.05

[a] From $C_{16}H_{33}P^+Bu_3Br^-$.
[b] $k = k_{obs}/[Q^+Y^-]$.

TABLE 4 Second-Order Rate Constants[a] for Displacement of n-$C_8H_{17}OMs$ with Various Nucleophiles (Y^-)[b] at 35°C

Y^-	PhCl-H_2O	PhCl-50% aq. NaOH	Anhydrous PhCl
N_3^-	2.9	11.6	11.7
Cl^-	0.26	3.4	3.4
Br^-	0.42	1.1	1.1
I^-	0.29	0.42	0.45

[a] $k \cdot 10^3$ ($M^{-1}s^{-1}$).
[b] From $(C_8H_{17})_4N^+Y^-$.
Source: Ref. 14.

Moreover, the high reactivity of low hydrated OH^- enables replacement of strong and dangerous bases such as sodium methoxide, *t*-butoxide, sodium hydride, and sodium amide. In fact NaOH has been successfully used for deprotonation of substrates with pK_a up to 38, oxidation of methylene groups up to pK_a 33, and alkylations of substrates up to pK_a 24.

A similar behavior was found with the fluoride anion, whose utility as proton abstractor in base-promoted reactions is well known [19]. In fact, when the hydration number n of $hexyl_4N^+F^- \cdot nH_2O$ is reduced from 6 to 1.7 the rate of the Hofmann-like elimination reaction (Scheme 5) increases by nearly four orders of magnitude, and is extrapolated to be seven orders of magnitude in the hypothetical case of anhydrous F^- [12] (Scheme 5).

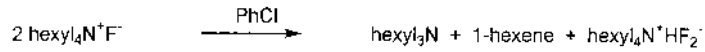

SCHEME 5

A comparison with data reported in Table 2 indicates that the basicity of F^- is much more affected by specific hydration than its nucleophilicity is, therefore confirming that anhydrous tetra-alkylammonium fluorides are not stable compounds with the single exception of $Me_4N^+F^-$, which cannot undergo Hofmann-like elimination.

C. Influence of the Organic Solvent

The best solvents for LL-PTC are those that are aprotic and immiscible with water in order to avoid strong interactions with ion pairs decreasing their reactivity. As clearly shown in Table 5, where extraction constants of tetrabutylammonium bromide in several solvents are reported, the extraction capability strongly depends on the solvent polarity [20]. Indeed, this is the main rationale to be considered for the choice of the solvent in PTC reactions unless the ion pair to be extracted is very lipophilic, e.g., $(n\text{-}C_8H_{17})_4N^+Br^-$.

Chloroform and dichloromethane are particularly favored from this point of view with the single limitation that they cannot be used in the presence of concentrated alkaline solution due to deprotonation. However, potentially reactive solvents can often be used when reactions proceed rapidly.

An outstanding merit of LL-PTC is that in many cases reactions involving liquid substrates can be carried out without any organic solvent, the organic phase being the neat reactant itself. An appreciable change of polarity of the organic phase may therefore occur as the reaction proceeds due to variation of composition of the organic phase. This can modify ion-pair partition as well as the reaction rate. The effect on the latter is usually small, whereas an appreciable modification of catalyst partition can produce relevant accelerations if its solubility in the product formed is considerably higher than in the starting material. In such a case the amount of catalyst in the organic phase increases as the reaction proceeds, producing acceleration of the reaction [21].

D. Salt Effects

The extraction constants of quaternary onium salts are measured after equilibration of an organic solution of Q^+X^- with an aqueous solution of the inorganic reactant. Values reported in the literature are usually taken at constant ionic strength of the aqueous phase. In fact, the extraction of organic salts from the aqueous to the organic phase is facilitated as the concentration of the aqueous phase increases.

For example, in the nucleophilic substitution reaction of *n*-octyl methanesulfonate with bromide in a chlorobenzene–water two-phase system the catalytic activity of $Bu_4N^+Br^-$ was found to increase 20 times as the aqueous KBr concentration was increased from 1 to 6 M [22].

The same salting-out effect enables the use of quaternary onium salts such as TEBA or $Bu_3MeN^+Cl^-$, usually unfavorably partitioned in the organic phase, in base-promoted reactions carried out with 50% aqueous NaOH.

Moreover, the presence of a high concentration of salts in the aqueous phase enables solvents partially or fully miscible with water, e.g., acetonitrile or tetrahydrofuran (THF), to be used in LL-PTC processes since they form a separate organic phase under these conditions.

III. MECHANISM OF PHASE TRANSFER CATALYSIS

In the original mechanism proposed by Starks [23] and depicted in Scheme 1 the quaternary onium salt, partitioned in both the aqueous and organic phase, transfers the reacting

TABLE 5 Apparent Extraction Constants of $Bu_4N^+Br^-$[a]

Solvent	$E_{Bu_4N^+Br^-}$	Solvent	$E_{Bu_4N^+Br^-}$
CH_3NO_2	168	PhCl	0.1
$CHCl_3$	47	*o*-C_6H_4-Cl_2	0.1
CH_2Cl_2	35	CH_3COOEt	0.2
$ClCH_2CH_2Cl$	6.1	$EtCOCH_3$	0.1
CCl_4	0.1	Et_2O	0.1

[a] Calculated from the distribution of 0.1 M $Bu_4N^+Br^-$ between water and solvent.

Source: Ref. 8.

anion from the aqueous to the organic phase, at the same time returning the leaving group to the aqueous phase. On the other hand, it has been found that, under a given set of reaction conditions, the efficiency of a phase transfer catalyst increases with its solubility in the organic phase. A modified mechanism, requiring no migration of cation between phases (Scheme 6), was therefore put forward by Landini et al. [24].

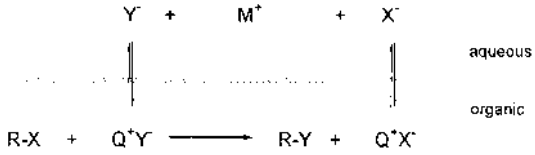

SCHEME 6

This modified mechanism has been validated by experiments using liquid membranes [24] or indicators [20], at least in the case of catalysts 100% partitioned in the organic phase.

Numerous evidence clearly indicates that the reaction occurs in the organic phase. In particular, the irreversible nucleophilic substitution (Scheme 2) in the presence of an excess of anionic nucleophile in the aqueous phase follows pseudo first-order kinetics:

$$\text{Rate} = k_{\text{obs}}[\text{RX}] \tag{11}$$

The observed rate constants are linearly correlated with the concentration of the catalyst in the organic phase:

$$k_{\text{obs}} = k[\text{Q}^+\text{Y}^-]_{\text{org}} \tag{12}$$

It is well known that interfacial reaction rates increase as stirring speed is increased until reaching a plateau around 600–1700 rpm (revolutions per minute) [25]. On the other hand, PTC reaction rates are independent of the stirring speed above 200–350 rpm, necessary to level concentration gradients at the interphase. When neutral reagents are involved, it is thus possible to exclude the contribution of interfacial phenomena to the PTC processes.

The kinetics of PTC reactions, Eqs (11) and (12), demonstrate that it does not proceed through the formation of micelles. In fact in this case the rate of reaction should have a sharp increase near the "critical micelle concentration" (CMC) instead of being linearly correlated with the concentration of the catalyst.

Dilute organic solutions of quaternary onium salts exist as ion aggregates in equilibrium with ion pairs. For example, aggregation numbers of 1–15 have been found for a series of quaternary ammonium and phosphonium salts in low-polarity anhydrous solvents in the range of concentration of practical use in PTC [26]. The presence of associated species in anhydrous PhCl is shown by the enhancements in second-order rate constants on decreasing the salt concentration [11]. This behavior contrasts with results obtained in the same solvent under PTC conditions where a linear relationship between rate constants and catalyst concentration [Eq. (11)] is observed. A comparison between the two systems indicates that the presence of a limited amount of water associated with the onium salt is enough to inhibit aggregate formation to a low level, thereby having no effect on reaction rates [11].

A. Mechanism in the Presence of Concentrated Aqueous Bases

A wide variety of PTC reactions are carried out in the presence of strong bases, usually concentrated alkaline aqueous solutions, to generate reactive anions. Indeed, reactions such as C-, O-, and N-alkylation, H/D exchanges, additions, α- and β-eliminations, and many other PTC reactions promoted by strong bases are among the most extensively used for practical applications [1].

The pK_a of the substrate plays an important role in influencing the reaction pathway. Relatively strong acids such as β-diketones ($pK_a \cong 9$–10) are dissolved in aqueous NaOH. The anion thus obtained is extracted by the PTC catalyst into the organic phase where the C/O alkylation occurs through the usual mechanism. In the case of relatively weak acids such as alcohols ($pK_a \cong 18$) the equilibrium [Eq. (13)] is largely shifted to the left, but the high hydrophilicity of OH^- enables alcoholate to be extracted into the organic phase as Q^+OR^-.

$$OH^- + ROH \rightleftharpoons RO^- + H_2O \tag{13}$$

The resulting mechanism is therefore the usual one allowing, e.g., the Williamson ether synthesis through alkylation of alkyl halides with alcohols in the presence of 50% NaOH and $Bu_4N^+HSO_4^-$ as catalyst [27].

An interfacial mechanism was proposed by Mąkosza in the case of substrates having pK_a values in the range 22–25 [28]. In fact, due to the negligible extractability of OH^- in the organic phase, deprotonation of substrate SH cannot occur in the bulk organic phase but occurs at the aqueous–organic interface. The resulting anion S^-_{int} is transferred to the organic phase by the PTC catalyst Q^+X^- as a quaternary ion pair $[Q^+S^-]$ and reacts with the electrophilic counterpart RX (Scheme 7).

$$SH_{org} + Na^+OH^-_{aq} \rightleftharpoons Na^+_{int} + S^-_{int} + H_2O$$

$$S^-_{int} + [Q^+X^-]_{org} \rightleftharpoons [Q^+S^-]_{org} + X^-_{aq}$$

$$[Q^+S^-]_{org} + RX \rightleftharpoons RS + [Q^+X^-]_{org}$$

SCHEME 7

The ion pair Q^+S^- is extracted anhydrously since concentrated NaOH is dehydrating [14,15] and any adventitious water, being a stronger acid, would decompose the ion pair.

The interfacial mechanism is confirmed by stirring rates around 700–800, necessary to obtain reproducible results [29]. Moreover, a number of interfacial deprotonations and further reactions of carbanions are described in the absence of catalysts. For example, phenylacetonitrile is alkylated by 1-iodobutane and 50% aqueous NaOH at 80°C. Under these conditions the concentration of phenylacetonitrile in the aqueous phase and its carbanion sodium salt in the organic phase were less than 2 and 5 ppm, respectively [30].

A modified interfacial mechanism has been proposed by Starks [1] assuming that tetraalkylammonium hydroxide, generated at the interphase by ion exchange between ammonium halide and sodium hydroxide, acts as a base for substrate deprotonation. This mechanism has been disputed by Mąkosza through competitive addition of CCl_3^- anions to *N*-alkylpyridinium salts and carbanion acceptors such as vinyl acetate [31].

IV. ANIONIC REACTIVITY OF QUATERNARY ONIUM SALTS

A successful PTC catalyst transfers one reactant, usually anionic, into the normal phase of the other reactant in a highly reactive form. In other words, cation–anion interactions should be minimized in the reactive ion pair. This can be accomplished by using bulky quaternary onium salts or cation complexing agents such as crown ethers or cryptands instead of small metal cations. According to Coulomb's law [Eq. (14)], increasing the dielectric constant ε of the medium is also useful.

$$E_{\pm} = e^2 N/\varepsilon r = 33.18/\varepsilon r \text{ kcal/mol} \tag{14}$$

where ε is the electron charge; N is Avogadro's number, and r is the cation–anion interatomic distance (Å).

The interaction energies between ions in K^+Br^- and $Bu_4N^+Br^-$ were found to be 4.5 and 2.4 kcal/mol, respectively, in dioxane ($\varepsilon = 2.2$) whereas the corresponding values were 0.26 and 0.13 kcal/mol in acetonitrile ($\varepsilon = 39$).

As reported in Table 6 the nucleophilic displacement of 1-bromobutane in dioxane or acetonitrile proceeds faster with $Bu_4N^+PhO^-$ than with PhO^-K^+ (Scheme 8).

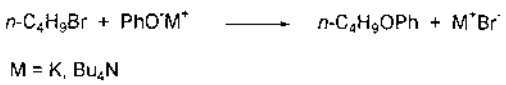

(15)

SCHEME 8

This is in agreement with the expected decrease in the free energy of activation as the interactions between cation and anion decrease with increasing interionic distance in ammonium phenate. Moreover, with PhO^-K^+ the rate of reaction increases by three orders of magnitude (4000:1) by exchanging a low ε solvent such as dioxane with a high ε solvent such as acetonitrile, due to increased separation between the ions, whereas the rate of reaction is nearly unchanged in the case of $Bu_4N^+PhO^-$ [32].

The increase observed by using $Bu_4N^+PhO^-$ instead of PhO^-K^+ is dramatic with dioxane (33,000:1) and appreciable but not relevant with acetonitrile (7.5:1). In general, it may be concluded that the effect of dielectric constant is relevant only when the ionic radius is small, whereas the effect of the latter is strongest with low dielectric constant solvents where ion pairs or ion-pair aggregates are present.

Since it has been demonstrated by conductimetry that both K^+ and Bu_4N^+ phenoxides are in the form of ion pairs in dioxane and are largely dissociated in acetonitrile [33], the increased reactivity of ammonium phenoxide in dioxane can be ascribed to the greater interionic distance.

TABLE 6 Influence of Interionic Distance and Dielectric Constants on Rates of Reaction (15)

		$k \times 10^5\,(M^{-1}s^{-1})$		$k_{Bu_4N^+}/k_{K^+}$
Solvent	ε	PhO^-K^+	$Bu_4N^+PhO^-$	k_{Q^+}/k_{K^+}
Dioxane	2.2	0.01	330	33,000
Acetonitrile	39	40	300	7.5

Source: Ref. 32.

A highly reactive ion pair may, therefore, be obtained by using a quaternary cation soluble in a low dielectric constant organic solvent. This is usually accomplished with onium salts with at least one long alkyl chain or symmetrical Bu_4N^+.

It is generally accepted that under PTC conditions the chemical reactivity is due to ion pairs or higher aggregates since the reaction occurs in the apolar organic phase where free ions are practically absent. The same conclusion can be drawn on the basis of kinetic measurements. In fact, as described above, the observed rate constants are linearly correlated with the concentration of Q^+Y^- within a wide range of concentrations. On the other hand, rates should be proportional to the square root of Q^+Y^- concentration if the free ion is the reactive species [20].

A. Influence of the Onium Cation Structure

Although there are cases where many different catalysts perform more or less the same, the choice of the proper catalyst is usually crucial in order to optimize a given PTC process. For example, a less lipophilic, and therefore less effective, catalyst may be preferred if it is separated more easily from reaction products by water extraction.

A comparison between literature data about performances of different catalysts in a particular reaction is not always an easy task to achieve. In fact when the reaction is not run under the same reaction conditions correct comparisons are difficult since various factors are usually simultaneously involved, often counteracting each other. Therefore, evaluation of the important requirements for a PTC process such as catalyst lipophilicity, selective anion extraction, cation–anion separation within the ion pair, and poor anion solvation may be not sufficient for useful predictions. Other factors such as the structure of the substrate or anion hydration, interaction with solvent, or ionic strength of the aqueous phase may assume great importance.

In the nucleophilic displacement of a hydrophilic leaving group such as methanesulfonate with bromide (Scheme 9), carried out under LL-PTC conditions with onium catalysts of different types, their lipophilicity is important whereas the cation structure is not [11].

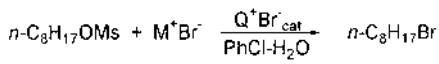

SCHEME 9

Although pseudo first-order rate constants span up to two orders of magnitude, the second-order rate constants, which include the actual concentration of the catalyst in the organic phase, are similar (Table 7), the highest rates being reached with catalysts 100% partitioned in the organic phase.

It is worth noting that a higher anionic reactivity is produced by increasing steric hindrance around the cation. This can be achieved by increasing the length of alkyl chains or by shortening the heteroatom–carbon bond using ammonium instead of phosphonium salts.

For example, in the series of hexadecyltrialkylammonium salts a dramatic increase in anionic reactivity is observed when a triethyl derivative is used instead of trimethyl as reported in Table 8. Kinetic constants were calculated for an anhydrous homogeneous system since trimethyl and triethyl derivatives are not suitable for LL-PTC as they are surfactants and generate stable emulsions when contacted with organic–aqueous biphasic systems [11].

TABLE 7 Influence of Cation Structure on Rate Constant for Nucleophilic Displacement of *n*-Octylmethanesulfonate with Bromide[a]

Q^+	$k_{obs} \times 1000$ (s^{-1})	$k \times 1000$ ($M^{-1}s^{-1}$)	Percentage of Q^+ in organic phase
Pr_4N^+	0.2	2.4	2.5
Bu_4N^+	12.0	3.6	83
BnN^+Pr_3	1.3	1.9	17
$C_{16}H_{33}N^+Bu_3$	17.3	4.3	100
$C_{16}H_{33}P^+Bu_3$	12.8	3.6	100
Bu_4P^+	10.4	2.7	97
$(C_8H_{17})_4N^+$	20.4	5.1	100

[a] In PhCl–H_2O at 60°C.
Source: Ref. 11.

When the same reaction is carried out in a dipolar aprotic solvent such as DMSO all catalysts tested show comparable reactivity, noticeably lower than in chlorobenzene.

The chemical stability of the onium salt is the main rationale to be considered for the choice between ammonium and phosphonium salts. The latter salts are thermally stable up to 150°–170°C whereas ammonium salts are rapidly decomposed above 110°C [34]. Although the difference in thermal stability is quite relevant, nevertheless it has no great impact on the choice between ammonium and phosphonium salts since PTC reactions are usually carried out at temperatures well below 110°C. On the other hand, phosphonium salts are much less stable in the presence of hydroxide anions that generate the corresponding phosphine oxides at 50°C [35,36].

V. OTHER PTC CATALYSTS

Specific complexation of cations by polyethylene oxide chains (PEGs **1**), macrocyclic (crown ethers **2–4**) or macrobicyclic (cryptands **5**) polyethers facilitates salt dissolution in low-polarity solvents, at the same time providing nonsolvated highly reactive anions by increasing ion-pair dissociation (Chart 1) [37].

TABLE 8 Influence of Steric Hindrance Around Cation on Rate Constant for Nucleophilic Displacement of *n*-Octyl Methanesulfonate with Bromide[a]

Q^+	PhCl [$k \times 1000$ ($M^{-1}s^{-1}$)]	DMSO [$k \times 1000$ ($M^{-1}s^{-1}$)]
$C_{16}H_{33}N^+Me_3$	3.9	3.2
$C_{16}H_{33}N^+Et_3$	18.6	2.9
$C_{16}H_{33}N^+Pr_3$	19.2	3.5
$C_{16}H_{33}N^+Bu_3$	18.2	3.2
Bu_4N^+	20.2	3.2
$C_{16}H_{33}P^+Bu_3$	8.7	3.5

[a] At 60°C.
Source: Ref. 11.

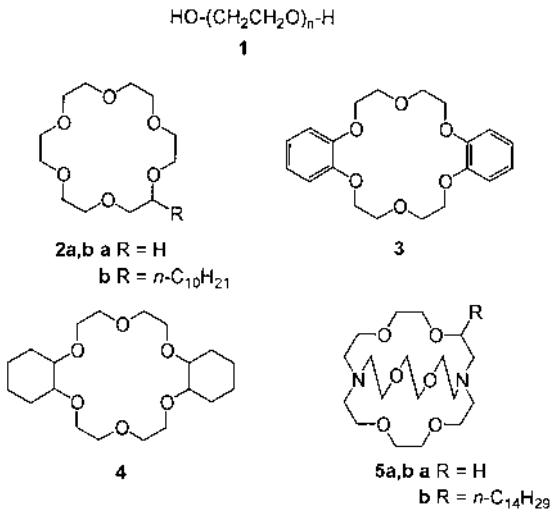

CHART 1

Crown ethers and cryptands have a central cavity where cations of opportune dimensions are held by chelation, enabling formation of complexes with other species. The stability of the complexes thus obtained depends on radii and electronic configurations as well as on the topology of the ligand. Open-chain PEGs behave in a similar way although the stability of their complexes is much lower.

PEGs **1** and unsubstituted crown ethers such as **2a** are hygroscopic water-soluble compounds. In low-polarity organic–aqueous two-phase systems they are almost completely partitioned in the aqueous phase, thus resulting in limited utility in LL-PTC. On the other hand, their solubility in low-polarity organic solvents is strongly increased by the presence of aromatic rings and alkyl chains. For example, dibenzo-18-crown-6 (**3**) and dicyclohexano-18-crown-6 (**4**) (PHDB18-C-6) are soluble in apolar organic solvents commonly used in LL-PTC and are commercial compounds.

A high complexation constant between the ligand and the salt in the organic phase, together with a high partition ratio for the complexed crown ether in the organic phase, are both prerequisites to the successful use of crown ethers as catalysts in aqueous–organic biphasic systems [38,39].

Various factors such as the relative size of the cation and macrocyclic cavity, the degree of solvation of both anion and cation crown complexes, the number and nature of ligand atoms in the ring, and the effect of steric and conformational factors in the ring, all contribute in determining the stability constant of the complex.

The complexed cation, being surrounded by organophilic groups, resembles an onium cation and is extracted into lipophilic medium along with its counteranion. Other conditions such as substrate, nucleophile, and leaving group being the same, the unsolvated anion concentration in the organic phase increases with ligand lipophilicity.

Nucleophilic displacements under two-phase conditions in the presence of catalytic amounts of crown ether, **4**, which is completely dissolved in the organic phase, follow the classical PTC mechanism and the observed pseudo first-order rate constants are linearly correlated with the amount of complexed crown ether in the organic phase. A narrow reactivity range was found for different anionic nucleophiles in the displacement of *n*-octyl methanesulfonate (Scheme 10).

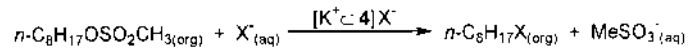

SCHEME 10

Results are compared in Table 9 with those obtained under the same conditions with a typical lipophilic onium salt such as hexadecyltributylphosphonium bromide [38].

Although second-order rate constants are similar with both catalysts, the catalytic performance of crown ether **4** is quite different from that observed with a typical onium salt such as $C_{16}H_{33}Bu_3P^+Br^-$.

In fact, the actual concentration of the anion in the organic phase in the case of complexed crown ethers is strongly related to the nature of the anion through the stability constants of the complex. These are high for soft anions such as I^- and low for hard anions such as Cl^- [10]. As a consequence of low complexation, in the case of Cl^-, reaction with crown ether **4** is much slower than the onium salt-catalyzed reaction, whereas the opposite is true for iodide due to its high complexation.

The hydration of the complexed polyether under two-phase conditions includes the specific hydration of anions, similar to that found with onium salts, and two molecules of water associated with the uncomplexed ligand. Removal of the hydration sphere of the anions in going from two phase to anhydrous conditions is balanced by a larger cation–anion interaction. This behavior causes very little variation in anionic reactivity in contrast with that observed with onium salts [40]. The hydration sphere determines in both cases the anomalous nucleophilicity scale found under PTC conditions with respect to dipolar aprotic solvents.

It may be concluded that lipophilic crown ethers can be efficiently used as catalysts for LL-PTC reactions only in the case of easily polarizable anions. Even hydrophilic crown ethers such as **2a**, when complexed with highly lipophilic anions in strongly alkaline solutions, are favorably partitioned in the organic phase and show good performances under LL-PTC conditions. On the other hand, the higher cost with respect to onium salts limit their applications only to special cases, e.g., in the presence of concentrated alkali where onium salts are less stable.

TABLE 9 Nucleophilic Displacement of *n*-Octyl Methanesulfonate with Nucleophiles X^- Under LL-PTC with PHDB18-C-6 (**4**) or $C_{16}Bu_3P^+Br^-$[a]

	4. K^+X^-				$C_{16}H_{33}Bu_3P^+Br^-$		
X	k_{obs} (s^{-1})	Complexation (%)	$k \times 100$[b] ($M^{-1}s^{-1}$)	Relative rates	k_{obs} (s^{-1})	$k \times 100$[c] ($M^{-1}s^{-1}$)	$k_{obs(4)}k_{obs\ (Q^+Br^-)}$[d]
N_3^-	25.1	13.3	5.1	2.8	188	4.7	0.13
CN^-	3.5	12.2	0.72	0.4	120	3.0	0.03
Cl^-	0.3	2.0	0.38	0.2	17	0.44	0.02
Br^-	10.7	16.8	1.6	0.9	29.6	0.74	0.4
I^-	66.8	92.8	1.8	1.0	27.6	0.69	2.4
SCN^-	6.6	83	0.2	0.1	5.2	0.13	1.3

[a] At 70°C in PhCl-H_2O.
[b] $k = k_{obs}$/[complexed **4**].
[c] $k = k_{obs}/[C_{16}Bu_3P^+Br^-]$.
[d] $Q^+ = C_{16}H_{33}Bu_3P^+Br^-$.
Source: Ref. 38.

Azamacrobicyclic ethers such as **5** form stable inclusion complexes (cryptates) in which the metal cation is fully sequestered inside a 10 Å spherical cavity taking the place of the solvation sphere. The resulting "solvent separated" ion pairs are particularly reactive in low-polarity media due to their scarce stabilization by the solvent and the cation.

As previously described for lipophilic crown ethers, simple cryptands such as **5a** show low solubility in apolar organic medium whereas substituted **5b** are easily dissolved. These compounds behave as a classic PTC catalysts, and the observed pseudo first-order rate constants are linearly correlated with the concentration of the cryptate in the organic phase. In a chlorobenzene–aqueous two-phase system it is 100% partitioned in the organic phase and nearly quantitatively complexed. The hydration state of anions is the same as that in quaternary salts; however, even in the presence of 53% KOH, the dehydrating effect is not complete. The extent of residual hydration is more significant for anions with less polarizable charge such as Cl^-, Br^-, and N_3^-, whereas anions with polarizable charge such as I^- and SCN^- are almost completely dehydrated. As a consequence, rate constants increase in comparison with those found in PTC conditions without reaching those of anhydrous solutions [40]. In cryptates the lower energy of interaction between the anion and complexed cation is balanced by a higher interaction of the anion with the solvent, namely, its higher hydration energy. Although the hydration state of anions in cryptates [$K^+ \subset$ **5b**] is the same as found in quaternary salts, second-order rate constants are greater. Moreover, in anhydrous homogeneous conditions the unsolvated anions show the highest reactivity found in solution. However, cryptands have found even fewer practical applications than crown ethers because of their higher cost.

VI. SYNTHETIC APPLICATIONS

A. Solid–Liquid PTC

As described previously, when PTC reactions are carried out in an aqueous–organic two-phase system any kind of PTC catalyst extracts some water into the apolar organic phase as a specific solvation sphere of the anion. Although the amount of water is generally limited, nevertheless it could be deleterious to the desired process. In such cases the problem can be overcome by using a solid anionic reagent in the presence of an anhydrous organic solution of the substrate and the PTC catalyst. The catalyst transfers the anion from the crystal lattice to the organic phase.

A typical case is the synthesis of dichlorocyclopropanes (**9**) by thermal decomposition of solid sodium trichloroacetate (**6**) in the presence of catalytic amounts of an onium salt and an organic alkene solution (Scheme 11) [41,42].

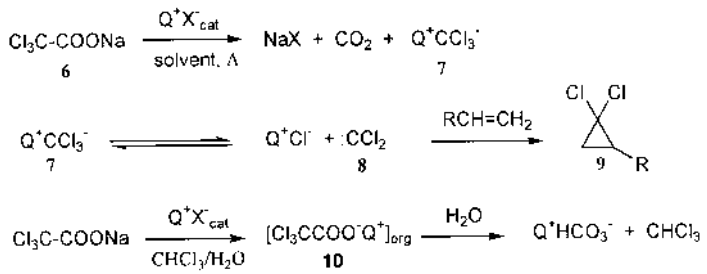

SCHEME 11

The generated dichlorocarbene (**8**) reacts with the alkene in the organic phase as soon as it is formed. The same process cannot be carried out in aqueous–organic media since the trichloroacetate anion is extracted by quaternary salts together with some water of hydration that promotes chloroform and onium bicarbonate formation. However, the same reaction can be successfully carried out with aqueous concentrated alkaline hydroxide and a quaternary ammonium salt. The carbenes thus generated undergo no hydrolytic side reactions since they are extracted into the organic phase in an anhydrous state and high yields of the expected dichlorocyclopropanes are usually obtained [43].

In SL-PTC processes the rate-determining step is often salt dissolution that may be further inhibited by coating of its surface due to the salt generated during reaction. It is well known that the addition of small amounts of water to a solid–liquid reaction mixture can produce large effects on reaction rates. This is due to the formation of a third phase that has been given the name "omega phase," which contains various species during the course of the reaction and provides an alternative lower energy pathway for transfer of species across phases [44].

Although a limited amount of water (0–25% with respect to the solid salt) can form a local saturated water layer on the crystal surface that facilitates anion exchange, in some cases the faster reaction is obtained under strictly anhydrous conditions [45].

B. Ion Pair Extraction

When leaving groups featuring high nucleofugacity and lipophilicity, e.g., I^- and TsO^-, are involved, LL-PTC affords poor results due to ineffective delivery of these anions to the aqueous phase. An alternative procedure is "ion-pair extraction," developed by Brändström in the early 1970s [8], which relies on the quantitative extraction of an anionic reactant into the organic phase from an aqueous solution with equimolar amounts of onium salts. A quaternary salt with a highly hydrophilic ion such as HSO_4^- allows the selective extraction into the organic phase of the desired anion. Reactions may therefore be carried out under strictly anhydrous conditions with highly reactive substrates. The obvious drawback of such a procedure is the need to recover and recycle the onium salt.

For example, olefin hydroboration has been performed, generating borane in situ by reacting equimolar amounts of $Bu_4N^+BH_4^-$ with an alkyl halide R^2X (Scheme 12) [46].

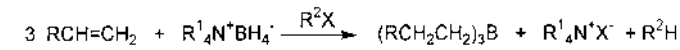

SCHEME 12

It is worth noting that the same reaction has been recently carried out under LL-PTC conditions by stirring a mixture of an *n*-butyl bromide solution of the olefin and a saturated aqueous solution of $NaBH_4$ in the presence of lipophilic onium salts (Scheme 13) [47].

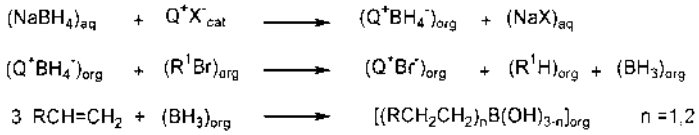

SCHEME 13

The crucial point for the outcome of the overall process is the gradual generation of borane in the organic phase where it reacts with the olefin faster than it is decomposed by water. Alkylboranes can be subsequently oxidized in situ to the corresponding alcohols with alkaline hydrogen peroxide. The sequential synthesis of alcohols from olefins can, therefore, be carried out through an environmentally friendly procedure avoiding anhydrous and dangerous solvents.

C. Inverse Phase Transfer Catalysis

Although LL-PTC is classically performed by extracting an anionic reagent from the aqueous into the organic phase where the reaction occurs, examples are known where the opposite is true, namely, a lipophilic reagent is transferred into the aqueous phase where it reacts with an hydrophilic reactant. The latter procedure has been given the name of inverse phase transfer catalysis (IPTC) [48] and remained quite an unexplored field until recently when it received increasing interest with regard to the use of water as a cheap and environmentally friendly solvent. Cyclodextrins [49], pyridine derivatives [50], and calixarenes [51] have been used as catalysts. On the other hand, the chalcone epoxidation by H_2O_2 in a water/heptane two-phase system in the presence of dodecyltrimethylammonium bromide as a surfactant has been investigated. Results indicated competition between an IPTC and an interfacial process, depending on the reaction conditions [52].

D. Phase Transfer Catalysis in Supercritical Fluids

During the last few years, phase transfer catalyzed reactions between a supercritical phase and a second phase have been investigated in order to find more environmentally friendly solvents than those commonly employed in PTC processes. In addition to the well known advantages deriving from the use of supercritical CO_2 ($scCO_2$) as solvent [53], the accessibility of the critical properties ($T_c = 31^\circ C$, $P_c = 74$ bar) permits its use when thermally labile reactants and catalyst are involved.

The nucleophilic displacement of benzyl chloride with solid potassium bromide [54] or potassium cyanide [55] has been carried out with tetraheptylammonium salts as catalysts. The kinetic data together with the determination of catalyst solubility clearly indicate that the reaction proceeds through formation of a catalyst-rich third phase on the surface of the solid salt phase, where the reaction occurs. The low solubilities of traditional PTC catalysts in the CO_2 phase do not hamper the process but facilitate catalyst removal and recovery.

The S_N2 displacement of *n*-octyl methanesulfonate by bromide and iodide anions has been performed using silica-supported ammonium or phosphonium phase transfer catalysts with $scCO_2$ as solvent, both in SL- (stoichiometric amounts of functionalized silica) and LL-PTC (added aqueous KBr or KI) conditions [56]. The anionic reactivity is comparable to that found in conventional organic solvents; however, environmental benefits and simple recovery of the catalyst through filtration are evident.

Alternative supercritical fluids are to be explored in cases where the intrinsic acidity of $scCO_2$/aqueous systems is undesirable.

E. Gas–Liquid PTC

Gas–liquid PTC is a continuous-flow procedure where gaseous reagents flow through a molten phase transfer catalyst supported on a solid in the absence of any solvent. For this

reason it received great attention with regard to developing new clean procedures for manufacturing organic compounds. For example, the selective monomethylation of various substrates with dimethylcarbonate has been carried out by feeding reagents over a solid bed composed of K_2CO_3 coated with a film of PEG 6000, which is in a molten state at operating temperature [57].

F. Asymmetric Phase Transfer Catalysis

Despite the great impact of PTC in organic synthesis since its discovery, catalytic asymmetric synthesis using chiral phase transfer catalysts has been poorly investigated for quite a long time, but has taken a fast growing pace in the last few years [58,59]. Only isolated examples [60] of asymmetric PTC appeared in the literature until O'Donnell in 1989 reported the enantioselective PTC alkylation of the benzophenoneimine of glycine derivatives catalyzed by *Cinchona* alkaloid-derived ammonium salts (Scheme 14) [61].

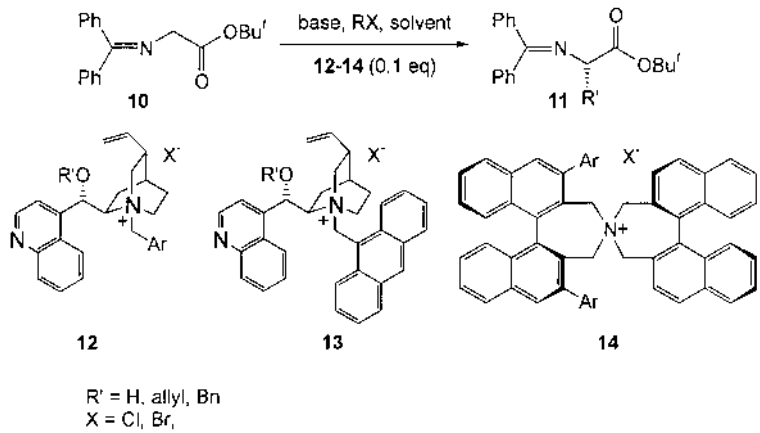

SCHEME 14

Although ees were at the onset only modest, further catalyst improvements allowed excellent ees to be obtained by various groups both under SL-(CsOH–Corey) and LL-PTC (50% KOH–Lygo; Schwesinger bases–O'Donnell) conditions. This topic has been recently reviewed by O'Donnell [62]. The enantioselective alkylation is made possible through formation of a tight, highly structured, ion pair of an ammonium cation and enolate, where the three-dimensional arrangement leaves a single face of the nucleophilic carbon center of the enolate free for attack by the alkylating agent [63].

Excellent results were also reported recently by Maruoka and coworkers by using 50% aqueous NaOH in toluene and a (*S*)-BINAP-derived C_2-symmetric ammonium catalyst **14** [64]. The steric and/or electronic properties of this new class of catalysts can be finely tuned in order to improve reactivity and enantioselectivity. The N-spiro structure along with their high lipophilicity make such catalysts much more reactive than the traditional PTC catalysts, e.g., $Bu_4N^+Br^-$, in otherwise identical conditions [65]. Excellent ees are usually obtained in short reaction times with 1% of catalyst only; moreover, they should be more stable under basic conditions than ammonium salt derived from *Cinchona* alkaloids since they do not undergo Hofmann elimination resulting from lack of β-hydrogens. However, they are not as easily prepared as *Cinchona* ammonium catalysts and are expected to be quite expensive since they are not derived from the chiral pool. On

the other hand, *Cinchona* ammonium catalysts, usually required in a 10% amount, can be recovered and recycled through simple procedures [63,66].

The reaction can be dramatically speeded up through sonication of the reaction mixture, affording comparable chemical yield and enantioselectivity [67].

Dimeric *Cinchona* alkaloid ammonium salts have also been evaluated in LL-PTC alkylation of *N*-(diphenylmethylene)glycine *tert*-butyl ester (Scheme 15). *meta*-Dimer **18** generates α-alkyl derivative **11** in excellent yield and ees, whereas *ortho* and *para* dimers afford lower and scarce enantioselective alkylations, respectively [68].

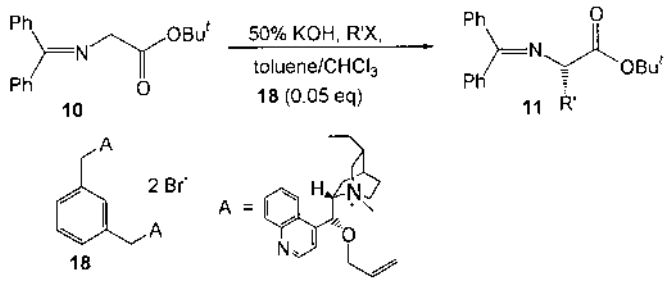

SCHEME 15

The asymmetric PTC alkylation of *t*-butyl glycinate Schiff base has recently been performed in water in the presence of a neutral surfactant such as Triton X-100 using 1 M KOH as base [69]. Alkylated compounds with the same configurations obtained by the LL- or SL-PTC conditions [62] are generated with 1% only of *N*-(9-anthracenylmethyl)-cinchonidium bromide (**13**) with good yields. Although surfactants are known to be phase transfer catalysts themselves, they only provide a hydrophobic area for the interaction between reagents and catalyst without affecting the stereochemical outcome. This solvent-free new procedure appears particularly attractive in the light of increasing demand for reductions in organic solvent use in order to develop environmentally benign processes.

The nucleophilic epoxidation of α, β–enones, pioneered by Wynberg et al. in the 1970s [70], has received considerable attention from various groups. In a recent study employing *N*-(9-anthracenylmethyl)–*Cinchona* alkaloids as PTC catalysts, 71–90% ees were obtained for a series of α, β-epoxyketones (Scheme 16) [71].

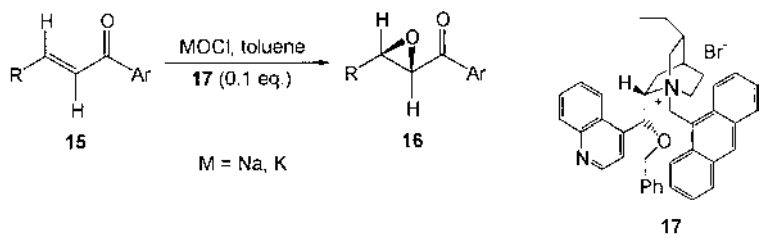

SCHEME 16

The use of 8 M KClO at lower temperature in order to reach higher ees and chemical yields has been reported by Corey and Zhang, together with a rationale of the observed stereoselectivity [72]. The chiral cation assembles the oxidant (KClO) and the α, β-enone in a three-dimensional arrangement that allows face-selective conjugate addition of ion-paired hypochlorite to the α, β-enone, held in proximity by electrostatic and van der Waals' forces.

The same reaction was later performed with high yields and ees with 15% aqueous NaOCl at room temperature in toluene with 1% only of the catalyst [73].

G. Catalyst Recovery

Catalyst separation from the reaction mixture is of primary importance for efficient product purification and catalyst recycling. This has usually been carried out through extraction, distillation, adsorption, and binding to an insoluble support [74].

Catalyst separation from reaction mixtures has been efficiently carried out by using solvent-resistant nanofiltration membranes [75]. Following an alternative approach to solving this problem a quaternary ammonium salt has been immobilized on a soluble poly(ethylene glycol) polymer support. The supported catalyst thus obtained, soluble in solvents commonly used in PTC such as dichloromethane and acetonitrile, was used in a series of standard reactions under PTC conditions with comparable results to those obtained with traditional PTC catalysts [76]. Moreover, it compares favorably to other quaternary salts immobilized on insoluble polystyrene supports [77]. The catalyst can be easily recovered by precipitation with ethereal solvent and filtration and shows no appreciable loss of activity when recycled three times.

VII. OUTLOOK

Although PTC has been on the stage for nearly four decades, no decrease of citations in *Chemical Abstracts* has been found in the last few years. Established PTC technology is expected to keep on greatly improving non-PTC industrial processes. The various benefits are related to the elimination of organic solvents and dangerous or expensive bases along with simplicity of the procedure and high yields and purity of the products. This is particularly attractive owing to the increasing number of environmental laws as PTC processes always produce much less industrial waste and consume less energy when compared with traditional processes [78].

In addition to the development and implementation of PTC processes, future advances of PTC in organic synthesis are expected in the field of supercritical-fluid PTC and from the incorporation of modern computational chemistry in the design of new, inexpensive chiral phase transfer catalysts.

Moreover, the integration of PTC with other technologies and disciplines outside organic synthesis, e.g., material science, biotechnology, bio-origin materials, and soil remediation, is expected to bring benefits to society.

ACKNOWLEDGMENTS

I wish to thank my beloved family for their understanding. I also wish to express my sincere gratitude to Professor Dario Landini and Dr. Michele Penso for helpful discussions and manuscript revision. Financial support from MURST (Project "Stereoselezione in Sintesi Organica: Metodologie ed Applicazioni") is gratefully acknowledged.

REFERENCES

1. (a) CM Starks, CL Liotta, M Halpern. Phase-Transfer Catalysis. Fundamentals, Applications, and Industrial Perspectives. New York: Chapman & Hall, 1994; (b) EV Dehmlow, SS Dehmlow. Phase Transfer Catalysis. 3rd ed. Weinheim: Verlag Chemie, 1993; (c) WE Keller. Phase Transfer Reactions. Fluka Compendium. vol. 3. Stuttgart: Georg Thieme Verlag, 1990; (d) Y Sasson, R Neumann, (ed.) Handbook of Phase Transfer Catalysis. London: Blackie Academic & Professional, 1997; (e) F Montanari, D Landini, F Rolla. Topics Curr Chem. 101:147–200, 1982. (f) M Mąkosza, M Fedorinsky. Adv Catal. 35:375–422, 1987.
2. (a) HJ Parker. Chem Rev 69:1–32, 1969; (b) C Reichardt. Solvent Effects in Organic Chemistry. Weinheim: Verlag Chemie, 1979.
3. (a) K Gustavii. Acta Pharm Suec 4:233–246, 1967; (b) K Gustavii, G Schill. Acta Pharm Suec 3: 241–258, 1966.
4. (a) K Gustavii, G Schill. Acta Pharm Suec 3:259–268, 1966; (b) A Brändström Adv Phys Org Chem, 15:267–330, 1977; (c) R Modin, G Schill. Acta Pharm Suec 4:301–326, 1967; (d) R Modin, A Tilly. Acta Pharm Suec 5:311–322; 1968.
5. NA Gibson, DC Weatherburn. Anal Chim Acta 58:159–165, 1972.
6. R Bock, GM Beilstein. Z Anal Chem 192:44–50, 1963.
7. JE Gordon, RE Kutina. J Am Chem Soc 99:3903–3909, 1977.
8. A Brändström. Preparative Ion Pair Extraction. Läkemedel: Apotekarsocieteten, AB Hässle, 1974.
9. D Landini, H Molinari, M Penso, A Rampoldi. Synthesis 953–954, 1988.
10. J March. Advanced Organic Chemistry. 4th ed. New York: John Wiley pp 261–263, 1992.
11. D Landini, A Maia, F Montanari. J Am Chem Soc 100:2796–2801, 1978.
12. D Landini, A Maia, A Rampoldi. J Org Chem 54:328–332, 1989.
13. D Landini, A Maia, A Rampoldi. Gazz Chim Ital 119:513–51, 1989.
14. D Landini, A Maia. Gazz Chim Ital 123:19–24, 1993.
15. D Landini, A Maia, F Montanari. Israel J Chem 26:263–269, 1985.
16. (a) D Landini, A Maia. Tetrahedron 47:1285, 1991; (b) D Albanese, D Landini, A Maia, M Penso. Ind Eng Chem Res 40:2396–2401, 2001.
17. D Landini, A Maia. Chem Commun 1041–1042, 1984.
18. DK Bohme, GI Mackay. J Am Chem Soc 106:2719, 1984.
19. HJ Clark. Chem Rev 80:429–452, 1980.
20. A Brändström. Adv Phys Org Chem 15:267–330, 1977.
21. CM Starks, RM Owens. J Am Chem Soc 95:3613–3617, 1973.
22. D Landini, A Maia, G Podda. J Org Chem 47:2264–2268, 1982.
23. CM Starks. J Am Chem Soc 93:195–199, 1971.
24. D Landini, A Maia, F Montanari. Chem Commun 112–113, 1977.
25. FM Menger. J Am Chem Soc 92:5965–5971, 1970.
26. (a) CM Starks, RM Owens. J Am Chem Soc 95:3613–3617, 1973; (b) D Landini, A Maia, F Montanari. Nouv J Chem 575–577, 1979; (c) L Horner, J Gerhard. Justus Liebigs Ann Chem 838–842, 1980.
27. HH Freedman, RA Dubois. Tetrahedron Lett 3251–3254, 1975.
28. M Mąkosza. Pure Appl Chem 43:439–462, 1975.
29. EV Dehmlow, M Lissel. Tetrahedron Lett 1783–1786, 1976.
30. Mąkosza, E Bialecka. Tetrahedron Lett 183–186, 1977.
31. Mąkosza, I Krylowa. Tetrahedron 55:6395–6402, 1999.
32. J Ugelstad, T Ellingsen, A Berge. Acta Chem Scand 20:1593, 1966.
33. DN Bhattacharyya, CL Lee, J Smid, M Szwarc. J Phys Chem 69:608–611, 1965.
34. (a) D Landini, A Maia, A Rampoldi. J Org Chem 51:3187–3191, 1986; (b) EV Dehmlow, V Knufinke. J Chem Res (S), 224–225, 1989.
35. S Samaan, F Rolla. Phosphorus Sulfur 4:145–148, 1978.

36. HJ Cristau, A Long, H Christol. Tetrahedron Lett 349–352, 1979.
37. CJ Pedersen, HK Frensdorff. Angew Chem, Int Ed Engl 11:16–25, 1972.
38. D Landini, A Maia, F Montanari, FM Pirisi. J Chem Soc, Perkin II 46–51, 1980.
39. PE Stott, JS Bradshaw, WW Parish. J Am Chem Soc 102:4810–4815, 1980.
40. D Landini, A Maia, F Montanari. J Am Chem Soc 106:2919–2923, 1984.
41. EV Dehmlow. Tetrahedron Lett 91–94, 1976.
42. EV Dehmlow, T Remmler. J Chem Res 72–73 (S); 766 (M), 1977.
43. M Mąkosza, W Wawrzyniewicz. Tetrahedron Lett 4659–4662, 1969.
44. CL Liotta, J Berkner, J Wright, B Fair. ACS Symp Ser 659:29–40, 1997.
45. EV Dehmlow, HC Raths. J Chem Res 384 (S), 2901 (M), 1988.
46. A Brändström, U Junggreen, B Lamm. Tetrahedron Lett 31:3173–3176, 1972.
47. D Albanese, D Landini, M Penso. Synlett 997–998, 2000.
48. LJ Mathias, RA Vaidya. J Am Chem Soc 108:1093–1094, 1986.
49. (a) H Bricout, L Caron, D Bormann, E Monflier. Catal Today 66:355–361, 2001; (b) R Widehem, T Lacroix, H Bricout, E Monflier. Synlett 722–724, 2000.
50. YL Lu, JJ Jwo. J Mol Catal 170:57–65, 2001.
51. S Shimizu, S Shirikawa, T Suzuki, Y Sasaki. Tetrahedron 57:6169–6173, 2001.
52. B Boyer, A Hambardzoumian, J-P Roque, N Beylerian. Tetrahedron 56:303–307, 2000.
53. PJ Jessop, T Ikariya, R Noyori. Chem Rev 99:475–493, 1999.
54. AK Dillow, SLJ Yun, D Suleiman, DL Boatright, CL Liotta, CA Eckert. Ind Eng Chem Res 35:1801–1806, 1996.
55. K Chandler, CW Culp, DR Lamb, CL Liotta, CA Eckert. Ind Eng Chem Res 37:3252–3259, 1998.
56. J DeSimone, M Selva, P Tundo. J Org Chem 66:4047–4049, 2001.
57. S Memoli, M Selva, P Tundo. Chemosphere 43:115–121, 2001.
58. MJ O'Donnell. In: I Ojima, ed. Catalytic Asymmetric Synthesis. New York: John Wiley, 1999.
59. T. Shioiri. Ref. 1d, pp 462–479.
60. U-H Dolling, P Davis, EJJ Grabowski. J Am Chem Soc 106:446–447, 1984; (b) DJ Cram, GDY Sogah. Chem Commun 625–628, 1981.
61. MJ O'Donnell, WD Bennett, S Wu. J Am Chem Soc 2353–2355, 1989.
62. MJ O'Donnell. Aldrichim Acta 34:3–15, 2001.
63. EJ Corey, F Xu, MC Noe. J Am Chem Soc 119:12414–12415, 1997.
64. (a) T Ooi, M Kameda, K Maruoka. J Am Chem Soc 121:6519–6520, 1999; (b) T Ooi, M Takeuchi, M Kameda, K Maruoka. J Am Chem Soc 122:5228–5229, 2000.
65. T Ooi, K Doda, K Maruoka. Org Lett 3:1273–1276, 2001.
66. B Lygo, J Crosby, TR Lowdon, JA Peterson, PG Wainwright. Tetrahedron 57:2403–2409, 2001.
67. T Ooi, E Tayama, K Doda, M Takeuchi, K Maruoka. Synlett 1500–1502, 2000.
68. S Jew, B-S Jeong, M-S Yoo, H Huh, H Park. Chem Commun 1244–1245, 2001.
69. T Okino, Y Takemoto. Org Lett 3:1515–1517, 2001.
70. R Helder, JC Hummelen, RWPM Laane, JS Wiering, H Wynberg. Tetrahedron Lett 1831, 1976.
71. B Lygo, PG Wainwright. Tetrahedron 55:6289–6300, 1999.
72. EJ Corey, F-Y Zhang. Org Lett 1:1287–1290, 1999.
73. B Lygo, DCM To. Tetrahedron Lett 1343–1346, 2001.
74. CM Starks. Ref. 1a, pp 292–302.
75. SS Luthra, X Yang, LM dos Santos, LS White, AG Livingston. Chem Commun 1468–1469, 2001.
76. R Annunziata, M Benaglia, M Cinquini, F Cozzi, G Tocco. Org Lett 2:1737–1739, 2000.
77. SL Regen. J Org Chem 42:875–879, 1997; (b) MS Chiles, DD Jackson, PC Reeves. J Org Chem 45, 2915–2918, 1980; (c) H Molinari, F Montanari, S Quici, P Tundo. J Am Chem Soc 101:3920–3927, 1979.
78. M Mąkosza. Pure Appl Chem 72:1399–1403, 2000.